IN VITRO METABOLIC PATHWAY CONSTRUCTION IN AN IMMOBILISED ENZYME MICROREACTOR (IEMR)

Amanatuzzakiah Binti Abdul Halim

A thesis submitted for the degree of
Doctor of Philosophy
to
University College London

Department of Biochemical Engineering
University College London
Torrington Place
London
WC1E 7JE
2013

'I, Amanatuzzakiah Binti Abdul Halim, confirm that the work presented in this thesis is my own. Where information has been derived from other sources, I confirm that this has been indicated in the thesis.'

Abstract

The concept of *de novo* metabolic engineering through novel synthetic pathways offers new directions for multi-step enzymatic synthesis of complex molecules. This has been complemented by recent progress in performing enzymatic reactions using immobilised enzyme microreactors (IEMR). This work is concerned with the construction of *de novo* designed enzyme pathways in a microreactor synthesising a chiral molecule. An interesting compound, commonly used as the building block in several pharmaceutical syntheses, is a single diastereoisomer of 2-amino-1,3,4-butanetriol (ABT). This chiral amino alcohol can be synthesised from simple achiral substrates using two enzymes, transketolase (TK) and ω-transaminase (TAm).

This project involves the design and the development of an IEMR using His_6-tagged TK and TAm immobilised onto Ni-NTA agarose beads and packed into tubes to enable multi-step enzyme reactions. The IEMR was first characterised based on the operational and storage stability. Furthermore, kinetic parameters of both enzymes were determined using single IEMRs evaluated by a kinetic model developed for packed bed reactors.

For the multi-step enzyme reaction, two model systems were investigated. The first model investigated was the dual TK (pQR 791)-TAm (pQR 801) reaction. With initial 60 mM (HPA and GA each) and 6 mM (MBA) substrate concentration mixture, the coupled reaction reached approximately 83% conversion in 20 minutes at the lowest flow rate. On the other hand, the second model reaction comprises of three sequential enzyme reaction, TAm (pQR 1021)-TK (pQR 791)-TAm (pQR 1021). A 6% yield of ABT was produced from initial substrate mixture of 100 mM serine and 40 mM GA at flow rate of 0.5 μL/min.

Further considerations to improve the system would allow for better yield of the target product and potentially make this IEMR system a powerful tool for construction and evaluation of *de novo* pathways as well as for rapid determination of various enzymes kinetics.

Acknowledgements

Table of Contents

List of Figures

List of Tables

Nomenclature

A_0	initial substrate concentration (mM)
C	reaction capacity (mol.h^{-1})
ºC	degrees centrigrade
D	dilution rate (h^{-1})
D_p	spherical diameter of the particle (m)
ε	void fraction of the bed
f	fraction of substrate converted to product during reaction
k_{cat}	enzyme turnover rate (s^{-1})
K_m	Michaelis−Menten constant (mM)
$K_{m\,(app)}$	apparent Michaelis−Menten constant (mM)
L	length of the bed (m)
OD	optical density
OD_{600}	optical density at 600 nm
Δp	pressure drop (Pa)
Q	volumetric flow rate (mL.h^{-1})
Re	Reynolds number
ρ	density of the fluid (kg.m^{-3})
μ	dynamic viscosity of the fluid (kg.m^{-1}.s^{-1})
τ	space time (or holding time) (h)
$t_{1/2}$	half life (h)
v	volumetric flow rate of the substrate (mL.h^{-1})
V	total volume of the reactor (mL)
v_o	initial reaction rate (mM.s^{-1})
V_{max}	maximum velocity at saturating substrate concentration (mM.s^{-1})
$V_{max(app)}$	apparent maximum reaction velocity (mM.s^{-1})
V_s	superficial velocity (m.s^{-1})

Abbreviations

ABT	2−amino−1,3,4−butanetriol
ACN	acetonitrile
AP	acetophenone
β-A: P TAm	β−alanine: pyruvate transaminase
BSA	bovine serum albumin
CO_2	carbon dioxide
DNA	deoxyribonucleic acid
E.coli	*Escherichia coli*
EDTA	ethylenediaminetetraacetic acid
ERY	erythrulose
FE−SEM	field-emission scanning electron microscopy
g	grams
GA	glycolaldehyde
H_2O	water
His_6	6x~histidine−tagged
Li−HPA	Lithium−hydroxypyruvate
HPLC	high performance liquid chromatography
IEMR	immobilised enzyme microreactor
IPTG	isopropyl β-D-thiogalacto pyranoside
kDa	kilo Dalton
LB	Luria−Bertani
M	molar
MBA	methylbenzylamine
mg	milligrams
Mg^{2+}	magnesium ion
Min	minutes
mL	milliliters
mM	millimolar
mmol	millimoles
ms^{-1}	metres per second

M.W.	molecular weight
MWCO	molecular weight cutoff
NADH	nicotinamide adenine dinucleotide
NaOH	sodium hydroxide
Ni−NTA	nickel−nitrilotriacetic acid
OD	optical density
PDMS	polydimethylsiloxane
PET	polyethylene terephthalate
PLP	pyridoxal phosphate
R.sphaeroides	*Rhodobacter sphaeroides*
RTD	residence time distribution
[S]	substrate concentration
SBP	soybean peroxidase
SDS−PAGE	sodium dodecyl sulfate polyacrylamide gel electrophoresis
TAm	transaminase
TFA	trifluoroacetic acid
TK	transketolase
TK−TAm	transketolase and transaminase pathway
TPP	thiamine pyrophosphate
Tris	tris(hydroxymethyl)aminomethane
UV	ultraviolet
V.fluvialis	*Vibrio fluvialis*
v/v	volume by volume
w/v	weight by volume
μL	microlitre
μm	micrometer
μ_{max}	maximum specific growth rate
μmol	micromole

1 Introduction

1.1 Microfluidics and its Characteristic features

Microfluidic is the field that studies and exploits the behavior of fluids confined to small channels with dimensions of ten to hundreds of micrometers (Folch, 2013; Whitesides, 2006). This technology originated from microanalytical methods that used electrophoresis back in 1940s by J. St. L. Philpot, a biochemist from Oxford University (Folch, 2013). Later in 1990, Manz et al. (1990) invented the first HPLC microfluidic device. After decade of development, microfluidics have shown to advance in many areas including analytical chemistry, biology, diagnostics and biomedical research inline with novel microfabrication techniques. As the microfluidic applications expand, several microfluidic structures, such as microvalves, micropumps and micromixers (Beebe et al., 2002; Laser & Santiago, 2004; Oh & Ahn, 2006; Zhang et al., 2007) are being developed. Integration of these different functional components give rise to the new emerging technology that is called micro total analysis systems (μ-TAS) or also known as lab-on-a-chip.

Owing to their miniature size, microfluidic system requires only a small volume of reagent, shorter processing time and can be parallelized using lab-on-a-chip technology (Chow & Hong, 2002; Edel & DeMello, 2009). In addition, a small quantity of processing volume allows for the precise control of reaction variables, such as reagent mixing, flow rates, reaction time, and heat and mass transfer (Schmid et al., 2001; Hong et al., 2009; Mark et al., 2010). It is a perfect alternative for direct synthesis on demand production in small-scale plant (Maehara et al., 2008). In contrast with conventional procedures, microreactors are easily scalable, rendering a device capable of both analytical and semi-preparative scales of production. Finally, the microreactor format is amenable to automation of reaction optimization (Quiram et al., 2007).

This technology is being developed by taking advantage of the same microfabrication techniques used to pattern integrated circuits on silicon wafers, with incorporation of the design and development of miniaturized fluidic devices

that manipulate samples at nanolitres volumes (Breslauer et al., 2006). Detection systems for product analysis is now accessible not only using fluorescence but also newly introduced techniques; optical methods of chemiluminescence, refraction and thermooptics, as well as the electrochemical methods of amperometry, conductimetry and potentiometry (Schwarz & Hauser, 2001). The application of microfluidic devices has been extensively increased over the years especially for conditions screening purpose. With the miniaturisation concept, multiple samples of biochemical, genetic, proteomic data can be processed, thus high-throughput screening (HTS) technology has emerged to meet the demand (Hsieh et al., 1998; Wu et al., 2003; Hong et al., 2009; Cho et al., 2011).

Furthermore, the microfluidic market was estimated to worth £1 billion in 2011 with an average of 19% annual growth (Frédéric, 2011). The demand for microfluidics devices for research in pharmaceuticals and life sciences is expected to thrive in the coming years with projection of 23% growth in 2016, pushing the sector to almost £2.5 billion sales (Frédéric, 2011). Despite the rapid development, commercialisation is still a major challenge of this technology. High initial investments and running fabrication cost are among the hurdles of market entry. Mark et al. (2010) proposed the concept of a well-defined microfluidic platform, whereby combining individual microfluidic unit operations within a consistent fabrication technology may results in lower production cost and less financial risks.

1.2   Application of Microfluidics

We have seen rapid developments on microfluidics technology in the recent years. Annual numbers of publication on the topic of microfluidics increases dramatically over the last 10 years, whereby 10,000 of journal papers have been published and this number continue to proliferate (Mark et al., 2010). The main driving force behind the fast growth of this technology is due to its potential to be exploited for a wide range of biological applications such as high-throughput screening in drug development (Pihl et al., 2005; Dittrich & Manz, 2006; Lombardi & Dittrich, 2010), bioanalyses (Huh et al., 2005; Breslauer et al., 2006), single cell and molecule

studies (Wheeler et al., 2003; Lemke et al., 2009), drug delivery and advanced therapeutics (Pihl et al., 2005; Dittrich & Manz, 2006; Lombardi & Dittrich, 2010), and point of care diagnostics (Lee & Lee, 2004; Whitesides, 2006; Mark et al., 2010).

1.2.1 Micro Total Analysis System (µTAS)

Term micro total analysis system (µ-TAS) was first coined in the early 1990s by Manz et al. (1990) on their miniature system of the wet chemical and electrical detection for chemical sensing. This term was gradually expanded to lab-on-a-chip (LOC) with increasing application in tissue engineering and cell biology studies (Folch, 2013). An important aspect of µ-TAS is the ability to perform complete an analytical microsystem in a single device. The various functional units usually include sample acquisition, pretreatment, separation, post-treatment and a detection system (Lee & Lee, 2004) (Figure 1.1).

Fluid and particle handling
pressure driven-flow
electrokinetic control
electroosmotic flow control

Sample preparation
sonication
extraction
preconcentration

Reactors and mixers
micromixer
chemical reactor
enzymatic reactor
immunoassay reactor
postcolumn labeling

Separation
chromatography
electrophoresis
isoelectric focusing
diffusion

Detection
chemiluminescence
electrochemical detection
fluorescence
nonfluorescence optical measurement
mass spectrometry

Microfluidic systems

Figure 1.1: Schematic diagram of micro-Total Analysis System (μ-TAS). Key technologies and units that need to be incorporated into μ-TAS. Image reproduced from (Lee & Lee, 2004).

Development of miniaturised protein analysis is progressing and it is more likely to be used widely in the near future. With the low sample requirement feature, a microfluidic approach appears to be an attractive choice to overcome the limited protein sample problem compared with DNA, which can be amplified by PCR. The advantages offered by microfluidic system will allow for high-throughput processing of multiple samples in an integrated microfluidic system for proteome analysis. High-sensitivity peptide mapping was developed that used micro-column high-performance liquid chromatography (HPLC) and capillary zone electrophoresis (CZE) separations (Cobb & Novotny, 1989). In this work, separations of 100 ng (4 pmol) of tryptic digest samples of β-casein were achieved with micro-column HPLC, while separations of approximately 2 ng (80 fmol) of β-casein tryptic digest (from a total sample size of 50 ng) were possible with CZE. Integration of on-line coupling with MALDI (matrix assisted laser desorption/ionization) has become one of the alternatives for mass spectrometric analysis as it offers an extended range of mass limit for biomolecules over 300,000 Da (Ekström et al., 2000). They devised a platform, which integrates automated sampling pretreatment, microchip IMER, microdispenser for sample deposition and automated MALDI-TOF-MS system analysis as shown in Figure 1.2.
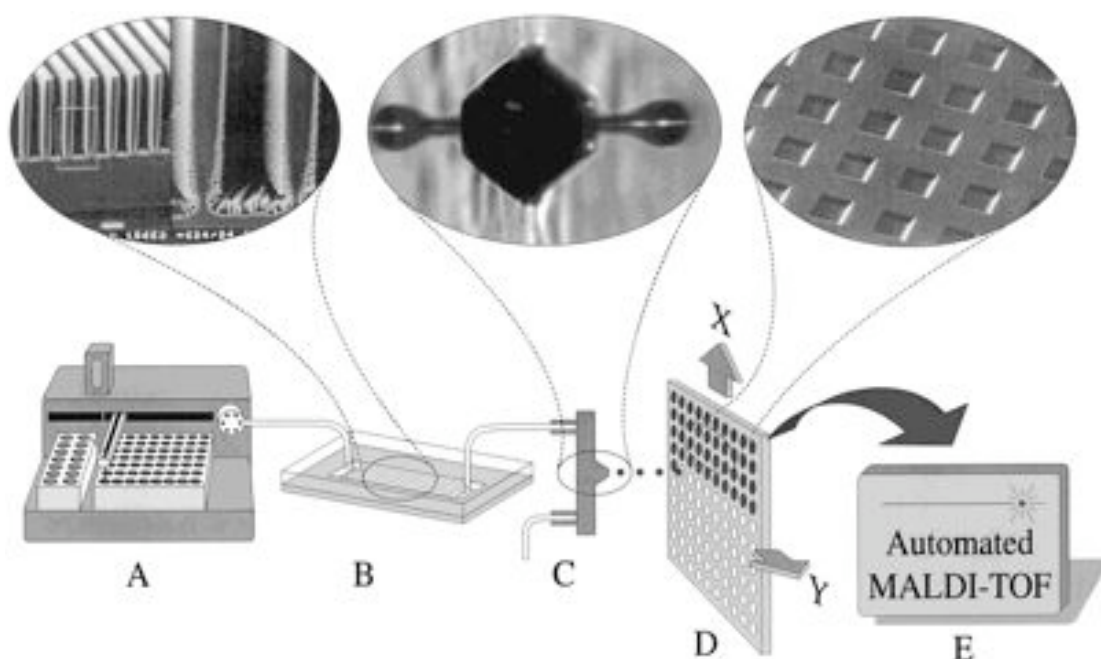
Figure 1.2: Integration of on-line coupling with matrix assisted laser desorption/ionization (MALDI). Total analysis system and its different parts; (A) automated sample pretreatment and injection; (B) microchip IMER (the photo inset shows a SEM picture of the lamella structure with the porous layer; (C) the microdispenser used to deposit sample into microvials, (D) shallow nanovials on the MALDI target plate; and (E) automated MALDI-TOF MS analysis. Image reproduced from (Ekström et al., 2000).

μ-TAS in DNA application has progressed rapidly since the completion of the human genome project in 2003. New platforms are being developed to enhance speed, sensitivity and high-throughput of the DNA analysis systems. DNA microchip for genomic analysis was developed for gene sequencing (Fodor et al., 1991) which then has been commercialized by Affymetrix. This technique used light to micropattern the chemical synthesis of oligonucleotides. Fan et al. (1999) demonstrated the use of paramagnetic beads for gene expression analysis in a microfluidic chip that takes a few seconds for the hybridization process to complete. An advanced integrated microfluidic device that allows for automated multistep genetic assays was developed by Anderson et al. (2000). This sophisticated device was tested for the detection of mutations in a 1.6 kb region of the HIV genome from serum samples. It has the ability to perform various analysis processes, which include microliter chemical amplification, serial enzymatic reactions, metering mixing and nucleic acid hybridization. With plastic as the fabricated material, this

system could be applied for low cost portable DNA analysis instruments for many different applications.

As the utilization of microreactors for bioassays becomes widely used, system integration and design complexity are expected to increase dramatically. Automation offers great benefits in terms of reducing human effort, enable high-volume production, ease in optimization, time saving and provide safer operations. Chakrabarty & Zeng (2005) described different actuation mechanisms for microfluidics-based biochips, as well as associated design automation trends and challenges. A microreactor system for gas-phase catalysed reactions was coupled with an automation system that employed process logic controller with a human-machine interface for display of sensors and monitoring of process control loops (Quiram et al., 2007). This system was able to operate at 500 Hz with all 24 microreactor heaters being under closed-loop PID control.

Thorsen et al. (2002) innovated large-scale integration of microfluidic chips that contain micro-pumps, micro-valves, and micro-channels, which exploits the usage of fluidic multiplexor to run the network. Pollack et al. (2002) superseded the use of conventional pumps, valves or channels with manipulation of discrete droplets. This system based upon direct electrical control of the surface tension or also known as electrowetting allowed the experiment to successfully transferred droplets of 0.7 – 1.0 l of 100 mM KCl solution between adjacent electrodes at voltages of 40 – 80 V. The switching rate of the electrode up to 20 Hz and average velocities of 30 mm/s was achieved and this illustrates nearly 100-fold increase compared to the previous electrical methods.

1.3 Materials and Microfabrication

1.3.1 Construction materials

There are many options on the type of material used to fabricate the microreactors, but it is all dependent on the application desired. Most common materials used in microfluidic systems are silicon, polymer, glass and metal. Silicon and glass were

26

widely used in the earliest development of microfluidic as the fabrication method was adopted from the micromechanical systems (MEMS). These materials are often not the ideal material for microfluidic applications due to the expensive fabricating cost, difficulty in component integration and surface characteristics (especially permeability to gases) that are not well suited to biological applications (Beebe et al., 2002; Verpoorte & Rooij, 2003). Moreover silicon is opaque to visible and ultraviolet light that make it impractical for optical method detection. Nonetheless, silicon and glass would be a perfect candidate for the material used in chemistry applications that require strong solvents, high temperatures or chemically stable surfaces (Woolley & Mathies, 1994; Mellors et al., 2008).

The trend of using a polymer as the material for microfluidic devices has increased tremendously in recent years. The most widespread used polymer is PDMS (polydimethylsiloxane). PDMS exhibits excellent attributes that make it suitable for the current microfluidic devices, that include inexpensive cost, optical transparency, low toxicity and permeability to gases (Verpoorte & Rooij 2003; Whitesides 2006; Hong et al. 2009). This elastomer is easy to handle and being used extensively for creation of prototype devices under non-clean room conditions. Integration of valves, pumps and mixer in the system is possible by using multilayer soft lithography (Hong et al. 2009). However, this material is prone to swelling in the presence of organic solvent.

1.3.2   Microfabrication methods

In the early development of microfluidic devices, fabrication was performed through a micromachining process where silicon was used as the fabricating material. This method can be divided into two types, which are bulk micromachining and surface micromachining. Bulk micromachining refers to those processes that lead to structures in the single-crystal wafer, whereas surface micromachining results in structures located on the wafer surface (Verpoorte & Rooij, 2003). These methods offer high precision quality for the devices. However, most of the microfluidic devices do not require the precision that micromachining offers. This fabrication method appears to be less adopted in many microfluidic

devices as it is time consuming, expensive, labor intensive and requires highly specialized skills and facilities (Beebe et al., 2002; Malek, 2006).

The need for flexible and rapid processes is increasing in all fields of microsystem technologies. Rapid prototyping becomes more appealing as to promote the usage of microfluidic devices. A simple method for fabrication has been introduced that is called soft lithography. The process involves the casting of solution (polymer), typically PDMS into the master that has been structured for specific design. The master can be moulded by using micromachining or photolithography techniques. The application of soft lithography has been reported extensively by many recent works. Park et al. (2010) used a micro-macro hybrid soft-lithography master (MMHSM) fabrication technique to create a PDMS microdevice having two integrated macroscale reservoirs and 40 fluidic interfaces. Li et al. (2005) demonstrated the multiple replication of the PMMA master for PDMS-based devices, which contain normal deep microfluidic channels and a much deeper optical fiber channel, and allows for laser-induced fluorescence (LIF) detection. A multidimensional layer of microfluidic devices has been fabricated by Anderson et al. (2000) using the membrane sandwich method. This method combines a convenient process for microfabrications rapid prototyping based on high resolution printings with multilevel photolithography, replica molding, and supported membrane transfer. The simplicity and flexibility that this method offers make it practical for prototyping microfluidic devices.

Injection moulding could also be used in fabrication of microfluidic devices for polymers. It was widely used in macroworld fabrication before it is been introduced in microfluidic system. Typically the polymer material is heated up at a certain glass transition temperature and injected with high pressure into the mould. Rapid cooling will take place as the mould is maintained at lower temperature and the moulded part is ready within a few minutes. The advantage of this technique is the ability to form three-dimensional objects in particular, the integration of fluidic interconnects (Gärtner et al., 2007). Furthermore, this process is preferable over the hot embossing technique with regard to the fabrication time and relatively cheap for

high volume manufacturing. However, this method requires complicated moulding tools that can withstand the operation conditions and imposes limitation on the resolution and material choices (Becker & Gärtner, 2008).

Another method for rapid prototyping for microfluidic devices is laser ablation. This technique involves directing laser pulses at the plastic surface in defined regions, which causes degradation of the plastic at those spots as a consequence of a combination of photochemical and photothermal degradation processes (Verpoorte & Rooij, 2003). Yin et al. (2005) presented a microfabricated approach to a nano liquid chromatography system by employing the laser ablation method to produce channels, ports, and frit structures on the chip. Furthermore, the laser ablation technique can be further used to modify surface charge on specific surfaces within a preformed plastic microchannel. This results in better control, adjustment, and modulation of the electroosmotic flow without using wall coatings or changing the geometry of the channel to achieve the desired flow profile (Johnson et al., 2001). Roberts et al. (1997) demonstrated fabrication of a miniaturized liquid-handling systems on polymer substrate chips using the same technique. Efficient sealing was obtained, while photoablated surfaces showed an increase in their hydrophilicity and rugosity, which indicates a correlation between the ablative changes in surface conditions and the resulting electroosmotic flow. All in all, the laser ablation method offers a highly precise, fast and contactless alternative to classic machining. Malek (2006) has discussed in detail the use of laser processing for microfluidics application.

1.4   Microreactors

Microreactor technology has immense potential to notably improve chemical and biological analyses as well as abundant applications in medical diagnostics and therapeutic devices. Microreactors have been developed to facilitate work in chemical and biochemical analysis as well as being integrated as parts of the lab-on-a-chip and µTAS (Urban et al., 2006). Owing to their miniature size, microreactors offer many advantages to the industry especially in organic synthesis which include;

improved selectivity and reliability, faster speed to market, safety, cost savings and easier scale-up (Ehrfeld et al., 2000).

The application of microreactors in fine-chemical industries is driven by the ability of the technology to ease the practical difficulties related to performing the chemical reactions using traditional methods (Haswell & Skelton, 2000). A high level of safety issue which include explosive, toxic and hazardous materials are the most common bottleneck presence in the conventional chemical reaction method. This safety aspect was addressed successfully in the production of organic peroxides from acid chlorides (Srinivasan et al., 1997), synthesis of hydrogen cyanide (Ehrfeld, 1999) and fluorine-containing organic compounds (Chambers & Spink, 1999) performed on a microreactor platform.

Besides that, many works have been demonstrated in enzyme microreactors applications. These cover the area in protein and peptide mapping analysis (Ekström et al., 2000; Guo et al., 2003; Kato et al., 2004), nucleic acids (Zhang & Yeung, 1998; Lee et al., 2000; Ke et al., 2004) and model enzymatic systems (Koh & Pishko, 2005; Hickey et al., 2007, 2009; Ngamsom et al., 2010; Alam et al., 2011; Matsuura et al., 2011). The incorporation of the enzyme may be either in immobilised (heterogeneous) form or in solutions (homogeneous biocatalysis). However, most of the reported works were based on immobilised enzymes due to its ability to be recycled, therefore reducing the operational cost. The applications of immobilised microfluidic enzymatic reactors were discussed in detail by Matosevic et al. (2011) and Nidetzky (2013).

1.4.1   Biocatalyst in microreactors

Biocatalysis posseses very compelling features that make it as one of the important tools in bioprocess industry especially in the biotechnology applications. This is mainly due to the ability of the biocatalyst to perform complex chemical conversions under mild environmental conditions with high specificity and efficiency (Christen & Metzler, 2005; Pollard & Woodley, 2006). Moreover, the continuing progress in medical research, genomics, proteomics and related

emerging biotechnology fields also lead to the exponential growth of the application of biocatalysis. The potential that biocatalysis has, makes it a perfect alternative to chemical processes particularly the exquisite regioselective and stereoselective properties that enable rather difficult syntheses to be performed with fewer steps and more benign conditions (Figure 1.3).
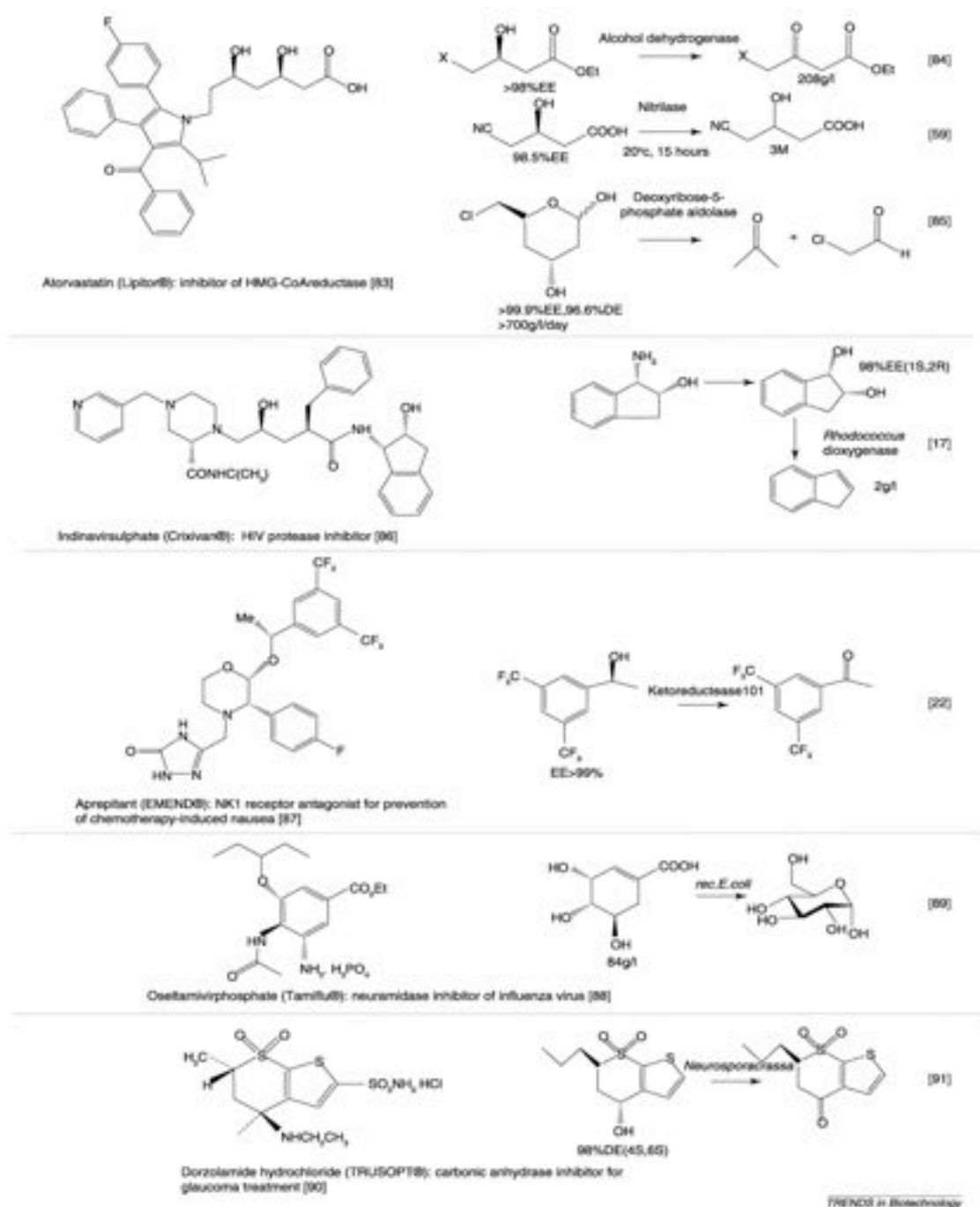
Figure 1.3: Complex drug compounds with multiple chiral centres and the biocatalytic step(s) associated with the development of each synthetic route. Image reproduced from Pollard & Woodley (2007). References: [17] (Buckland et al., 1999), [22] (Pollard et al., 2006), [59] (DeSantis et al., 2003), [83] (Roth, 2002), [84] (Yasohara et al., 1999), [85] (Greenberg et al., 2004), [86] (Lin et al., 2002), [87] (Brands et al., 2003), [88] (Federspiel et al., 1999), [89] (Guo & Frost 2004), [90] (Blacklock, 1993), [91] (Holt, 1996).

With the increasing demand from the industry to seek new routes to produce complex molecules, there is a need to have a system or tools as a platform to guide the development of new biocatalytic processes. Where typically, large scales incur higher expenses, there are other much lower-scale devices that can be used. One such technology are microreactors as they allow a reaction to be conducted which only requires a small volume of reagent, short processing time, and most of all, the ability to be integrated with various analytical system.

1.4.2 Batch and continuous microreactors

One of the important factors affecting bioreactor performance is the mode of operation. The most common modes of bioreactor operation are batch and continuous. The choice of operating mode has a significant effect on the substrate conversion, product concentration, susceptibility to contamination and process reliability (Doran, 2013). A batch reactor measures the rate of substrate conversion to product as a function of time. Whereas, in a continuous flow reaction, they operate at steady state and remain unchanged for as long as the flow rates are kept constant (Denbigh, 1944). In industry, a large number of processes in the production of polymers, specialty and fine chemicals as well as pharmaceuticals are operated in batch (Friedrich & Perne, 1995). While many chemical processes are produced in batch reactors, the direction in process industries is moving towards continuous reactors for commercial manufacture. A defining feature of continuous flow systems is continuous flow processing, which further brings inherent safety and economical advantage to the process (Watts, 2004). Moreover, the scale-up difficulties commonly occur in batch reactors can be improved in continuous flow reactors (Anderson, 2001; Brivio et al., 2006).

In addition, a batch microreactor is commonly associated with its limitation on the reagents mixing time (Gleason & Carbeck, 2004). With a small dimension of the microreactor, the Reynolds numbers are usually small and flow is laminar, whereby the mixing is dependent almost completely on diffusion (Jähnisch et al., 2004). The characteristic time for diffusive mixing is given by the following equation:

$$\frac{x^2}{D} = t$$

where x is distance travelled and t is time for the reagents to mix, and D is the diffusion coefficient.

Therefore, batch reactors are characterised by a "dead time". This is the time it takes for the reactants to mix before kinetic data can be collected. Based on the equation, the dead time is estimated to be on the order of seconds in a micrometer-sized batch reactor (Gleason & Carbeck, 2004). This would account for a significant loss that could prevent the study of fast enzyme kinetics when operated in batch mode.

Numerous studies have been demonstrated with an immobilised biocatalyst run in continuous flow mode. The operation can be performed advantageously due to the shorter average residence time spent by the substrate molecules within the reactor. This results in a far greater productivity from a fixed amount of enzyme than is achieved in batch process as well as minimizing dead time operation. This type of operation was demonstrated in many microreactors application, whereby the reactions provide improved yields and selectivity when performed in a continuous manner at the microscale as compared to the batch process (Greenway et al., 2000; Wilson & McCreedy, 2000; Kobayashi et al., 2004). In addition the yield of a reaction could be improved dramatically by removing the inhibitory product by performing the reaction in a continuous flow mode (Shin & Kim, 1999; Andrić et al., 2010).

1.4.3 Kinetic analysis

Another application of microreactors is as a platform for analysing kinetic parameters of particular enzyme. Utilising the attributes of this system allows the study of enzyme kinetics in a simpler manner where hundreds of enzyme reactions can be conducted simultaneously with minimal amount of material at very short

time. Besides that, immobilisation of enzyme permits the device to be reused again while preserving the stability of the enzyme. Nonetheless, study of enzyme kinetics plays a very important role in developing new biocatalysts that could be used for a wide range of applications.

The ability of enzymes to speed up the rate of reaction by many orders of magnitude, and the selectivity towards substrate make it as a valuable element in biochemical reactions. With the study of enzyme reactions, one can explain mechanisms of enzyme catalysis and regulation. Enzyme kinetics deals with time-dependent enzyme reaction outside equilibrium. The reactions usually follow the well-known Michaelis-Menten kinetics under steady state conditions. Besides that, there are several factors that affect the kinetics of the enzyme that include, temperature, pH, enzyme and substrate concentration. Most enzymes work at optimum pH and temperature at which the activity is the greatest.

Kinetic data for the enzyme is important to study specific reactions catalysed by the enzyme. One of the models to study the kinetics is that of Michaelis–Menten (Michaelis et al., 1913). The Michaelis–Menten equation relates the initial reaction rate, v to the substrate concentration, [S]. The corresponding graph is a rectangular hyperbolic function and the maximum rate is described as V_{max} (Eq 1.1)

$$v = \frac{V_{max}[S]}{K_m + [S]}$$

(1.1)

This equation can be rearranged to obtain linear relationships, which permit more precise fitting to the experimental data, and estimation of the values of K_m and V_{max}. There are several linear regression methods that can be used to fit to the Michaelis Menten model. This includes Lineweaver−Burke (Lineweaver & Burk, 1934), Eadie−Hofstee (Eadie, 1942; Hofstee, 1952) and Hanes−Woolf (Hanes, 1932). The Lineweaver-Burk double reciprocal plot rearranges the Michaelis-Menten equation as:

$$\frac{1}{v} = \frac{1}{V_{max}} + \frac{K_m}{V_{max}} \cdot \frac{1}{[S]}$$

(1.2)

However, this double reciprocal plot is prone to errors inherent in all inverse plots. Moreover often most points on the plot are found far to the right of the y-axis where the concentration of the substrate is lower. These are the points at which the precision of determining the rate of reaction is lowest, because the smallest amount of product has been formed. Alternatively, the Eadie-Hofstee plot (Eq. 1.3) can be used for the linear regression plot. This plot reduces the error of the undue weight given to points at low substrate concentration. Nevertheless, both axes of the plot use dependent variables, which increase the errors in estimating the kinetics value.

$$\frac{[S]}{v} = \frac{[S]}{V_{max}} + \frac{K_m}{V_{max}}$$

(1.3)

1.5   Immobilised Enzyme Microreactors (IEMRs)

1.5.1   Overview of Enzyme Immobilisation

The integration of an immobilised biocatalyst in a microreactor expands the application of this system especially in the production of many biotechnological products with applications in biosensor, diagnostics and therapeutics (Guilbault et al., 1991; Lombardi & Dittrich, 2010; Yeo et al., 2011). The main feature of the enzyme immobilisation is the ability to reuse the enzyme, separation from the solvent system and extensive use over a longer period of time (Tischer & Kasche, 1999; Pollard & Woodley, 2007). The biocatalyst can be immobilised either using the isolated enzymes or the whole cells. Moreover, it can be coenzyme dependent or coenzyme independent. For coenzyme dependent, employment of whole cells is more desirable. This approach enables the cell to regenerate the cofactor internally so that no external addition is necessary (Stewart, 2001). Despite of the efficient way for the cofactor regeneration *in situ*, whole cells are not able to tolerate high substrate or product concentration (>1g/L), restricted use with organic solvents and generation of unwanted side products (multiple enzyme reaction) are other issues to consider (Pollard & Woodley, 2007).

In spite of the advantages that enzyme immobilisation brings, experimental investigations have revealed unfavorable results, such as significant reduction in enzyme activity compared with soluble enzymes (Mao et al., 2002; Gleason & Carbeck, 2004; Delouise & Miller, 2005; Kerby et al., 2006). They suggested that the loss of activity of the immobilised enzyme might due to the mass transfer effect, altered conformation of enzyme and steric hindrance. However, improved stability under working conditions and the reusability factor can compensate for such drawbacks, resulting in an overall benefit.

Several changes can be made in practice to mitigate the problems present in enzyme immobilisation. Mass transfer effect can be reduced by decreasing the particle size of the carriers (<100 μm), reducing the enzyme loading for enzymes with high specific activity and opting for preferential binding at the outer shell of carrier

materials (Tischer & Kasche, 1999). Spacer molecule can be introduced to the larger proteins to improve steric accessibility to the active sites (Nouaimi et al., 2001).

While the cost of enzyme is rather high, the implementation of immobilised enzyme can reduce the operational costs. With the possibility of the enzyme to be reused and separation from the solvent system, the cost saving can only be achieved by the repeated or prolonged use of the immobilised enzyme (Figure 1.4).
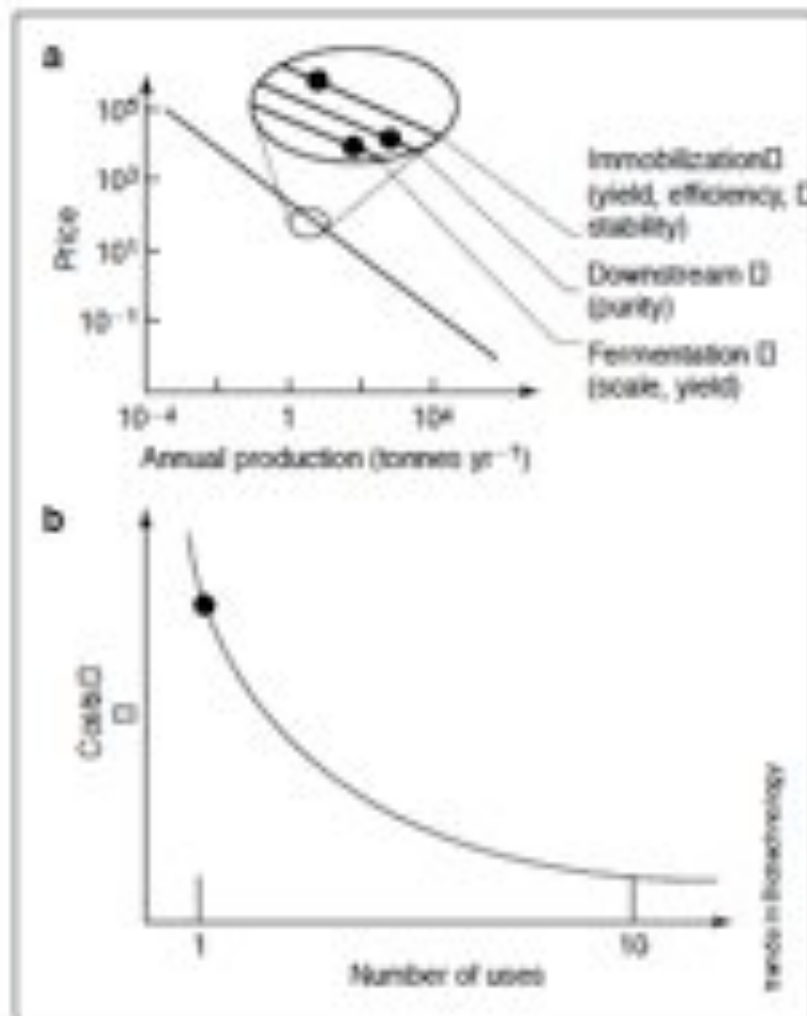
Figure 1.4: Manufacturing cost for immobilised enzymes (price per gram enzyme) are reduced as their annual production increases, roughly along a straight line when plotted on a logarithmic scale. Image reproduced from (Tischer & Kasche, 1999).

1.5.2 Choice of supports

The characteristics of the matrix are of paramount importance in determining the performance of the immobilised enzyme system. The ideal matrix for the immobilisation process should have the following characteristics: (i) large surface area, (ii) permeability, (iii) hydrophilic character, (iv) insolubility, (v) chemical, mechanical and thermal stability, (iv) high rigidity, (vii) chemical reactivity for coupling of the ligands, and (viii) resistance to microbial and enzymatic attack (Krenková & Foret, 2004). There are many types of supports available commercially that can be classified as organic and inorganic according to their chemical composition (Table 1.1)

Table 1.1: Classification of supports

Organic

Natural polymers

- Polysaccharides: cellulose, dextrans, agar, agarose, chitin, alginate

- Proteins: collagen, albumin

- Carbon

Synthetic polymers

- Polystrene

- Other polymers: polyacrylate, polymethylacrylates, polyacrylamide, polyamides, vinyl and allyl-polymers

Inorganic

Natural minerals: bentonite, silica

Processed materials: glass (nonporous and controlled pore), metals, controlled pore metal oxides

1.5.3 Methods of Immobilisation

Several methods are available for enzyme immobilisation. Miyazaki & Maeda (2006) have summarized typical techniques for preparation of immobilised enzyme microreactor (IEMR) as shown in Table 1.2. These techniques include particle entrapment, surface modification and membranes using various types of media. Advantages of IEMR are discussed in the next section.

Table 1.2: Typical techniques for preparation of immobilised enzyme microreactor

Technique	Media	Immobilisation method	Immobilised enzyme	Reference
Particle Entrapment	Glass	Cross-linking (3-aminopropylsilane glutaraldehyde)	Xanthine oxidase	(Richter et al., 2002)
			Horseradish peroxidase	
	Polystylene	Biotin-Avidin (avidin- coated beads were used)	Horseradish peroxidase	(Seong & Crooks, 2002)
	Agarose	Complex formation (Ni-NTA and His tag)	Bacterial P450	(Srinivasan et al., 2004)
	Magnetic beads	Cross-linking (3-aminopropylsilane glutaraldehyde)	Glucose oxidase	(Nomura et al., 2004)
	Polymer monolith	Entrapment (2-vinyl-4-4-dimethylazlactone, ethylene dimethacrylate, 2-hydroxyethyl methaacrylate, acrylamide)	Trypsin	(Sakai-Kato et al., 2004)
	Silica monolith	Entrapment within porous silica	Trypsin	(Sakai-Kato et al., 2003)
			Protease P	(Kawakami et al., 2004)
	Aluminium oxide	Cross-linking (3-aminopropylsilane glutaraldehyde)	Horseradish peroxidase	(Heule et al., 2003)
Surface Modification	SiO_2 surface	Physical adsorption of biotinylated polylysine/biotin avidin	Alkaline phosphatase	(Gleason & Carbeck, 2004)
	PDMS (O_2 plasma treated)	Physical adsorption of lipid bilayer/biotin avidin	Alkaline phosphatase	(Mao et al., 2002)
	PDMS	Physical adsorption of fibrinogen/photochemical reaction of fluorescein-biotin	Alkaline phosphatase	(Holden et al., 2004)
	Silicon	Cross-linking (3-aminopropylsilane	Trypsin	(Ekström et al.,

		glutaraldehyde)		2000)
	Fused silica (sol-gel modified)	Cross-linking (3-aminopropylsilane succinate)	Cucumisin	(Miyazaki et al., 2003)
			Lipase	(Miyazaki et al., 2004)
			L-lactic dehydrogenase	(Miyazaki et al., 2005)
	PMMA-modified with butyl methacrylate and/γmethyl acryloy propyltrimet hoysilicane	Cross-linking (Si-O bond between modified surface and silica monolyth)	Trypsin	(Qu et al., 2004)
	PDMS (O$_2$ plasma treated)	Cross-linking (Si-O or Si-O-Al bond between titaniaor alumina monolyth)	Trypsin	(Wu et al., 2004)
	Fused silica	Cross-linking between physically immobilised silica particle (3-aminopropylsilane/succinate)	Lipase	(Nakamura, 2004)
	PDMS	Entrapment within hydrogel formed on the surface	Alkaline phosphotase	(Koh & Pishko, 2005)
			Urease	
Membrane	PDMS/Glass	Place PVDF membrane which adsorb enzymes	Trypsin	(Gao et al., 2001)
	Glass	Covalent cross-linking with Nylon membrane formed at liquid-liquid interface (glutaraldehyde)	Horseradish peroxidase	(Hisamoto et al., 2003)
	PTFE	Enzyme-embedded membrane formation using glutaraldehyde/paraformaldehyde	Chimotrypsin	(Honda et al., 2005)
			Trypsin	

1.5.4   Characteristic Features of IEMRs

1.5.4.1 Enhanced Stability of the enzyme

Generally enzymes in solution are not stable for extended time and lose their activity during storage. However, immobilisation of enzymes can overcome these problems by facilitating their application under harsh environmental conditions of temperature, pH and organic solvents (Sakai-Kato et al., 2002; Nomura et al., 2004). Immobilised enzymes also reduce the risk of autolysis and can be recycled (Fernandes, 2010). Sakai-Kato et al. (2002) immobilised trypsin via encapsulation by sol-gel method, which was conducted under mild conditions. This technique is required to maintain the enzyme catalytic activity and the encapsulated trypsin displayed increased stability during prolonged use compared to that in free solution.

In the work described by Srinivasan et al. (2004), nickel-nitrilotriacetic (Ni-NTA) agarose beads were used to immobilised PikC hydroxylase into a microfluidic biochip. The high enzyme loading enabled the rapid hydroxylation of the macrolide YC-17 to methymycin and neomethymycin in about equal amounts with a conversion of >90% at a flow rate of 70 nL/min. Nevertheless, stability of the enzyme was enhanced which enables the half-life of the enzyme to be extended from 3 hours in free solution to 9 hours in the immobilised form.

Magnetic microbeads were also used in a microreactor where it can be readily injected into the flow analysis, and the retention takes place within the flow line by a small permanent magnet located near the detector (Nomura et al., 2004). The immobilised enzymes were shown to be stable and active for more than 8 months when stored at 10°C. Utilization of silica-based particles has been recognized to be highly effective as the scaffold for enzyme immobilisation. As reported by Berne et al. (2006), polyethyleneimine (PEI)-mediated silica encapsulation showed improvement in mechanical properties of the immobilised enzyme and excellent operational stability. More than 90% conversion of nitrobenzene was observed during continuous use for more than 3 days at room temperature and a flow rate of 5

μL/min.

1.5.4.2 Improved Reaction Efficiency

One of the main applications of IEMR is the protein digestion for peptide mapping. This process consumes immense time with manual sampling system and extended proteolytic digestion. Efficient protein or peptide digestion can be carried out through enzymes immobilisation. The feature of this method permits high concentration of enzymes to be immobilised onto the surface and finally results in rapid catalytic turnover. Ekström et al. (2000) described their work on immobilisation of protease enzymes on μ-chip IEMR by following the standard procedures for enzyme coupling to silica matrixes. Larger surface area was obtained by treating the silicon with anodization in an HF/ethanol solution, yielding a thin, porous surface layer on the channel walls. This resulted in significant increase in the speed of the digested protein, which was 200-1000 faster than in solution digestion. Furthermore, the immobilised protease prevents autolytic interferences from the proteolytic enzyme in the mass spectra.

In the work by Miyazaki et al. (2005), His-tagged dehydrogenase enzyme was immobilised onto a microchannel surface through Ni-complex. High concentration of immobilised enzymes were achieved as a result of multilayer binding of the enzymes on the surface and higher performance of the microreactor was reported compared to free enzyme reaction. A layer-by layer self-assembly technique onto silicon was introduced by Jones et al. (2004) where urease enzyme was incorporated into microchannels of a polymeric matrix of polydimethylsiloxane (PDMS). The multilayers comprise of polydimethyldiallyl ammonium chloride (PDDA) and polystyrene sulfonate (PSS) to which urease enzyme was attached. This method displayed greater stability of the enzyme than those entrapped in PDMS and obtained high conversion of urea with a proportional increase in residence time and enzyme loading.

1.5.4.3 Utilisation of Crude Enzyme

Generally, high purity of enzyme is used for the immobilisation of biocatalyst to ensure high-throughput analysis. However, researchers have to bear the cost incurred for the purification of the enzymes. Miyazaki et al. (2005) incorporated crude cell extracts for the immobilisation of enzyme. Supernatant of cell lysate of BL21 (DE3) cells expressing L-lactic dehydrogenase was immobilised in the same way as performed for the purified sample. The same amount of protein was immobilised and the performance of the microreactor indicated the same results as the purified protein. This technique may create a new route for simplification of protein purification whereby enabling integration of purification and immobilisation of enzymes in one step.

1.5.5   Enzyme Immobilisation Through His-Tag

Perhaps the most general approach for the immobilisation of oriented protein molecules is the use of recombinant tags, particularly poly histidine (His-tag). This technique is stemmed from immobilised metal ion affinity chromatography (IMAC) and has been applied extensively to protein immobilisation (Block et al., 2009; Cheung et al., 2012). In this method, a chelate group (iminodiaacetic acid (IDA) or nitrolotriacetic acid (NTA)) is attached to a solid support which then can bind strongly to a metal ion such as Ni^{2+} or Cu^{2+} via three or four binding sites, leaving three or two vacant sites for coordination to imidazole group of polyhistidine units on the tagged protein molecule. Complex formation between Ni-NTA and His-tag renders stability for the immobilisation and the interaction can be easily uncoupled through incorporation of imidazole or EDTA.

With the advent of recombinant protein technology, the incorporation of His-tag to either C-terminus or N-terminus to the target protein becomes feasible. Roche obtained patents on the use of nitrilotriacetic acid (NTA) as a ligand for immobilizing metals in affinity chromatography and for the incorporation of histidine affinity tags into recombinant proteins, whilst QIAGEN is the distributor for the expression vectors, Ni-NTA purification matrices, and the EasyXpress Protein Synthesis system. This elegant technique offers fast and specific binding

and allows protein immobilisation without pre-purification steps. Moreover, the His-tag does not usually interfere with the structure or function of proteins and does not affect the secretion, compartmentalization, or folding of fusion proteins within cells (Cha et al., 2004). The tag also allows for purifying recombinant proteins in denaturing conditions because its mode of action is dependent only on the primary structure of proteins.

Application of the immobilisation of protein molecules via a His-tag has been successfully demonstrated. Site-specific immobilisation which orientates all proteins uniformly was performed by Abad et al. (2005), where His-tagged of horseradish peroxidase and ferredoxin- $NADP_+$ reductase, confirmed the full functional attachment of the protein to the NTA-Co(II)-platform. These functionalized nano particles thus represent an attractive ready-to-use tool for protein immobilisation on nanoparticles. Besides that, immobilisation of His-tagged *Rhodotorula gracilis* D-amino acid oxidase (*Rg*DAO) on Ni-NTA magnetic beads was demonstrated by Kuan et al. (2008). The immobilisation of *Rg*DAO enhanced its stability against thermal inactivation where the relative activity of the immobilised enzyme was 56% while the free enzyme was completely inactivated after incubation at 50°C for 1 h. The residual activity and the storage stability were also improved in the immobilised form of the enzyme. Cha et al. (2005) described that enzymes immobilised through poly His-tag exhibits similar activities as in the free solution as a result of highly specific orientation offered by the His-tag linkage.

1.5.6   Enzyme Immobilisation in Fused-Silica Microcapillary

Microcapillaries are originally used as analytical columns in gas chromatography (GC) analysis. A glass capillary was first used before it was replaced by a fused silica capillary in the early 1980s, which the application then has been extended in many other miniaturized analytical columns in various separation techniques. The fused-silica capillary is now widely available, relatively cheap and easy to handle. It also allows UV and fluorescence detection to be performed directly on the capillary. The fused-silica capillary is available in several different dimensions with internal diameter typically between 1 and 700 μm and outer diameter between 150 and 850

µm.

In order to take full advantage of the fused-silica capillary, and to extend the range of its application, it is necessary to treat the surface of the capillary to suit the application of interest. Miyazaki et al. (2003) developed a simple method to form a nanostructure suitable for catalyst immobilisation on a fused-silica capillary surface by a solution of 3-aminopropylsilane (Figure 1.5). They applied the sol–gel procedure, which has been utilized for porous structure preparation in batch systems. After treatment of the surface modification, the serine protease cucumicin was successfully immobilised as multilayers on the surface and the activity of the enzyme was demonstrated. This work was further studied (Miyazaki et al., 2004), where the cucumisin-immobilised microreactor showed high efficiency that enabled hydrolysis of substrate within 2 seconds. Moreover, the system was improved with a reversible immobilisation method that allowed denatured enzyme to be replaced. In addition, Amankwa & Kuhr (1992) demonstrated the immobilisation of trypsin via a biotin-avidin-biotin couple onto surface of a fused-silica capillary. The strong coupling method produces a highly stable and reusable catalytic active capillary. Matosevic et al. (2009) performed quantification of immobilised transketolase kinetics based on the reversible immobilisation of His_6-tagged enzymes via the Ni-NTA linkage to surface derivatised silica. The capillary derivatisation protocol was adopted from Miyazaki et al. (2005). The kinetics data obtained was comparable with reaction in free solution indicating that the microreactor is a powerful tool for enzyme kinetic parameter quantification.
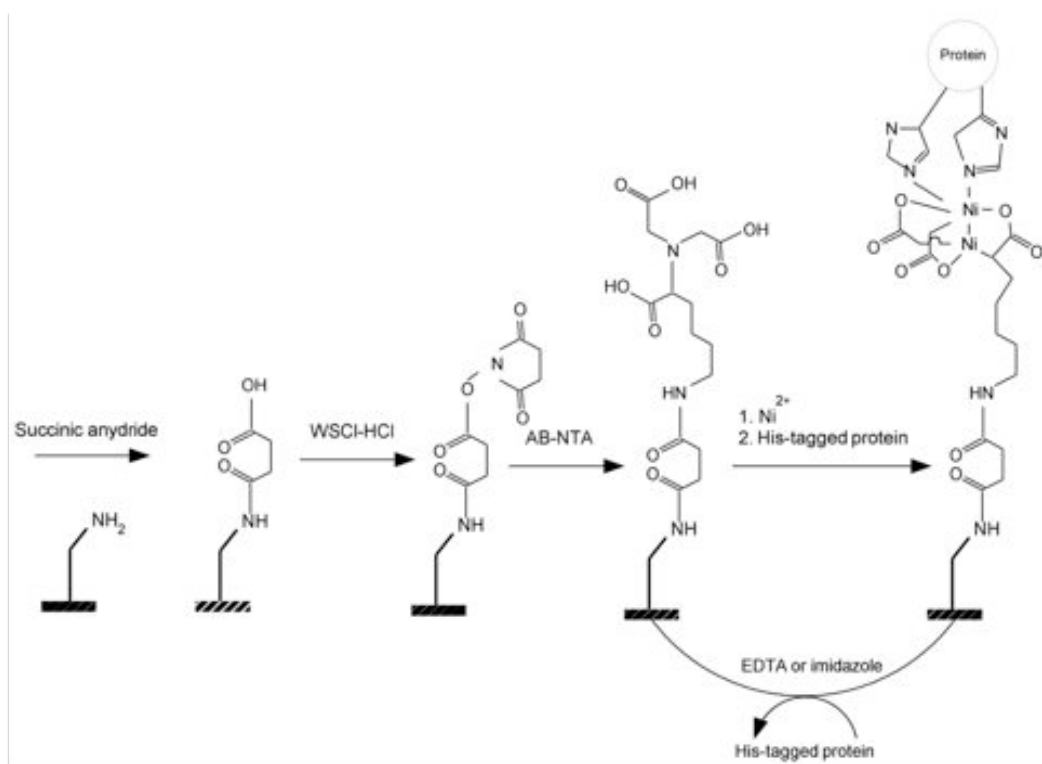
Figure 1.5: Surface modification process for reversible immobilisation of proteins. The fused silica surface was modified with a mixture of 3-aminopropyltriethoxysilane/methyltriethoxysilane prior to the above treatment. (Miyazaki et al., 2005)

1.6 Multi-Step Enzyme Reactions in Microreactors

1.6.1 Enzymes to be studied

1.6.1.1 Transketolase Enzyme and Reaction

Transketolase (TK) (EC 2.2.1.1) is an important enzyme that is responsible for the reversible transfer of a two-carbon ketol moiety from a ketose to an aldose in a key step of the pentose phosphate pathway (Meining et al., 2000; Chen et al., 2007). It does also catalyze a reaction in the Calvin cycle in photosynthesis process (Henkes et al., 2001). Transketolase can be isolated from many sources which include, yeast (Effenberger et al., 1992; Kobori et al., 1992) , spinach (Demuynck et al., 1991; Dalmas & Demuynck, 1993) and recombinant *Escherichia coli* strains (Hobbs et al., 1993; Sprenger et al., 1995). Over expressed TK in *E coli* can be optimised to

48

get higher level of TK expression up to 4 kg of enzyme from a 1000-L glycerol-fed fermentation (French & Ward, 1996) with TK represented around 35% of the intracellular protein expressed by the cell.

The functional form of the enzyme is homodimer with a subunit molecular weight of 74,200 Da, with both active sites having equal catalytic activity (Meining et al., 2000). Each monomer comprising a pyrophosphate (PP)-binding, pyridinium (Pyr)-binding, and C-terminal domain (Figure 1.6). For TK to become fully functional, it requires reconstitution of cofactors which are magnesium (II) ions and thiamine diphosphate (TPP) (Kochetov, 1982; Aucamp et al., 2008). TPP binds at the interface between the subunits and interacts with residues from both subunits and it is regenerated in each cycle of the reaction. The cofactor is noncovalently bound to the enzyme in the less energetically favorable but activated ''V'' conformation (Muller et al., 1993). The apoenzyme form of TK turns to completely functional form of holoenzyme with the binding of cofactors.
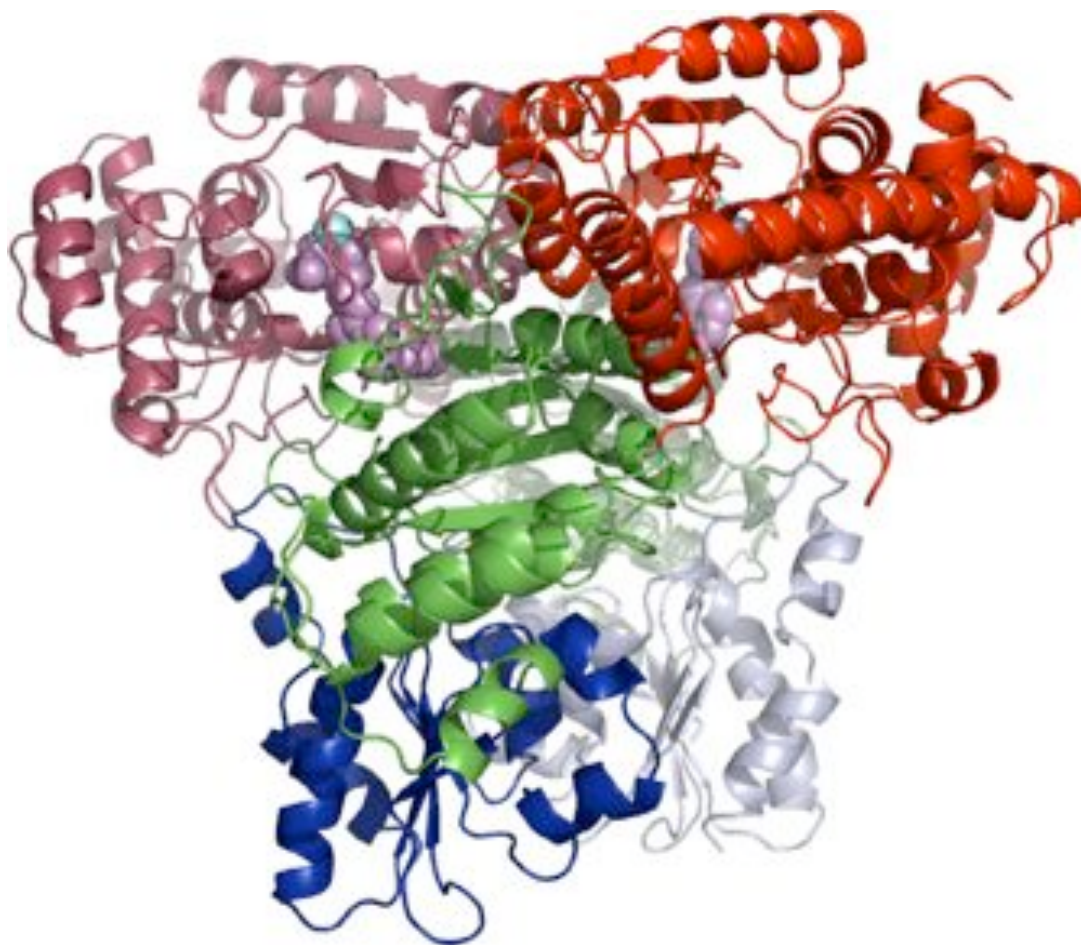
Figure 1.6: Structure of *E. coli* holo-transketolase (holo-TK). The homodimer is highlighted with chain A dark and chain B light, the domains coloured as PP (red), Pyr (green), and C-terminal (blue), the two TPP cofactors as violet spheres, and two Mg^{2+} ions as cyan spheres. Image reproduced from Jahromi et al., 2011.

The potential substrates for this enzyme are D-xylulose-5-phosphate, D-fructose -6-phosphate, D-sedoheptulose-7-phosphate and hydroxypyruvate (HPA) as donors of the transferred glycolaldehyde (GA) group (Sevostyanova et al., 2004). As acceptor substrates, it catalyses D-ribose-5-phosphate, D-glyceraldehyde-3-phosphate, D-erythrose-4-phosphate, and glycolaldehyde (Sevostyanova et al., 2004). *In vivo*, the reaction remains reversible, however with HPA as a ketol donor, the reaction renders irreversible, with the release of CO_2 and formation of a compound containing a new carbon-carbon bond and a chiral hydroxy group (French & Ward, 1996). Figure 1.7 shows the TK reaction catalysed the carbon-carbon bond formation using HPA and GA. Many works involving glycolaldehyde as the aldehyde acceptor were demonstrated which produces erythrulose and CO_2 with

HPA as the ketol donor (Lilly et al., 1996; Mitra et al., 1998). Moreover, the assay for this reaction can be easily carried out using HPLC (Mitra & Woodley, 1996) or a colorimetric assay (Smith et al., 2006) that allows for simple and rapid measurement and kinetic study of TK.
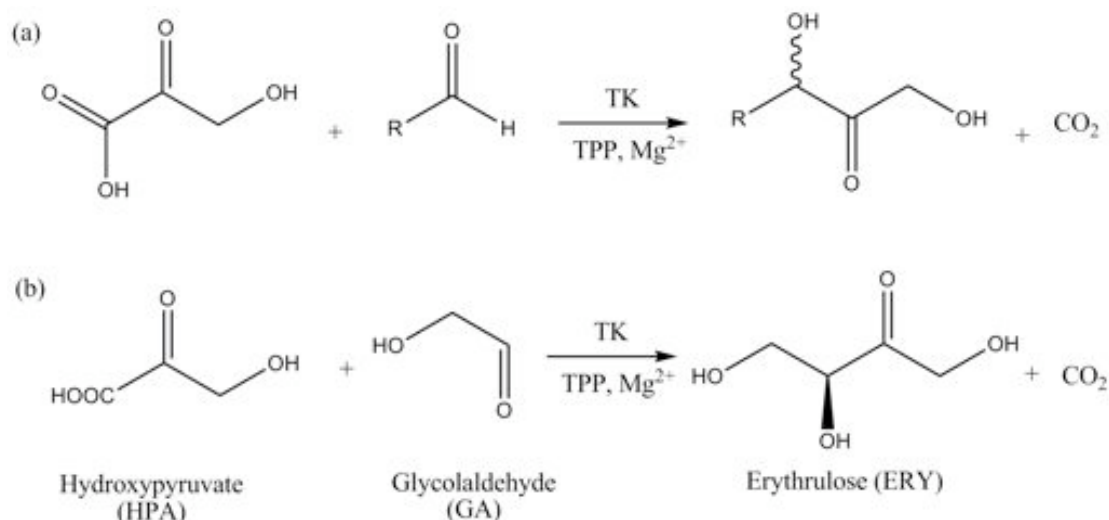
Figure 1.7: (a) General reaction scheme of TK mediated carbon–carbon bond formation using hydroxypyruvate as ketol donor, (b) Transketolase-mediated erythrulose (ERY) synthesis via-hydroxypyruvate (HPA) and glycolaldehyde (GA) reaction.

TK used in this study is originating from *E. coli*, whereby the TK coding gene has been engineered into high copy number plasmid pQR791 (Martinez-Torres et al., 2007) to increase expression and has been tagged with six histidine residues to facilitate rapid purification and facile immobilisation process. This enzyme has been extensively studied in both purified and lysate forms (Matosevic et al., 2009; Jahromi et al., 2011; Rios-Solis et al., 2011; Payongsri et al., 2012). In this work, the HPA and GA substrate model system was used. The optimum conditions and kinetic analysis for TK-catalysed reaction for the model system of HPA and GA was discussed in details by Matosevic et al. (2009) in batch reaction as well as in continuous flow reaction. TK was found to be relatively stable at ambient temperature and neutral pH. Moreover, TK kinetics parameters evaluated based on a Michaelis-Menten model, in the IEMR were shown to be comparable to those measured in free solution (Matosevic et al., 2009).

1.6.1.2 ω -Transaminase Enzyme and Reaction

Transaminase (TAm) (EC 2.6.1) falls under transferases group that catalyses a type of reaction between an amino acid and α-keto acid. This high stereoselectivity

52

enzyme converts a carbonyl group to an amino group to form chiral amino alcohols, but would need a broad specificity to accept substrates other than keto acids or ketones (Kaulmann et al., 2007). Figure 1.8 shows the general reaction catalyses the transfer of an amine and ketose substrate using pyridoxal-5'-phosphate (PLP) as the cofactor. Other enzymes that exhibit the same characteristics as TAm are acid dehydrogenases and amine dehydrogenases (Crump & Rozzell, 1992; Brunhuber & Blanchard, 1994). In contrast to the amino dehydrogenase reaction, TAm does not require cofactor recycling which makes it the perfect choice for industrial processes (Kaulmann et al., 2007).
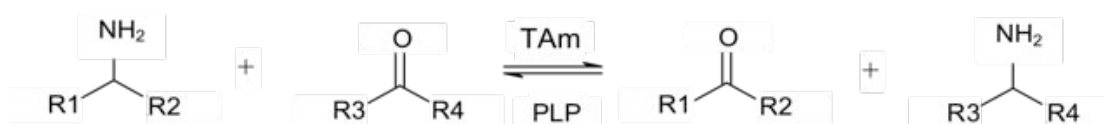
Figure 1.8: General scheme of transaminase catalysed reaction. TAm catalyses the transfer of an amine functionality between an amine and a ketose substrate in a reaction requiring a pyridoxal phosphate (PLP) cofactor.

Transaminases can be categorized into four subgroups based on their mutual primary structure, and also correspond to the specialization of the enzymes for substrate specificity within subgroups (Mehta et al., 1993). ω-TAms fall under group III as defined by Pfam while $\alpha-$TAms are classified under group I, II, IV and V (Punta et al., 2012). Distinct feature of ω-TAms as compared to $\alpha-$TAms is on the ability of ω-TAms to accept substrates that do not contain α-amino acid or α-keto acid, which is required for $\alpha-$TAms. The TAm used in this work was isolated from *Chromobacterium violaceum,* which was first reported by Kaulman et al. (2007). Apart from this, many other sources of ω -TAms from different microorganisms have been studied. Among them are *Klebsiella pneumoniae* JS2F, *Bacillus thuringiensis* JS64 and *Vibrio fluvialis* JS17 (Shin et al., 2003; Mishra et al., 2007). These strains showed high enantioselectivity (E>50) towards (S)-α-Methylbenzylamine (MBA) and catalyse the amination of keto acids, aldehyde and ketone (Shin & Kim, 2002). The studies concluded that among the three strains, *V.*

fluvialis JS17 displayed the best in kinetic resolution and asymmetric synthesis to produce enantiomerically pure chiral amines (Cho et al., 2003; Yun et al., 2005).

The CV-ωTAm is a homodimer with a molecular mass of ~100 kDa. Each monomer has an active site at the dimeric interface that involves amino acid residues from both subunits. The active site contains a PLP-binding pocket and a substrate-binding region. In the holo form, pyridoxal 5′-phosphate (PLP) is joined by a covalent Schiff base linkage to the ε-amino group of the catalytic lysine. The TAm enzymatic reaction can be described by a ping-pong bi-bi mechanism (Christen & Metzler, 1985) (Figure 1.9). In the first half-reaction, the donor binds to the enzyme, the PLP coenzyme is aminated to pyridoxamine 5′-phosphate (EPMP) and the respective keto product is released. The transamination cycle is completed by transferring the amino group from enzyme-bound (EPMP) to the acceptor and regenerates the co-factor (EPLP).
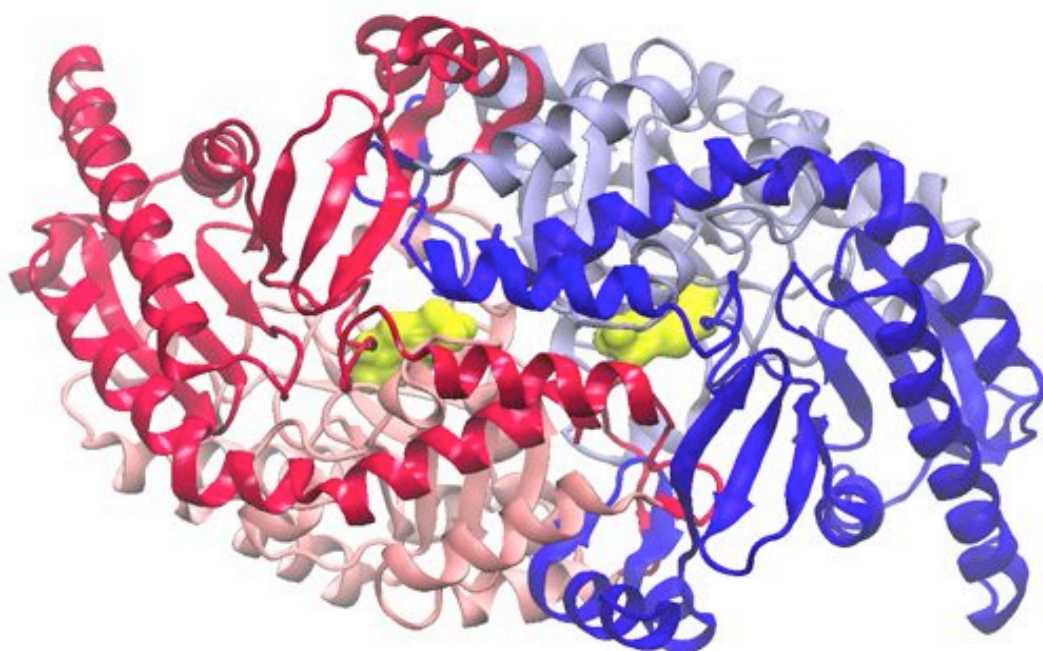
Figure 1.9: Structure of *C. violaceum* holo-ω-transaminase (dimer) The large domains are coloured light red and blue respectively, and the small domains are coloured dark red and blue respectively, PLP is shown as spheres.
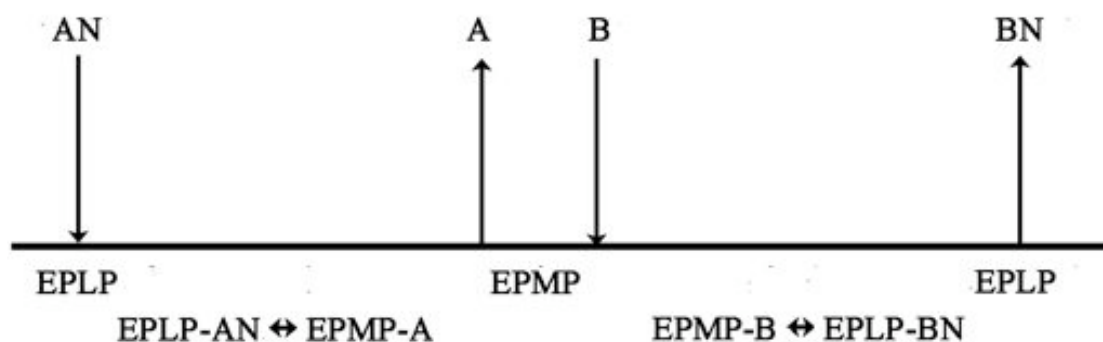
Figure 1.10: Schematic representation of the ping-pong bi-bi ordered reaction mechanism of ω - TAm.

Despite many advantages that ω-TAms can offer, the industrial use of these enzymes have been limited mainly due to the low equilibrium constants in the reactions (Shin & Kim, 2002). Moreover, severe substrate and product inhibition was also observed which further hampered the use of high concentration of amine substrate (Shin & Kim, 1999; Mishra et al., 2007).

The substrate spectrum with different amine donors and pyruvate was investigated with *C. violaceum,* TAm CV2025 (Kaulmann et al., 2007). CV2025 ω-TAm showed high activities towards aromatic (*S*)-amines such as MBA and (*S*)-aminoindane and the three most efficient amine donors were 1- aminoindane, 1-methyl-3-phenylpropylamine and benzylamine. The amination of pyruvate by MBA as the amino donor displayed high conversion reaction with almost complete conversion to acetophenone and alanine (Figure 1.10). Glyoxylate proved to be the best acceptor and aliphatic and aromatic aldehydes were both readily converted. This study also managed to demonstrate the amination of aromatic 2-keto-1,3-diols that was later quantified.
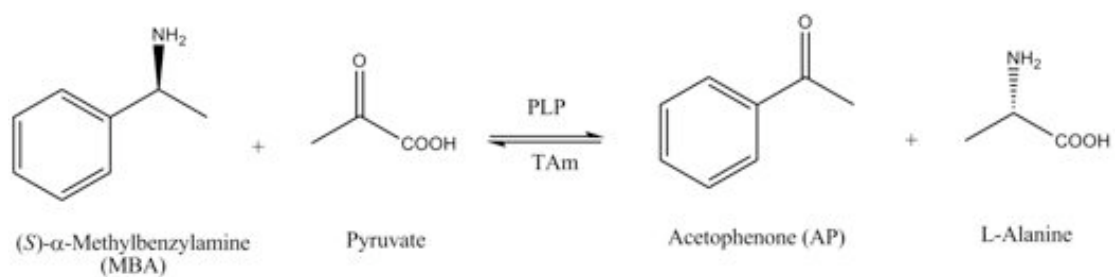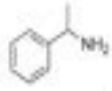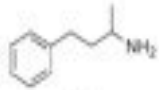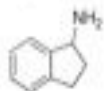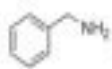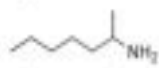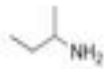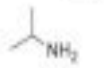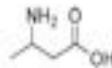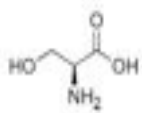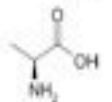
Figure 1.11: Reaction scheme of the transamination between (S)-α-Methylbenzylamine and pyruvate to synthesise acetophenone and L-Ala

Table 1.3: Specificity of CV2025 ω -TAm towards various amino donors. Table reproduced from (Kaulmann et al., 2007).

		Relative initial rates (%)	
		CV2025 TA[a]	V. fluvialis TA[b]
Amines			
(±)-α-Methylbenzylamine (MBA)		100(69.4)	100(112.0)
(±)-1-Methyl-3-phenylpropylamine		148.6	54.2 (61.4)
(±)-1-Aminoindane		183.0 (157.9)	156.5 (161.7)
Benzylamine		133.9	115.6
(±)-2-Aminoheptane		19.4	42.9
(±)-2-Amino-6-methylheptane		35.2	24.4
(±)-sec-Butylamine		<4[c]	6.8
Isopropylamine		<4[c]	3.6
Amino acids and derivatives			
(±)-3-Aminobutyric acid		4.7	7.0
γ-Aminobutyric acid		7.2	<1
6-Aminohexanoic acid		10.3	<1
L-α-Ser		9.0	6.4
L-α-Ala[d]		165.0	10.0
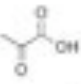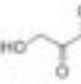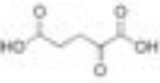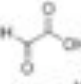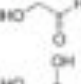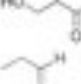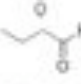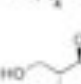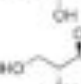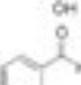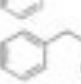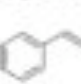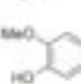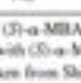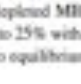
[a] Reaction conditions: 10 mM pyruvate and either 20 mM racemic donor, 10 mM enantiomer or 10 mM achiral donor, 0.4-0.8 U/ml CV2025 TA, 37 °C, pH 7.0. Values in parentheses represent relative reactivities of 10 mM (S)-enantiomers in comparison to the respective 20 mM racemic mixtures. For arylic donors, initial rates were determined from donor depletion, for aliphatic donors from pyruvate depletion.

[b] Relative initial rates determined by Shin and Kim [26]. Note that initial rates have been determined with half the substrate concentrations and from 10 min reactions.

[c] The detection limit for pyruvate depletion was ca. 4%. Other tested substrates with relative reactivities of less than 4% were: 2-aminoisobutyric acid, β-Ala, taurine, L-α-Asp, (±)-3-amino-1,2-propanediol; of less than 4% (detection limit for arylic amino donor depletion): (R)-α-MBA, L-α-Phe, (±)-3-amino-3-phenyl propionic acid, anthranilic acid, (1S,2S)-APP, (1R,2R)-APP. L-α-Ala was not tested with pyruvate as the acceptor.

[d] The reactivity of L-α-Ala was measured by using glyoxylate as an amino acceptor and compared with that of (S)-α-MBA with glyoxylate. For comparison: the relative initial rate for the L-α-Ala/glyoxylate reaction with V. fluvialis TA as determined by Shin et al. [19].

Table 1.4: Specificity of CV2025 ω-TAm towards ketoacids and aldehyde acceptors. Table reproduced from (Kaulmann et al., 2007).

		CV2025 TA[a]		V. fluvialis TA[b]
		Conversion at equilibrium (%)[c]	Relative initial rate (%)	Relative initial rate (%)
Keto acids				
Pyruvate		95–100	100	100
HPR		65	144.1	29.2
α-Ketoglutarate		<5	<5	0.3
Aldehydes				
Glyoxylate		95–100	176.2	60.2
Glycolaldehyde		47–57	106.6	n.d.
(±)-Glyceraldehyde		40	116.1	n.d.
Propanal		60–70	132.3	36.4
Butanal		74–78	122.9	113.5
Hexanal		8–14	81.3	106.2
Nonanal		8–10	78.2	0.9
D-Erythrose		14–22	60.6	n.d.
D-Fructose		n.d.	<5	n.d.
Benzaldehyde		90	91.2	72.8
Phenylacetaldehyde		68	107.0	68.5
(E)-Cinnamaldehyde		>60[d]	79.7	31.5
Vanillin		>60[d]	61.7	n.d.

[a] Reaction conditions: 10 mM (S)-α-MBA, 10 mM acceptor, 0.4–0.8 U/ml CV2025 TA, 37 °C, pH 7.0. Initial rates were calculated from MBA depletion in 3 min and related to the rate obtained with (S)-α-MBA/pyruvate. The detection limit was 5%.
[b] Relative initial rates were taken from Shin and Kim [26].
[c] Based on concentration of depleted MBA. Data were obtained from three independent experiments and generally varied by no more than 6% from the mean (exception: data variation of up to 25% with nonanal). The reactions were monitored until equilibrium was reached (mostly after 2–3 h).
[d] The reactions were not run to equilibrium.

Further study on substrate specificity was carried out by Ingram et al. (2007) using β−alanine: pyruvate transaminase (β-A:P TAm) from *Pseudomonas aeruginosa* PAO1. In this work, (S)-α-MBA and erythrulose was used to produce acetophenone (AP) and the chiral amino alcohol, 2-amino-1,3,4-butanetriol (ABT) (Figure 1.11). They demonstrated a *de novo* TK-TAm pathway where L−erythrulose, product of the TK−catalysed reaction was aminated by β-A:P TAm producing 2-amino-1,3,4-butanetriol (ABT) from achiral substrates glycolaldehyde (GA) and β-hydroxypyruvate (HPA) (Figure 1.12). This novel synthetic pathway offers new directions for multi-step enzymatic synthesis of complex molecules. The resulting product from this pathway contains both a chiral aldehyde group and a chiral amine group making an excellent industrial synthon (Section 1.6.2).
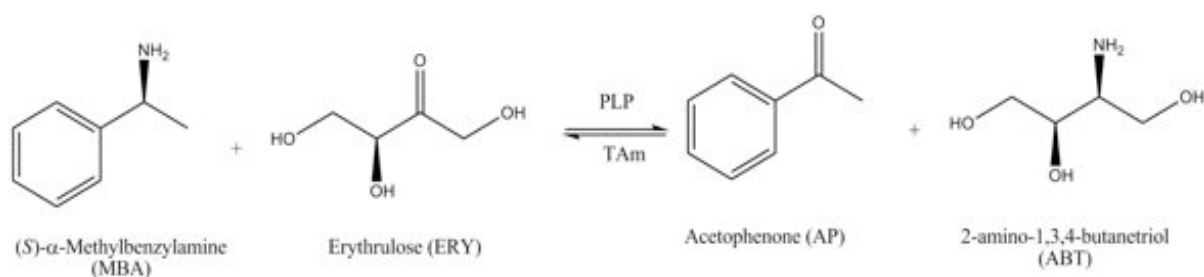
Figure 1.12: Reaction scheme of the transamination between (S)-α-methylbenzylamine and erythrulose to synthesise acetophenone and 2-amino-1,3,4-butanetriol (ABT).
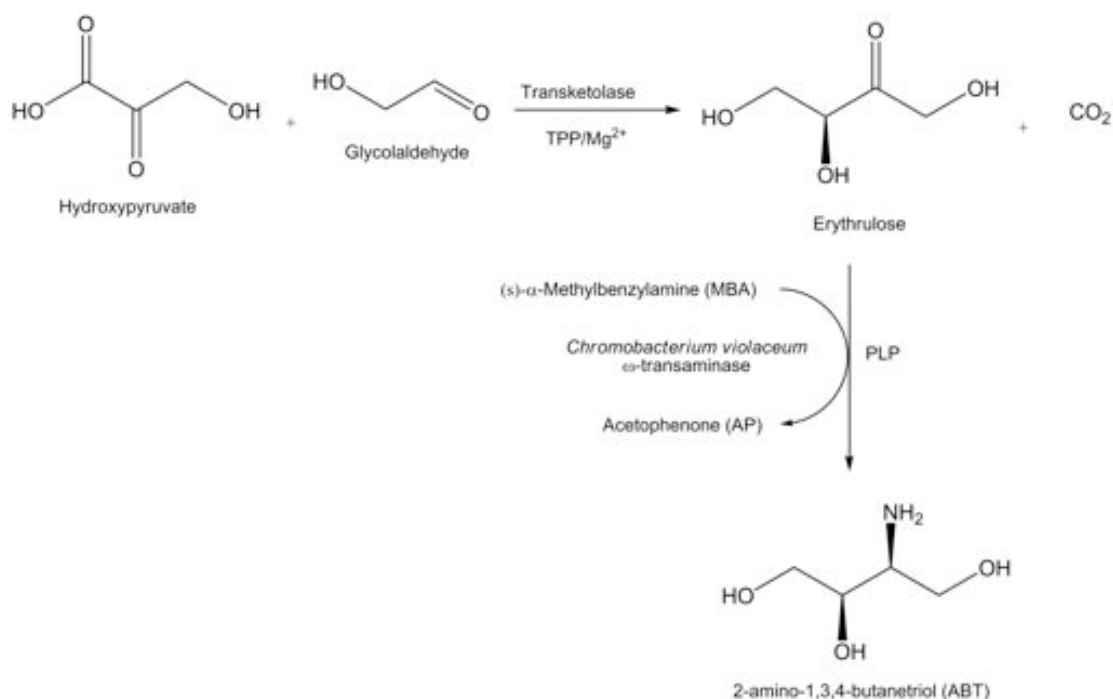
Figure 1.13: The synthesis of chiral amino alcohol 2−amino1,3,4−butanetriol from achiral substrates glycolaldehyde and hydroxypyruvate using a TK−TAm pathway.

1.6.2 Aminodiol synthesis

Chiral aminodiols play significant roles in production of many pharmaceutical products. These molecules are important synthons for the production of a wide range of chiral chemicals. Moreover, the increasing size and complexity of these molecules frequently results in multiple chiral centers that can be exploited for extensive use in many complex chemicals syntheses.

Wang et al. (1995) synthesised an aminodiol that act as HIV protease inhibitor. Optically pure aminodiols are also used as chiral ligands for asymmetric syntheses such as in the enantioselective addition of diethylzinc to aromatic aldehydes (Szakonyi, 2008) and as an intermediate compound in the synthesis of detoxinine, an agent used to reduce the toxicity of an antibiotic treatment for rice blast disease (Monache et al., 1999). Moreover, chiral aminodiols are also opted as the starting materials for the syntheses of oxazines or oxazolidines, which are compounds that exert potent antibacterial properties (Mishra et al., 2007).

1.6.3 De-novo pathway engineering

The rapid growth of the pharmaceutical industry requires more sophisticated, facile, and uncomplicated ways of synthesising complex compounds with high optical purity that are superior compared to the conventional chemical synthesis. Academic researchers and industry have shown great interest in the idea of *de novo* pathway engineering as one of the alternative to improve efficiency and productivity in pharmaceutical syntheses. *De novo* pathway engineering through integration of multi-step enzyme reactions provides an attractive alternative for the creation of molecules with increased complexity and has been complemented by recent progress in performing enzymatic reactions on chips using IEMRs. There were several studies conducted where various enzymes have been immobilised within microchannels. Worth noting here that, the main target of multienzyme reaction is the ability to perform *in vitro* metabolic pathway manipulation for high-throughput biotransformations. To attain this goal, multiple enzymes that function in series must be functional on the microfluidic chip, wherein the product of one reaction acts as the substrate for the subsequent reaction and so forth.

Babich and co-workers (2012) demonstrated the synthesis of a complex chiral carbohydrate analogue in a three-step cascade reaction consisted of immobilised acid phosphatase, fructose-1,6-diphosphatase aldolase and acid phosphatase in a packed bed system reactor. This flow system was able to synthesise a yield of 0.6 g of D-fagomine precursor product. Moreover, a seven continuous flow enzymatic reaction was established by Liu et al. (2002) to produce uridine diphosphate galactose (UDP-galactose). All of the enzymes were immobilised individually on Ni-NTA agarose bead, which was packed into a column. The synthesis was performed in three main pathways, i) main pathway to form UDP-galactose from galactose, ii) the uridine triphosphate supply pathway and, iii) the adenosine triphosphate (ATP) regeneration pathway. The authors achieved 50% conversion of UMP into UDP-galactose in 48 hours and the stability of the immobilised enzyme was also improved compared to the enzyme in solution.

Multiple reactions in one pot mode are also an attractive option in organic synthesis. This mode of operation is usually associated with the benefits of improved yield, enhanced reaction rates, the ability to shift reaction equilibria, overcoming of inhibition effect and solubility problems (Ricca et al., 2011). This method is well exploited in the case of compounds with similar structures, conversion and selectivity >99% are desired in industry because product separation can heavily affect the overall costs (Goldberg et al., 2006). Several successful studies were reported that utilized the one-pot reactions. For example, pure D-xylulose-5-phosphate was prepared in gram quantities (>82% overall yield) by the multi-enzymatic one pot procedure (Zimmermann et al., 1999). Schoevaart et al. (2000) demonstrated a four-step enzymatic reaction for the one-pot synthesis of non-natural carbohydrates from glycerol. The production of N-acetyl-D-neuraminic acid (Neu5Ac) was conducted by Tao et al. (2011). This important pharmaceutical compound was synthesised by utilizing a robust engineered whole-cell catalyst, which was integrated in the process for the one-pot synthesis of Neu5Ac in a safe and economic manner. On the other hand, the one-pot mode poses some disadvantages that include non-agreeable optimal conditions among the multiple reactions, the presence of side reactions and enzyme inhibition (Ricca et al., 2011). The optimal conditions for the one-pot system however can be predicted by conducting a mathematical modeling (Chen et al., 2006).

A chemoenzymatic microfluidic reactor was developed by Luckarift et al. (2007) that merged a single chemical reaction with a multi-step enzymes reaction. Individual microfluidic chips containing metallic zinc, silica-immobilised hydroxylaminobenzene (HAB) mutase and silica-immobilised soybean peroxidase (SBP) were connected in series to produce 2-aminophenoxazin-3-one (APO), an intermediate in the synthesis of anti-fungal compound known as antinomycins. In the first step, nitrobenzene was reduced by immobilised metallic zinc to HAB, subsequently HAB was converted into 2-aminopenol (2-AP) by HAB mutase that was also immobilised in the microchannel. The final stage involved immobilised SBP, which catalysed the conversion of 2-AP to 2-aminophenoxazin-3-one (APO). However, the results showed a decrease in efficiency that was down to 19% of the overall conversion compared to 52% conversion with only HAB and SBP catalysed

reactions. This percentage however could be improved by optimizing the zinc conversion step.

1.7 Aim and Objectives of the Project

Microreactor technology has immense potential to notably improve chemical and biological analyses as well as abundant applications in medical diagnostics and therapeutic devices. Owing to their miniature size, they require only a small volume of reagent, shorter processing time and can be parallelized using lab-on-a-chip technology (Hong et al., 2009; Mark et al., 2010) Moreover, the integration of immobilised enzymes in microreactor systems has great impact in many emerging technologies employing biocatalytic and biorecognition events. Several reports show that a microreactor can be an ideal platform for enzyme reactions (Hickey et al., 2007, 2009; Ngamsom et al., 2010; Alam et al., 2011; Matsuura et al., 2011). Rapid screening can be done with the capacity of multiple usage of the immobilised enzyme (Forsberg et al., 2004; Matosevic et al., 2011). In addition to that, enzymes are found to gain higher stability facilitating their application under harsh environmental conditions of temperature, pH and organic solvents (Sakai-Kato et al., 2002; Nomura et al., 2004; Berne et al., 2006) .

There are many applications of IEMRs available for biocatalysis reported to date (Section 1.5). Different types of technique and method for enzyme immobilisation were introduced (Table 1.2). A variety of methods of the immobilisation of protein have been demonstrated, such as non-specific physical adsorption of trypsin on N-vinyl-2-pyrrolidinone matrix (Jiang et al., 2012), affinity-based adsorption of alkaline phosphotase immobilised in a microchannel (Mao et al., 2002), covalent attachment of ribonuclease A to macroporous methacrylate-based monolith supports (Ponomareva et al., 2012) and hydrophobic adsorption of monoamine oxidase (MAO) on an immobilised artificial membrane (IAM) liquid chromatographic stationary phase (Markoglou et al., 2004). Most of these types of immobilisation were found to affect the intrinsic properties of the enzyme, which in turn altered the catalytic activity. The catalytic modification may be caused by the changes in the three-dimensional conformation of the protein especially if the functional groups of the enzyme involved in the binding linkage to the support (Krenková & Foret, 2004). This non-orientated immobilisation may impose a critical effect on the enzymatic activity and therefore would compromise the observed kinetic

performance of these systems (Kerby et al., 2006).

In contrast to more complex attachment chemistries, reversible immobilisation of oriented protein molecules through affinity interactions, His_6-tag is considered simpler and highly selective. This elegant technique offers fast and specific binding and allows protein immobilisation without pre-purification steps. Moreover, the His_6-tag does not interfere with the structure or function of proteins and does not affect the secretion, compartmentalization, or folding of fusion proteins within cells (Cha et al., 2004). The use of His_6-tag for the applications of IEMR has been widely demonstrated to study the kinetics performance of enzyme systems. However, only a few studies were conducted that used fused silica capillary and Ni-NTA beads as the solid support. These studies also lacked a thorough quantification in kinetic studies and the enzymatic behavior inside the IEMR needs further consideration. Ultimately, different enzymes combinations could be incorporated in the IEMR to synthesise optically pure compounds.

The aim of this project is to design and characterise a novel microscale reactor based on the reversible immobilisation of His_6-tagged enzymes. The versatility of the immobilisation method makes the system amenable to a wide range of biocatalysts to be integrated in order to create a variety of synthetic pathways for rapid synthesis and screening purposes.

The specific objectives are:

- Chapter 3: To gather baseline data of enzymatic activity in a batch solution. In this chapter, two enzymes, i.e. transketolase and transaminase will be first characterised by looking at several parameters, which include storage stability, effect of different co-factor concentration and kinetic parameters. Additionally, preparation and purification of the enzyme catalyst in pure form will be studied with respect to its activity and compared to the crude form. The validated data from the batch solution reactions will be used for further investigation of enzymatic activity in IEMR.

- Chapter 4: To design and construct a reversible immobilised enzyme microreactor (IEMR). In the first part of the chapter, two types of solid support will be investigated for the construction of the IEMR, which are the functionalised microbeads and derivatised surface silica capillary. The feasibility of both methods will be compared and one method will be chosen for further study of the IEMR. The IEMR will be further characterised based on the operational enzymatic activity, storage and reusability for both enzymes. Besides that, an online UV detection system using the Actipix instrument will be incorporated with the IEMR and this system will be tested on one of the enzyme model system as a proof of concept.

- Chapter 5: Having established the IEMR prototype with known enzymatic conversions, the IEMR will be used for the kinetic evaluation of the transketolase (TK)-catalysed production of L-erythrulose (ERY) from hydroxypyruvate (HPA) and glycolaldehdye (GA) as substrates, and the second enzyme ω-transaminase (TAm)-catalysed reaction between S-methylbenzylamine (MBA) and ERY to produce 2-amino-1,3,4-butanetriol (ABT) and acetophenone (AP). This chapter will investigate the kinetic performance of both enzymes in continuous flow reaction using Lilly-Hornby (Lilly et al. 1966) kinetics model.

- Chapter 6: This final results chapter will demonstrate the versatility of the IEMR in the multistep enzymatic reaction to synthesise a complex chiral aminodiol. In this chapter two model systems will be studied. The first one is a two-step TK-TAm catalysed reaction and the second one is a three-step TAm-TK-TAm catalysed reaction. Single IEMRs will be arranged in series whereby the product of the first reaction will be the substrate of the subsequent step. Furthermore, the best matching enzyme combinations will be identified allowing high conversion for production of the chiral aminodiol. Actipix online detection will be also integrated into the three-step enzymatic system to enable direct quantification of the bioconversions. This *in vitro* study of the multi-step enzymatic reaction will provide insight into the

behaviour of *de novo* engineered pathway prior to cloning them into engineered whole cell biocatalysts.

- Chapter 7: This chapter will give a summary of the main findings and conclusions of the study as well as suggestions for future work.

2 Materials and Methods

2.1 Reagents and chemicals

All reagents were of analytical grade and were obtained from Sigma-Aldrich (Gillingham, UK) unless stated otherwise. Reverse osmosis (RO) water was used in all of the experiments.

2.2 Biocatalyst production

2.2.1 Enzyme production

Stocks of *E.coli* BL21gold (DE3) containing plasmid pQR791 (His$_6$-TK) (Martinez-Torres et al., 2007) or pQR801 (His$_6$-TAm) (Kaulmann et al., 2007) (previously cloned from expression constructs provided by Prof. John Ward, Department of Biochemical Engineering, UCL) were used. Cells were grown for 16 hours at 37 °C on agar plate containing LB-glycerol nutrient broth (yeast extract 5 g/L, tryptone 10 g/L, NaCl 10 g/L, glycerol 10 g/L), 15 g/L agar and 0.15 g/L selection antibiotic ampicillin (TK cultures) or kanamycin (TAm cultures). A single colony was inoculated into a sterile 250 mL shake flask containing 20 mL of the LB-glycerol medium and grown on an orbital shaker (Stuart Scientific, Redhill, UK) at 250 rpm for 12-16 hours at 37°C.

20 mL of inoculum prepared earlier was transferred into 2 L shake flask containing 180 mL of LB-glycerol with 0.15 g/L antibiotic. The culture was incubated for 7-8 hours at 37°C and 250 rpm on an orbital shaker. For TAm production isopropyl β-D-1-thiogalactopyranoside (IPTG) of 0.2 mM was added after 3 hours of fermentation at optical density (OD): 0.6. The OD$_{600nm}$ of the solution was measured every hour to check bacterial growth until it reached stationary phase. 0.2 mM of pyridoxal-5'-phosphate (PLP) was added to the transaminase cells upon harvesting. Following the fermentation, culture broth was centrifuged at 4000 rpm for 10 minutes at 4°C. The supernatant was discarded and the pellets were stored at –20°C.

For plasmid pQR1021 (His$_6$-TAm), the overnight cultures were prepared in 2XYT (tryptone 16 g/L, yeast extract 10 g/L, NaCl 5 g/L, glycerol 20 g/L) with 0.15 g/L kanamycin. Cells were subcultured using 1% v/v inoculum in 2 L shake flasks containing 500 mL of the same supplemented broth at 37°C and 250 rpm. Transaminase was induced with 1 mM of IPTG when growing in early exponential phase (OD$_{600}$ = 0.7), and temperature was dropped to 30°C until harvesting. Cells were harvested by centrifugation after 5 hours of induction. 0.2 mM of pyridoxal-5'-phosphate (PLP) was added to the cells upon harvesting. The culture broth was centrifuged at 4000 rpm for 10 minutes at 4°C. The supernatant was discarded and the pellets were stored at –20ºC.

2.2.2   Optical Density (OD) measurement

The optical density (OD) of liquid cultures was measured in triplicate at every hour by absorbance at 600 nm using a ATI Unicam UV/VIS spectrophotometer (Spectronic, Leeds, UK). The OD was measured by diluting the fermentation samples with fresh LB medium in order to keep the value between 0.1–0.9

2.2.3   Quantification of protein concentration

2.2.3.1 Sodium dodecyl sulfate polyacrylamide gel electrophoresis (SDS-PAGE) and densitometry analysis

Pre-cast gels (1.0 mm x 12 wells) of SDS 12% Tris-Glycine (Novex, Paisley, UK) were used for SDS-PAGE protein analysis as described by King and Laemmli (King & Laemmli, 1971). Gels were run in Tris-Glycine buffer (Novex, Paisley, UK) using a Mini-155 Protean II system (Bio-Rad Laboratories Inc., Hemel Hempstead, UK) at a power of 80-150 V for about 90 minutes. The gel was then rinsed twice for 5 minutes with 100 mL of RO water. Next, the gel was stained with sufficient SimplyBlue SafeStain (~20 mL) (Novex, Paisley, UK) to cover the gel for 1 hour at room temperature with gentle shaking. Then the gel was de-stained with de-staining buffer (40% v/v methanol, 10% v/v acetic acid and 50% v/v RO water)

for 2-3 hours. Finally, the mini gel was washed with 100 mL of RO water for 1-3 hours.

All gels were visualized and quantified on a Gel-Doc-it bioimaging system with Labworks 4.5 software (Bioimaging systems, Cambridge).

2.2.3.2 Protein concentration determination

Quantification of protein was carried out by UV absorbance of the purified enzyme at 280 nm using ATI Unicam UV/VIS spectrophotometer (Spectronic, Leeds, UK). Absorbance measurements were converted to protein concentration using the Beer-Lambert law:

$$A = \varepsilon \lambda c$$

Where A = absorbance at 280 nm, ε = extinction coefficient (for transketolase 93,905 $M.cm^{-1}$ and transaminase 78,000 $M.cm^{-1}$), λ = path length (1 cm), and c = protein concentration (mol. L^{-1}).

Quantification of the enzyme concentration in crude and purified form were carried out using a Bradford Assay based on the method of Bradford (Bradford, 1976). Bradford Reagent was used with bovine serum albumin (BSA) as the standard protein. Absorbance measurements at 595 nm were carried out on an ATI Unicam UV/VIS spectrophotometer (Spectronic, Leeds, UK). Crude extracts enzyme was quantified using Bradford assay as it contains contaminants such as nucleic acids that have absorption maxima near 260 nm with considerabe absorption extending to 280 nm.

2.3   Preparation of enzyme lysate for activity analysis

Frozen cell pellets from the fermentation were thawed at room temperature. The pellet was resuspended in a small quantity of 50 mM Tris-HCl at pH 7.0 (TK) or 7.5 (TAm) (1:25 v/v) and vortexed. The suspension was sonicated on ice using a

Soniprep 150 sonicator (MSE, Sanyo, Japan, 10 cycles of 10 seconds ON, 10 seconds OFF). The solution was centrifuged using a Hettich Universal 320R mid-bench centrifuge (DJB Labcare, Newport Pagnell, UK) for 10 minutes at 4000 rpm and 4°C. The supernatant was decanted and the pellets were discarded. The supernatant was filtered using a 0.2 μm pore filter (GE Healthcare, Buckinghamshire, UK). The clarified lysates was stored in the freezer at -20°C.

2.4   Purification of His_6-tagged enzymes

Frozen cell pellets from the fermentation were thawed at room temperature. The pellet was resuspended in a small quantity of 50 mM Tris-HCl at pH 7.0 (TK) or 7.5 (TAm) (1:25 v/v) and vortexed. The suspension was sonicated on ice using a Soniprep 150 sonicator (MSE, Sanyo, Japan, 10 cycles of 10 seconds ON, 10 seconds OFF). The solution was centrifuged using a Hettich Universal 320R mid-bench centrifuge (DJB Labcare, Newport Pagnell, UK) for 10 minutes at 4000 rpm and 4°C. The supernatant was decanted and the pellets were discarded. The supernatant was filtered using a 0.2 μm pore filter (GE Healthcare, Buckinghamshire, UK). Purification of His_6-tagged enzymes was performed using Ni-NTA superflow cartridges (Qiagen, Sussex, UK). The cartridge was equilibrated with 10 mL of binding buffer (pH 8.0) (50 mM NaH_2PO_4, 300 mM NaCl and 10 mM imidazole). The clarified lysate was loaded into the cartridge and subsequently washed with 20 mL of wash buffer (pH 8.0) (50 mM NaH_2PO_4, 300 mM NaCl and 20 mM imidazole). The enzyme was eluted with 2.5 mL of elution buffer (pH 8.0) (50 mM NaH_2PO_4, 300 mM NaCl and 250 mM imidazole).

2.5   Dialysis of His_6-tagged enzymes

The purified enzyme contains imidazole in the solution due to the presence of this compound in the buffers. To remove this, 50 mM of Tris-HCl at pH 7 (for TK) and pH 7.5 (for TAm) was added to 0.5 L of water (0.2 mM of PLP was added to the buffer for TAm). The purified enzyme-imidazole solution was placed inside a dialysis semi-permeable membrane with a MWCO of 14,000 Da (BioDesign,

Carmel, NY, USA) and this was positioned in a beaker containing the prepared buffer with gentle magnetic stirring. By stirring this at 4°C overnight the imidazole moves out of the dialysis membrane leaving pure enzyme. 100 μL of pure enzyme was taken for SDS-PAGE analysis. The dialysed enzyme solution was stored in the fridge at 4°C. This enzyme solution was used throughout this work.

2.6   Desalting of His₆-tagged enzymes

The purified enzyme contains imidazole in the solution due to the presence of this compound in the purification buffers. PD-10 desalting column (GE Healthcare, Buckinghamshire, UK) with a MWCO of 5,000 Da was used to remove the imidazole. The column storage solution was removed by taking off the seal at the bottom. Next, the column was filled up with 25 mL of 50 mM Tris-HCl at pH 7 (for TK) and pH 7.5 (for TAm) (0.2 mM of PLP was added to the buffer for TAm) and the flow-through solution was discarded. 2.5 mL of purified enzyme sample was added to the column and the flow-through was discarded. Elution was carried out by adding 3.5 mL of 50 mM Tris-HCl at pH 7 (for TK) and pH 7.5 (for TAm) (0.2 mM PLP was added to the buffer for TAm) to the column and the eluate was collected in a universal tube. The desalted enzyme was stored in the fridge at 4°C. This enzyme solution was used throughout this work.

2.7   Standard enzyme activity in solution

2.7.1   Assay for TK activity in microwells

The enzyme activity assay was carried out at room temperature in 50 mM Tris-HCl buffer (pH 7.0). One unit of TK enzyme was defined as the amount that catalyses the formation of 1 μmol of erythrulose (ERY) per minute using 50 mM of glycolaldehyde (GA) and lithium-hydroxypyruvate (HPA) at pH 7.0. TK reactions were conducted using model substrates, 50 mM HPA and 50 mM GA unless stated otherwise. The enzyme was incubated with cofactors, 2.4 mM thiamine pyrophosphate (TPP) and 9 mM $MgCl_2$ of for 30 minutes to reconstitute the holoenzyme. Substrate solutions of HPA and GA were added to make the total

reaction volume of 300 µL. 20 µL of samples were taken from this reaction mixture and 180 µL of 0.1% TFA was added to the sample to stop the TK activity at certain time interval. Reactions were monitored for HPA depletion and ERY production by HPLC assay.

2.7.2 Assay for ω-TAm (pQR 801) activity in glass vials

The enzyme activity assay was carried out at room temperature in 50 mM Tris-HCl buffer (pH 7.5). One unit of TAm enzyme was defined as the amount that catalyses the production of 1 µmol of acetophenone (AP) per minute using 100 mM ERY and 10 mM *(S)*-α-methylbenzylamine (MBA) at pH 7.5. TAm reactions were conducted using 10 mM of MBA and 100 mM of ERY unless stated otherwise. Substrate solutions of MBA and ERY and 0.2 mM cofactor pyridoxal-5'-phosphate (PLP) were added to the enzyme solution to make the total reaction volume of 300 µL. 20 µL of samples were taken from this reaction mixture and 280 µL of 0.1% TFA was added to the sample to stop the TAm activity at certain time interval. Reactions were monitored for MBA depletion and AP production by HPLC assay.

2.7.3 Assay for ω-TAm (pQR 1021) activity in glass vials

The enzyme activity assay was carried out at room temperature in 50 mM Tris-HCl buffer (pH 7.5). One unit of TAm enzyme was defined as the amount that catalyses the production of 1 µmol of HPA per minute using 100 mM *L*-serine (SER) and 10 mM GA at pH 7.5. Substrate solutions of SER and GA and 0.2 mM PLP were added to the enzyme solution to make the total reaction volume of 300 µL. 20 µL of samples were taken from this reaction mixture and 280 µL of 0.1% TFA was added to the sample to stop the TAm activity at certain time interval. Reactions were monitored for HPA production by HPLC assay.

2.7.4 TK kinetics in solution

TK kinetics parameter was determined by following a modified assay for TK activity (Section 2.7.1). The enzyme was incubated with cofactors, 2.4 mM TPP and 9 mM MgCl$_2$ for 30 minutes to reconstitute the holoenzyme. Substrate solutions of HPA and GA (Table 2.1) were added to make the total reaction volume of 300

μL. 20 μL of samples were taken from this reaction mixture and 180 μL of 0.1% TFA was added to the sample to stop the TK activity at certain time interval. Reactions were monitored for ERY production by HPLC assay.

2.7.5 TAm kinetics in solution

TAm kinetics parameter was determined by following a modified assay for TAm activity (Section 2.7.2). Substrate solutions of MBA and ERY (Table 2.1) and 0.2 mM PLP were added to the enzyme solution to make the total reaction volume of 300 μL. 20 μL of samples were taken from this reaction mixture and 280 μL of 0.1% TFA was added to the sample to stop the TAm activity at certain time interval. Reactions were monitored for AP production by HPLC assay.

Table 2.1: Compositions of substrate solutions for TK and TAm kinetics in solution

TK				TAm			
HPA (mM)	GA (mM)	GA (mM)	HPA (mM)	ERY (mM)	MBA (mM)	MBA (mM)	ERY (mM)
100	10	100	10	100	1	10	50
100	25	100	25	100	5	10	100
100	50	100	50	100	7.5	10	200
100	100	100	100	100	10	10	300

2.8 HPLC analysis

HPLC analysis was conducted using a microbore HPLC system (Dionex, Surrey, UK) controlled by Chromeleon 6.8 software with a multiwell plate autosampler (Spark, Emmen, Holland). HPA and ERY were analysed using an Aminex 87H column (Bio-Rad, Hertfordshire, UK) and analysis were conducted at 60°C using a

mobile phase of 0.1% (v/v) TFA in water at 0.6 mL/min. Detection was at 210 nm and the retention time was around 8.8 and 11.5 minutes for HPA and ERY respectively.

AP and ABT were analyzed using an ACE5 C18 reverse phase column (150x4.6 mm, Advanced Chromatography Technologies, Aberdeen, UK) on the Dionex HPLC system. The mobile phase for AP detection comprised of 0.1% TFA at 1.0 mL/min with a gradient of acetonitrile from 15% to 72% over 9 minutes. The gradient was followed by a 2 minute equilibration. UV detection was carried out at 250 nm with retention time for AP was around 7.3 minutes. For ABT analysis, the samples were derivatised by addition of an excess of 6-aminoquinolyl-N-hydroxysuccinimidyl carbamate (AQC). The derivatising reagent was made in house based on Cohen and Michaud (1993) protocol and the HPLC method reported by Ingram et al. (2007) was used. AQC powder was added in dry acetonitrile and heated at 55°C until the powder dissolves. The samples were mixed with borate buffer and the AQC solution. This mixture was then vortexed for few seconds prior to transfer to HPLC vial. The retention time of derivatised ABT was around 8.9 minutes.

2.8.1 Quantification of HPLC standard

Standard calibration curves were used to quantify the absorbance responses for the reaction substrates and products from the HPLC assay. Standard ERY, HPA, MBA, AP and ABT were prepared separately with a known concentration and analysed with the HPLC. Example of chromatogram for each compound can be found in Appendix 1.

2.9 Synthesis of derivatising reagent

The derivatising reagent AQC was made in house based on Cohen and Michaud (Cohen and Michaud, 1993) protocol. Di (N-succinimidyl) carbamate (3 g, 6 mmol) was dissolved in 100 mL of dry acetonitrile and heated to reflux. Dropwise addition of a 6-aminoquinoline (1.5 g, 10 mmol) solution in dry acetonitrile was carried out

over 45 min. Following a further 30 min reflux, the reaction mixture was concentrated to about half of the original volume by rotary evaporation. The solution was stored at 4°C overnight. The crystals were then filtered off and stored in a desiccator.

2.10 Immobilised Enzyme Microreactor (IEMR) setup

2.10.1 Derivatised fused silica capillary

2.10.1.1 Microreactor setup

The microreactor system setup consists of fused silica capillary microreactor that was connected to KDS100 syringe pump (KD Scientific, Holliston, MA, USA) (Figure 2.1). The NanoTight fittings (Presearch Ltd, UK) were used to connect the capillary tubing into standard 10-32 threaded, coned ports (Quick Connect Luer adapter) (Presearch Ltd, UK) which then joined to the syringe. These are made of chemically inert PEEK™ polymer nuts with a high-pressure ferrule. The 1.6" long NanoTight sleeves are manufactured from fluoropolymer (FEP) and can withstand up to 50˚C. The sample of bioconversion was collected at the other end of the capillary.
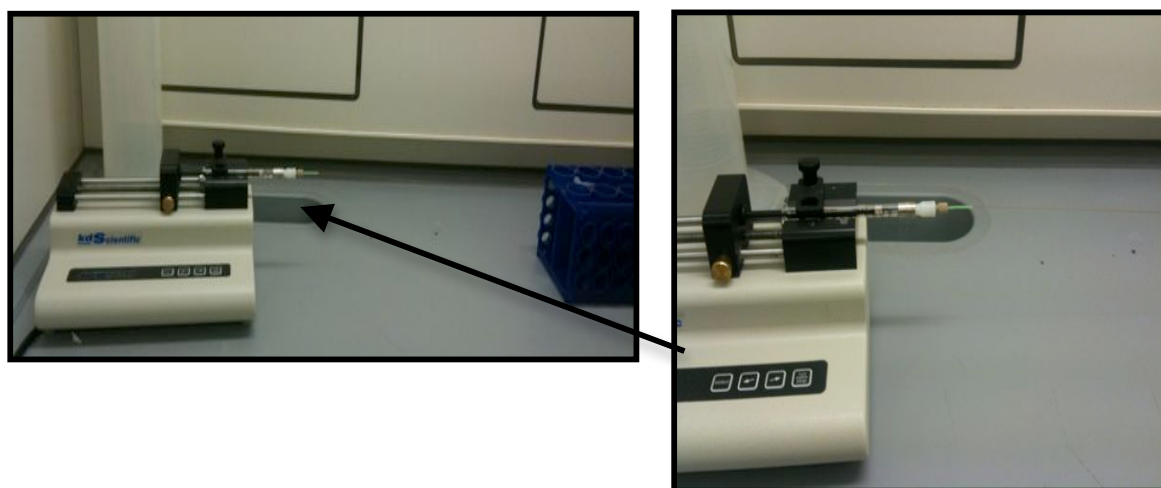
Figure 2.1: Stop flow microreactor setup. Photos showing the setup of the derivatised fused silica capillary. The microreactor consists of capillary with I.D of 200 μm and total reaction volume of ~13 μL.

2.10.1.2 Microcapillary surface derivatisation

A fused silica capillary with I.D of 200 µm was used for the microcapillary reactor. Derivatisation protocol was conducted under laboratory safety hood in room temperature. The immobilisation procedure was adopted from previous work (Miyazaki et al., 2005). A new, untreated capillary was treated with a 3:1 (v/v) piranha solution (H_2SO_4 and 30% H_2O_2) at a flow rate of 1 µL/min overnight to strip the inner surface from any organic residues prior to chemical treatment, followed by washing with 150 µL ultrapure water at a flow rate of 5 µL/min. The capillary was then reacted with a 30% of 1:1 v/v solution of 3-aminopropyltriethoxysilane and methyltriethoxysilane in 97% ethanol in water for 1 hour and left to incubate for an additional hour. After washing with low volume ethanol (1:1 v/v), the capillary was heated to 115˚C for 1 hour. This caused polymerisation of the silanes on the surface and resulted in a visible white layer forming inside. The amino functionalized microcapillary prepared above was treated with 20 mM solution of succinic anhydride in dimethylformamide (DMF) for 2 hour at room temperature at a flow rate of 5 µL/min to create the carboxyl function. After washing with DMF, the resulting carboxyl group was reacted with 1 M solution of 1−Ethyl−3−(3−dimethylaminopropyl) carbodiimide hydrochloride (WSCI−HCl) and N-hydroxysuccinimide (NHS) in DMF for 1 hour, followed by washing with DMF. The nickel-nitrilotriacetic acid (Ni-NTA) chemistry could now be complexed to the surface. A 250 mM DMF solution of Nα-Nα-bis(carboxymethyl)-l-lysine hydrate in water was loaded to the capillary and reacted for 4-6 h at a flow rate of 5 µl/.min and left to incubate overnight. AB-NTA forms white solid deposits on the surface. Nickel was then complexed to the surface by incubation with 40 mM Ni_2SO_4 solution for 12 hours. The derivatised capillary was stored at 4°C. The chemistry immobilisation diagram is shown in Figure 1.5.

2.10.1.3 Enzyme immobilisation and elution

Enzyme immobilisation was carried out at room temperature. An AB-NTA derivatised microcapillary was treated with a 40 mM aqueous solution of nickel sulphate for 6 hours at a flow rate of 5 µL/min. Incubation of nickel was for an additional 6 hours in stop-flow mode. After washing with 50 mM Tris-HCl, the enzyme solution (~0.2-0.3 mg/mL) in 50 mM Tris-HCl containing 5 mM imidazole was loaded into the capillary at a flow rate of 5 µL/min. The enzyme was left to incubate for an additional 2 hours following immobilisation and later washed with 50 mM Tris-HCl (with 5 mM imidazole) to remove unbound enzyme.

Enzyme was removed by treating the capillary with a 50 mM solution of EDTA (pH 8.0) at 5 µL/min. The amount of EDTA used did not exceed 100 µL. The collected solution was analysed for protein content by SDS-PAGE or absorbance at 280 nm. When absorbance was measured, the readings were blanked with EDTA buffer to minimise background absorbance.

2.10.1.4 Transketolase reaction in microcapillary

TK activity in microcapillary was conducted based on modified procedures in microwells using similar model substrates, HPA and GA. One unit of TK enzyme was defined as the amount that catalyses the formation of 1 µmol of ERY per minute using 50 mM GA and 50 mM HPA at pH 7.0. Cofactors of TPP, 2.4 mM and $MgCl_2$, 9 mM was loaded at 5 µL/min in the immobilised TK capillary for 30 minutes to reconstitute the holoenzyme. Solution substrates of 50 mM HPA and 50 mM GA were loaded at 5 µL/min and left incubated at certain residence time. Samples were taken from this reaction mixture and 0.1% TFA was added to the sample to stop the TK activity. Reactions were monitored for HPA depletion and ERY production by the HPLC assay (Section 2.8).

2.10.2 Packed tube IEMR

2.10.2.1 Packing of a FEP tube with microbeads

HIS-Select Nickel Affinity agarose beads (45-165 µm) were used as the packing material. They were first washed with 50 mM of Tris-HCl and left in suspension in the same buffer. A Nanobaume (Presearch Ltd, UK) pressurised container was used to pack the beads in the tube (Figure 2.2). The bead slurry containing 5% (v/v) beads was placed in a glass vial. A stir bar was put in the vial and the vial was placed into the pressurized container. The container was then set on top of a magnetic stirrer. The fluorinated ethylene propylene (FEP) tube (500 µm ID, Presearch Ltd, UK) was attached to the container while a microfilter assembly (2 µm, Presearch Ltd, UK) was connected at the end of the tube. A two-way valve was connected to the pressurised container while the other end was connected to a nitrogen gas cylinder. A pressure of 5 bar was applied to the system and the pressure drop was monitored by the pressure gauge installed. The packing took 5-10 minutes.
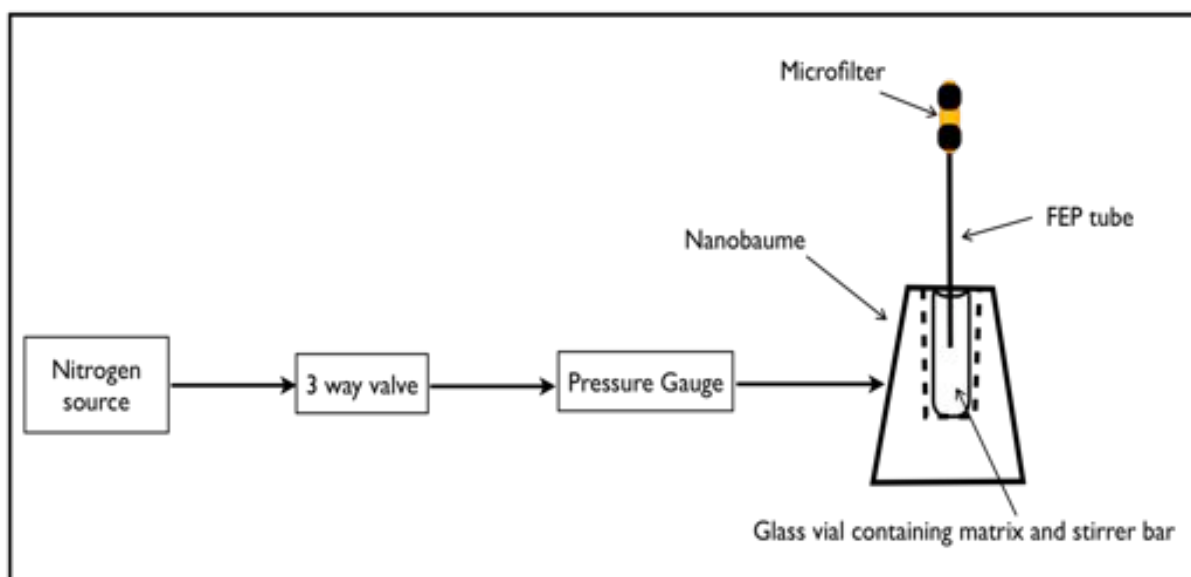
Figure 2.2: A schematic of the nanobaume pressurized container: The nitrogen gas source was compressed into the system through the 3 way valve at 5 bar. A bead slurry of 5% (v/v) was continuously stirred in the glass vial and then packed into the fluorinated ethylene propylene (FEP) tube (500 µm ID) by positive pressure. Excess liquid left through the filter while the beads were retained inside the FEP tube.

2.10.2.2 Enzyme immobilisation and elution

The packed tube IEMR was first equilibrated with binding buffer (500 mM NaCl, 20 mM Tris-HCl, 5 mM imidazole; pH 7.0 or 7.5) at 5 µL/min for 15 minutes. Enzyme concentrations used were 0.05-2.0 mg/mL. The purified enzyme (100 µL) was loaded into the tube at 5 µL/min and was left to incubate for an additional 1 hour following immobilisation. Non-specific binding of the enzyme on the beads was removed by treating the tube with washing buffer (50 mM Tris-HCl; pH 7.0 or 7.5) at 25 µL/min for 20 minutes. Bound enzyme was removed by treating the tube with elution buffer (1 M imidazole, 500 mM NaCl and 20 mM Tris-HCl; pH 7.0 or 7.5) at 5 µL/min for 10 minutes.

2.10.2.3 Transketolase reaction in packed tube IEMR

The packed tube IEMR (5 cm length) was connected to a KDS100 syringe pump (KD Scientific, Holliston, MA, USA) on one end and connected to a microfilter assembly (2 µm, Presearch Ltd, UK) at the outlet. The enzyme activity assay was carried out at room temperature in 50 mM Tris-HCl buffer (pH 7.0). One unit of TK

enzyme was defined as the amount that catalyses the formation of 1 μmol of ERY per minute using 50 mM GA and 50 mM HPA at pH 7.0. TK reactions were conducted using model substrates, 50 mM HPA and 50 mM GA unless stated otherwise. The enzyme was incubated with cofactors, 2.4 mM TPP and 9 mM MgCl$_2$ at 5 μL/min for 30 minutes to reconstitute the holoenzyme. Substrate solutions of HPA and GA with the cofactors were loaded continuously at various flow rates and 20 μL samples were taken from the outlet of the tube at regular time intervals. The samples were quenched with 0.1% TFA and analysed by HPLC. Reactions were monitored for ERY production by HPLC assay (Section 2.8).

2.10.2.4 Transaminase reaction in IEMR

The enzyme activity assay was carried out at room temperature in 50 mM Tris-HCl buffer (pH 7.5). One unit of TAm enzyme was defined as the amount that catalyses the production of 1 μmol of AP per minute using 100 mM Ery and 10 mM MBA at pH 7.5. TAm reactions were conducted using model substrates, 10 mM of MBA and 100 mM of ERY unless stated otherwise. Substrate solutions of MBA and ERY and 0.2 mM PLP were loaded continuously at various flow rates and 20 μL samples were taken from the outlet of the tube at regular time intervals. The samples were quenched with 0.1% TFA and analysed by HPLC. Reactions were monitored for AP production by HPLC assay (Section 2.8).

Table 2.2: Flow rates used in the continuous flow reaction corresponding to the residence times in the packed tube IEMR. The residence times were based on the 5 cm IEMR with total volume of 10 μL

Flow rate (μL/min)	Residence Time (min)
0.5	20
1	10
2	5
5	2
10	1
20	0.5
30	0.33

2.10.3 Actipix online detection system

Actipix D100 was integrated in the IEMR system to monitor the product conversion in a real-time. This detector has been designed for use in a variety of applications in research by providing quantitative imaging in the UV region. The Actipix D100 consists of a control box and a capillary cartridge with a miniature size detector (6.5 cm x 5.5 cm x 11.5 cm) (Figure 2.3). This system allows for wide range of UV detection by using different types of filter corresponding to the specific wavelength. Detection was performed at two different wavelengths. The first one was at 210 nm for the detection of product formation of HPA in the multi steps enzymatic reaction. And the second filter was at 280 nm for the detection of product formation of AP in the single TAm enzymatic reaction. Light was delivered via a fibre optic coupled light source. Readout of signals on the active pixel sensor and absorbance calculations were carried out at MHz rates, with all processing done in hardware on custom electronic assemblies. Processed data was output in real-time to a computer using a high-speed serial data or USB link. Paraytec data acquisition software was set up for data collection and output signal analysis.

2.10.4 Integration of Actipix online detection system in IEMR

The packed tube IEMR was connected to a KDS100 syringe pump on one end and connected to a microfilter assembly at the outlet. The Actipix detector capillary was joined at the outlet by connecting the outlet tube with a sleeve that allow for direct flow of the bioconversion mixture to flow through the detector. Substrate solution was loaded at flow rates ranging from 1-30 μL/min, with detection taking place in real time through the Actipix cartridge window and data was recorded as .cvs files via the propriety software.

2.10.5 Quantification of Actipix standards

Standard calibration curves were used to quantify the absorbance responses for the product formation from the Actipix online detection system. Standard HPA and AP were prepared separately with a known concentration and run through the Actipix.
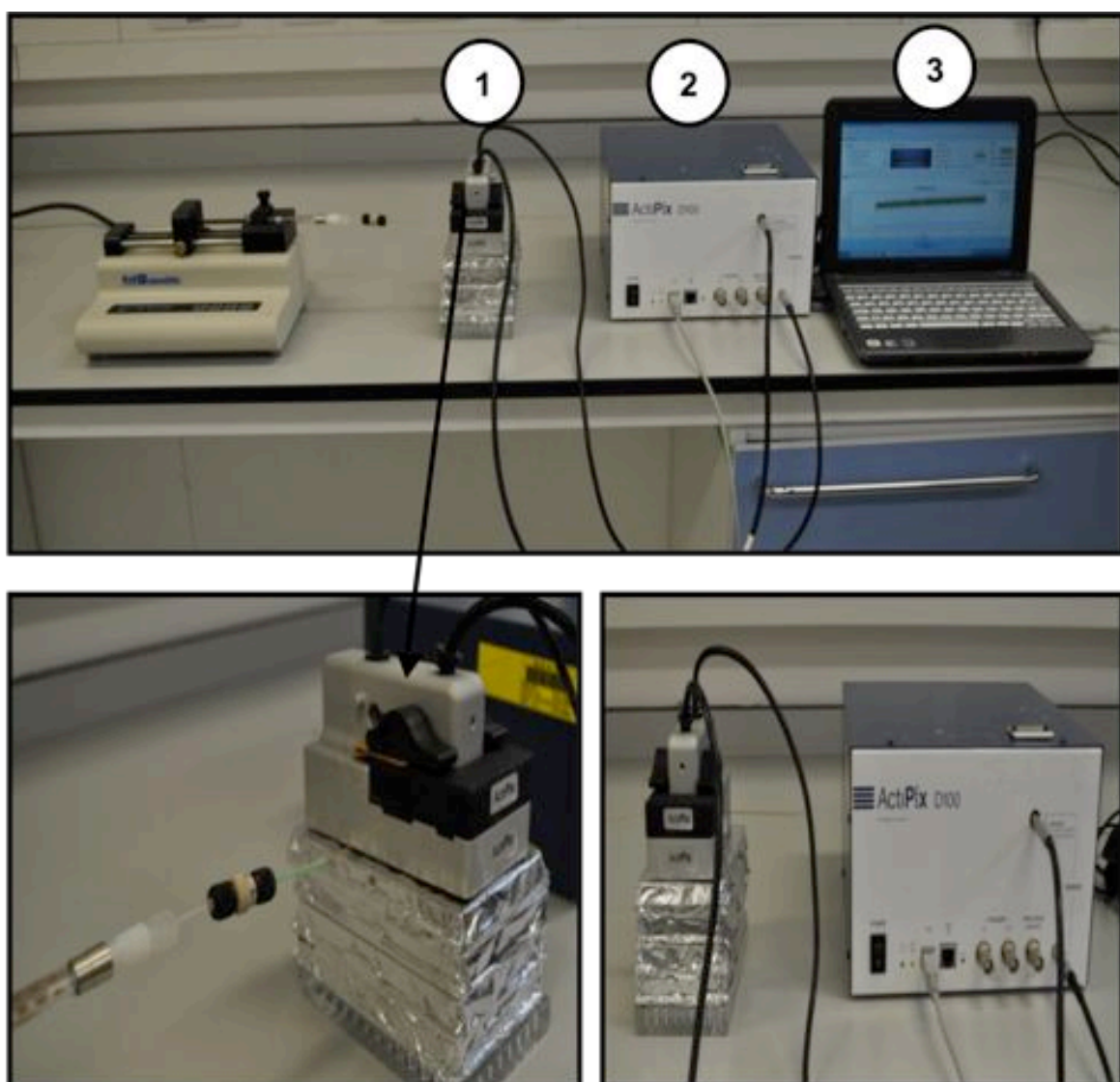
Figure 2.3: Continuous flow microreactor setup with Actipix detector. Photos showing the setup of the continuous flow microreactor coupled with Actipix (Paraytec, York) capillary detection system consisting of a capillary-holding sensor head (1) and the control box (2). Data is collected and processed through a computer interface (3).

2.11 Enzyme kinetics in IEMR

2.11.1 TK kinetics in IEMR

TK kinetics in the IEMR was determined by following a modified assay for TK activity as described in Section 2.10.2.3. The enzyme was first incubated with cofactors, 2.4 mM TPP and 9mM $MgCl_2$ at 5 µL/min for 30 minutes to reconstitute the holoenzyme. Substrate solutions (Table 2.3) were loaded continuously at flow rates ranging from 2-30 µL/min and 20 µL samples were collected from the outlet of the tube. The samples were quenched with 0.1% TFA and analysed by HPLC. Reactions were monitored for ERY production by HPLC assay (Section 2.8).

2.11.2 TAm kinetics in IEMR

TAm kinetics in the IEMR was determined by following a modified assay for TAm activity as described in Section 2.10.2.4. Substrate solutions (Table 2.3) and 0.2 mM PLP were loaded continuously at flow rates ranging from 2-30 µL/min and 20 µL samples were collected from the outlet of the tube. The samples were quenched with 0.1% TFA and analysed by HPLC. Reactions were monitored for AP production by HPLC assay (Section 2.8).

Table 2.3: Substrate composition for TK and TAm kinetics

TK		TAm	
HPA (mM)	GA (mM)	MBA (mM)	Ery (mM)
100	10	10	50
100	15	10	100
100	25	10	200
100	50	10	300

2.12 Multi-step enzymatic reaction in IEMR

2.12.1 Two step enzymatic reaction

The set-up of the IEMR cascade is shown in Figure 2.4. The enzyme immobilisation of individual IEMRs was conducted separately before assembly. Two separate (2x5 cm) of the packed tube IEMR were connected in series where the beads were retained using a microfilter assembly (2 µm, Presearch Ltd, UK). The second packed tube IEMR was connected to the first using a microferrule (Presearch Ltd). The two-tube system was connected to a KDS100 syringe pump (KD Scientific, Holliston, MA, USA) so that the inlet of the first tube was directly connected to the pump while its outlet was used to collect the samples for further off-line HPLC analysis. Coupled reactions were carried out using the TK (pQR 791)-TAm (pQR 801) model reaction. Solution substrates of GA, HPA and MBA at desired concentrations and cofactors for both enzymes at pH 7.5 were loaded together into the first tube containing packed beads immobilised with TK. The erythrulose required by the immobilised TAm was provided by the TK reaction step. The reaction was carried out continuously at flow rates between 1-30 µL/min.

20 µL samples were taken at different time intervals and quenched with 0.1% TFA. Reactions were monitored for ABT and AP production by HPLC assay (Section 2.8).
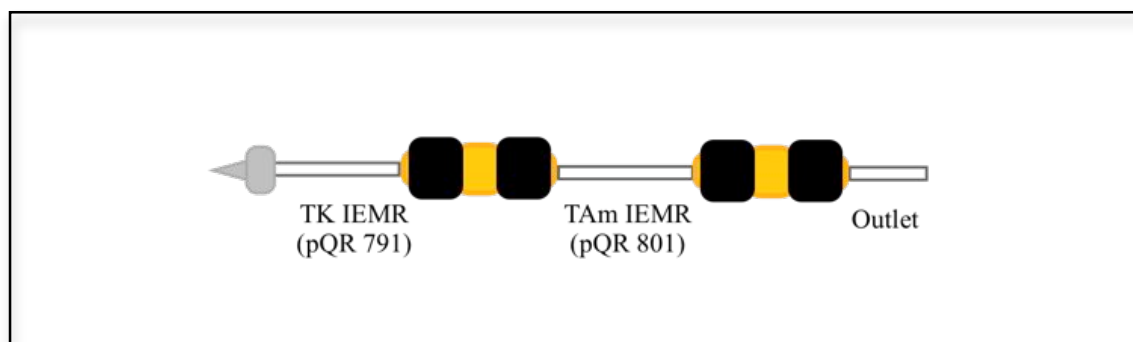
Figure 2.4: Schematic illustration of the IEMR used for analysis of TK-TAm reaction. An IEMR with ID of 500 µm and length of 5 cm gives a total reaction volume of ~10 µL. The prototype consisted of single IEMRs that were cascaded in series to allow multi-step enzymatic reaction. TK catalysed the reaction of hydroxypyruvate (HPA) and glycoaldehyde (GA) to L-erythrulose (ERY), and the second unit of the IEMR with immobilised TAm converted ERY into 2-amino-1,3,4-butanetriol (ABT) using (S)-α-methylbenzylamine (MBA) as amine donor.

2.12.2 Three step enzymatic reaction

The set-up of the IEMR cascade is shown in Figure 2.5. The enzyme immobilisation of individual IEMRs was conducted separately before assembly. Three separate (2x10 cm and 1x5 cm) of the packed tube IEMR were connected in series where the beads were retained using a microfilter assembly (2 µm, Presearch Ltd, UK). The second and third packed tube IEMR was connected to the first using a microferrule (Presearch Ltd). The three-tube system was connected to a KDS100 syringe pump (KD Scientific, Holliston, MA, USA) so that the inlet of the first tube was directly connected to the pump while its outlet was used to collect the samples for further off-line HPLC analysis. Coupled reactions were carried out using the TAm (pQR 1021)-TK (pQR 791)-TAm (pQR 1021) model reaction. Solution substrates of SER and GA at desired concentrations and cofactors for both enzymes at pH 7.5 were loaded together into the first tube containing packed beads immobilised with TAm. The HPA required by the immobilised TK was provided by the first TAm reaction step which then reacted with GA in the second step reaction to produce ERY (substrate used in the third step). The reaction was carried out

continuously at flow rates between 0.5-10 µL/min. 20 µL samples were taken at different time intervals and quenched with 0.1% TFA. Reactions were monitored for HPA production in the first step of TAm reaction through Actipix online detection whilst ABT and HPA production in the final step by HPLC assay (Section 2.8).
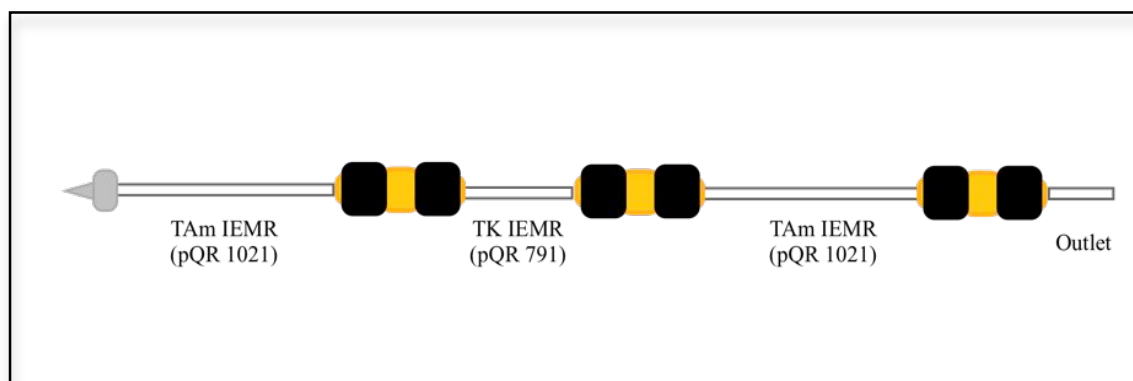
Figure 2.5: Schematic illustration of the IEMR used for analysis of TAm-TK-TAm reaction. Three IEMR with ID of 500 μm (2x10 cm and 1x5 cm) gives a total reaction volume of ~20 μL and ~10 μL respectively. The prototype consisted of single IEMRs that were cascaded in series to allow multi-step enzymatic reaction. TAm catalysed the reaction of Serine (SER) and glycolaldehyde (GA) to hydroxypyruvate (HPA) which was used in the second unit of the IEMR. Immobilised TK converted the reaction between HPA and GA to erythrulose (ERY) and this product was subsequently reacted with SER for the formation of 2-amino-1,3,4-butanetriol (ABT).

3 Characterisation of Transketolase and Transaminase in solution phase

3.1 Introduction

As described in Section 1.6.1.1, transketolase (TK) is an important enzyme that catalyses the transfer of a two-carbon ketol group to an aldose to form asymmetric carbon-carbon bond. Given the importance of this reaction in the synthesis of a wide range of molecules, interest on TK has been growing in recent years. TK applications have been widely reported, owing to its broad substrate tolerance (Takayama et al., 1997; Turner, 2000; Fessner & Helaine, 2001). To date, the most rapid TK reaction using HPA as a ketol donor is in the production of erythrulose (ERY) from glycolaldehyde (GA), which releases carbon dioxide as a by-product (Bolte et al., 1987; Dalmas & Demuynck, 1993) (Figure 1.7b). The assay for this reaction can be easily analysed using HPLC (Mitra & Woodley, 1996) that allows for simple and rapid measurement and kinetic study of TK. This model system has been extensively studied for investigating transketolase-catalysed reaction. Details of biotransformation characterisation of TK was reported by Mitra et al. (1998) and kinetic measurements was performed by Gyamerah et al. (1997) and Chen et al. (2007). Guidelines for reactor design and operation condition was also demonstrated (Woodley et al., 1996) and *in situ* product removal (ISPR) of erythrulose from the bioconversion was developed (Chauhan et al., 1997).

Apart from transketolase enzyme, transaminase is also among the frequently studied enzymes due to its potential in the production of amino acids and chiral amines (Taylor et al., 1998; Chao et al., 1999). In this research, CV2025 ω–TAm from *C. violaceum* was used to investigate transaminase-catalysed reaction. This enzyme showed high activity towards (*S*)-α-methylbenzylamine (MBA), the amino donor (Kaulmann et al., 2007) and reacted with erythrulose to produce 2-amino-1,3,4-butanetriol (ABT) and acetophenone (AP) (Figure 1.12). The ketodiol needed for this reaction can be synthesised via the transketolase enzyme, therefore making it a perfect model for investigating TAm-catalysed reaction, which can be further

coupled in the TK-TAm reaction for the production of chiral aminodiol (Figure 1.13).

This chapter details the characterisation of two main enzymes that were used throughout this project, which were transketolase (TK) and transaminase (TAm) in enzyme solution. A good understanding of the enzyme activity of both TK and TAm in solution phase is very important for effective optimisation of immobilised enzyme microreactor (IEMR). Key insight can be gained into the enzyme behaviour involved in the IEMR, which will facilitate future implementation of the multienzyme microreactor. The validated data will be used for further investigation of enzyme activity in IEMR.

The key objectives of this chapter are:

- Characterisation of His_6-tagged transketolase and transaminase with respect to its bioconversion for purified and crude enzyme.

- Characterisation of His_6-tagged transketolase and transaminase with respect to its stability in different storage conditions.

- Evaluation of kinetic parameters of the His_6-tagged transketolase and transaminase in solution phase.

3.2 Characterisation of Transketolase (TK) enzyme

3.2.1 Transketolase production

3.2.1.1 Production of His$_6$−TK by *E.coli* fermentation

Stocks of *E.coli* BL21gold (DE3) containing plasmid pQR791 (His$_6$-TK) (Martinez-Torres et al., 2007) was used. Cells were grown in a 2 L shake flask with a total working volume of 200 mL using LB-glycerol media. The OD$_{600nm}$ of the solution was measured every hour to check bacterial growth until it reached stationary phase. This data ensures that the cell is harvested at the optimum level, hence offers substantial amount of TK for the subsequent purification step. Figure 3.1 shows a typical growth profile for *E.coli* fermentation expressing His$_6$-tagged TK pQR791 as determined by OD$_{600nm}$ measurements. The cell reached a plateau after a period of approximately 7 hours. The fermentation was stopped and the cells were harvested.

Based on the growth profile, the fermentation underwent a short lag phase which due to high inoculum volume 10% v/v, as well as using similar medium in the fermentation to the inoculum. Following the lag period, growth started in the exponential phase for about 7 hours before it reached stationary phase. For the particular fermentation data shown in Figure 3.1, the maximum specific growth rate was 0.73 hr^{-1} with a doubling time, t$_d$ of 0.95 hr. A similar fermentation procedure was used throughout this project and data shown in Figure 3.1 is representative of each fermentation performed. Expressed His-TK constituted about 28% of the total cell protein as estimated by SDS-PAGE.
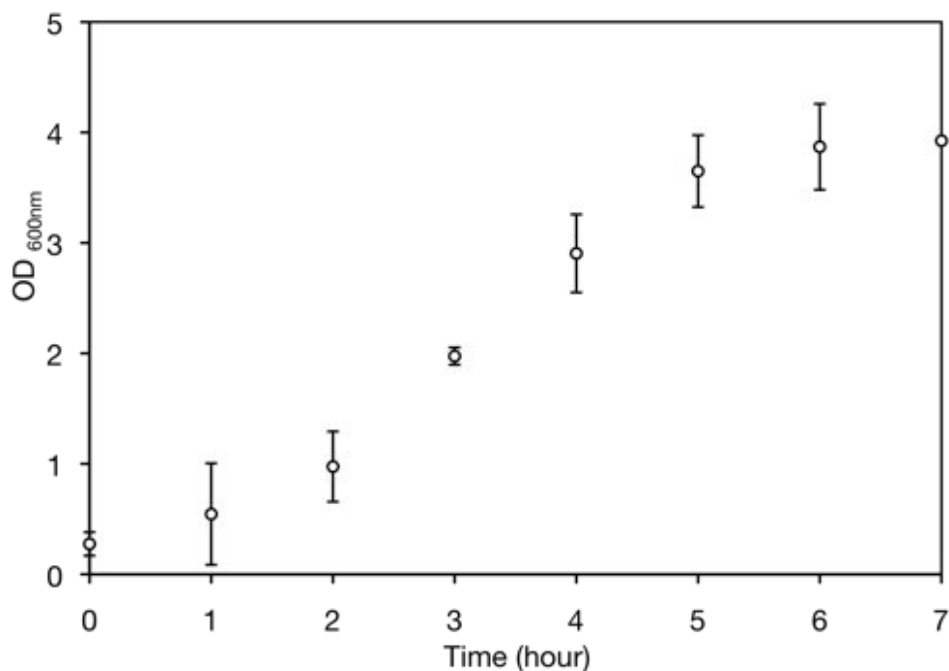
Figure 3.1: Growth of *E.coli* strain BL21gold (DE3) pQR791 expressing His_6-TK. Cells were cultured in 200 mL LB glycerol media with the addition of 0.15g/L ampicillin, in a 2 L shake flask at 37°C, 250 rpm with a 10% v/v inoculum grown overnight as previously described (Section 2.2.1). 10 g/L of glycerol as the carbon source to the media was added to promote growth. Growth was monitored by OD_{600nm} measurements (Section 2.2.2). Error bars represent one standard deviation about the mean (n = 3).

3.2.1.2 Purification of His$_6$−tagged TK

Characterisation and kinetics studies of His-tagged TK in solution phase and immobilised form were conducted using purified enzyme. Pure enzyme offers cleaner reaction product and easier workup when reaction is complete (Kirst et al., 2001). In contrast to the crude form, purified enzyme enhances the enzyme specificity whilst minimising non-specific reactions. These features are absolutely paramount to the investigation of the enzyme kinetics. Instead of using crude enzyme for direct immobilisation with the Ni-NTA derivatised capillary and microbeads, the use of purified enzyme feed minimises non-specific binding during immobilisation and allows for improved characterisation of the enzyme behaviour.

3.2.1.2.1 Ni-NTA affinity purification

With the advent of recombinant protein technology, the incorporation of an affinity tag offers a feasible way for enzyme purification. Among the variety of affinity tags, more than 60% of the proteins produced include a polyhistidine tag (Derewenda, 2004), which normally results in high yields of more than 90% purity, making it economically favourable (Arnau et al., 2006). Numerous application of his-tag purification have been reported (Chaga et al., 1999; Derewenda, 2004; Chatterjee et al., 2005). Purification of His-tagged proteins is based on the affinity binding of histidine residues to several types of immobilised metal ions (Ni^{2+} or Cu^{2+}) that is in complexed with an immobilised chelating agent (immobilised metal-ion affinity chromatography, IMAC). Complex formation between Ni-NTA and His-tag renders stability for the immobilisation and the interaction can be easily uncoupled through incorporation of imidazole or EDTA.

Purification of His-tagged TK was demonstrated successfully by Hibbert et al. (2007) using sepharose fast-flow Ni-NTA resin and Matosevic et al. (2009) using Ni^{2+} affinity cartridge. In this work, purification of His-tagged TK was performed using Ni-NTA superflow cartridge from Qiagen. Purification is based on the affinity between the neighbouring histidines of the His•Tag sequence of the expressed TK and an immobilised metal ion (Ni^{2+}) in the cartridge. The cartridge

was first loaded with equilibration buffer before the crude TK was loaded through the cartridge. Any non-specific protein binding was removed by washing buffer and the target protein was recovered in the elution buffer (Section 2.4). This procedure produced high purity of TK (>90%) as indicated by the band appeared in the SDS-PAGE gel in Figure 3.2. The Ni-NTA superflow cartridge was used up to ten times without any major enzyme loss before being discarded. In addition, the Ni-NTA superflow cartridge can also be used for purifying proteins in an automated procedure, which was successfully demonstrated by using the syringe pump.
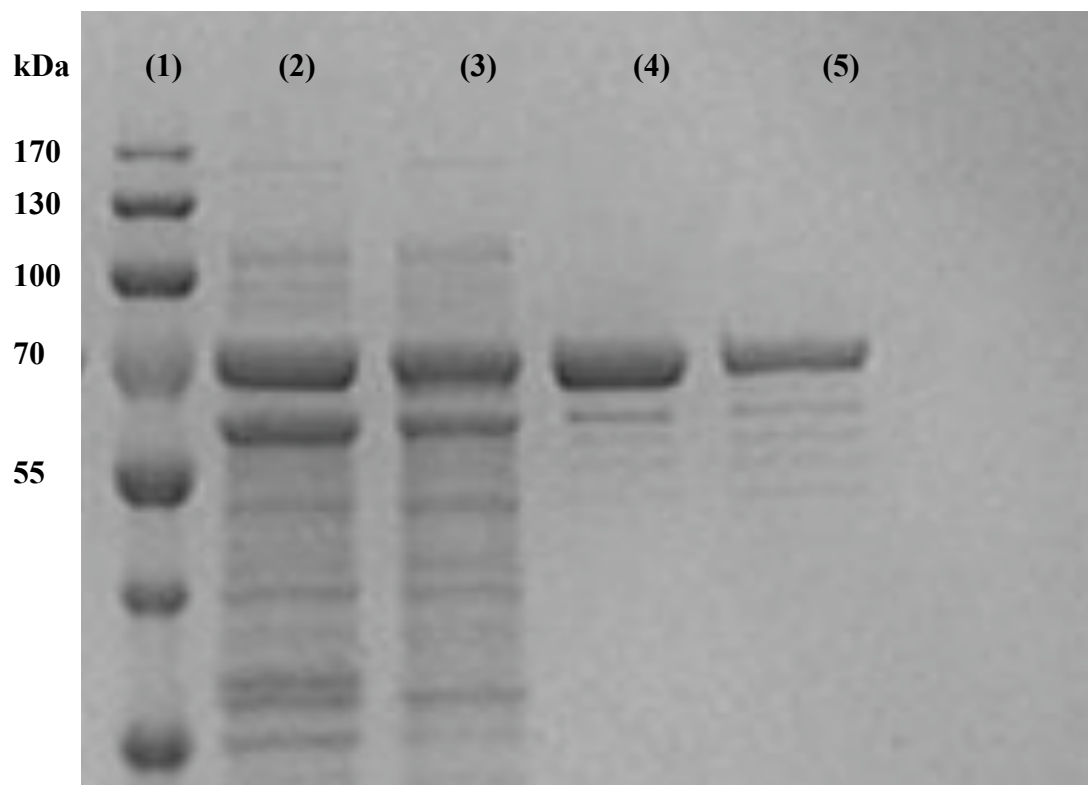
Figure 3.2: Purification of His$_6$−tagged transketolase. His$_6$−tagged TK was purified from 200 mL culture scale on Ni-NTA superflow cartridge. The TK band in each lane at 72 kDa corresponds to the monomeric form of the enzyme. Lane (1) protein marker, (2) *E.coli* lysate obtained by sonication, (3) supernatant following sonication and centrifugation, (4) purified His$_6$-TK eluted with a 250 mM solution of imidazole, (5) purified His$_6$-TK following removal of imidazole by desalting method. His$_6$-TK was determined to make up about 28% of the total cell protein. Purification performed as described in Section 2.4

3.2.1.2.2   Removal of imidazole from purified His$_6$-TK

Imidazole was added during the purification process to allow for the recovery of the purified His$_6$-TK from the purification column (Section 2.4). Imidazole was passed in excess through the column to displace the His$_6$-TK from nickel co-ordination, and freeing the enzyme. No more than 250 mM is suggested for the elution buffer since many proteins will elute with imidazole levels as low as 100-200 mM. Free imidazole can be removed from the eluted sample by dialysis, desalting column or gel filtration. Alternatively, EDTA can be used to elute His$_6$-TK from the column. However, the downside of this method is that EDTA strips nickel ions from the resin, which limits the reusability of the purification column.

Two methods were tested to demonstrate the removal of imidazole from purified His$_6$-TK. Dialysis works by separating molecules in solution by the difference in their rates of diffusion through a semi-permeable membrane. The TK-imidazole solution was placed inside a dialysis semi-permeable membrane with MWCO of 14,000 Da and incubated in 50 mM Tris-HCl at pH 7 (Section 2.5). By stirring this at 4°C overnight (14-16 hours) the imidazole moves out of the dialysis membrane leaving pure transketolase. The pore size is significantly lower than the size of the enzyme molecule (~144,000 Da), thus minimising losses that might occur during the process.

The second method was by using the desalting column with a MWCO of 5,000 Da (Section 2.6). This method allows for rapid group separation of salts and other impurities from the high molecular weight substances of interest. The sensitivity of this column was even higher and the desalting process took less than one hour to perform. The desalted sample however was diluted by more than 30% from the initial enzyme feed. Samples from both methods were quantified and run on SDS-PAGE (Figure 3.3). The quality and band size of both samples, as visualized from the gel were similar. Quantification of the enzyme concentration was carried out to support this data. After normalising the final volume of the samples, the concentration of purified His$_6$-TK from dialysis was 2.38±0.055 mg/mL while sample from desalting column was 2.44±0.056 mg/mL. This result suggests that no

significant leakage of enzyme occurred during the dialysis process compared to the desalting method, despite the long hours process.

Based on the information acquired from this study, desalting method appeared to be more favourable compared to the dialysis method. While both methods showed almost similar results, desalting method was chosen due to its simpler protocol and shorter processing time. In addition, the desalting method was found to be relatively cheap as the desalting column could be recycled up to ten times before discarding. Therefore, desalting method was used for further post purification process for removal of imidazole. The effect of dialysis and desalting process on the His$_6$-TK activity was further investigated in Section 3.2.4.
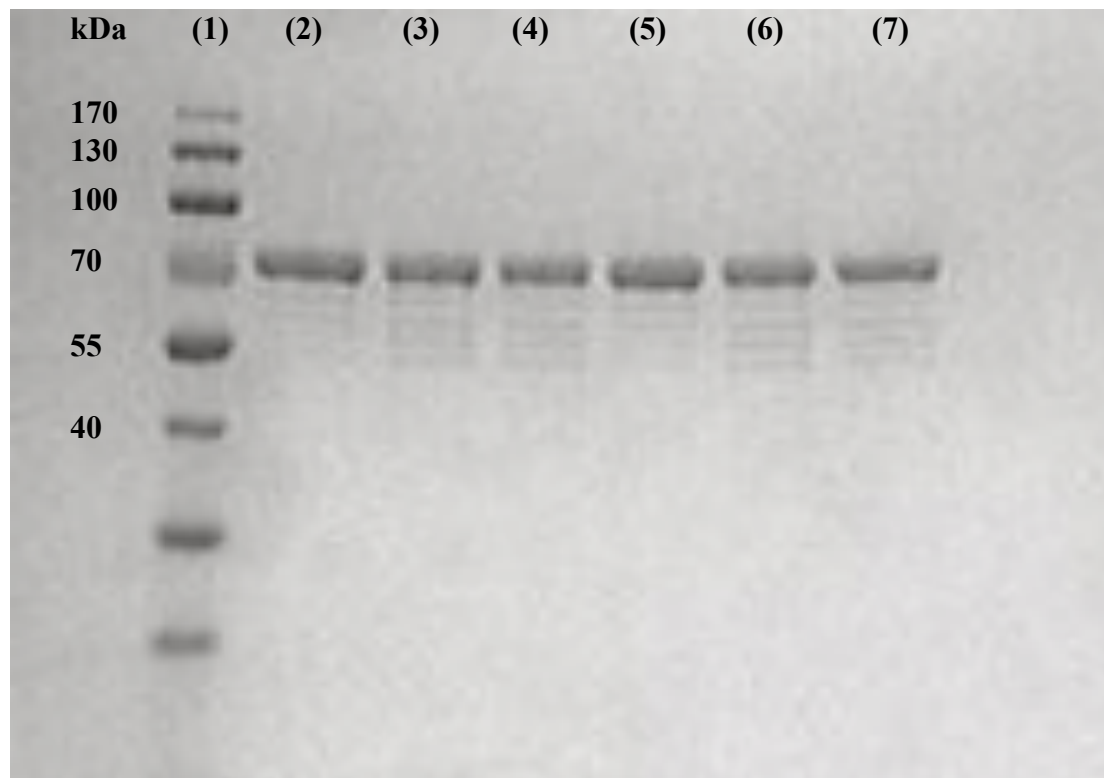
Figure 3.3: SDS PAGE for dialysis and desalting process sample of purified His_6-TK. (1) Protein marker, (2 and 5) Purified His_6-TK prior to removal of imidazole, (3 and 6) Purified His_6-TK after dialysis, (4 and 7) Purified His_6-TK after desalting process. Dialysis of His_6-TK was performed as described in Section 2.5 and desalting process in Section 2.6.

3.2.1.3 Quantification of His$_6$−tagged TK

The quantification of His$_6$-TK concentration was conducted after the purification process using three techniques, which were absorbance by spectrophotometer, SDS-PAGE and Bradford assay. Protein concentration was determined at 280 nm with an extinction coefficient (ε) of 93905 L mol^{-1} (Martinez-Torres et al., 2007). This measurement is based on the content of Trp, Tyr and cystine (disulfide bonds) (Pace et al., 1995). The relationship of absorbance to protein is linear. Using the known ε value, the concentration of the TK was calculated using Beer-Lambert equation (Section 2.2.3.2).

The concentration of purified TK was measured to be 1.58±0.19 mg/mL. The variability of the TK concentration might be due to the OD measurement of the fermentation and the recovery process of the protein, which includes the sonication process and purification.

From the SDS-PAGE analysis, the recovery process of the purified TK was demonstrated. A significant loss of TK was observed during centrifugation process whereby about 10-15% of protein was lost based on the band compared to that of the sonicated sample. This fraction of protein loss was the inclusion bodies that were formed during the high-level expression of *E.coli* cells. The removal of this aggregated protein will ensure there is no misfolded protein presence in the purified TK. The centrifugation processes were carried out twice with the first step was the recovery of the pellet after the fermentation. The purity of His-tagged purified TK was consistently high (>90%) indicating that the purification process with Ni-NTA superflow cartridge was effective in removing the vast majority of the contaminants.

Finally, the Bradford assay (Section 2.2.3) was used to validate the results obtained by the other methods. This simple technique relies on the binding of the dye Coomassie Blue G250 to protein. Bovine serum albumin (BSA) was used for constructing the calibration curve and the absorbance was taken at 595 nm. Results

were found to be in agreement with slight variation in values with this method compared to the previous method. The difference may be subject to variation in sensitivity between individual proteins and impurities presence in the sample (Hammond and Kruger, 1988). Unless the protein is free of other compunds that absorb light at 280 nm, the results will be inaccurate. For example, nucleic acids contain purine and pyrimidine rings that have absorption maxima near 260 nm with considerabe absorption extending to 280 nm. In addition, the variability in the values could also be due to other factors arising from SDS-PAGE preparation, such as the reducing agent used and staining and the staining and destaining processes (Neuhoff et al., 1985).

3.2.2   Investigation of activity of His$_6$-TK in solution

The standard activity of TK was conducted in 96-SRW microwell with total reaction volume of 300 µL (Section 2.7.1). A comparison of activity of purified TK and TK in lysate form was performed for a period of two hours (Figure 3.4). The activity of TK lysate reached 80% after one hour reaction compared to purified TK that only achieved 64% conversion. The concentration of enzyme used in the reaction was 0.1 mg/mL and 0.05 mg/mL for lysate and purified TK respectively. When normalised by the corresponding amount of enzyme, the specific activity of erythrulose formation were 19 ± 0.25 $\mu mol.min^{-1}.mg^{-1}$ (lysate) and 23 ± 0.13 $\mu mol.min^{-1}.mg^{-1}$ (purified His$_6$-TK).

These results indicate that productivity per unit of enzyme of purified His$_6$-TK was higher than lysate, which was likely due to less competing side reactions present. Despite losing some enzyme during the purification, this data suggests that the purification procedure had no detrimental effect on the His$_6$-TK enzyme activity. Therefore, further bioconversion studies were performed using the His$_6$-TK in purified form.

(a)
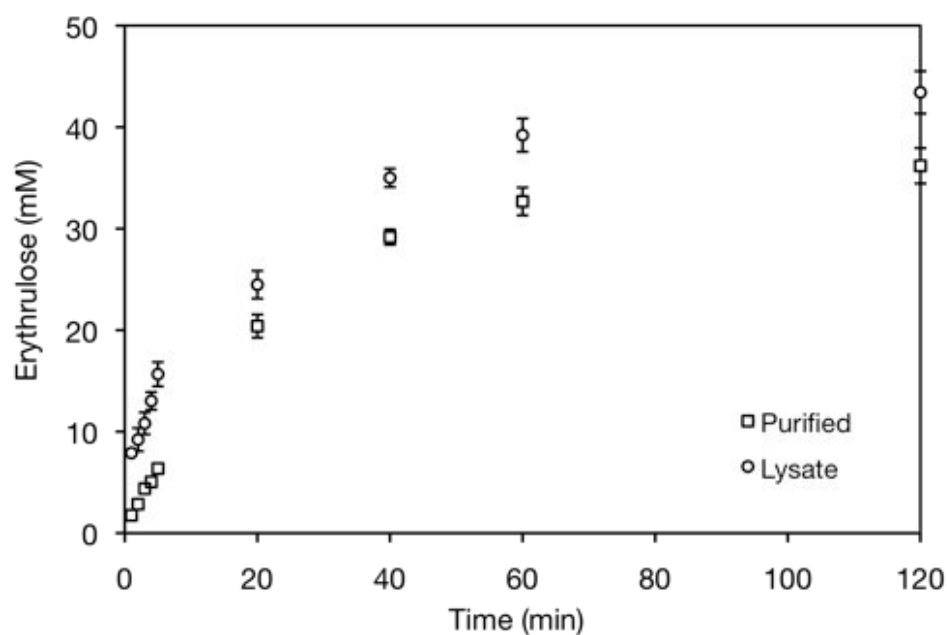
(b)
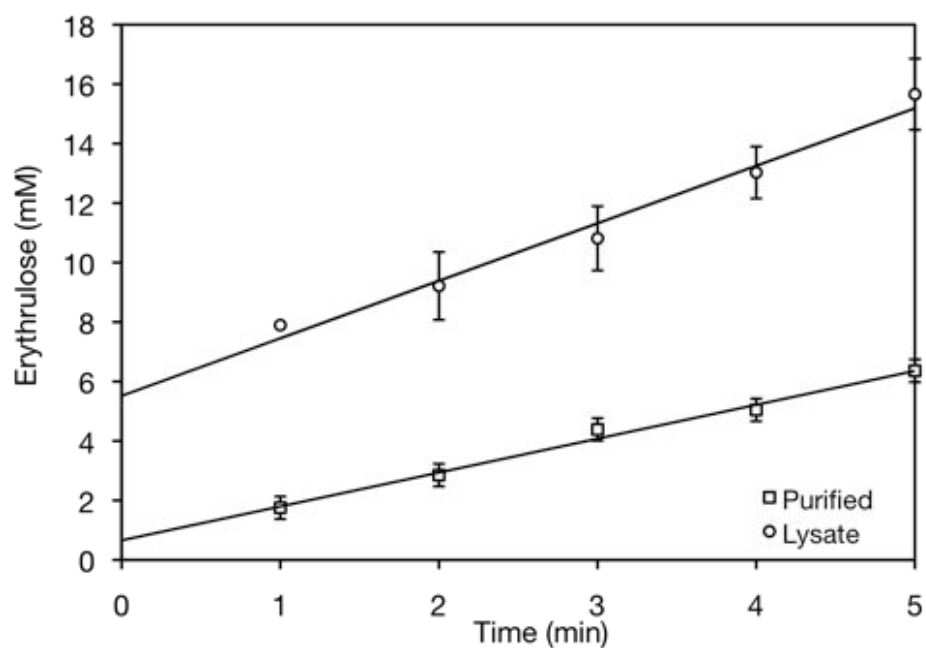
Figure 3.4: Activity profile of pure and crude form of His$_6$-TK. Comparison of purified His$_6$-TK with His$_6$-TK in lysate form. (a) The TK reaction profile with model substrate of 50 mM hydroxypyruvate (HPA) and 50 mM glycolaldehyde (GA) in 50 mM Tris−HCl buffer, pH 7.0 with cofactors thiamine pyrophosphate (TPP), 2.4 mM and MgCl$_2$, 9 mM at room temperature (Section 2.7.1). Concentration of enzyme used for purified TK was 0.05 mg/mL and lysate was 0.1 mg/mL in 300 μL total volume reaction. (b) Initial reaction rates of purified and lysate His$_6$-TK. Error bars represent one standard deviation about the mean (n = 2)

3.2.3 Investigation of His$_6$-TK storage stability

Understanding the stability of an enzyme is paramount to both commercial and scientific interest. There are several parameters that can be studied to determine the stability of an enzyme such as temperature, pH, oxidative stress, solvent used and presence of surfactant (Eijsink et al., 2005). Mitra et al. (1998) evaluated the stability of TK based on the effect of pH and substrates, while Jahromi et al. (2011) further investigated the effect of organic solvents, extreme pH and high temperature on the activity and stability of TK. To date there is no reported data on TK stability at different storage conditions. The viability and activity of TK over time is very important to ensure the enzyme does not degrade nor destabilise during investigation. Any reduction in enzyme activity would compromise the evaluation of the enzymatic behaviour.

Effect of storage at three different temperatures on enzyme stability was investigated. The temperatures selected were 4°C, -20°C and room temperature (22°C). The effect of storage on the stability of TK in the fridge at 4°C was minimal for a period of up to 15 days with average specific activity of 21± 2.16 μmol.min^{-1}.mg^{-1} (Figure 3.5). Significant loss of enzyme activity was observed with only 58% of TK activity was retained after 30 days of storage. For prolonged use of purified TK, the enzyme was best stored in -20°C. The activity of the purified TK was almost constant for up to 30 days and a minimal loss (15%) of activity was observed after 60 days (Figure 3.6). This data suggests that the enzyme is stable for longer period of time, which minimises the number of purifications required to obtain sufficient enzyme for TK activity assays.

Stability of purified TK was evaluated during the first 24 hours at room temperature. Reduced activity was noticed whereby about 22% of enzyme activity loss was observed (Figure 3.7). This assessment is important, as the enzyme will be immobilised in the IEMR for a period of up to 24 hours. However, the evaluation of TK stability in IEMR is not conclusive based on this finding. As the reaction was conducted in solution phase, they were likely to be less representative of the immobilised TK. Significant improvements are usually observed with immobilised

enzyme in storage and operational stability as well as decreased autolysis reaction (Sakai-Kato et al., 2002; Nomura et al., 2004; Fernandes, 2010).

Enhanced stability of immobilised TK on derivatised surface capillary was reported by Matosevic et al. (2009) with constant activity up to 96 hours. Moreover, the stability of TK immobilised on different resins were studied, where Eupergit-C® matrix (Brocklebank et al., 1996) showed to be stable for up to 5 hours reaction while immobilisation on Sepharose 4B matrix (Kochetov & Solocbeva, 1977) was reported to retain 50% of its specific activity compared to the free enzyme. While some immobilisation proved to increase the enzyme stability, the type of immobilisation or matrixes used plays an important role in determining the stability of an enzyme.

(a)
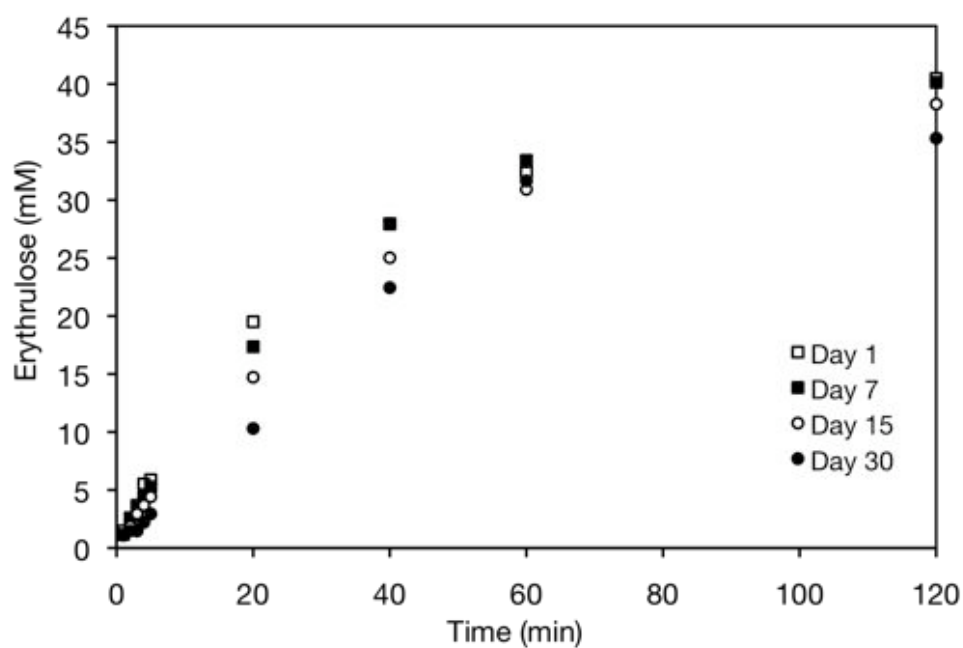
(b)
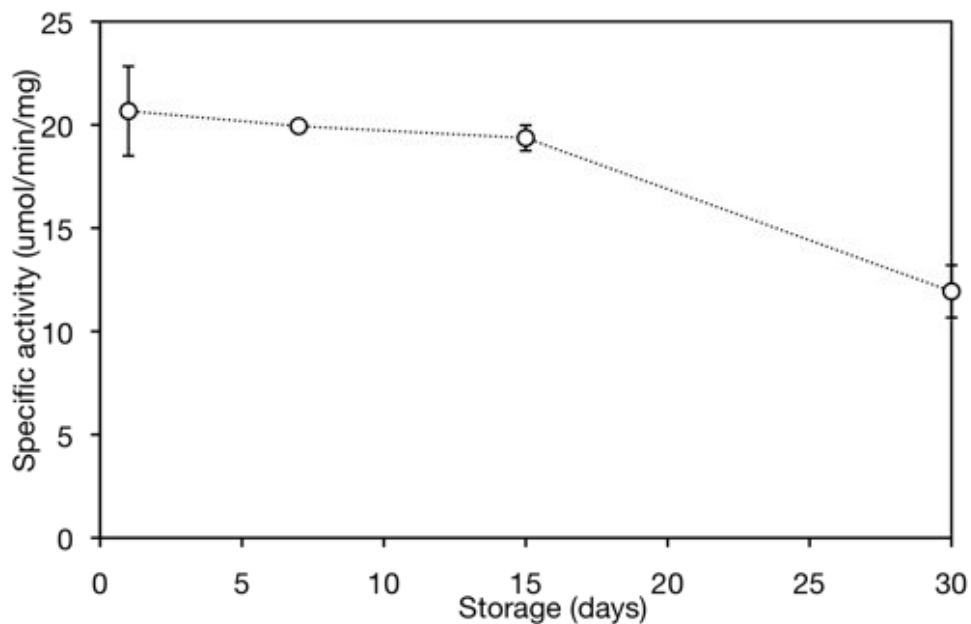
Figure 3.5: Stability of His$_6$-TK upon storage at 4°C. (a) Graph showing the production of erythrulose by purified His$_6$-TK assessed at different time. (b) Specific activity of His$_6$-TK measured over a period of 30 days. The assays were conducted with 50 mM HPA and GA (Section 2.7.1) with enzyme concentration of 0.05 mg/mL. Error bars represent one standard deviation about the mean (n = 2)

(a)

(b)
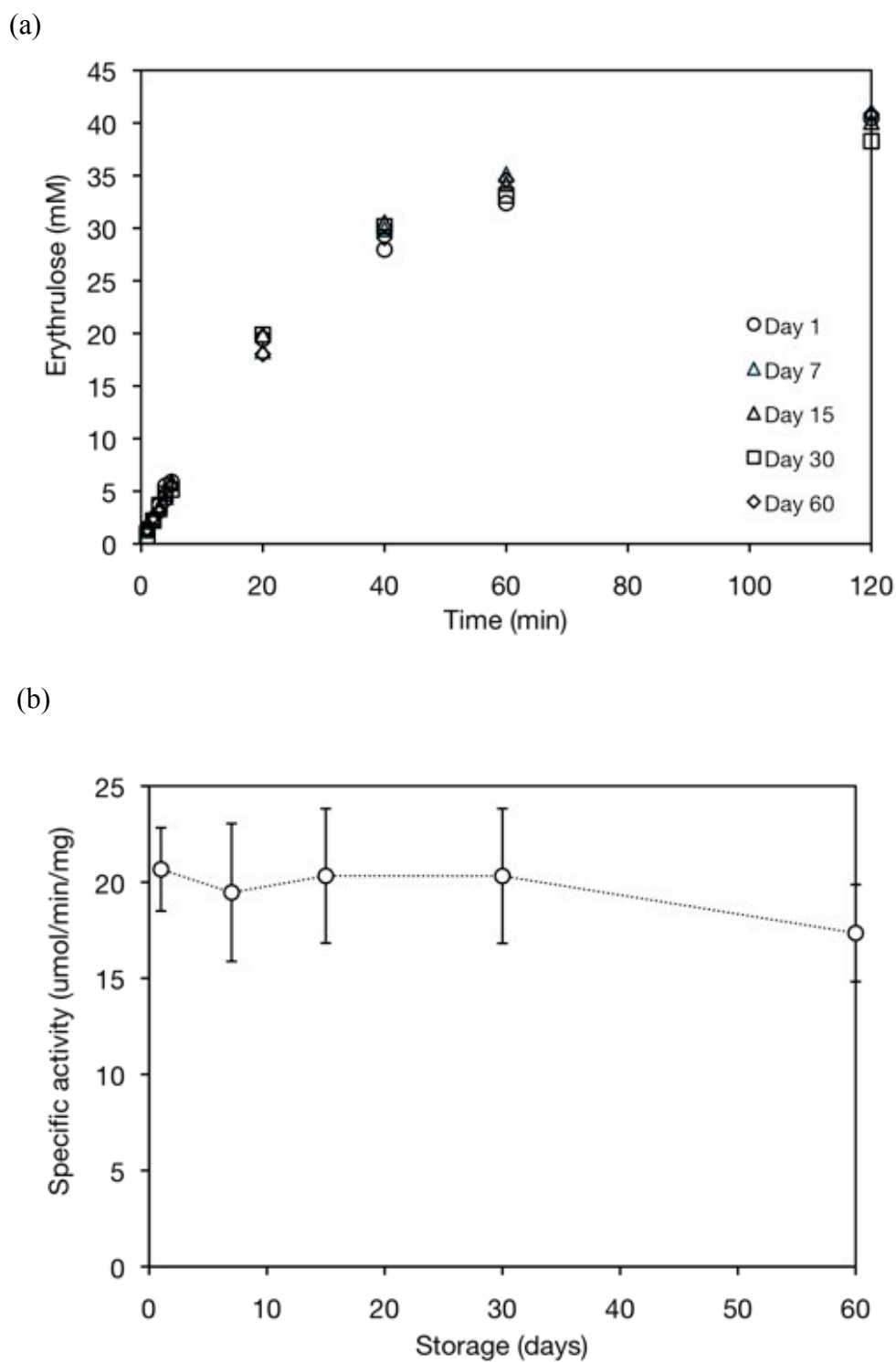
Figure 3.6: Stability of His$_6$-TK upon storage at -20°C. (a) Graph showing the production of erythrulose by purified His$_6$-TK assessed at different time. (b) Specific activity of His$_6$-TK measured over a period of 60 days. The assays were conducted with 50 mM HPA and GA (Section 2.7.1) with enzyme concentration of 0.05 mg/mL. Error bars represent one standard deviation about the mean (n = 2)

(a)
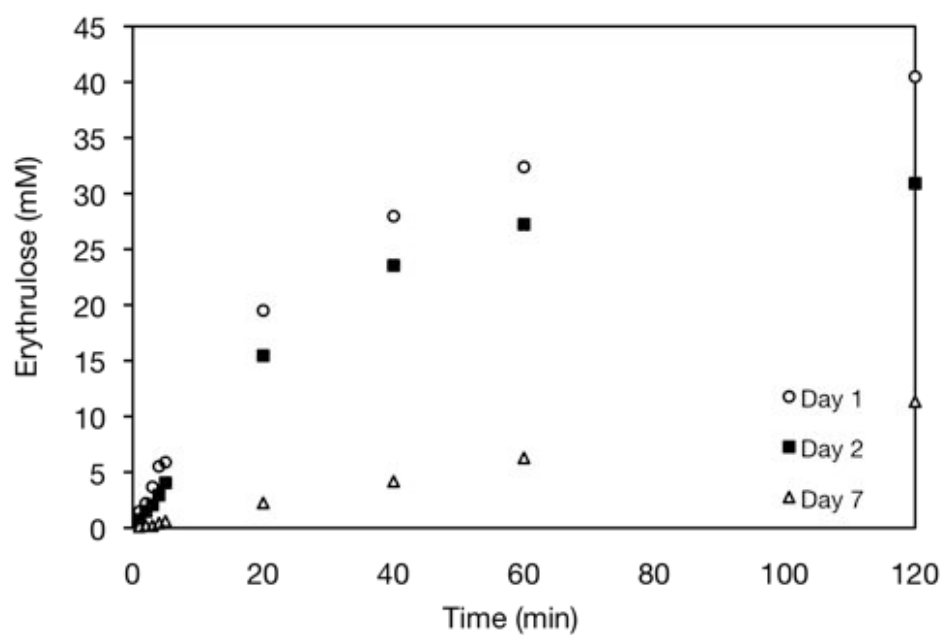
(b)
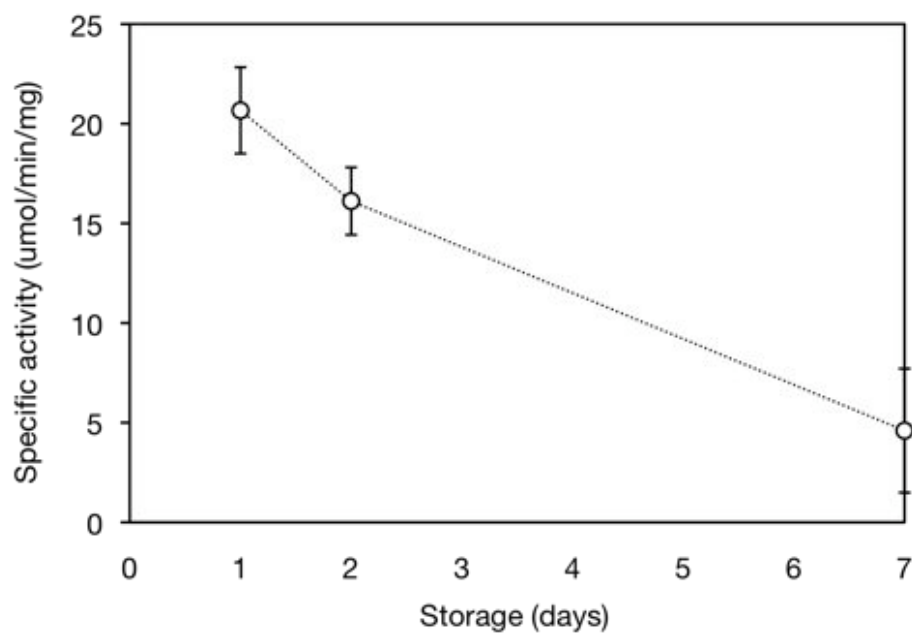
Figure 3.7: Stability of His$_6$-TK upon storage at room temperature. (a) Graph showing the production of erythrulose by purified His$_6$-TK assessed at different time. (b) Specific activity of His$_6$-TK measured over a period of 7 days. The assays were conducted with 50 mM HPA and GA (Section 2.7.1) with enzyme concentration of 0.05 mg/mL. Error bars represent one standard deviation about the mean (n = 2)

3.2.4   Effect of dialysis and desalting on the activity of His$_6$-TK form

Further investigation on the effect of dialysis and desalting on the TK activity in solution was carried out using the standard protocol for TK activity assay (Section 2.7.1). The activity of His$_6$-TK showed to be comparable for both methods with initial rates of 1.015±0.13 mM/min and 1.02±0.14 mM/min for dialysis and desalting column, respectively (Figure 3.8). However, the desalting column appeared to be more preferable due to its simpler protocol and high efficiency in removing imidazole. This method was adopted for the post purification process.
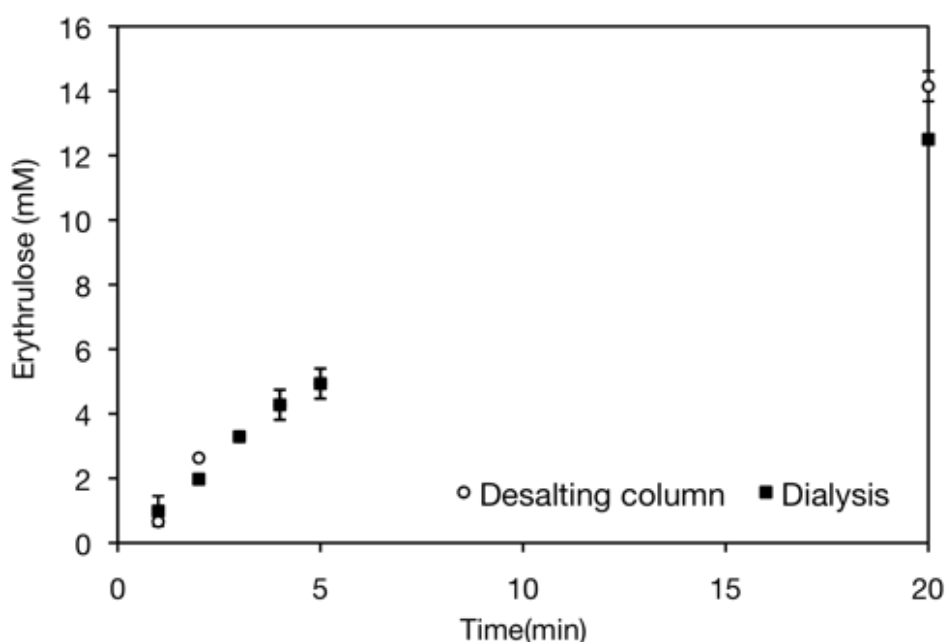
Figure 3.8: Activity of purified His$_6$-TK following dialysis and desalting process. Dialysis (Section 2.5) and desalting process (Section 2.6) were carried out for post purification process for the removal of imidazole. The assay was conducted with 50 mM HPA and GA (Section 2.7.1) with enzyme concentration of 0.05mg/mL. Error bars represent one standard deviation about the mean (n = 2)

3.2.5 Kinetic data of purified His$_6$-TK in solution phase

Determination of kinetic data is important in order to quantify and predict specific chemical reactions catalysed by the enzyme. The most common model to study the kinetics is Michaelis–Menten model (Michaelis & Menten, 1913). The Michaelis–Menten equation (Eq. 3.1) relates the initial reaction rate v to the substrate concentration [S]. The corresponding graph is a rectangular hyperbolic function (Figure 3.9); the maximum rate is described as V_{max}.

$$v = \frac{V_{max}[S]}{K_m + [S]}$$

(3.1)

Where K_m = Michaelis Menten constant, [S] = substrate concentration, v = initial rate of product formation, and V_{max} = maximum reaction rate of product formation.

The Michaelis constant is an approximation of the affinity of the enzyme for the substrate based on the rate constants within the reaction, which is equivalent to the substrate concentration when the rate of conversion is half of V_{max}. Smaller K_m value indicates higher affinity towards the enzyme, hence will approach V_{max} more quicker. Very high [S] values are required to approach V_{max}, which is reached only when [S] is high enough to saturate the enzyme.
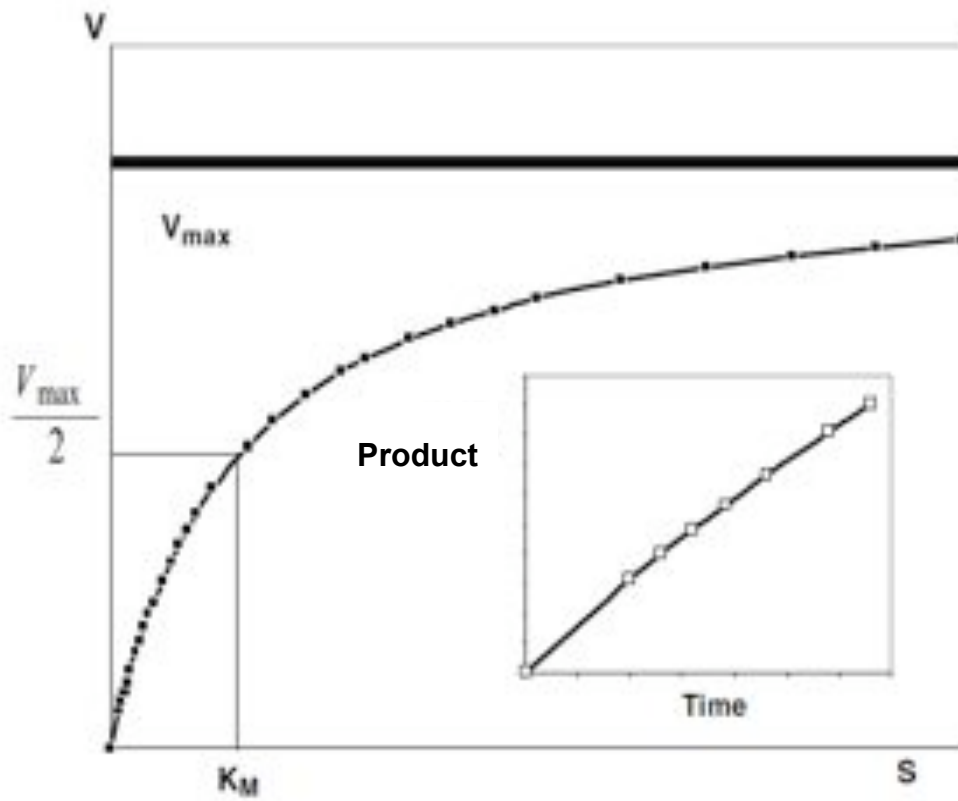
Figure 3.9: Michaelis-Menten representation of enzyme activity data. V represents the initial velocity rate of a given enzyme reaction and is calculated from the initial portion of the measurement as depicted in the inset. S is the limiting substrate concentration for each rate experiment. Image reproduced from (Cooney, 2011).

In order to evaluate the His$_6$-TK enzyme kinetics, the reaction rates were first measured at different substrate concentrations (Figure 3.10). These data were used to construct Lineweaver-Burk and Eadie-Hofstee plots. Enzyme kinetics was shown to have no significant inhibition by the products within the substrates concentration range studied. The K_m and V$_{max}$ values estimated from both plots showed to be in agreement with slight difference in their estimation of kinetic parameters for His$_6$-TK (Table 3.1). The Michaelis constant for GA of 37 mM obtained in this study was of the same magnitude as the value of 16 mM (Chen et al., 2009), 16.1 mM (Gyamerah et al., 1997) and 14 mM (Sprenger et al., 1995) reported in previous studies.

Comparable Michaelis constant value was also obtained for HPA which was 21 mM as compared to 18 mM (Chen et al., 2009), 13.2 mM (Gyamerah et al., 1997) and 18 mM (Sprenger et al., 1995) reported from the same studies. The difference in values may be accounted for the fact that our assays were performed using a purified His$_6$-TK compared to lysate in the described studies. Variation of pH, temperature and the way the assay was conducted could also have contributed to the variation in the results produced. Data of the kinetic parameters in various studies was summarized in Table 3.2.

(a)
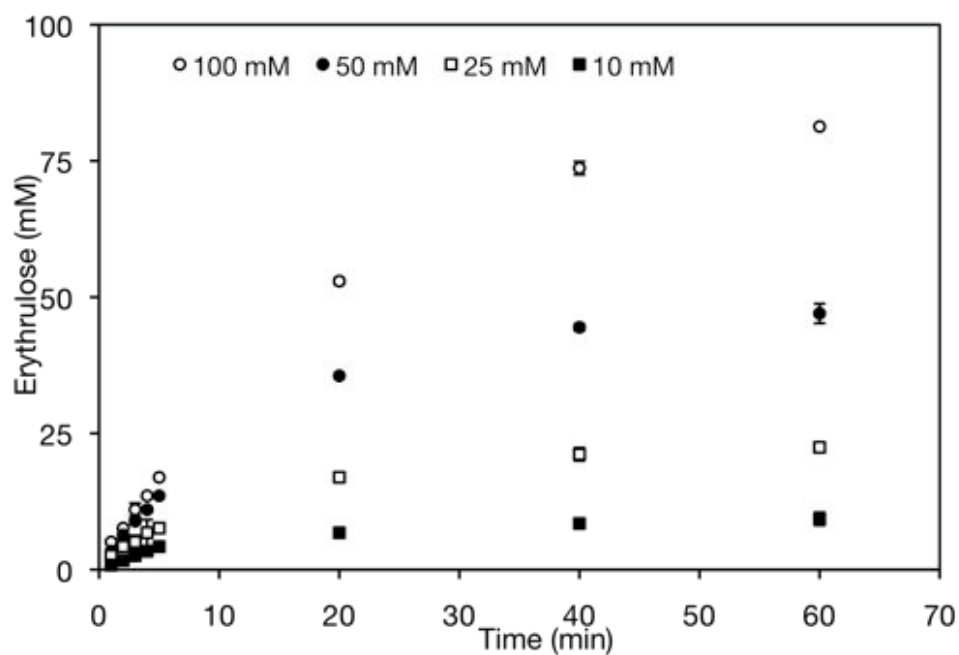
(b)
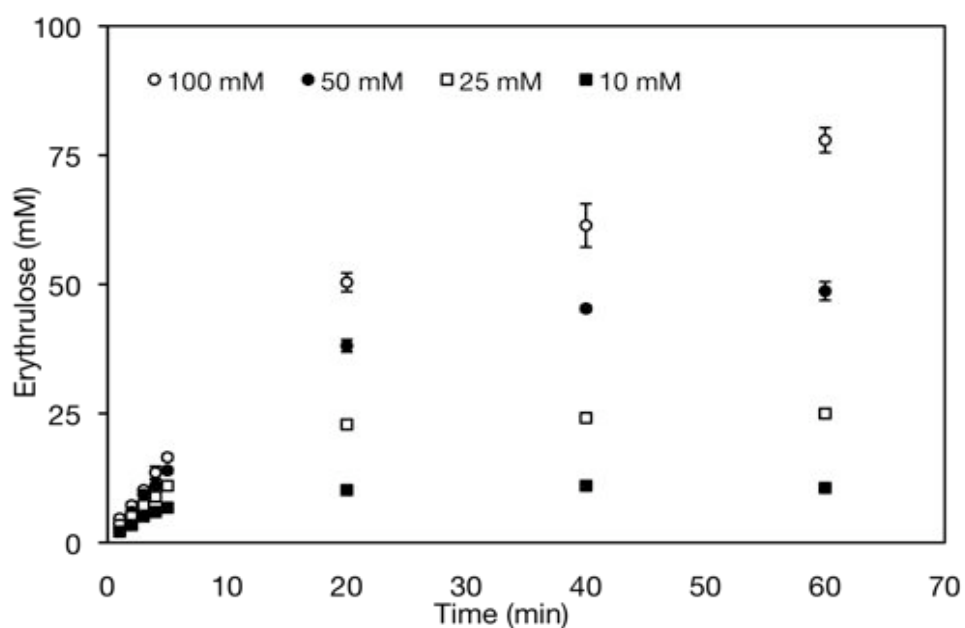
Figure 3.10: Purified His$_6$-TK activity assay at different substrate concentrations. Erythrulose formation over 60 min reaction with different substrate concentration. (a) Reaction with various glycolaldehdye (GA) concentrations (100-10 mM) when the concentration of second substrate hydroxypyruvate (HPA) was kept constant at 100 mM, (b) Reaction with various hydroxypyruvate (HPA) concentrations (100-10 mM) when the concentration of second substrate glycolaldehyde (GA) was kept at 100 mM. Reactions were performed as described in Section 2.7.4 and His$_6$-TK concentration of 0.05 mg/mL was used. Error bars represent one standard deviation about the mean (n = 3).

(a)
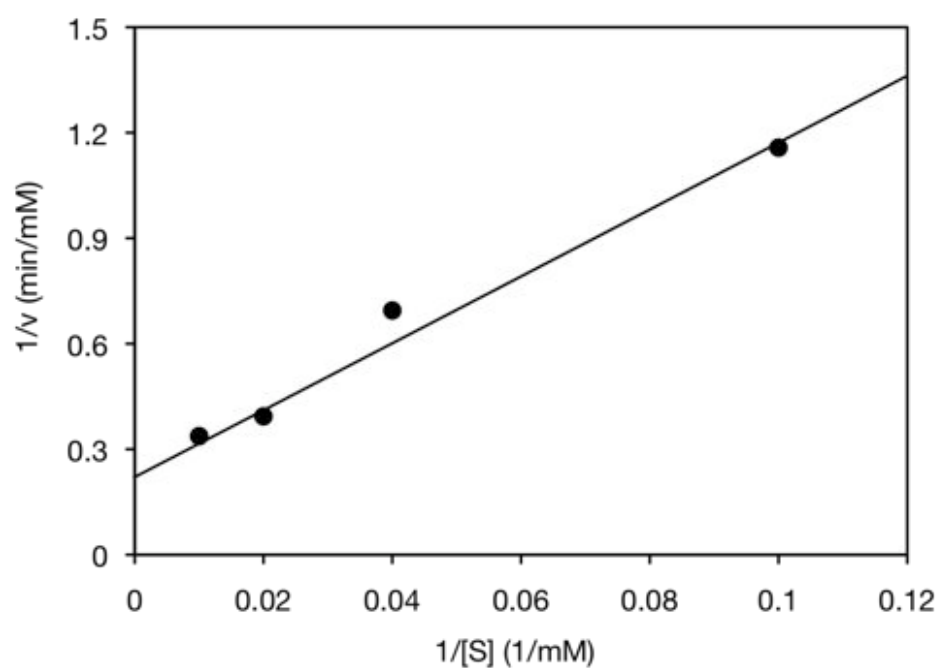
(b)
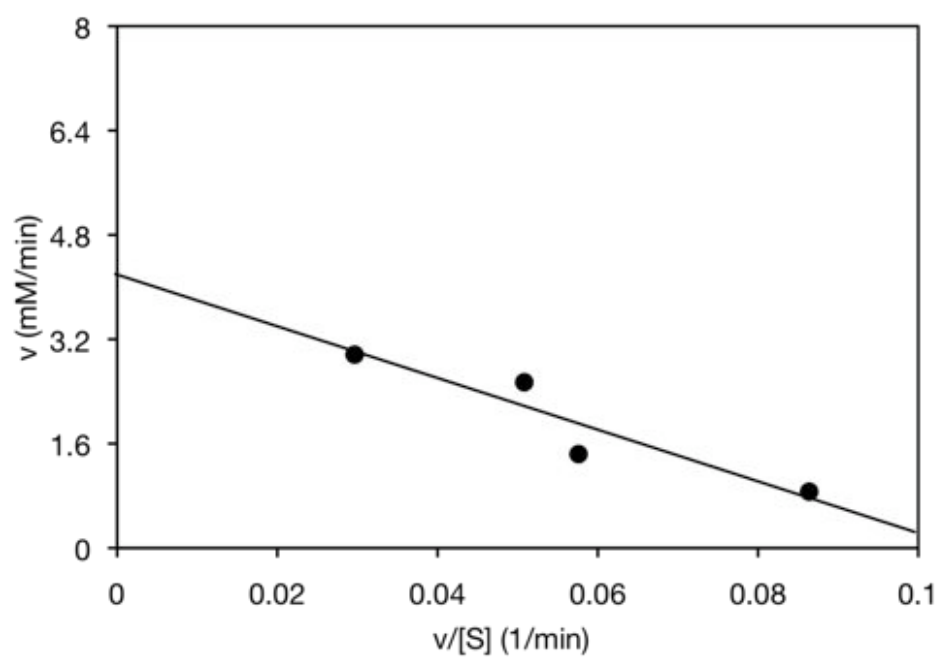
Figure 3.11 Kinetic analysis of purified His$_6$-TK in solution phase. (a) Lineweaver-Burke and (b) Eadie-Hofstee plots. Initial rate data for different glycolaldehyde (GA) concentrations was used to obtain these plots. K_m values obtained with both plots were in agreement.

(a)
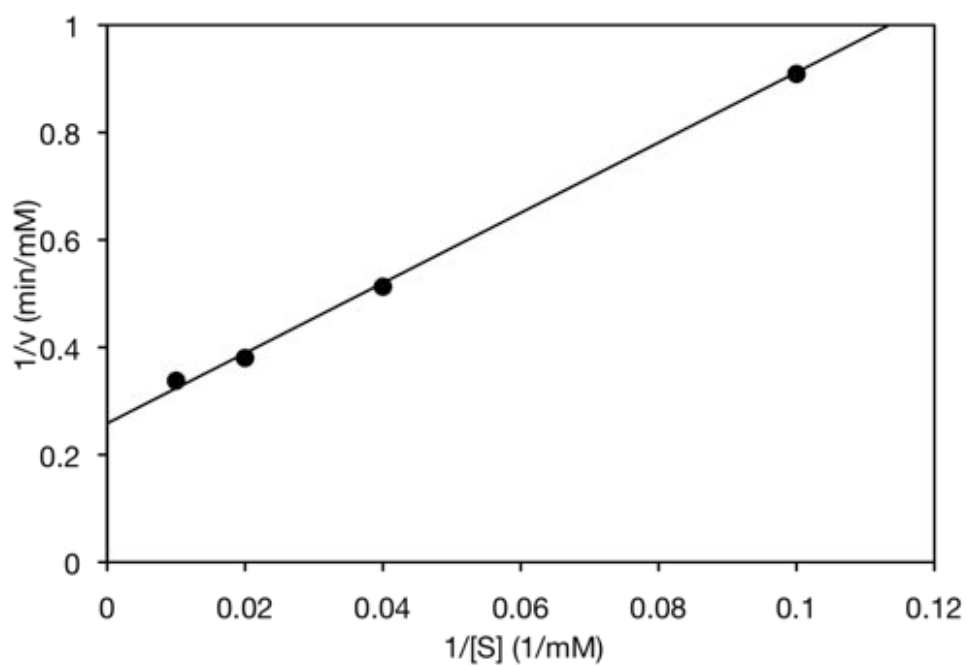
(b)
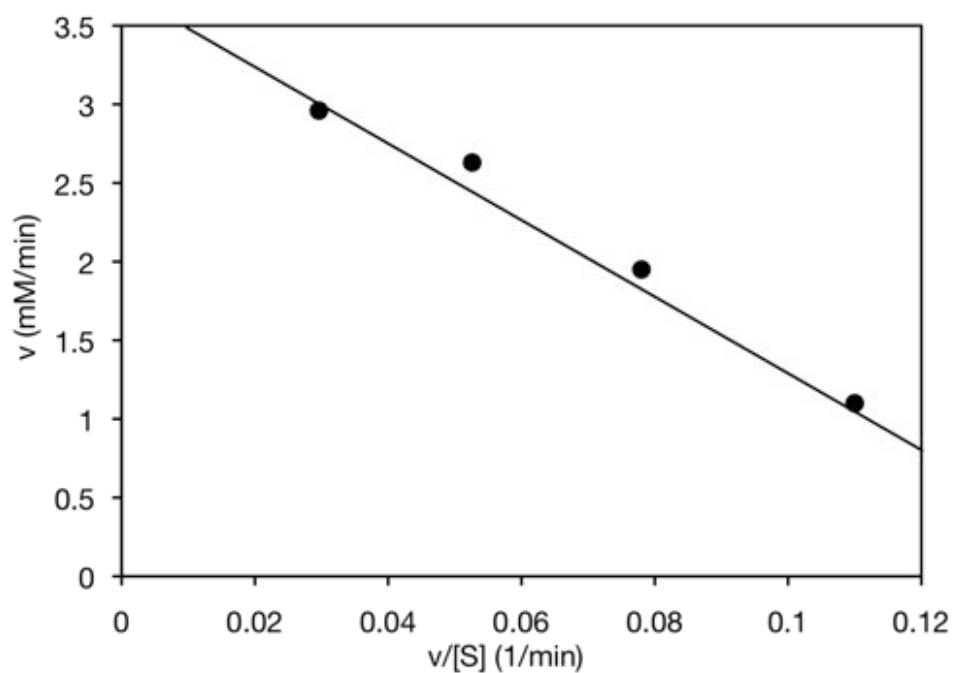
Figure 3.12: Kinetic analysis of purified His_6-TK in solution phase. (a) Lineweaver-Burke and (b) Eadie-Hofstee plots. Initial rate data for different hydroxypyruvate (HPA) concentrations was used to obtain these plots. K_m values obtained with both plots were in agreement.

Table 3.1: Kinetic parameters for purified His$_6$-TK in solution phase. Comparison of kinetic parameters analysed using Lineweaver-Burke and Eadie-Hofstee plots (Figure 3.11 and Figure 3.12). Table shows mean values ± one standard deviation (n=3).

	Michaelis-Menten kinetic parameters			
	Lineweaver-Burke		Eadiee-Hofstee	
	V_{max} (mM/min)	K_m (mM)	V_{max} (mM/min)	K_m (mM)
Glycolaldehyde (GA)	3.8±0.3	35±1	4±0.1	37±1
Hydroxypyruvate (HPA)	3.7±0.3	21±5	3.7±0.1	21±4

Table 3.2: Summary of kinetic parameters for transketolase reaction using HPA and GA as substrate model in various studies.

Kinetic parameters	This work	(Chen et al., 2009)	(Gyamerah et al., 1997)	(Sprenger et al., 1995)
K_m for HPA (mM)	21	18	13.2	18
K_m for GA (mM)	37	16	16.1	16.1
V_{max} (mM/min)	4.0	-	5.3	-
k_{cat} (s^{-1})	95	40.7	84.6	-

3.3 Characterisation of Transaminase (TAm) enzyme

3.3.1 Transaminase production

3.3.1.1 Production of His$_6$−TAm by *E.coli* fermentation

The *E.coli* (containing plasmid pQR801) (Kaulmann et al., 2007) expressing ω–TAm from *C. violaceum* was firstly grown in a 2 L flask with working volume of 200 mL for 7-8 hours at 37°C and 250 rpm (Section 2.2.1). Optical density (OD) of the solution was measured every hour at 600 nm to check for bacterial growth at stationary phase. 0.2 mM IPTG was added after 2 hours fermentation (early exponential phase). The growth of the cells begins to reach stationary phase after seven hours fermentation and the optical density measurement taken at eight hours confirmed the bacterial growth plateau. This data ensures that the bacteria culture is harvested at the optimum level, hence offering substantial amount of TAm for the subsequent purification step. Following fermentation, 0.2 mM PLP was added to the culture broth to stabilise the cells.

Based on the growth profile, the fermentation underwent a short lag phase, due to the high inoculum volume 10% v/v and as a result of using similar inoculum medium in the fermentation. Following the lag period, growth started in the exponential phase for about 7 hours before it reaches stationary phase. For the particular fermentation data shown in Figure 3.13, the maximum specific growth rate was 0.84 hr^{-1} with a doubling time, t_d of 0.83 hr. Similar fermentation procedure was used throughout this project and data shown in Figure 3.13 is representative of each fermentation performed. The expressed His-TAm constituted about 40% of the total cell protein as estimated by SDS-PAGE.
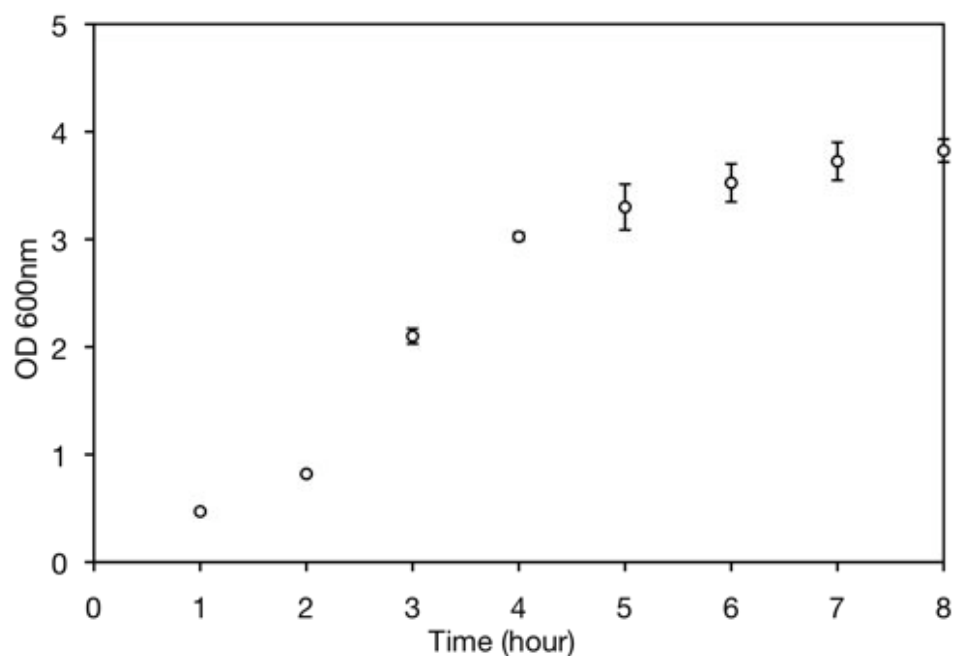
Figure 3.13: Growth of *E.coli* strain BL21gold (DE3) pQR801 expressing His_6−TAm. Cells were cultured in 200 mL LB glycerol media with the addition of 0.15g/L kanamycin, in a 2 L shake flask at 37°C, 250 rpm with a 10% v/v inoculum grown overnight as previously described (Section 2.2.1). 10 g/L of glycerol as the carbon source to the media was added to promote growth. The cell was induced with 0.2 mM of IPTG after 2 hours of fermentation. Growth was monitored by OD_{600nm} measurements (Section 2.2.2). Error bars represent one standard deviation about the mean (n = 3)

3.3.1.2 Purification of His$_6$−tagged TAm

TAm purification was conducted using Ni-NTA superflow cartridge (Qiagen) that is specially designed for histidine tagged protein purification. A similar protocol as the His$_6$-TK purification was adopted with additional of 0.2 mM of PLP in the purification buffers (Section 2.4). The presence of the PLP stabilises the enzyme by covalently binding to the apoenzyme via internal aldimine linkage with the ε-amino group of an active −site lysine (Shin et al. 2003).

The desalting process was carried out after the purification, to remove the remaining imidazole (Section 2.6). The purification process was monitored and analysed by running some samples on the SDS-PAGE and quantification by Bradford assay and spectrophotometer at 280 nm.

From the SDS-PAGE analysis, the recovery process of the purified His$_6$-TAm was demonstrated (Figure 3.14). A significant loss of His$_6$-TAm was seen during centrifugation, with about 40-50% loss based on the band compared to the sonicated sample. This was due to the inclusion bodies formation, which was previously observed by Ingram et al. (2007). The purification column produced high purity of His$_6$-TAm as indicated by the band appeared in the SDS-PAGE gel with almost >90% purity was achieved. The concentration of His$_6$-TAm was determined by the Bradford assay with an average concentration of 2.4±0.2 mg/mL. The value obtained was in agreement with spectrophotometer reading (Section 2.2.3.2). The reading was blanked with 0.2 mM PLP to reduce any background noise.
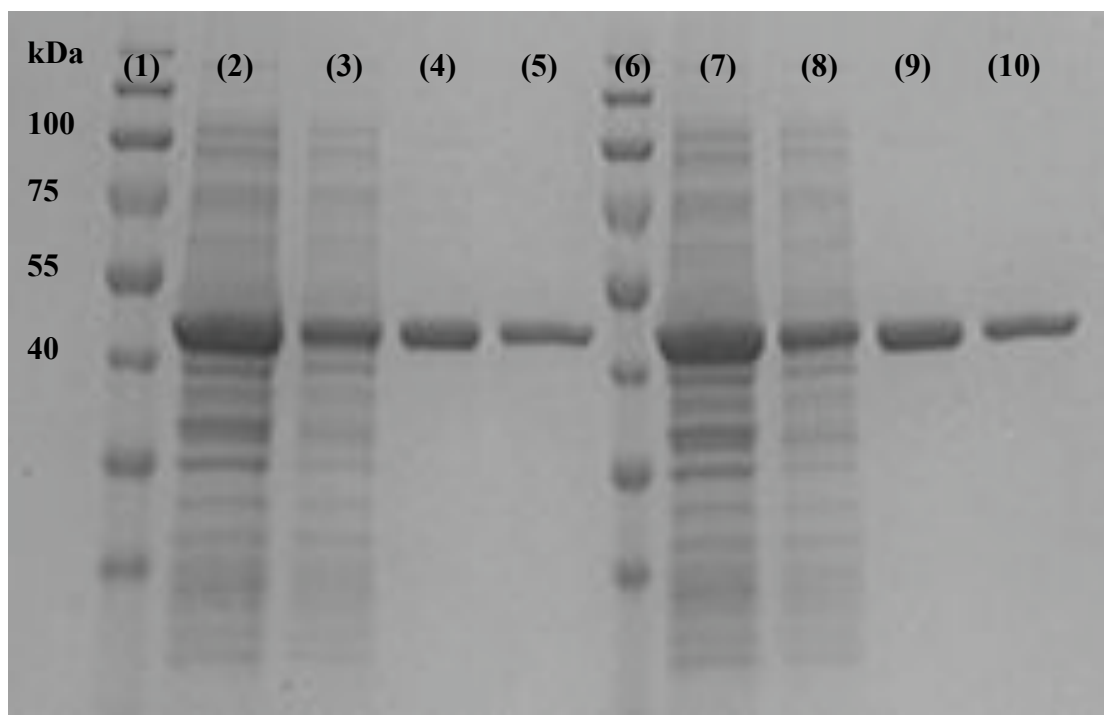
Figure 3.14: Purification of His$_6$−tagged transaminase. His$_6$−tagged TAm was purified from 200 mL culture scale using Ni-NTA superflow cartridge. The TAm band in each lane at 50 kDa corresponds to the monomeric form of the enzyme. Lane (1 and 6) protein marker, (2 and 7) *E.coli* lysate obtained by sonication, (3 and 8) supernatant following sonication and centrifugation, (4 and 9) purified His$_6$-TAm eluted with a 250 mM solution of imidazole, (5 and 10) purified His$_6$-TAm following removal of imidazole by desalting method. His$_6$-TAm was determined to make up about 40% of the total cell protein. Purification performed as described in Section 2.4.

3.3.2 Investigation of His$_6$- TAm activity in solution

His$_6$-TAm activity was demonstrated using MBA and ERY model substrates with cofactor PLP to produce ABT and AP (Section 2.7.2). The formation of the second product (ABT) was confirmed to follow the formation of AP by derivatising the ABT sample (Section 2.8). This allows for the ABT to be detected through HPLC. The mass balance of the product was consistent, with the AP and ABT formation was similar within error (Figure 3.15).

Similar activity of TAm from *C. violaceum* was reported for using MBA and ERY as model substrates with the enzyme in lysate (Kaulmann et al., 2007). With 0.45 U/mL of TAm, about 3% conversion was observed after one hour of reaction. On the other hand, higher conversion (84% in one hour) was achieved with pyruvate as the amino acceptor (Kaulmann et al., 2007). The activity of enzyme in lysate reached 37% conversion after one hour of incubation, whereas it was 25% for the purified enzyme (Figure 3.16). However, when normalised by the amount of enzyme present in the reaction, the specific activity of enzyme in lysate (0.13±0.03 μmol/min/mg) was slightly lower than that of the purified enzyme (0.15±0.04 μmol/min/mg). These values suggest that purification process had no adverse effect on the enzyme activity. Further bioconversion studies were performed using His$_6$-TAm in purified form unless stated otherwise.
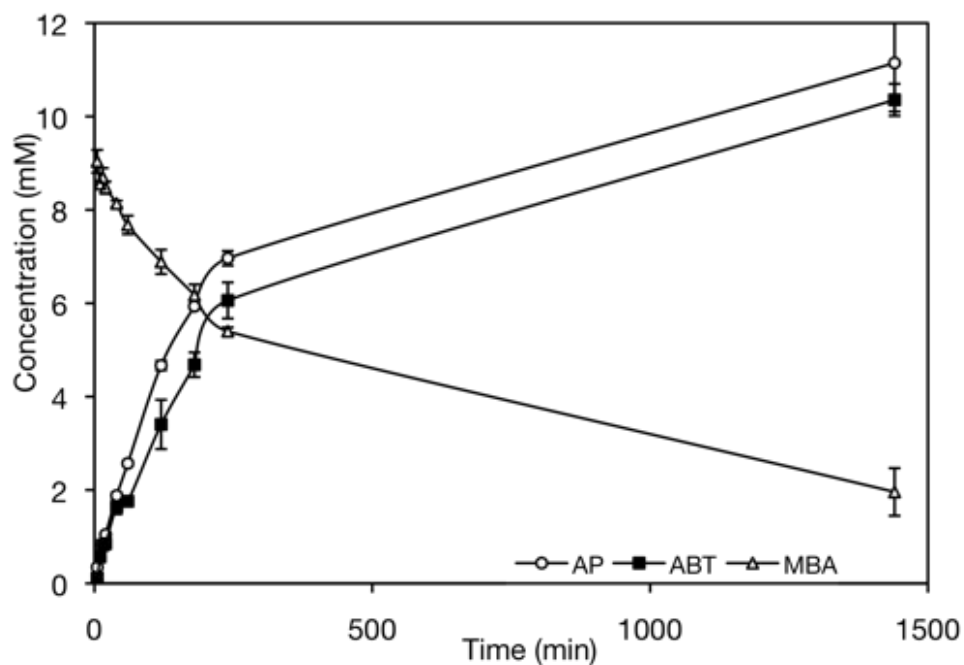
Figure 3.15: Profile of His$_6$-TAm reaction with analysis of MBA depletion, AP and ABT formation. His$_6$-TAm model reaction with 10 mM of (S)-α- methylbenzylamine (MBA) and 100 mM of L−erythrulose (Ery) as model substrates with 0.2 mM pyridoxal phosphate (PLP) to produce acetophenone (AP) and 2-amino-1,3,4-butanetriol (ABT), pH 7.5 and at room temperature (Section 2.7.2). Reaction was monitored on the depletion of MBA and production of AP and ABT by HPLC. Concentration of His$_6$-TAm used was 0.3 mg/mL in this reaction. Error bars represent one standard deviation about the mean (n = 3).

(a)
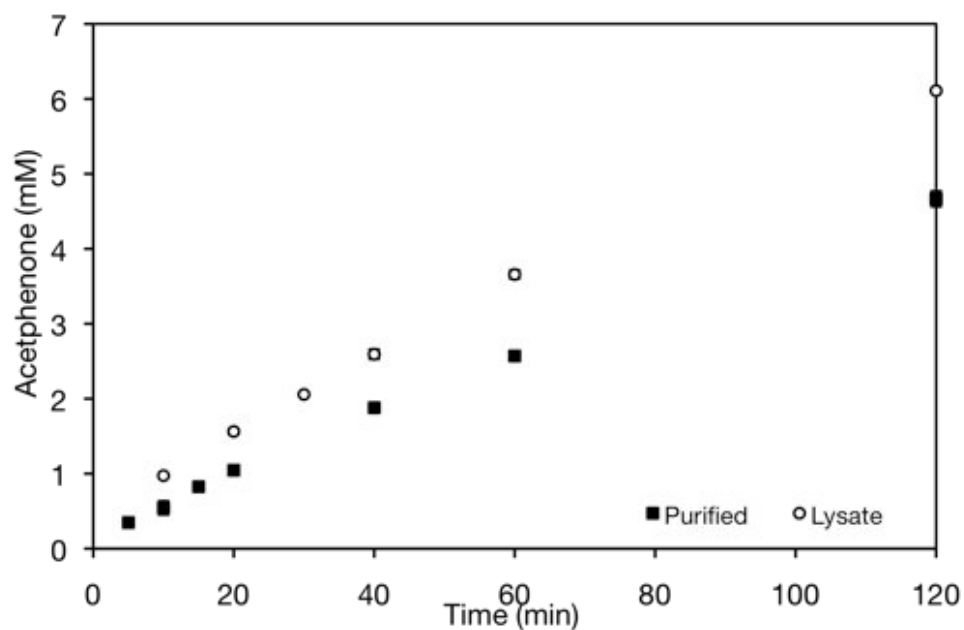
(b)
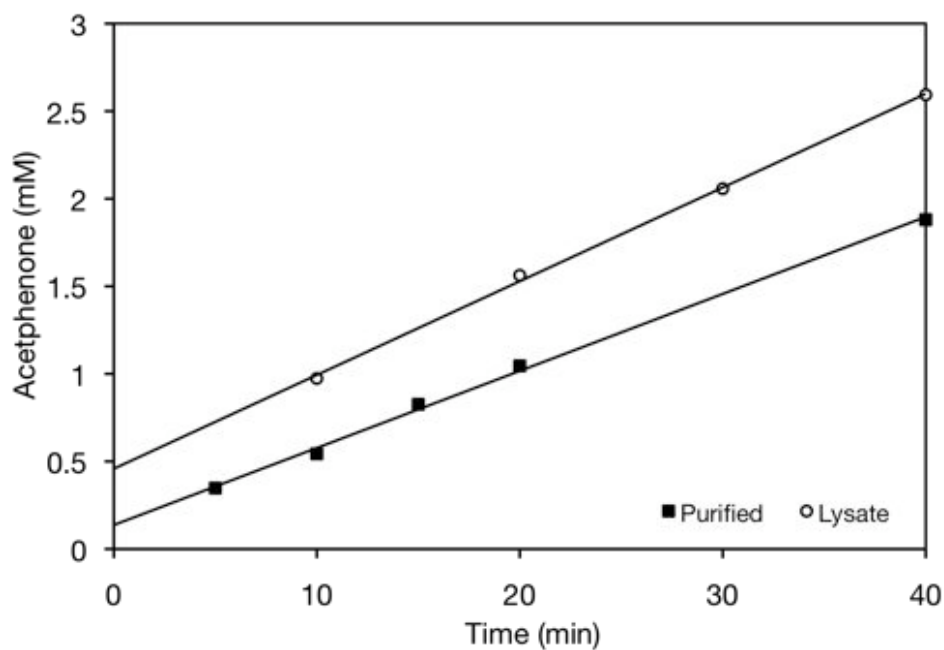
Figure 3.16: Activity profile of pure and crude form of His_6-TAm. Comparison of purified His_6-TAm with His_6-TAm in lysate form. (a) The TAm reaction profile with model substrate of 10 mM (S)-α- methylbenzylamine (MBA) and 100 mM L−erythrulose (ERY) in 50 mM Tris−HCl buffer, pH 7.5 with cofactor 0.2 mM pyridoxal phosphate (PLP) at room temperature (Section 2.7.2). Concentration of enzyme used for purified TAm was 0.3 mg/mL and lysate was 0.4 mg/mL in 300 μL total volume reaction. (b) Initial reaction rates of purified and lysate His_6-TAm.

3.3.3 Product inhibition effect on His$_6$-TAm

In spite of the many advantages that TAm offers, such as broad substrate specificity, high turnover rate and high stability, the industrial use of TAm has been limited, due to the low equilibrium constant of the transaminase reaction (Shin et al., 2003; Yun et al., 2005; Kaulmann et al., 2007). Moreover, high concentration of substrate in TAm bioconversion will become impractical as it would cause severe product inhibition (Shin & Kim, 1999). Ketone product was reported to inhibit the enzyme activity in ω-TAm from *V. fluvialis* JS17 (Shin & Kim, 1999; Shin & Kim, 2002; Shin et al., 2003). Similar inhibition was observed with ω-TAm from *C. violaceum* with exception of few amine acceptors (pyruvate, glyoxylate and benzaldehyde) that allowed for ≥90% conversion (Kaulmann et al., 2007).

A time course study was performed with MBA and ERY until no more conversion was observed. Equimolar concentration of substrate was used (50 mM MBA and ERY) and the reaction was monitored for 24 hours (Section 2.7.2). The reaction reached equilibrium after 6 hours and no increment in product formation was observed after 24 hours with the final reaction yield of only 17% (Figure 3.17). The low conversion observed here displayed the unfavourable equilibrium seen in many ω-TAm substrates that was influenced by a strong by-product (AP) inhibition. Conversely, the bioconversion of 50 mM MBA and pyruvate catalysed by ω-TAm from *Bacillus thuringiensis* JS64 resulted in almost 100% conversion with the equilibrium favouring product formation to produce L-alanine (Shin & Kim, 1998).

Many studies have been done to tackle this inhibition problem. Product can be removed to overcome the equilibrium problem by using whole cell biotransformation (Chao et al., 1999). Shin & Kim (1997) demonstrated an extractive biphasic reaction system that reduced the inhibitory AP concentration in the aqueous phase. However this method may pose a solvent toxicity problem on the enzyme and mass transfer limitation due to the interfacial area (Shin et al., 2001). In addition, an enriched culture method combined with random mutagenesis was shown to significantly reduce product inhibition by aliphatic ketones (Yun et al.,2005).
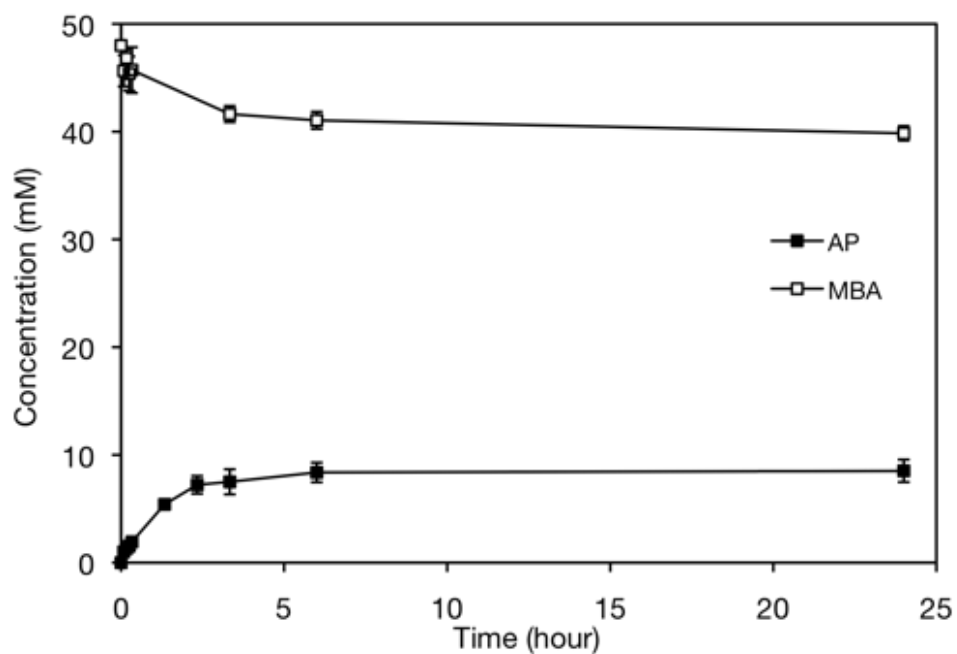
Figure 3.17: Reaction profile of His$_6$-TAm with 50 mM of MBA and 50 mM ERY. Profile of His$_6$-TAm reaction with analysis of MBA depletion and AP formation. Experimental conditions: 0.2 mM pyridoxal phosphate (PLP), pH 7.5 and at room temperature (Section 2.7.2). Concentration of His$_6$-TAm in lysate form used was 1.4 mg/mL. Error bars represent one standard deviation about the mean (n = 3).

3.3.4 Investigation of His$_6$-TAm storage stability

Enzyme stability plays a very important role due to the increasing number of enzyme applications. This study will help to realise the full potential of the enzyme, which reflects the commercial and scientific interest. The majority of enzymes on the market are in their native form and therefore, it is vital to the industrial biochemist to ensure the stability of the enzyme during storage and use. Storage stability of various enzymes under different storage conditions were successfully demonstrated (Cryer & Bartley, 1974; Jones, 1985; Hansen & Shultz, 2001). In general, storage stability tends to decrease significantly with increasing temperature. In pure aqueous solution, rapid inactivation takes place between 50-80°C, which completely destroys the enzyme activity within one to five hours (Euler & Pope, 1912). Alternatively, enzymes can be stored with glycerol solution to enhance their stability.

A similar study was conducted to evaluate the storage stability of His$_6$-TAm at three different storage conditions. His$_6$-TAm productivity dropped to ~70% after 24 hours and was nearly inactive after seven days when stored at room temperature (Figure 3.18). The stability of His$_6$-TAm was improved when stored in 4°C with slight decrease in productivity after three days reaction (Figure 3.19). This small fluctuation might be due to errors during the experiment and the HPLC analysis. However, a significant decline was observed on the enzyme productivity after seven days reaction where His$_6$-TAm only retained 45% of its initial productivity. For prolonged use of purified His$_6$-TAm, the enzyme could be stored at - 20°C for 30 days without any substantial loss of activity (Figure 3.20).

(a)
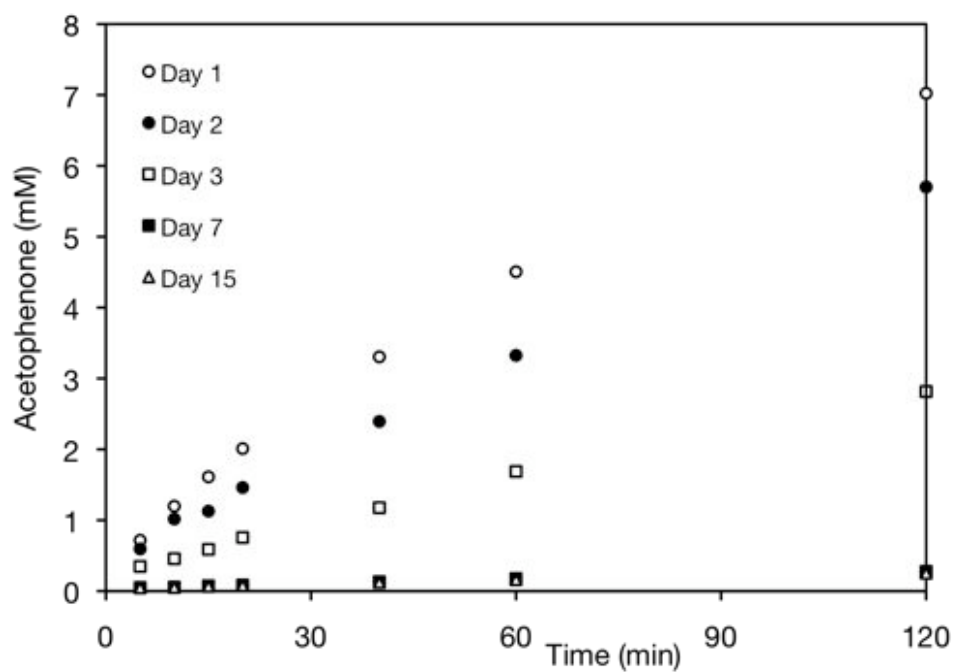
(b)
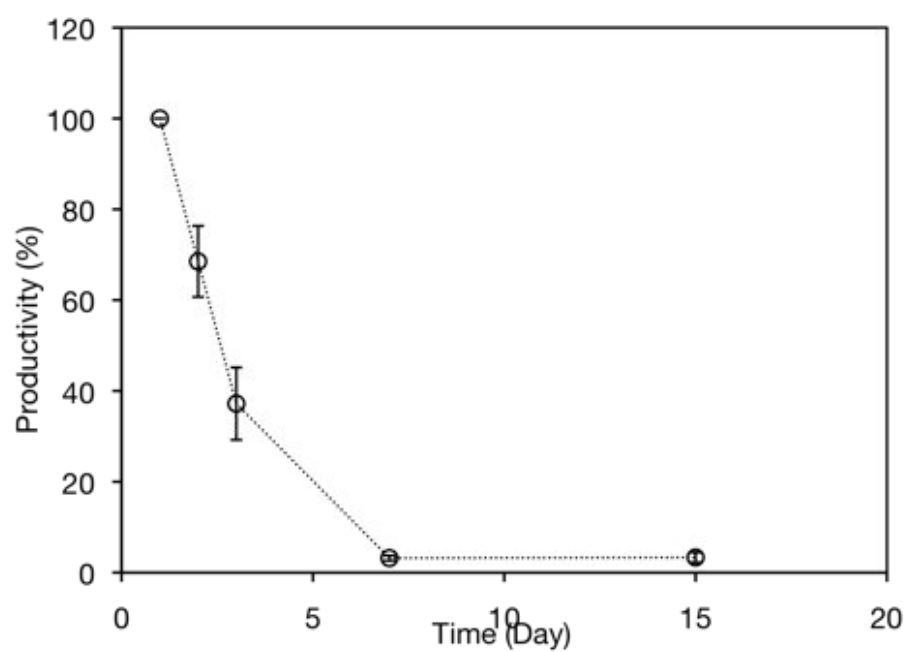
Figure 3.18: Reaction profile of His$_6$-TAm stored at room temperature. (a) Graph showing the production of acetophenone catalysed by purified His$_6$-TAm assessed at different times. (b) Productivity of His$_6$-TAm measured over a period of 15 days. The assay was conducted with 10 mM MBA and 100 mM ERY (Section 2.7.2) with enzyme concentration of 0.5 mg/mL. Error bars represent one standard deviation about the mean (n = 3).

(a)
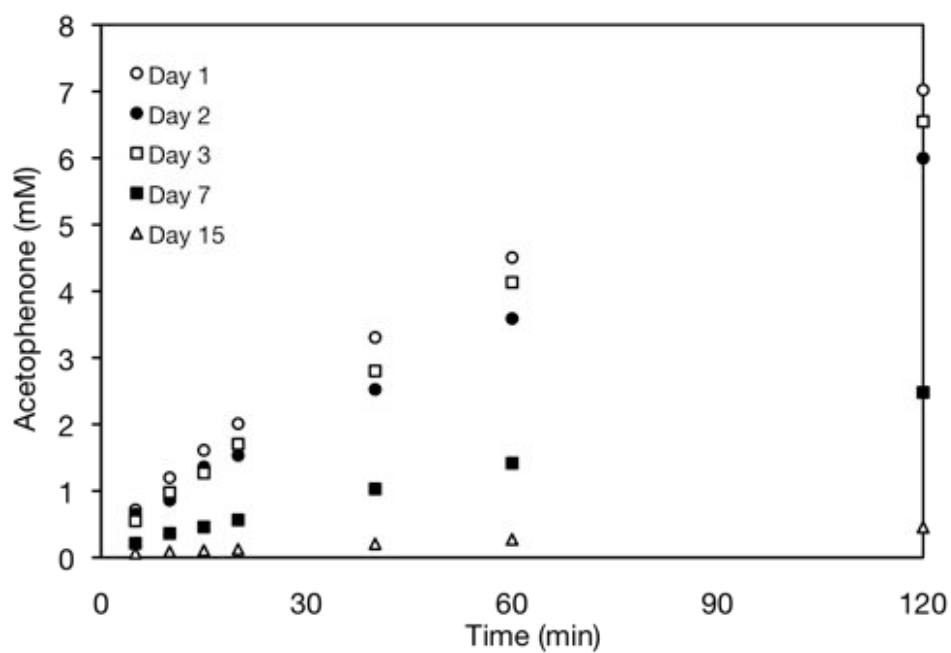
(b)
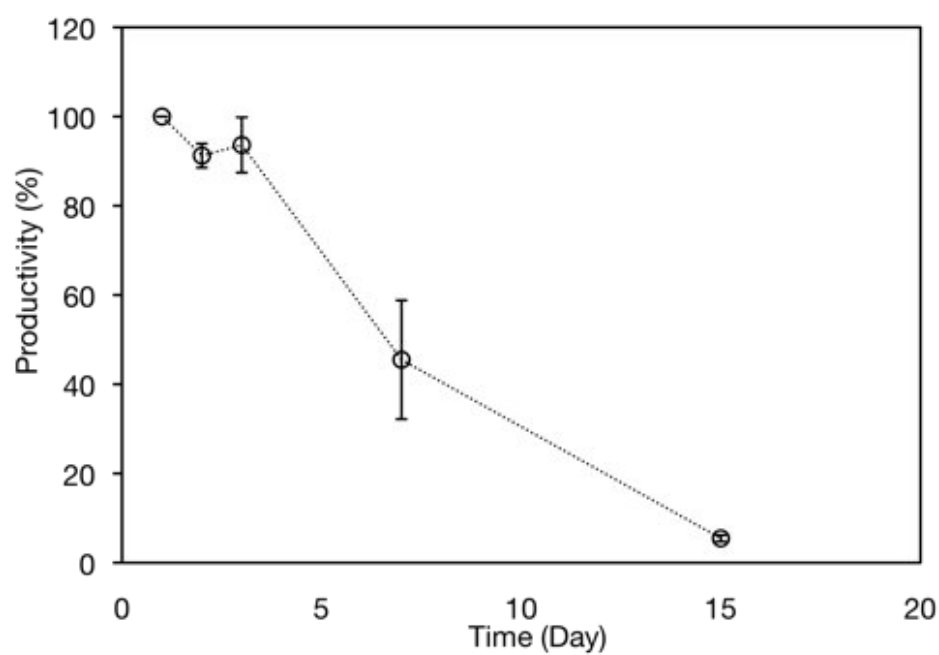
Figure 3.19: Reaction profile of His$_6$-TAm stored at 4°C. (a) Graph showing the production of acetophenone catalysed by purified His$_6$-TAm assessed at different times. (b) Productivity of His$_6$-TAm measured over a period of 15 days. The assay was conducted with 10 mM MBA and 100 mM ERY (Section 2.7.2) with enzyme concentration of 0.5 mg/mL. Error bars represent one standard deviation about the mean (n = 3).

(a)
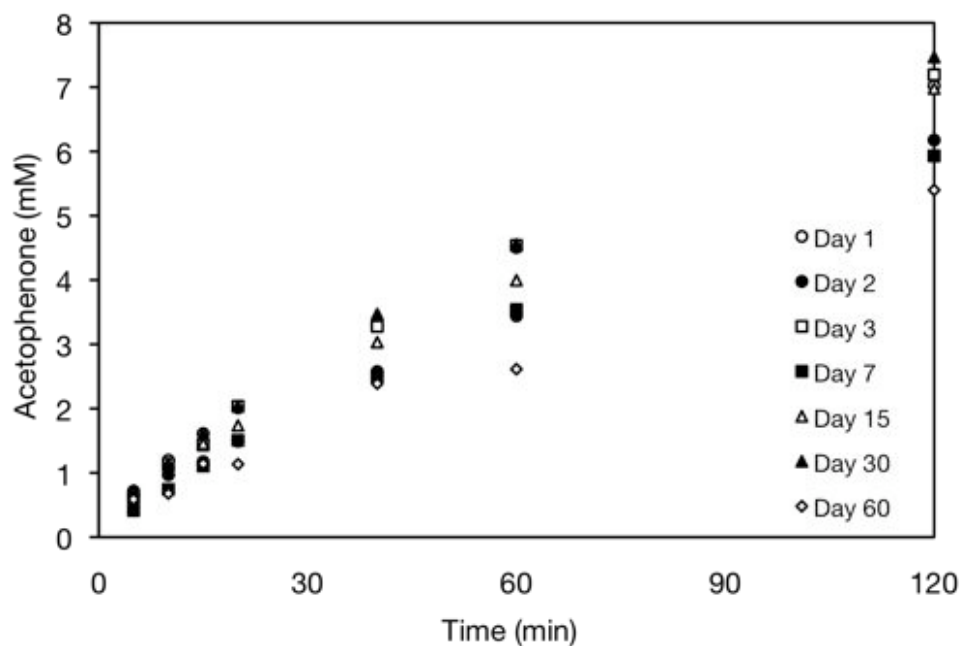
(b)
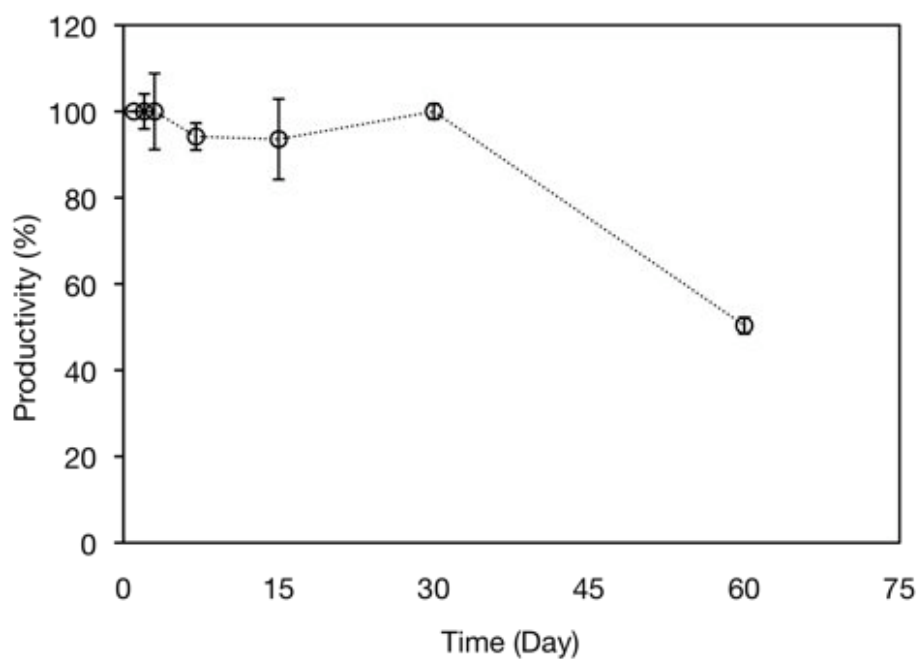
Figure 3.20: Reaction profile of His$_6$-TAm stored at -20°C. (a) Graph showing the production of acetophenone catalysed by purified His$_6$-TAm assessed at different times. (b) Productivity of His$_6$-TAm measured over a period of 60 days. The assay was conducted with 10 mM MBA and 100 mM ERY (Section 2.7.2) with enzyme concentration of 0.5 mg/mL. Error bars represent one standard deviation about the mean (n = 3).

3.3.5 Effect of PLP on His_6-TAm enzyme activity and storage stability

Pyridoxal-5'-phosphate (PLP) acts as a coenzyme in all transamination reactions and in some decarboxylation and deamination reactions of amino acids. The TAm enzymatic reaction demonstrates ping-pong bi-bi mechanism (Christen & Metzler, 1985). According to this mechanism, PLP is coordinated in the active site as an internal aldimine formed by a covalent Schiff base linkage to the ε-amino group of a catalytic lysine (Humble et al., 2012). The regeneration of the cofactor *in situ* after the reaction completes make it a perfect choice in industrial processes.

The presence of PLP in the transaminase reaction does not only act as a cofactor but also as a stabilizing agent (Shin et al., 2003; Yun et al., 2004; Yun et al., 2005). To evaluate the PLP effect on enzyme activity, a set of standard His_6-TAm activity assays (Section 2.7.2) were carried out using different PLP concentration (0.2-2.0 mM). No significant change was observed on the His_6-TAm activity (Figure 3.21a). This suggests that the range of PLP concentration used did not pose a drastic effect on the enzyme activity. Higher PLP concentration can be tested to see any obvious effect on the enzyme activity.

The effect of different PLP concentration on His_6-TAm storage stability was demonstrated. All samples were readily incubated in respective PLP concentration (0.2, 1.0, 2.0 and 5.0 mM) during the purification process and stored at 4°C. His_6-TAm activity was recorded over 15 days of reaction following the standard His_6-TAm assay (Section 2.7.2). Enzyme activity incubated in all of the PLP concentrations was quite similar for the first two days of reaction (Figure 3.21b). However, a more pronounced effect was observed on the enzyme activity on the seventh and 15th day of reaction. His_6-TAm incubated with 5 mM PLP retained 22% activity after 15 days compared to 4% activity in His_6-TAm incubated with 0.2 mM PLP. That was more than 5-fold improvement in the enzyme stability. This suggests that while moderate effect of PLP concentration on enzyme activity was observed on the early period of the experiment, the stabilizing effect at different PLP concentration only could be seen distinctly at a longer time period of time when the PLP starts to degrade.

129

Nevertheless, since the effect of the PLP concentration on the enzyme storage stability become apparent at longer time period, it is not necessary for the enzyme to be prepared at higher PLP concentration. The enzyme can be stored at 4°C with 0.2 mM PLP without compromising kinetic data collection if the enzyme is utilised within the first few days. Moreover, one can opt to store the enzyme at -20°C for longer storage time (>30 days without substantial loss in enzyme activity) (Figure 3.20).

(a)
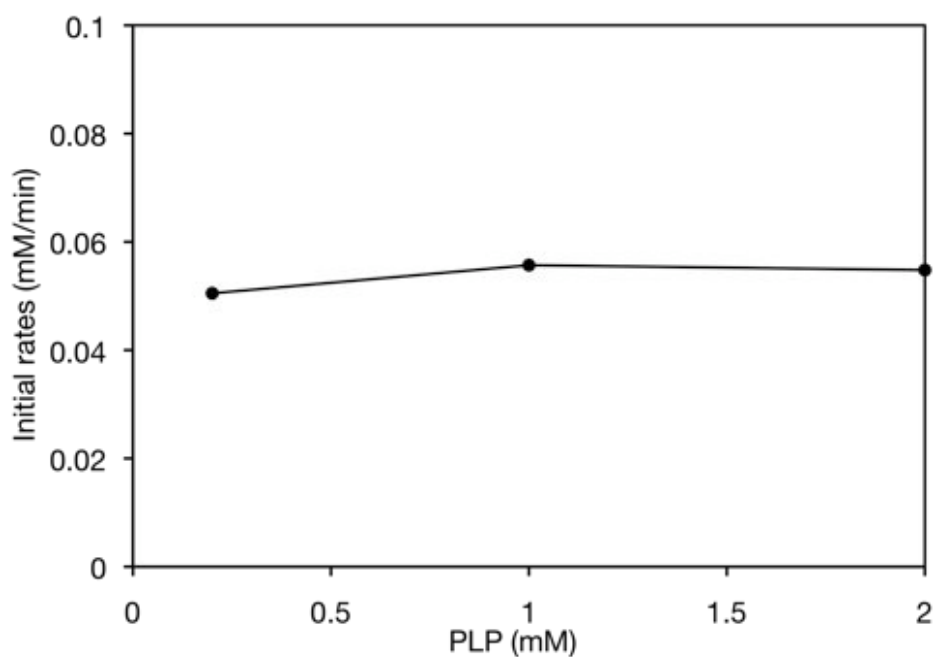
(b)
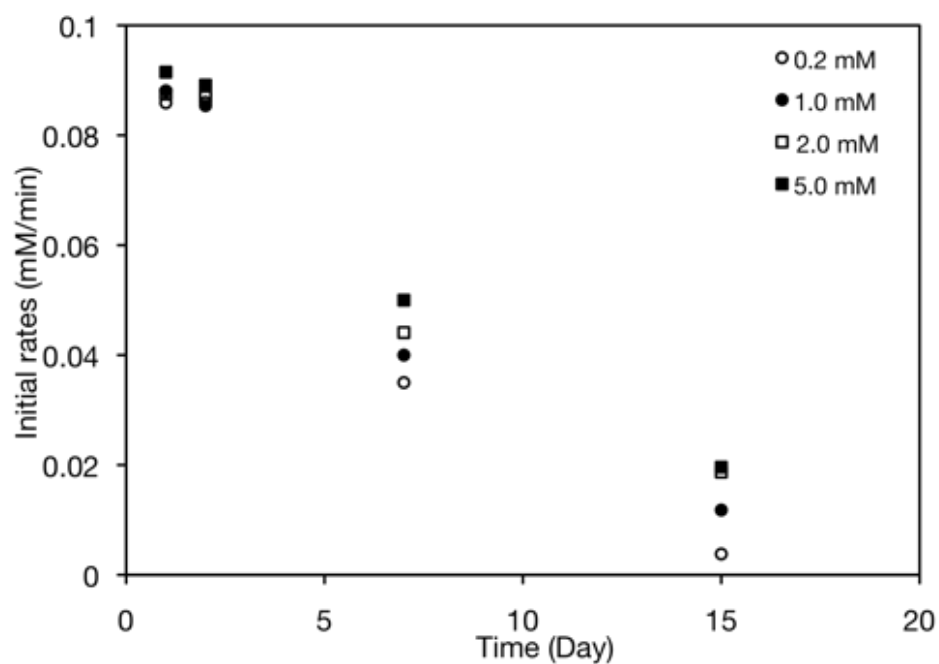
Figure 3.21: Effect of pyridoxal-5'-phosphate (PLP) on enzyme stability. Reaction was carried out with 100 mM ERY and 10 mM MBA substrate, 50 mM Tris-HCl buffer (pH 7.5) at room temperature. (a) Effect of different PLP concentration on the enzyme activity using 0.4 mg/mL His$_6$-TAm (b) Effect of different PLP concentration (0.2-5.0 mM) incubated with TAm, stored in 4°C over 15 days reaction using 0.5 mg/mL His$_6$-TAm.

3.3.6 Kinetic data of purified His$_6$-TAm in solution phase

The kinetic constants for the forward reaction between MBA and ERY were evaluated based on a single substrate assumption. Two sets of reaction were conducted, whereby in both sets, the concentration of one of the substrate was varied while the other substrate was kept fixed. All reactions were performed at room temperature and at pH 7.5 (Section 2.7.5). As expected, the reaction rates increase with higher substrate concentration (Figure 3.22). These data were fitted to a Michaelis Menten model using two plots, the Lineweaver–Burke and Eadie-Hofstee plots to estimate the V$_{max}$ and the K_m value. The V$_{max}$ for ERY and MBA calculated were 0.018 mM/min and 0.015 mM/min, respectively, and the Michaelis constant estimated for ERY was 80 mM and for MBA was 1 mM. Agreeable values of the kinetic parameters obtained from both plots apart from the slight different in K_m value for ERY and the catalytic constant k_{cat}, calculated for His$_6$-TAm was 0.19/s.

(a)
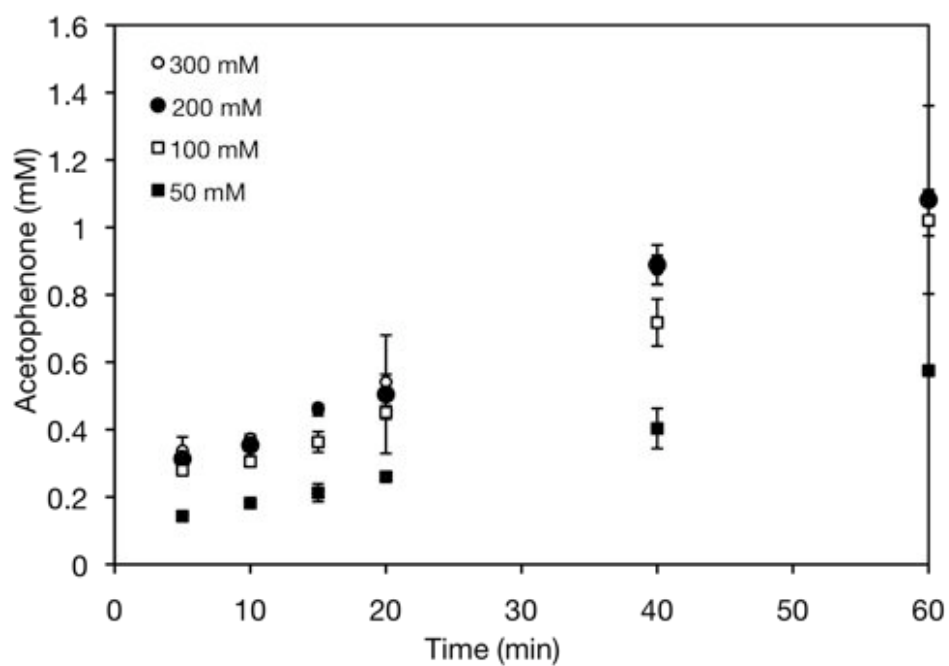
(b)
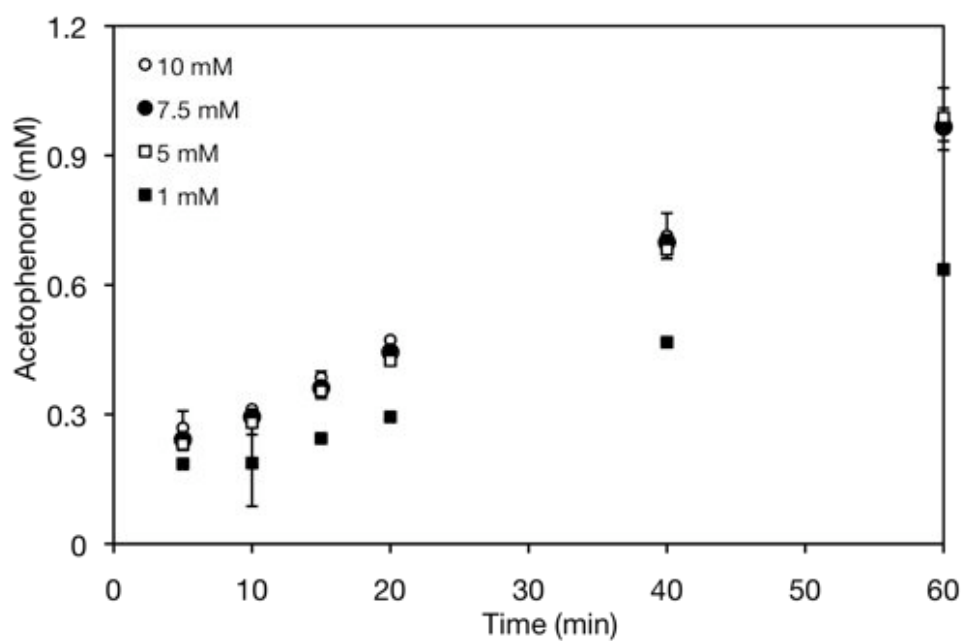
Figure 3.22: Activity profile of His$_6$-TAm at different substrate concentration (Section 2.7.5). Reactions were set up in 50 mM Tris-HCl, pH 7.5 with total reaction volume of 300 μL. (a) ERY concentration was varied (50-300 mM) with MBA concentration fixed at 10 mM. (b) MBA at different concentrations (1-10 mM) with ERY concentration maintained at 100 mM. Error bars represent one standard deviation about the mean (n = 3).

(a)
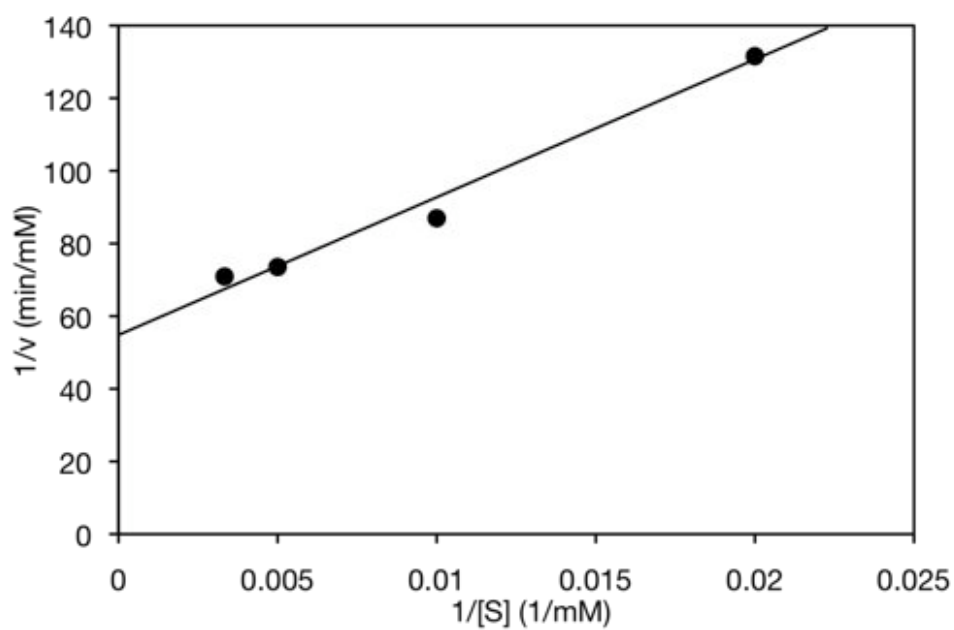
(b)
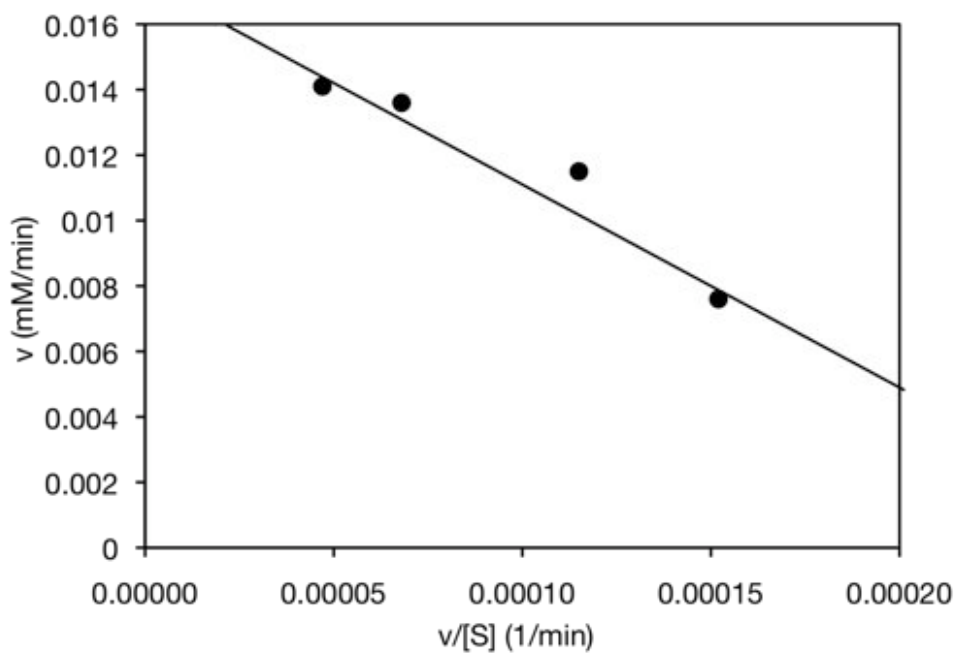
Figure 3.23: Kinetic analysis of His$_6$-TAm in solution phase. (a) Lineweaver-Burke plot and (b) Eadie-Hofstee plot at different ERY concentration.

(a)
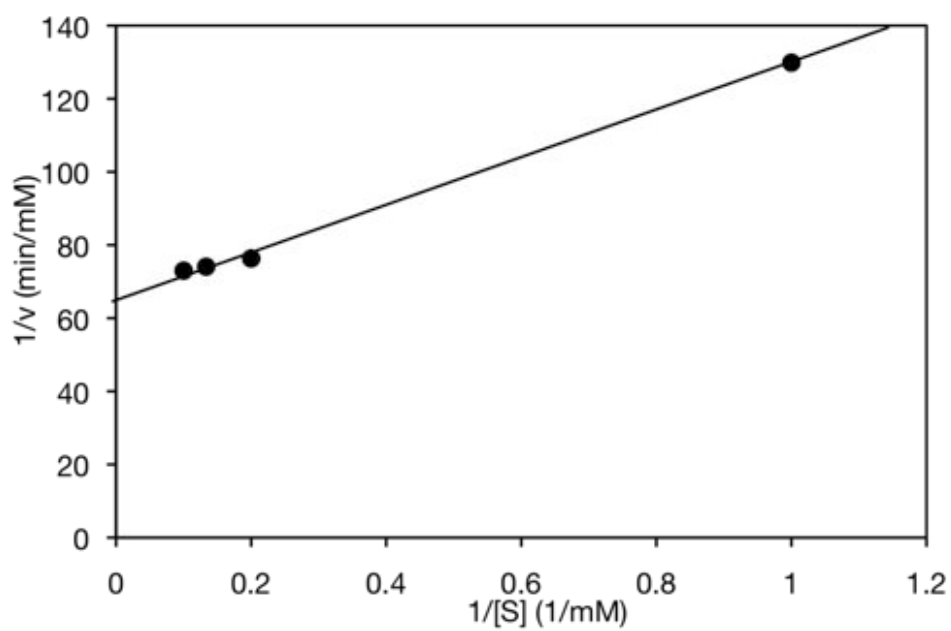
(b)
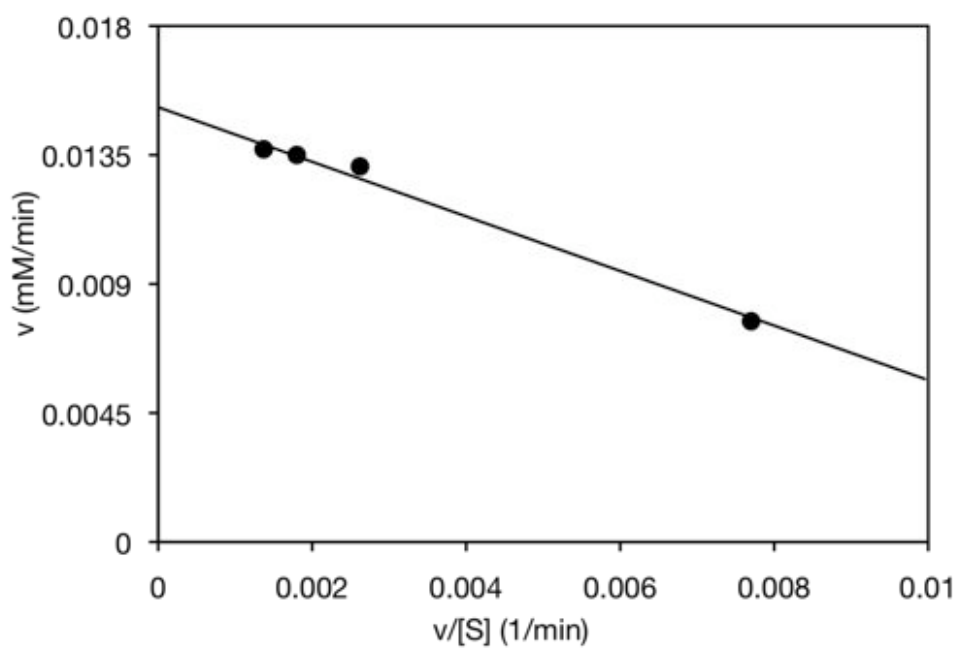
Figure 3.24: Kinetics of His$_6$-TAm in solution phase. (a) Lineweaver-Burke plot and (b) Eadie-Hofstee plot at different MBA concentration.

3.4 Summary

The work performed in this initial chapter demonstrated the utility of batch solution phase formats for the quantitative study of transketolase and transaminase bioconversion kinetics. The preliminary data gathered here provides a basis for studies in the subsequent chapter of the thesis.

The comparison of the enzyme activity in crude and purified form was investigated and the results showed the productivity per unit of purified enzyme was higher than lysate, which was likely due to less competing side reactions present (Section 3.2.2 and Section 3.3.2). Besides that, the characterisation of both enzymes in regards to its storage stability showed that the enzymes are best stored at -20°C for prolonged use of 30 days without showing any significant loss in enzyme activity (Section 3.2.3 and Section 3.3.4).

As for transaminase enzyme, the presence of PLP showed to have a significant effect not only as a cofactor but also as the enzyme stabiliser. Concentration of 0.2 mM of PLP stored in 4°C was chosen to be used in the TAm-catalysed reaction without compromising kinetic data collection provided that the enzyme is utilised within the first few days (Section 3.3.5). In addition, the activity of TAm reaction was found to be greatly inhibited by the by-product, acetophenone. The maximum product formed after 24 hrs reaction was ~9 mM (Section 3.3.3).

Finally, the specific activity for both enzymes showed that the conversion rate of TAm (Section 3.3.2) was relatively slower (~150x) compared to TK (Section 3.2.2) based on the investigated conditions. This preliminary data highlights the importance of matching the rates of the two enzymes to achieve optimal conversion rates in the multi-step enzymatic reactions (Chapter 6).

4 Development and Characterisation of Immobilised Enzyme Microreator (IEMR)

4.1 Introduction

The application of biocatalysts in microfluidic systems have attracted huge attention in recent years due to their potential for creating microscale analytical tools with minute volumes, high-throughput and attractive prospect for mass replication (Section 1.1). The aim of this research is to design and characterise a novel microscale reactor based on the reversible immobilisation of His_6-tagged enzymes. The flexibility of this microreactor allows for the system to be applied to a wide range of enzyme-catalysed bioconversions. Two reactors system were considered in this study, which were the derivatised fused-silica capillary and packed tube reactor as outlined in Section 2.10.1 and Section 2.10.2 respectively.

The fused silica capillary was commonly used in capillary electrophoresis but has progressed into capillary HPLC and electrochromatography (Wen et al., 1990). Series of chemical processes will be conducted in the capillary to create the desired functional group on the surface that allows for the immobilisation of an enzyme (Miyazaki et al., 2004). In the second system, a packed tube microreactor was employed. The microbeads, which were used as the solid support for the enzyme immobilisation, will be packed in the FEP tube that works as a packed bed reactor. These microreactors were based on the affinity-based attachment of the enzymes on the surface of a microchannel or microbeads employing His_6-Ni affinity. The reversible immobilisation of the His-tagged enzymes shows the versatility of these reactors that reflects the practicality and commercial interest of these systems.

Furthermore, there is a great need for the development of a microreactor that allows for rapid screening of biocatalytic conversion and kinetic determination. Conventionally, bioconversions are performed in a microwell system that requires a minimum volume of 100-300 μL. For this purpose, it is indispensable to provide

hydroxypyruvate, a rather expensive substrate in large quantities. On the other hand, immobilised enzyme microreactor (IEMR) is able to tackle this issue and other limitations presence in a microwell system such as shorter processing time, lower cost, better enzyme stability and potential of reusability of the reactor.

In this chapter, the prototype of the immobilised enzyme microreactor was developed. Both systems were constructed and the feasibility and efficiency of the system were investigated. The selected IEMR was further characterised in details for both TK and TAm enzymes. By knowing the behaviour of each single enzyme in the IEMR, key insight can be gained into the physics and chemistry involved during the bioconversion which will facilitate future implementation of the multienzyme reactor. Finally, the Actipix online detection system was incorporated into the microreactor system to allow for direct quantification of the product of interest.

The key objectives of this chapter are:

- Development of the reversible immobilisation of His_6-tagged enzymes microreactor.

- Characterisation of the IEMR using transketolase and transaminase enzymes with respect to its operational and storage stability.

- Investigation of the reusability of the IEMR

- Implementation of a continuous flow, UV-based online detection system for monitoring and evaluating immobilised enzyme reactions.

4.2 Construction of the immobilised enzyme microreactor

4.2.1 Derivatised fused silica capillary

4.2.1.1 Setup of the microreactor system

The setup of the microreactor was described in Section 2.10.1.1. As shown in Figure 2.1, the stopped-flow microreactor comprises of three main units, (1) inlet, (2) microreactor and (3) outlet/sample collector. With length of 40 cm and ID of 200 μm, the total reaction volume of the microcapillary was ~13 μL.

Figure 4.1: Fused silica capillary for the construction of the immobilised enzyme capillary reactor.

4.2.1.2 Microreactor preparation

A number of microreactors using fused silica capillaries have been demonstrated (Section 1.5.6). In this work, the surface of fused silica capillary was first treated to create the Ni-NTA group on the surface to allow the binding of His-tagged enzyme. The derivatisation method was adopted with slight modification based on Miyazaki et al. (2003). The protocol (Section 2.10.1.2) describes immobilisation method of His-tagged enzymes onto a microchannel surface.

The protocol involved several steps using different chemical reagents to create Ni-

NTA group on the capillary surface (Figure 1.5). The capillary surface was first modified using silanes mixtures to generate an amino group on the surface. Then the amino group formed was modified with succinic anhydride, followed by active ester formation by WSCI/NHS solution. This active ester was reacted with AB-NTA to enable the formation of a complex with Ni^{2+} ions. The capillary was ready for immobilisation of His-tagged enzymes after incubation of the Ni_2SO_4 solution. Incubating the capillary with Ni_2SO_4 solution can regenerate the derivatised capillary and a new batch of enzyme is ready to be immobilised.

(a)
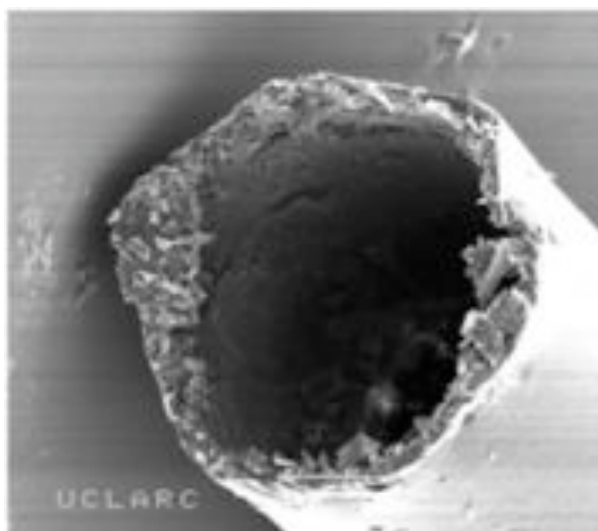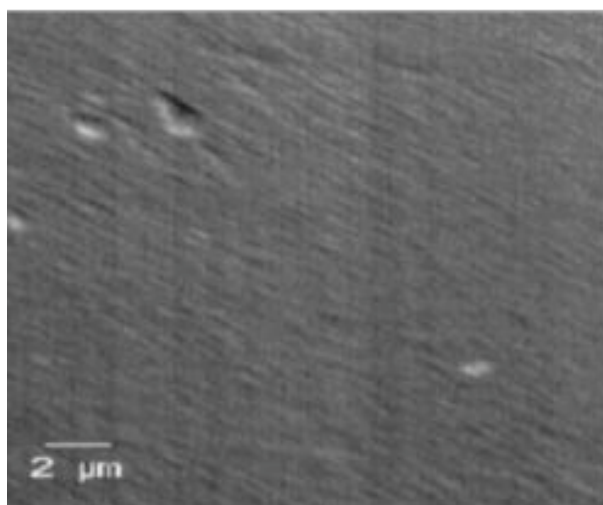
(b)   (c)
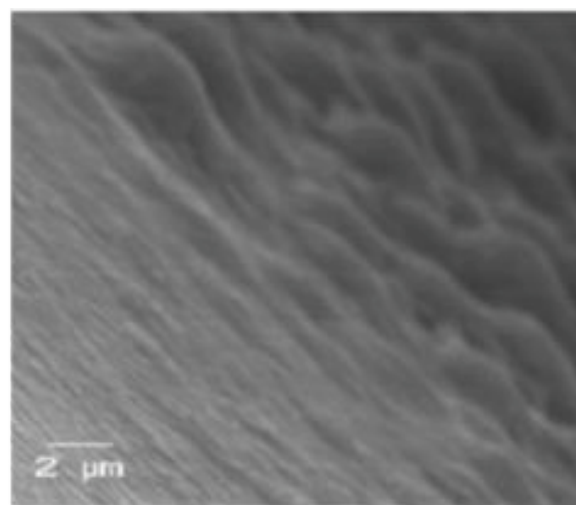
Figure 4.2: Field emission (FE)-SEM images of the inner surface of a fused silica capillary; (a) **3**700 magnification cross-section of 200 μm ID untreated capillary; (b) untreated capillary shows an entirely smooth inner surface at a **3**3,000 magnification; (c) **3**3,000 magnification of capillary surface treated with a solution of AB-NTA ready for enzyme immobilisation showing a rough inner topography. Image reproduced from (Matosevic et al., 2009) .

4.2.1.3 His$_6$-Transketolase immobilisation and elution

The immobilisation of His-tagged TK was carried out following the procedure in Section 2.10.1.3. Enzyme solution (~0.25-0.3 mg/mL) in 50 mM Tris-HCl (pH: 7.0) was loaded into the capillary at a flow rate of 5 μL/min. Theoretically, the immobilisation of His$_6$-TK is dependent on the concentration of amino group attached to the capillary surface as a result of the chemical derivatisation (Miyazaki et al., 2003). The functionalised Ni-NTA groups are proportional to the number of amino residues on the surface and in turn drive the binding between poly-histidine tags on the protein molecule.

Based on the dimension of the capillary reactor used (ID 200 μm and 40 cm length), the surface area available was 250 mm^2, which can accommodate about 1.3 μg of His$_6$-TK. This estimation was based on the saturated binding of His$_6$-TK on the inner surface of a fused silica capillary that forms a monolayer of spherical protein molecules. The quantity immobilised can be estimated based on the size of the protein and its density. The density of the enzyme was estimated to be approximately 1.3 g.cm^{-3} (Fischer et al. 2004). The full calculation is shown in the Appendix 2. The immobilisation of TK resulted in complete single layer coverage based on the quantification of the eluted enzyme sample, 0.018 mg/mL of His$_6$-TK concentration that was approximately equal to 1.8 μg. Samples from the immobilisation process were run on SDS-PAGE (Figure 4.3). Significant portion of the initial enzyme feed was not bound on the surface and can be easily removed after the washing step. Based on the measured concentration of the bound His$_6$-TK enzyme following the immobilisation and washing steps, the binding of His$_6$-TK was confirmed to be a complete single layer surface coverage.
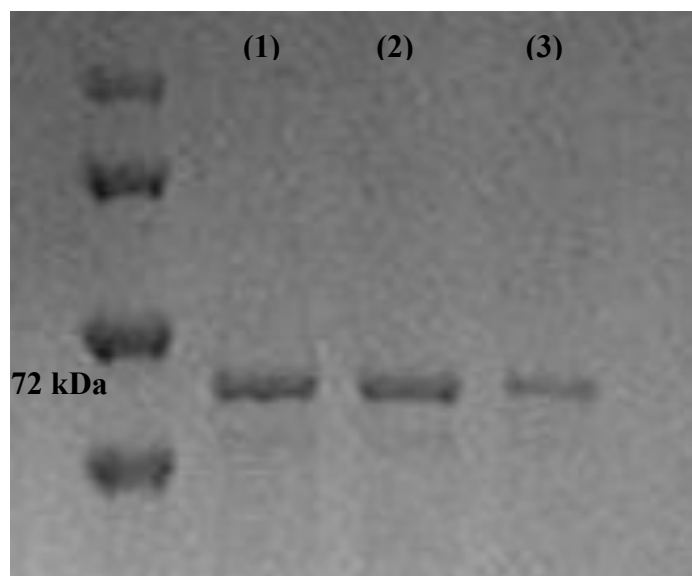
Figure 4.3: Immobilisation of His$_6$-TK inside microcapillary. SDS PAGE of enzyme immobilisation within the Ni-NTA derivatised fused silica capillary. (1) The purified His$_6$-TK feed, (2) His-TK remaining in solution after one pass through the microreactor, (3) His$_6$-TK remaining in solution after two additional passes through the microreactor. Immobilisation performed as described in Section 2.10.1.3.

4.2.1.4 His$_6$-TK microcapillary reaction

A standard assay of His$_6$-TK was conducted in the derivatised microcapillary following the immobilisation process. The same procedure was adopted as in the microwell with slight modification (Section 2.10.1.4). Initial substrate concentration of 50 mM of HPA and GA and cofactors were loaded at 5 µL/min and left incubated at room temperature. The stop-flow reaction was carried out at different residence times and the samples of the reaction were analysed using HPLC.

Based on Figure 4.4, the conversion yield of His$_6$-TK increased over time and after 12 hours reaction, His$_6$-TK catalysed approximately 50% conversion of the substrates. With length of 40 cm and ID of 200 µm the total reaction volume of the microcapillary was ~13 µL. This was still significantly below that of a standard reaction performed in the microwell (300 µL) scale. At this volume, the microreactor is characterised by laminar flow with a parabolic velocity profile, whereby the mixing is dependent almost completely on diffusion (Jähnisch et al., 2004). A number of stop-flow reaction kinetics have been demonstrated (Delouise & Miller 2005; Matosevic et al., 2009). In this system, diffusion is enhanced by an increase in residence time of the reaction mixture to allow longer contact between the substrate and the immobilised enzyme (Amankwa & Kuhr, 1992). In addition to that, immobilisation may result in some changes in enzymatic activity, optimum pH or the affinity with the substrate (Krenkova & Foret, 2004). Problems related to mass transfer and long diffusion times also contribute to the lower conversion in the microcapillary compared to the reaction in the microwell that has a homogenous reaction mixture.
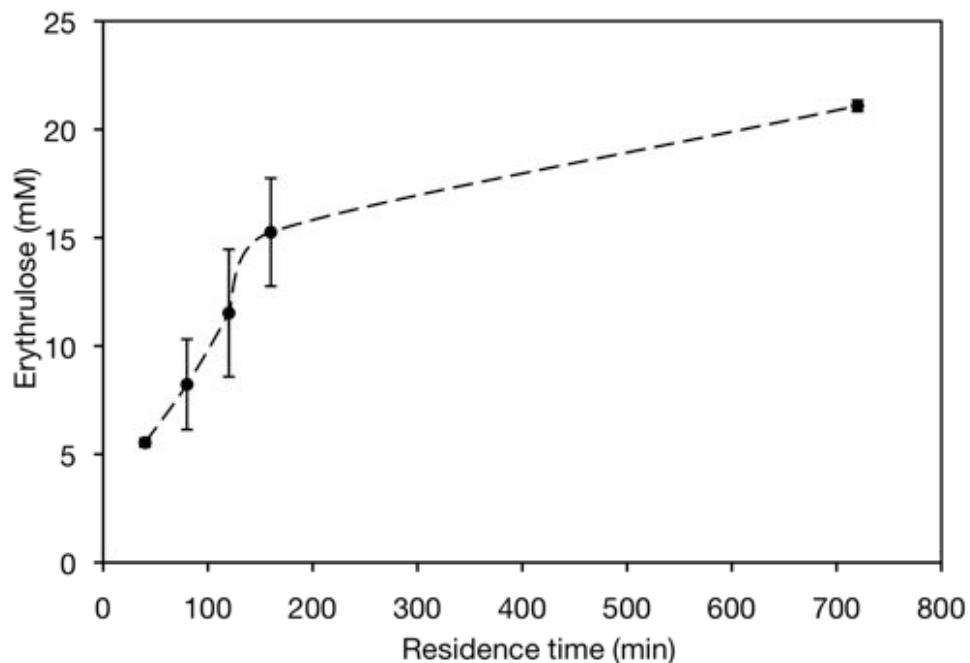
Figure 4.4: Reaction profile of His$_6$-TK in the microcapillary. The reaction was carried out using 50 mM of hydroxypyruvate (HPA) and glycolaldehdye (GA) in 50 mM Tris-HCl buffer at pH 7.0 in room temperature with 0.018 mg/mL of His$_6$-TK. The reaction was performed in stop-flow mode. Samples were removed at different residence time and the capillary was filled with new substrate for the next sampling. The reaction was performed as described in Section 2.10.1.4. Error bars represent one standard deviation about the mean (n = 3).

145

4.2.2　Packed tube microreactor

4.2.2.1 Setup of the microreactor system

A schematic illustration of the packed tube microreactor is shown in Figure 4.5b. The construction of the reactor was carried out using a transparent fluorinated ethylene propylene (FEP) tube that was packed with microbeads. A 500 μm FEP tube was chosen, as it allows at least five bead layers of packing while the length of the reactor was 5 cm. Packing of the tube was carried out using a Nanobaume pressurised container (Section 2.10.2.1). This method produced consistent and reproducible packed tubes according to the images produced from the microscope (Figure 4.6). The microfilter at the end of the capillary retained the microbeads and released excess liquid during packing. The dense packing in the tube was formed as a result of the compressibility property of the agarose beads used.

Besides the FEP tube, a fused silica capillary can also be employed for the reactor. However, the practicality of using the capillary was found to be more complicated. With the naturally bend coil characteristic, the capillary tends to break when packed with the beads and was extremely fragile especially when the top microfilter was applied. On the other hand, the FEP tube is more flexible and with the transparent tube, the progress of the packing can be monitored to avoid over compression during the packing process.

(a)

(b)
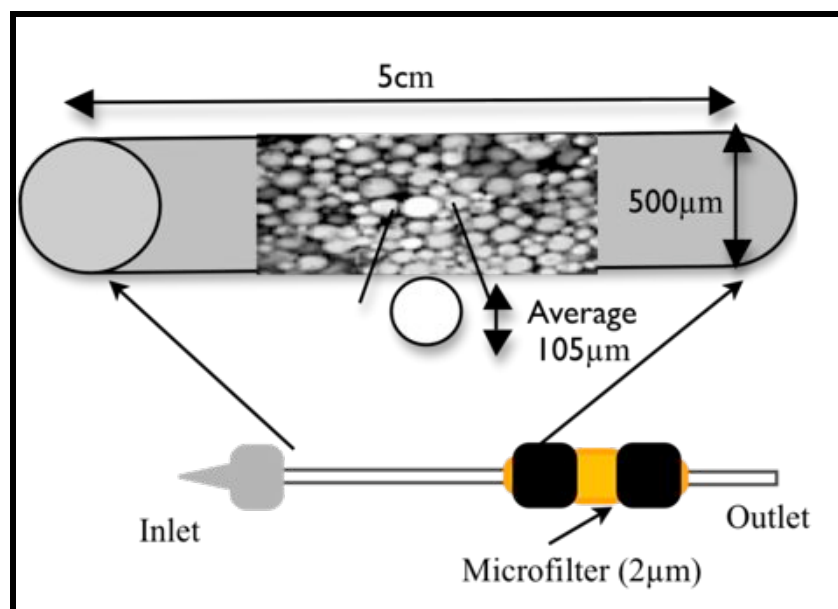
Figure 4.5: Schematic illustration of the packed tube reactor used for analysis of His_6-TK and His_6-TAm reactions. (a) A fluorinated ethylene propylene (FEP) tube used as the packing tube. The characteristics of this tube include high durability, low permeability, inert material and compatible with biological application. (b) A packed tube IEMR with ID of 500 μm and length of 5 cm gives a total reaction volume of ~10 μL.

(a)
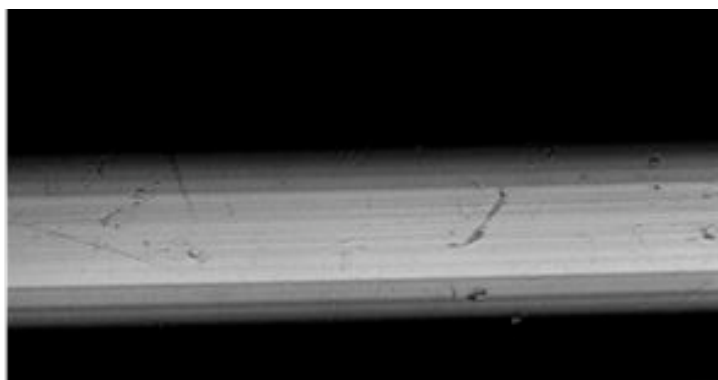
(b)
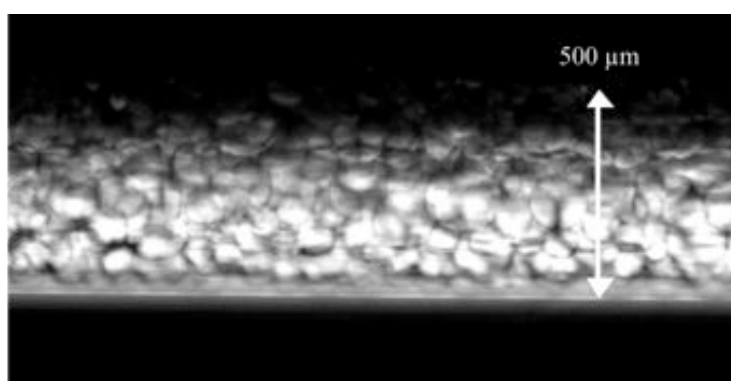
Figure 4.6: Microscope images of tube packing process. (a) Image of FEP tube with diameter of 500 µm, prior to the tube packing process. (b) Image of dense beads packing in the FEP tube using a Nanobaume pressurized container. HIS-Select Nickel Affinity agarose beads (45-165 µm diameter) were used as the packing material. Photos taken using standard light microscope (Leica microscope) with 5x magnification.

4.2.2.2 Enzyme immobilisation and elution

Purified enzymes were used in all immobilisation processes. Samples collected from the feed and elution steps were ran on SDS-PAGE and quantified (Section 2.2.3). The eluted enzyme purity was >90%, observed as a single band on the gel for TK and TAm (Figure 4.7). Following immobilisation of 0.2 mg/mL of the enzyme feed, 0.1± 0.01 mg/mL (10 µg) of the enzyme was recovered during the elution process. This showed approximately 50% of the feed was retained inside the microreactor while the remaining proportion was removed during the washing process. In order to test if the maximum enzyme loading capacity was reached the concentration of TAm in the feed was increased to 1.9 mg/mL, which resulted in a 10-fold increase of immobilised enzyme in the microreactor (1.1 ± 0.15 mg/mL). This suggests that enzyme loading increases gradually with higher enzyme concentration in the feed until it reaches the maximum capacity of the beads. The IEMR with higher TAm loading was later used in the dual enzyme reaction. In addition, no adsorption of protein on the surface of the FEP tube was detected when a similar immobilisation- washing- elution process was conducted on an empty tube. This eliminates any errors that might mask the actual enzyme activity in the packed tube IEMR.
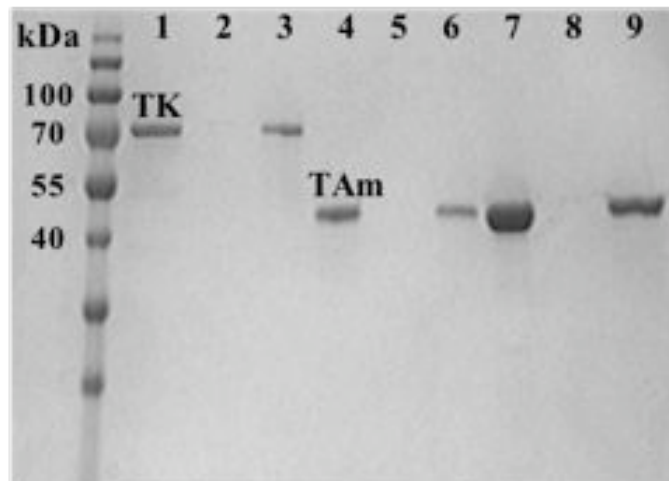
Figure 4.7: SDS-PAGE gel of enzyme immobilisation-elution process in a packed tube IEMR. The immobilisation- elution process was conducted as described in Section 2.10.2.2. (1) Purified TK (0.2 mg/mL) (2) Flow through from the IEMR, (3) Eluted TK (0.1 mg/mL) (4) Purified TAm (0.2 mg/mL) (5) Flow through from the IEMR (6) Eluted TAm (0.1 mg/mL), (7) Purified TAm (1.9 mg/mL), (8) Flow through from the IEMR, (9) Eluted TAm (1.1 mg/mL).

4.2.2.3 His$_6$-TK enzyme activity in packed tube reactor

The standard activity assay of His$_6$-TK was performed as described in Section 2.10.2.3. In a continuous flow reaction, the residence time needs to be adjusted to allow sufficient time for the bioconversion to occur at a detectable level. Due to the small dimension of a microreactor, the Reynolds number (Re) is usually between ~0.1 and 100 (Adeosun & Lawal, 2009). This indicates flow to be in a laminar regime. At this level, the flow can only rely on molecular diffusion, which is known to be very slow compared to convection. At such a low Re number, the flow is dominated by the balance between viscous stress and pressure gradient and the flow enfolding necessary for effective mixing is weak (MacInnes et al., 2005).

At a concentration of 0.2 mg/mL of His$_6$-TK, the conversion yield of the enzyme reached >90% after 10 minutes reaction (Figure 4.8). The highest activity was observed at the lowest flow rate (1 µL/min), which had longer residence time. Moreover, the conversion reached ~20% in less than one minute at the highest flow rate. This showed that the mass transfer effect was improved which is normally observed in a continuous flow mode reaction (Chen & Chen, 1998). Furthermore, the physical attribute of microbeads that were used as packing material enhanced the surface-to-volume ratio while reducing the long diffusion times present in a laminar flow condition (Krenková & Foret, 2004). Therefore shorter analysis time can be achieved.
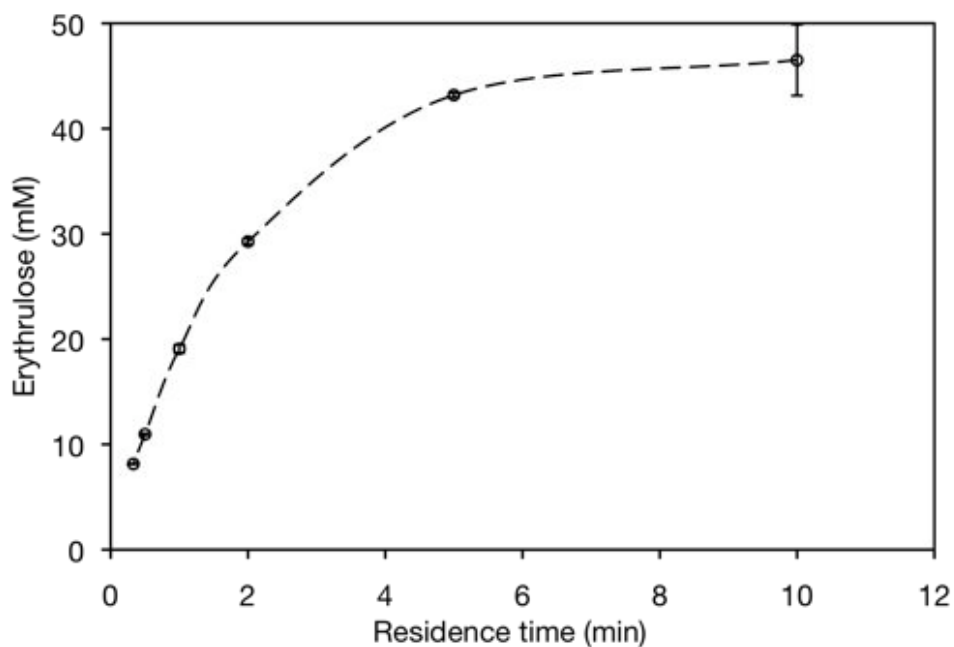
Figure 4.8: Reaction profile of His$_6$-TK in packed tube reactor. The reaction was carried with the model substrates of 50 mM hydroxypyruvate (HPA) and 50 mM glycolaldehyde (GA) in 50 mM Tris−HCl buffer, pH 7.0 with cofactors thiamine pyrophosphate (TPP), 2.4 mM and 9 mM MgCl$_2$ at room temperature. The reaction was performed in continuous flow mode. The substrate was loaded continuously at different flow rates (1-30 µL/min). The reaction was performed as described in Section 2.10.2.3. The concentration of immobilised TK was ~0.16 mg/mL. Error bars represent one standard deviation about the mean (n = 3).

4.2.3 Summary of microreactor evaluation

Both microreactor systems were investigated previously (Section 4.2.1 and Section 4.2.2). In the preliminary study, the development of a derivatised fused silica capillary and packed tube reactor were demonstrated. The first method requires a lot of preparation in terms of time (~ two days), effort and large amounts of reagents for every step. In contrast, the latter method appeared to be more facile and relatively inexpensive to prepare.

The activity assay of immobilised His_6-TK was performed following the immobilisation process. The conversion yield of His_6-TK immobilised on the surface of the microcapillary tube achieved approximately 11% completion in 40 min while 92% in 10 min for the packed tube reactor. When normalised by the corresponding amount of enzyme, the specific activity of His_6-TK for erythrulose formation in the microcapillary was lower than in packed tube reactor, which was 0.6 μmol/min/mg and 7.8. μmol/min/mg respectively. The low activity observed in the microcapillary was most likely due to the nature of the reaction (stop-flow mode) as well as a mass transfer issue that might affect it. Long diffusion time and small surface-to-volume ratio issues that is common among the open tubular IEMR was improved in the packed tube reactor system. Similar studies that utilised resins as packing material have been demonstrated elsewhere (Cobb & Novotny 1989; Wang et al., 2000; Seong & Crooks 2002).

Furthermore, the capacity of immobilised enzyme for both systems were also demonstrated. The packed tube reactor was able to accommodate a much higher enzyme concentration, which helps to speed up the reaction despite of having lower reactor volume than the microcapillary reactor. With a simple microreactor setup, higher enzyme capacity and improved mass transfer in the packed tube reactor, this system is ideal for the design and development of the multienzyme reactor that will be discussed in Chapter 6. Therefore, the packed tube microreactor was chosen for further enzyme kinetics investigation in IEMR.

4.3 Characterisation of packed tube IEMR

4.3.1 Pressure drop across the packed tube IEMR

The ability to determine pressure drop in packed bed system is of importance for the design of the reactor especially for the pump and column specification. The pressure drop of packed bed has been studied in details whereby the pressure drop is known to be dependent on the particle Reynolds number, the mean void fraction, the particle geometry and the particle size distribution (Eisfeld & Schnitzlein, 2001). To calculate the pressure drop value, the friction factor is considered which is attributed to Ergun equation. The Ergun equation that is commonly employed is given below:

$$ f_p = \frac{150}{\text{Re}_p} + 1.75 $$

Here the friction factor f_p for the packed bed and Reynolds number Re_p are defined as follows:

$$ f_p = \frac{\Delta p}{L} \frac{D_p}{\rho V_s^2} \left(\frac{\varepsilon^3}{1-\varepsilon} \right) \qquad\qquad \text{Re}_p = \frac{D_p V_s \rho}{(1-\varepsilon)\mu} $$

Δp: pressure drop

L: length of the bed

D_p: spherical diameter of the particle (1.05×10^{-4} m)

ρ: density of the fluid (1000 kg.m^{-3})

μ: dynamic viscosity of the fluid (1×10^{-3} kg.m^{-1}.s^{-1})

V_s: superficial velocity

ε: void fraction of the bed (0.3)

In the case of the continuous flow reaction, the packed tube IEMR is subjected to a constant flow of the substrates-cofactor mixture that creates a pressure drop within the packed tube reactor. With a compressible resin used as the packing material, the maximum flow rate through the reactor is limited by the collapse of the resin due to

compressive stresses imposed by the fluid flowing through it (Tran et al., 2007). Therefore, it is very important to estimate the range of working flow rate that will suit the design and dimension of the reactor as well as the capacity of the pump. Due to the small dimension of the microreactor, the Re number of the fluid flow is less than 1, which corresponds to the laminar flow regime. At this condition, the velocity of a particle in a fluid stream is not a random function of time and any streams flowing in contact with each other will not mix except by diffusion (Beebe et al., 2002). It was reported that the pressure drop in a column is directly proportional to the velocity when the flow is laminar (Joye, 2003). The pressure drop calculated for the packed bed tube IEMR (Figure 4.5b) for a flow rate of 30 μL/min is ~790 Pa and this data was used to evaluate the maximum force, F_{max} of the microreactor.

$$F_{max} = A_s \Delta P_{max}$$

where A_s: syringe surface area

Based on this data, the maximum force estimated was still very low compared to the maximum force capacity of the syringe pump ($F_{pump} > F_{max}$)(~80 N). Therefore, the current working flow rates and the microreactor dimension do not impose any critical risk on the packed tube reactor operation. This would allow for further modification on the operating condition as well as the reactor dimension.

(a)
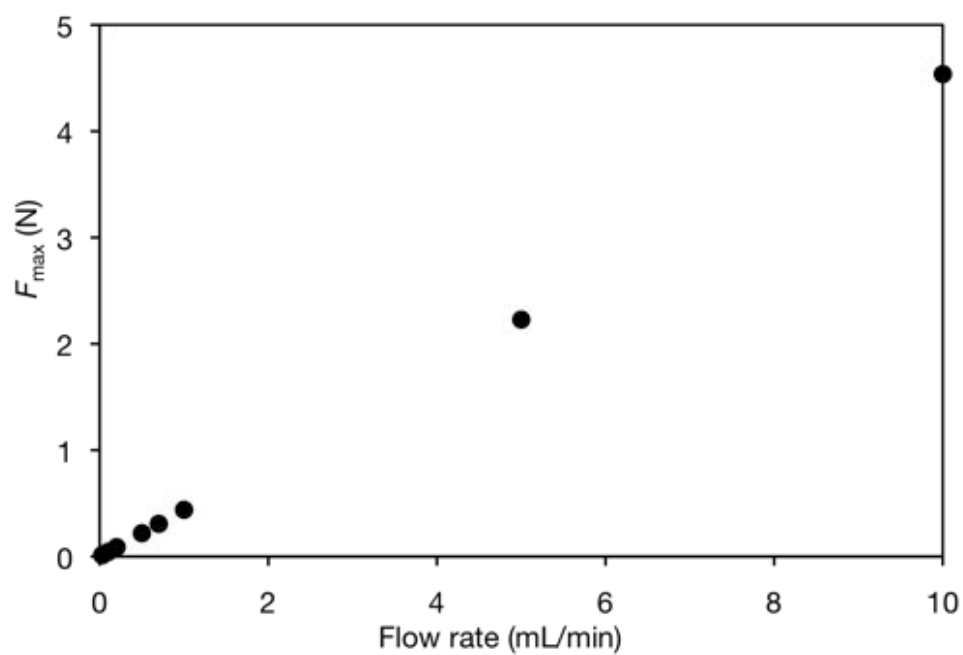
(b)
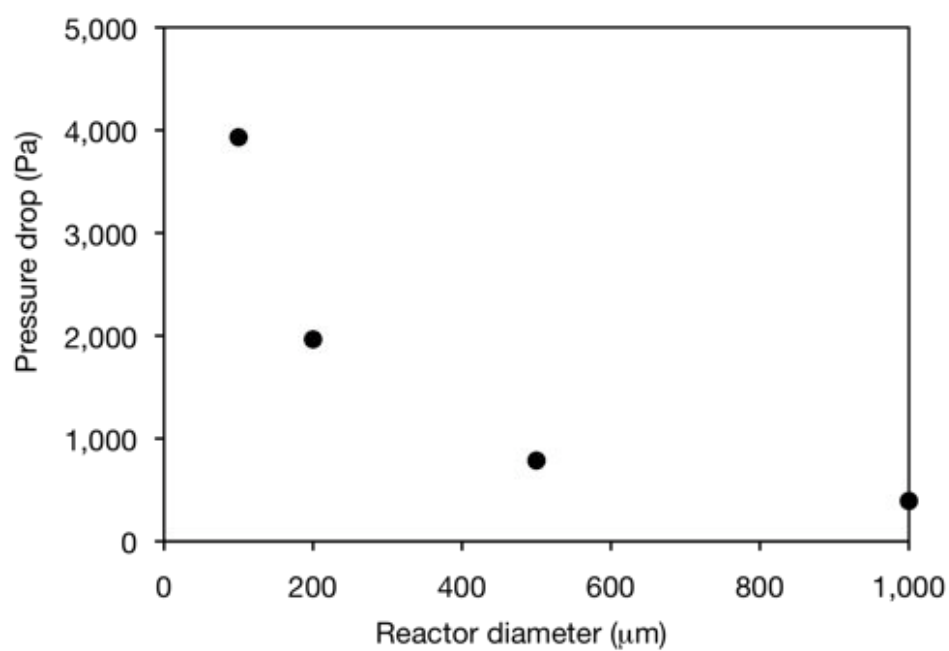
Figure 4.9: Reactor profile on the effect of flow rate and reactor diameter based on theoretical calculation. (a) Plot of F_{max} as a function of flow rate. The theoretical values of F_{max} calculated are much lower than the capacity of the maximum capacity of syringe pump (~80N). The reactor dimension as in Figure 4.5b was used in the calculation. (b) Plot of pressure drop as a function of reactor diameter. A pronounced effect was observed as the reactor diameter increases

4.3.2 Operational and storage stability study

One of the most important properties of an immobilised enzyme is its storage and operational stability (Krenková & Foret, 2004). Unless it is stable, it cannot be used over a prolonged period. The most realistic way to test storage and operational stability is by periodic measurement of the residual activity. Enhanced stability of immobilised enzyme is usually observed compared to their soluble form.

The operational stability of the immobilised His_6-TK was evaluated continuously for 48 hours at a flow rate of 1 µL/min. Samples were taken every 12 hours to measure the conversion of HPA and GA to ERY product. Immobilised His_6-TK was found to remain stable during the first 12 hours of reaction with 100% productivity (Figure 4.10a). However the productivity dropped to 76% after 48 hours of reaction. A similar test was performed with immobilised His_6-TAm where the productivity was determined continuously every hour at 1 µL/min. In contrast to TK, after only 8 hours of continuous reaction, the productivity of the immobilised His_6-TAm was reduced to 60% (Figure 4.10b).

The storage stability of immobilised TK in the packed tube stored at 4°C in 50 mM of Tris-HCl was measured over a period of 16 days. Immobilised TK retained almost 100% productivity after 16 days, when compared to the first day of reaction (Figure 4.11a). This consistency in activity of the immobilised TK enzyme, proved the high stability of TK in the immobilised form whilst ~7% of activity drop was observed with free enzyme (Figure 3.5). By contrast, immobilised TAm only retained ~7% of its initial productivity after 5 days (Figure 4.11b) compared to ~45% residual activity after 7 days in free enzyme (Figure 3.19). The sharp decrease in productivity showed that immobilisation significantly affect enzyme stability (Krenková & Foret, 2004; Ladero et al., 2006). This low catalytic stability of TAm was most likely due to the alteration in the three-dimensional conformation of the protein upon immobilisation, which led to rapid inactivation of TAm after repeated use. In addition, it was reported that CV2025 TAm has flexible structure and requires a large loop movement during the catalytic activity cycle (Sayer et al., 2013). This might now be restricted upon immobilisation. Besides that, the stability

of an enzyme was found to be highly dependent on the type of immobilisation support used. ω-TAm from *V. fluvialis* immobilised on chitosan beads exhibited higher stability compared to Eupergit C, whereby 70% of residual activity was retained after 3.5 weeks and only 10% for the latter one (Yi et al., 2007).

(a)
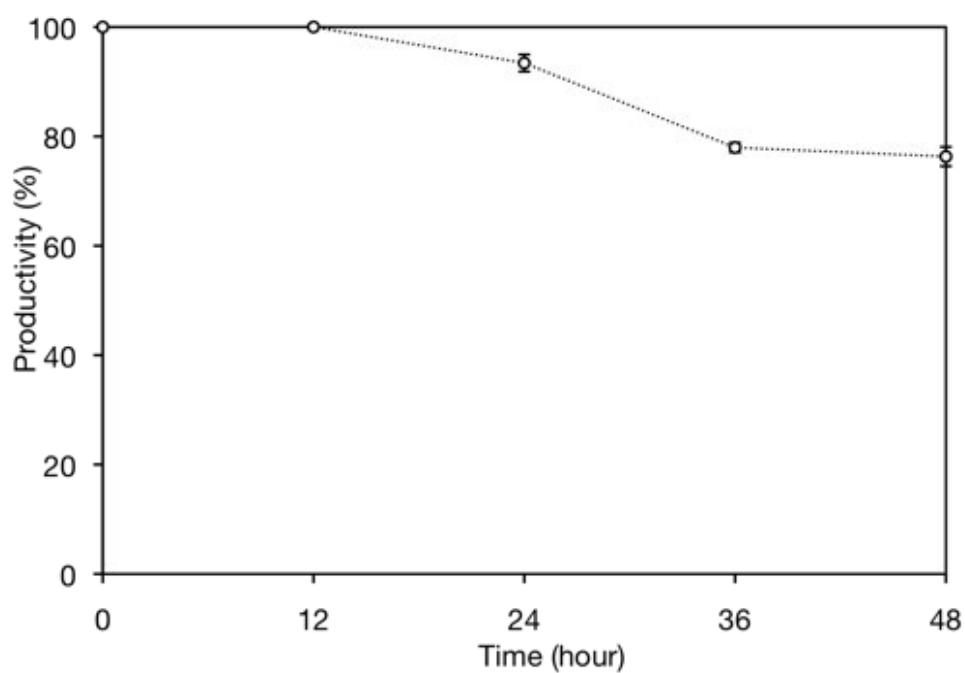
(b)
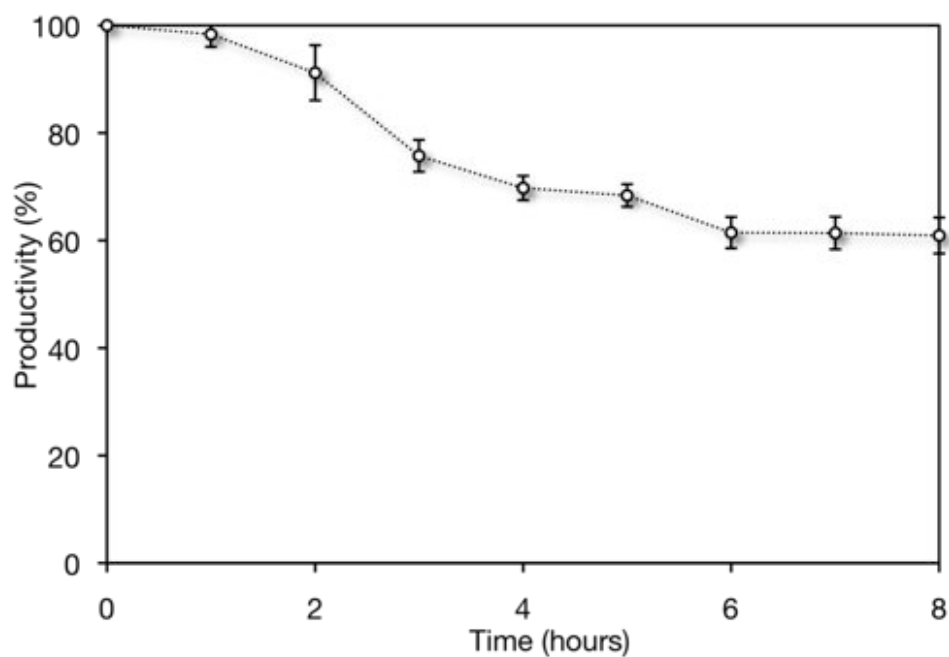
Figure 4.10: Operational stability of TK and TAm in IEMR. The productivity is defined as the amount of product generated over 12 h (TK) or 1 h (TAm) (per amount of enzyme) divided by the product formed of the starting enzyme activity determined in the same way. A productivity of 100% indicates no deactivation and degradation of the immobilised enzyme in the reactor. (a) Continuous reaction of TK in packed tube IEMR at 1 μL/min for 48 hours. (b) Continuous reaction of TAm in packed tube IEMR at 1 μL/min for 8 hours. Error bars represent one standard deviation about the mean (n = 3).

(a)
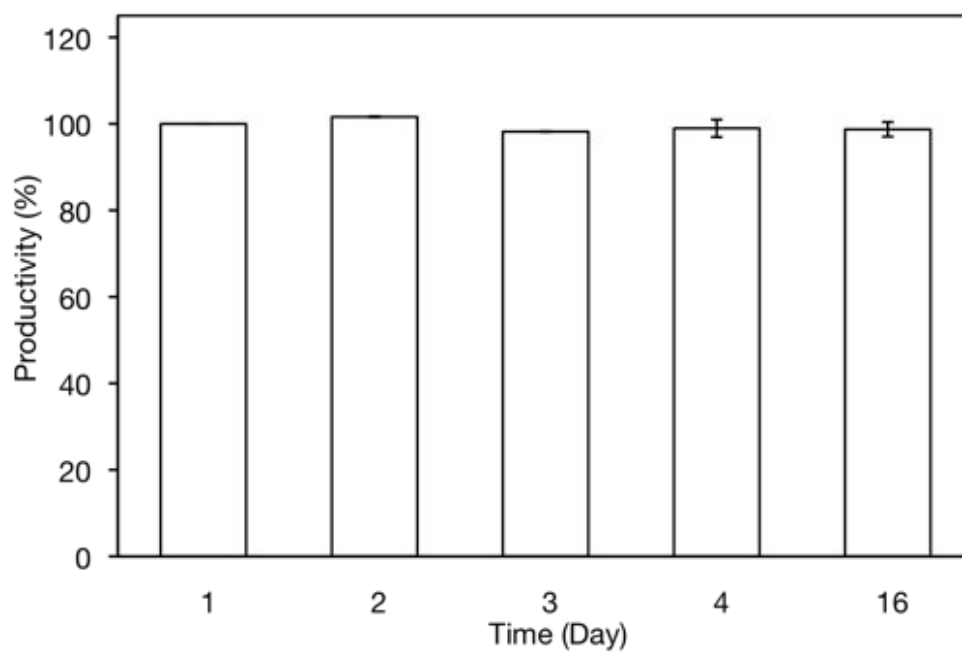
(b)
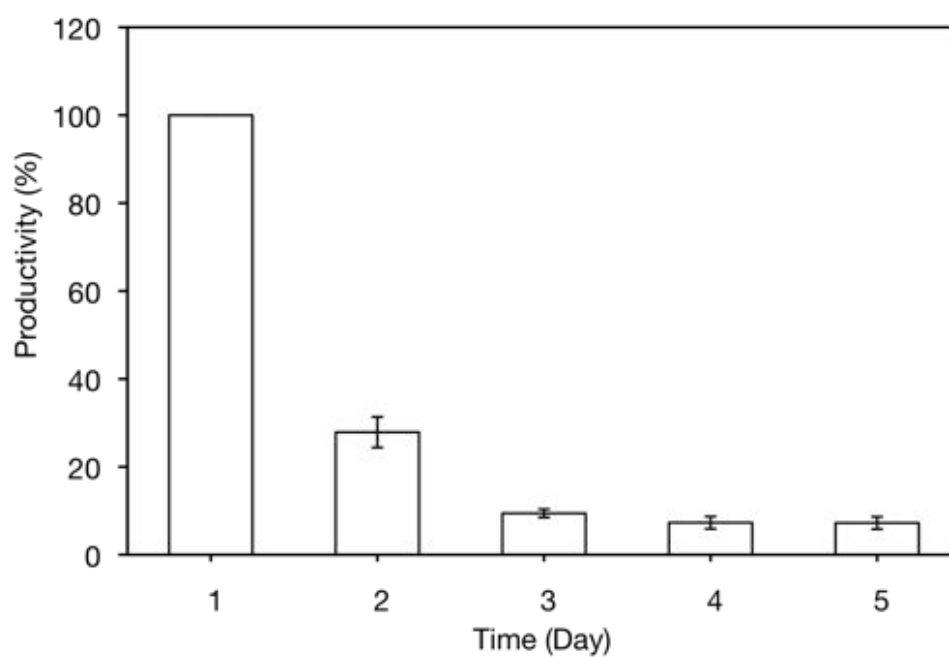
Figure 4.11: Storage stability at 4°C in 50 mM Tris-HCl of (a) TK IEMR and (b) TAm IEMR. The productivity of the IEMR was determined according to the standard TK and TAm assays (Section 2.4.3 and 2.4.4). The productivity is defined as the amount of product generated (per amount of enzyme) divided by the product formed of the starting enzyme activity determined in the same way. Error bars represent one standard deviation about the mean (n = 3).

4.3.3 Reusability of IEMR

The reusability of the microreactor was investigated by using the same packed tube reactor in seven TK immobilisation-elution processes. The activity of the immobilised enzyme was then tested (Section 2.10.2.2) to ensure the repeated immobilisation-elution process in the microreactor does not affect the activity of the enzyme. Based on the results shown in Figure 4.12, the productivity of the IEMR was retained over seven cycles of the immobilisation-elution process within a four week period. This is similar to the findings from work of Matosevic et al. (2009), however the reusability of the packed tube was made simpler compared to the surface derivatised capillary as it does not require a regeneration step before the subsequent immobilisation process. The same concentration of enzyme was used throughout the experiments to allow a direct comparison between each cycle of immobilisation-elution processes.
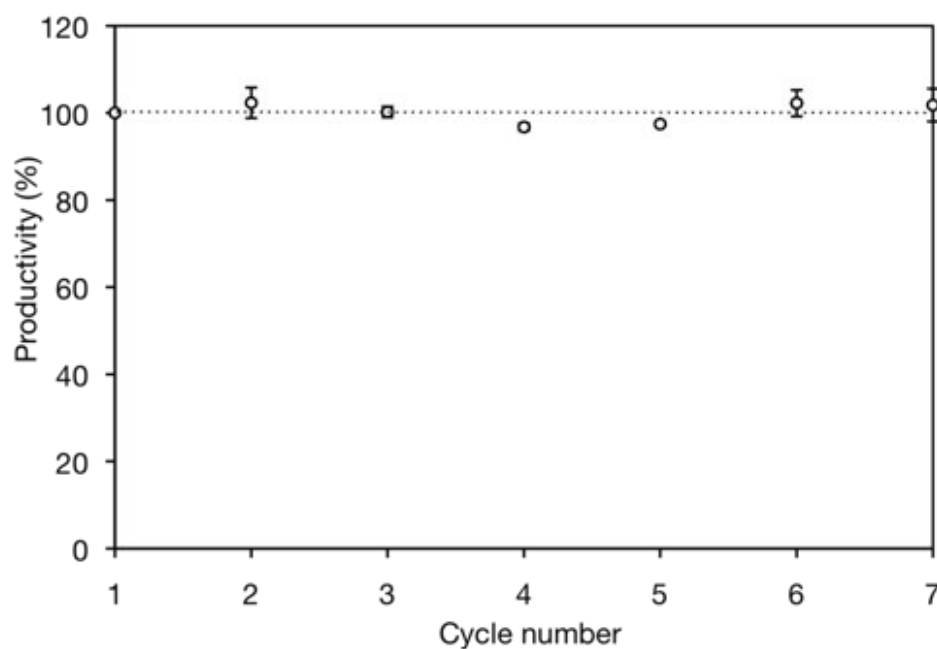
Figure 4.12: Reusability test of the IEMR. Reusability of packed tube was measured by productivity of the immobilised TK over seven cycles of immobilisation-enzyme reaction-elution processes using a single IEMR. Productivity of the IEMR was measured according to the standard TK assay (Section 2.10.2.3) over four week period. Error bars represent one standard deviation about the mean (n = 3).

4.4 Integration of Actipix online detection system

The various functional units of a microfluidic devices apart from sample acquisition, pretreatment, separation, post-treatment is the incorporation of an efficient detection system (Lee & Lee 2004). The detection system enables monitoring the reaction conditions in real time while reducing the processing times for high-throughput screening experiments. There are numerous detection methods available for these miniaturized systems, with the analyte of interest driving the choice of detection system (Baker et al., 2009). The most common detection systems employed are the optical (Benninger et al., 2007; Emory & Soper, 2008; Tong et al., 2009), electrochemical (Kim et al., 2007; Hayashi et al., 2008; Kang et al., 2008) and mass spectrometric method (An et al. 2008; Kim et al., 2009).

The most predominant detection method in microfluidic analyses by far has been with optical means (Baker et al., 2009). Within this system, ultraviolet (UV) absorbance-based detection can be considered routine. UV detection system has been used in many characterisation of a diverse range of liquid samples, including pharmaceutical drugs, peptides, protein and DNA.

The Actipix D100 detector was integrated in the IEMR system to monitor the product conversion in real-time. This detector has been designed for use in a variety of applications in research by providing quantitative measurements in the UV region. The Actipix D100 consists of a control box and a capillary cartridge with a miniature size detector (6.5 cm x 5.5 cm x 11.5 cm) (Figure 2.3). Processed data output was sent in real-time to a computer using a high-speed serial data or USB link. The Paraytec data acquisition software was set up for data collection and output signal analysis. The setup of the integration of the Actipix online detection system with the IEMR was previously described in Section 2.10.4. The absorbance of the analyte can be visually monitored based on the colour of the capillary image that corresponds to the detector output data (absorbance data) (Figure 4.13). Two capillaries in a cartridge were installed which allows for simultaneous multiple detections. However in this study only one capillary was used which correlates to the channel one in the detector output data. Calibration of the detector with RO

163

water through the capillary was performed and low absorbance reading (0-0.1 mAU) was obtained indicating minimal background interference from the capillary.

(a)
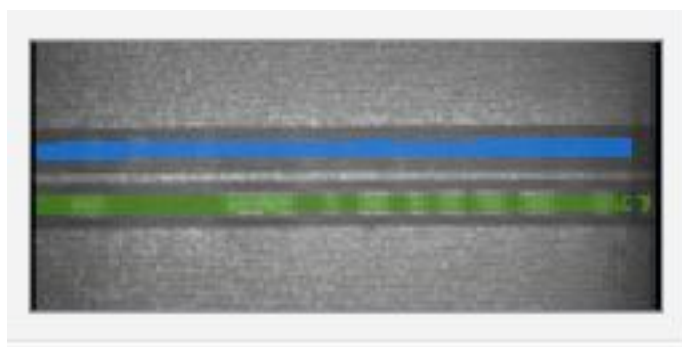
(b)
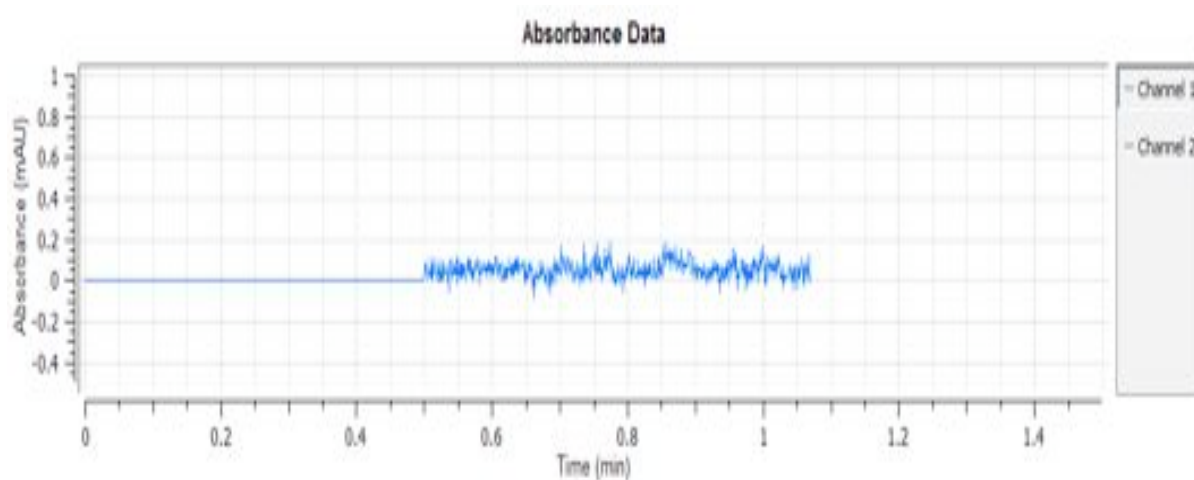
Figure 4.13: Paraytec Actipix detection window and UV detector data output. (a) The cartridge consists of two capillaries with a real time visual image through a 9 x 7 mm area on the Actipix detector head. Flow was provided via a single syringe pump at various flow rates. Absorbance data was collected directly and processed using the application software via a computer connected to the Actipix detector (b) Detector output data as collected through the application software. Data acquisition begins approximately 30 s after detector start time.

4.4.1 Absorptivity of TAm reaction components

The integration of the Actipix online detection in the packed tube IEMR was performed at detection wavelength of 280 nm. This detection system was tested on the TAm-catalysed reaction in the IEMR with model substrate of ERY and MBA to produce AP and ABT. It was previously reported that the by-product AP absorbs UV light at 280 nm (Fisher et al., 2001) while both of the substrates and ABT have negligible absorbance at the same wavelength. In order to determine the absorbance of the species, measurements at 280 nm were initially carried out on a bench scale spectrophotometer at room temperature. A solution of substrates was prepared in 50 mM Tris-HCl (pH:7.5) and the reading confirmed low absorptivity at this wavelength. However, the cofactor PLP required for TAm-catalysed reaction was found to absorb at 280 nm. In order to eliminate background interference by PLP, output absorbance readings were blanked with the initial absorbance of the PLP-substrates mixture.

In order to validate the previous results, the substrates solutions were run through the Actipix detector and the reading was observed. The results obtained were in agreement as in the spectrophotometer. The detection of product through the Actipix detector was calibrated with solution of pure product measured at different concentration (Figure 4.14). This calibration curve was used to quantify the AP production in the TAm-catalysed reaction.

a)
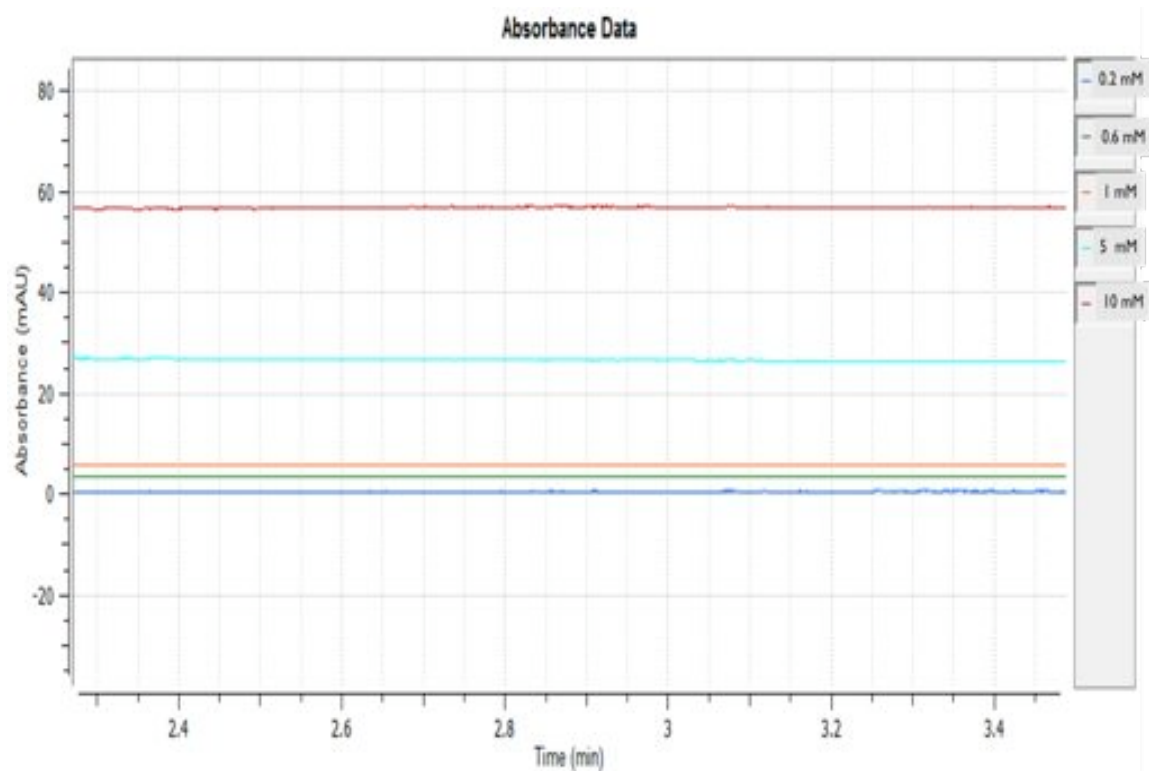
b)
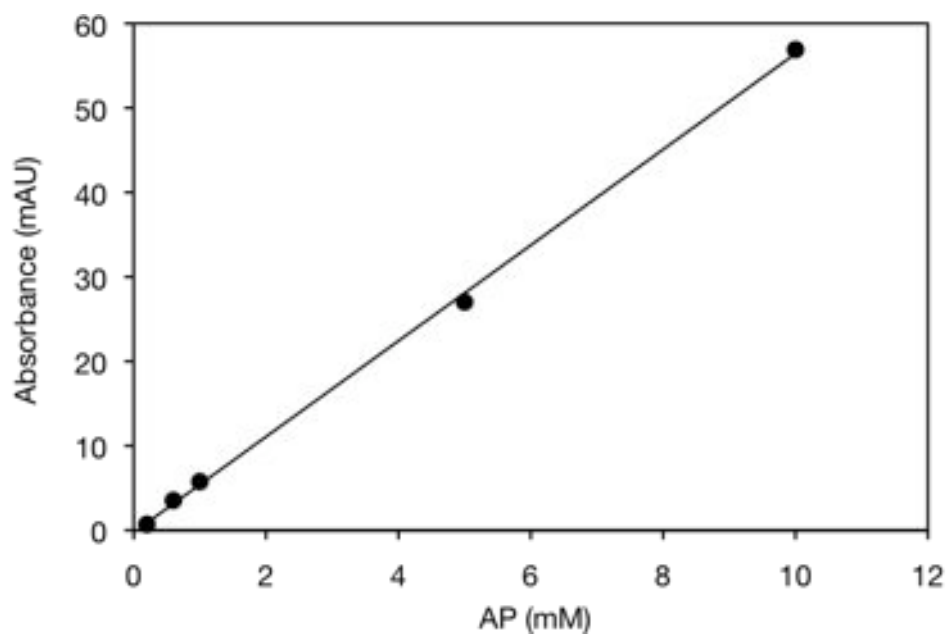
Figure 4.14: Actipix online detection of acetophenone at 280 nm. (a) AP absorbance at various concentrations (0.2-10 mM). The absorbance values were used to construct the (b) calibration curve for the quantification of AP product in the TAm-catalysed reaction in packed tube IEMR.

4.4.2 TAm-catalysed reaction with direct quantification of AP

His_6-TAm activity in the packed tube IEMR was demonstrated based on protocol described in Section 2.10.2.4. The setup of the experiment was described in Figure 2.3 and performed at room temperature. The reaction was evaluated by quantifying the by-product of AP via an Actipix online detection system and validated by the off-line HPLC.

The reaction profile of acetophenone production is shown in

Figure 4.15 as a function of flow rate and residence time. As expected, the product formation was highest at the lowest flow rate reflecting the longer residence time for the reaction to occur. With enzyme concentration of 1.0 mg/mL, the bioconversion reached almost 40% conversion at the slowest flow rate. The conversion can be easily improved by running the reaction at a slower flow rate. For instance, at flow rate of 1 μL/min the residence time in the packed tube IEMR is 10 minutes. The residence time can be increased up to 2 hours to get higher conversion without having significant effect on the stability of the His_6-TAm immobilised enzyme (Figure 4.10). A stable biocatalyst would retain activity over a number of reactions thereby minimizing the need of re-immobilisation.

The detection of the product was performed in a real time via the Actipix detector. Based on the residence time, different rates of conversion were achieved, as indicated by the change in the output signal response. In order to validate the data from the Actipix detector, the samples were run on the HPLC. The results from the Actipix were agreeable with the HPLC analysis with an average error of less than 20%. This discrepancy could be due to the dilution error added during preparation of samples for the HPLC analysis. Ultimately, the integration of the online detection system in the packed tube IEMR was performed successfully. The efficiency of this detection system shows a great potential for the system to be applied to other bioconversion models especially in the multi-step enzymatic reaction that will be discussed in Chapter 6.

(a)
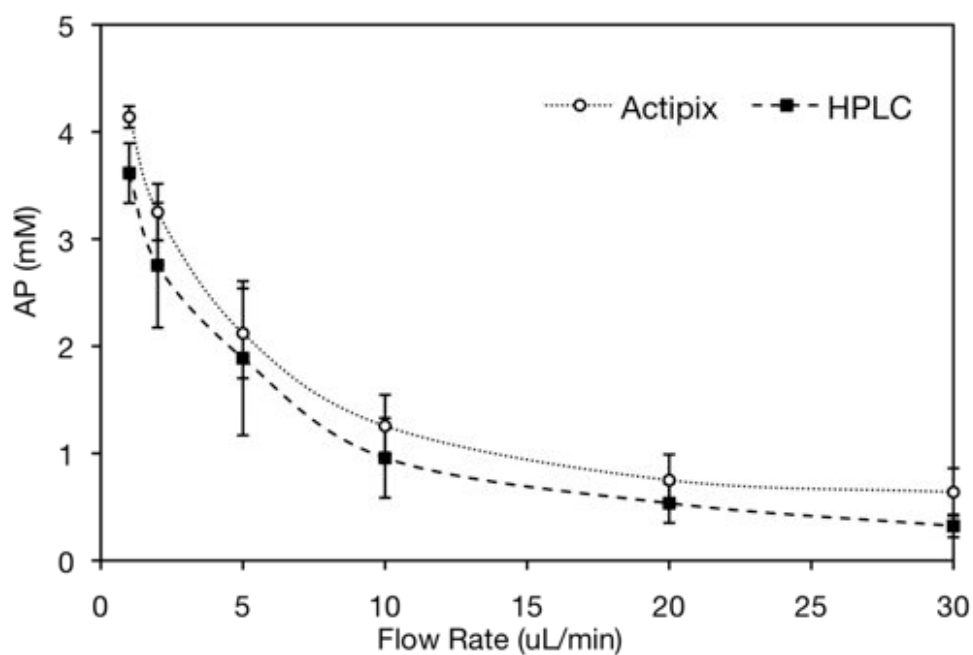
(b)
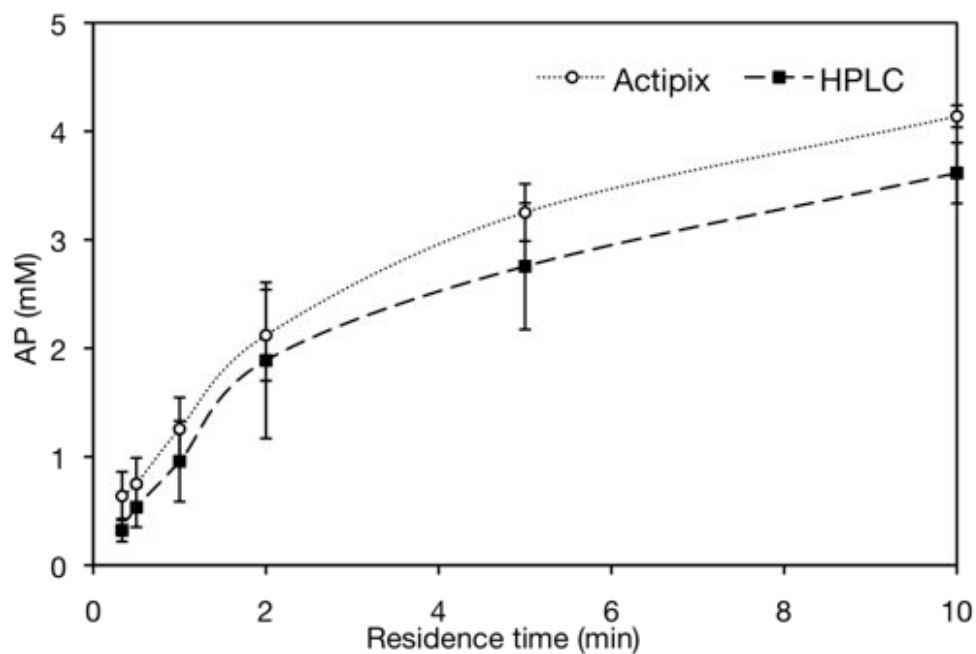
Figure 4.15: Continuous flow TAm-catalysed reaction integrated with Actipix online detection system. Profile of acetophenone (AP) formed as a function of (a) flow rate and (b) residence time. The reaction was carried out as described in Section 2.10.2.4 with the enzyme concentration of 1.0 mg/mL. Reaction was analysed for acetophenone production by the UV Actipix detector and validated by the off-line HPLC. Error bars represent one standard deviation about the mean (n = 3).

4.5 Summary

In this chapter, the implementation of a prototype enzyme microreactor based on the reversible immobilisation of His_6-tagged enzymes was demonstrated. A packed tube microreactor was selected over the derivatised fused silica capillary based on the outcomes discussed in Section 4.2.3. The reaction of the enzyme was downscaled from 300 μL to 10 μL in a 500 μm-ID packed tube IEMR. With the microreactor format, a small quantity of processing volume would allow for the precise control of reaction variables, such as reagent mixing, flow rates, reaction time, and mass transfer.

The strong coupling method of the His_6-tagged enzyme produces a highly stable and reusable IEMR. Moreover, the capacity of the packed tube IEMR was tested with several batches of enzyme immobilisation and the quantitative elution of the immobilised enzyme was demonstrated. The operational and storage stability of both enzymes on the immobilised form were also evaluated and reusability of the microreactor was performed over several cycles of immobilisation and elution.

Moreover, the integration of the UV online detection system in the packed tube IEMR was successfully demonstrated using the TAm model reaction. This detection system enables the monitoring of the reaction conditions in real time while reducing the sample processing time. The flexibility of this system would allow for a wide range of UV detection by simply changing to a different types of filter corresponding to the specific wavelength.

Overall, the microreactor configuration enables the biocatalytic reaction to be conducted rapidly for various TK and TAm libraries for screening purposes. The facile His tag-immobilisation method provides a stable heterogeneous catalyst, which can be easily incorporated into a FEP tube and is cost-effective due the low material cost and reusability property of the IEMR. Moreover, the problem of using expensive substrate such as hydroxypyruvate is alleviated in the microreactor

system compared to the microwell format as well as other limitations that include limited enzyme stability and higher operation cost.

Having established the IEMR prototype with known enzymatic conversions, the IEMR will be used for the kinetic evaluation of the transketolase (TK)-catalysed production of L-erythrulose (ERY) from hydroxypyruvate (HPA) and glycolaldehdye (GA) as substrates, and the second enzyme ω-transaminase (TAm)-catalysed reaction between S-methylbenzylamine (MBA) and ERY to produce 2-amino-1,3,4-butanetriol (ABT) and acetophenone (AP) (Chapter 5).

5 Determination of continuous flow enzyme kinetics in packed tube IEMR

5.1 Introduction

Microfluidic system has been used to characterise kinetics of various biochemical reactions and shows a huge potential to speed up processes especially in clinical diagnostics and drug discovery and screening (Section 1.2). Hadd et al. (1997) demonstrated the first enzyme kinetics analysis performed using microfluidic platform. Following that, numerous studies based on enzymatic microreactors have been reported in analytical chemistry or biochemistry.

Conventionally enzyme assays are performed based on homogenous reaction systems. Several reports of enzyme activity measured using microfluidic system have been conducted in homogenous solutions (Xue et al., 2001; Schilling et al., 2002; Miller & Wheeler, 2008; Wang et al., 2010). Alternatively, heterogeneous assays using immobilised enzymes can be adopted due to the attractive benefits that it can offer, such as ability to reuse the enzyme, easy separation of product and continuous flow analysis. Hickey et al. (2009) studied the effect of immobilised (+)-γ-lactamase within a capillary column microreactor in respect to its stability, activity, kinetics and substrate specificity. High stability of the immobilised enzyme was observed with the enzyme retained 100% of its initial activity at 80°C for 6 hr and 52% activity after 10 hr. Moreover, the data obtained on the substrate specificity of the enzyme in the immobilized form was in agreement with the data in free enzyme. On the other hand, reduced enzyme activity by 70% was reported. It was suggested that the exposure of the enzyme to formaldehyde during the immobilisation process contributed to the loss of the immobilised enzyme activity. In addition, Kundu et al. (2011) demonstrated the polymerization of lactones using immobilised *Candida antartica* Lipase B in a microreactor format. The apparent rate constant for the microreactor recorded was at least an order of magnitude higher than that observed for batch reactor. The small confined volume and higher surface-to-volume ratio of the microreactor attributed to the improved performance of the immobilised enzyme. As both of these examples were performed in

continuous flow mode, conversions were monitored as a function of position under steady-state conditions. In this case, all limits of dead time and difficulties with mixing were improved (Section 1.4.2).

In this chapter, the evaluation of enzyme kinetics in continuous flow mode was performed in a packed tube IEMR. Having established the IEMR prototype with known enzymatic conversions, the IEMR was used for the kinetic evaluation of the transketolase (TK)-catalysed production of L-erythrulose (ERY) from hydroxypyruvate (HPA) and glycolaldehdye (GA) as substrates, and the second enzyme ω-transaminase (TAm)-catalysed reaction between S-methylbenzylamine (MBA) and ERY to produce 2-amino-1,3,4-butanetriol (ABT) and acetophenone (AP). The apparent kinetic parameters of both enzymes in continuous flow reaction were determined using the Lilly-Hornby (Lilly et al., 1966) kinetics model. Several factors that affected the kinetics of immobilised enzyme were also discussed.

The key objectives of this chapter are:

- Demonstration of TK and TAm kinetics in a packed tube IEMR operated in continuous flow mode.

- Evaluation of the continuous flow kinetics using Lilly-Hornby (Lilly et al., 1966) kinetics model.

5.2 Evaluation of continuous flow enzyme kinetics

The kinetic parameters of the immobilised enzyme may result in different values compared to the solution-phase reaction due to conformational change of enzyme, partitioning effect, mass transfer restriction and enzyme deactivation. Among these, mass transfer limitation have been studied extensively from the viewpoint of heterogeneous catalysis (Kobayashi & Moo-Young, 1973; Toda, 1975; Lee et al., 1979; Ozdural et al., 2001; Kerby et al., 2006). Under these conditions, apparent kinetic constants are used to evaluate the kinetics of the immobilised enzyme. The Lilly-Hornby (1966) model is commonly employed to determine kinetic parameters for continuous packed-bed reactors where a plug flow assumption is made. Furthermore, the model is able to account for any mass transfer effects that may be present and can alter the overall enzyme kinetics. Under steady state conditions the apparent kinetic parameters in a packed-bed enzyme reactor can be determined by the following equation:

$$f[A_o] = K_{m \, (app)} \ln(1\text{-}f) + C/Q$$

Where f is the fraction of substrate reacted, $[A_o]$ is the initial substrate concentration, $K_{m \, (app)}$ is the apparent Michaelis constant, C is the reaction capacity of the reactor and Q is the flow rate.

If values of f are measured when various initial concentrations of substrates are perfused through the same reactor at identical flow rates (Q is constant), then $f[A_o]$ plotted against $\ln(1\text{-}f)$ will give a straight line if $K_{m \, (app)}$ and C are constant at this flow rate. The slope of the line will be equal to $K_{m \, (app)}$ and the y-intercept will be equal to C/Q. Thus $K_{m \, (app)}$ and C may be determined for any flow rate of substrate through the reactor.

The applicability of this model has been performed in many studies of enzyme kinetics, particularly for the packed bed microreactor (Ozdural et al., 2001; Seong et

174

al., 2003; Ozdural et al., 2001; Kerby et al., 2006). Most recently Matosevic et al. (2011b) demonstrated the kinetics evaluation of transketolase enzyme using this model in a microcapillary. The findings of the study will be compared with the present work in the next section.

5.3   Continuous flow kinetics in packed tube IEMR

Determination of kinetic parameters of the continuous flow mode packed tube IEMR were conducted for both enzymes at flow rates ranging from 2-30 µL/min. For TK, the concentration of GA was varied from 10 to 50 mM while HPA was kept at 100 mM and for TAm, the concentration of ERY was varied from 50 to 300 mM with MBA kept at 10 mM. The progression curve for each substrate concentration was shown to follow the standard TK and TAm reaction profile in solution-phase, with conversion yield increasing proportionately to substrate concentration (Figure 5.1). Data from these graphs were then used to plot the Lilly et al. (1966) kinetic model and determine the kinetic parameters for the continuous flow reaction (Figure 5.2). The slopes of the fitted lines were evaluated to give the $K_{m(app)}$ for each flow rate.

From Figure 5.3, a pronounced effect of flow rate was observed on $K_{m(app)}$, where the values increased with lower flow rates. This can be explained by the presence of a diffusion layer surrounding the immobilised enzyme (Lilly et al., 1966). At high flow rates, the mass transfer effect is less pronounced as the diffusion layer around the bead gets thinner, while the effect is more significant at lower flow rates, which could be observed as an elevation of the $K_{m(app)}$ values. This diffusion layer theory fits the trend displayed in Figure 5.3, where an approximately linear decrease was seen for $K_{m(app)}$ between 2-10 µL/min, and then the values started to level-off between 10-30 µL/min. Toda (1975) addressed the problem of inter-particle mass transfer in connection with the overall kinetics of gel-entrapped enzymes packed in a fixed bed reactor. He suggested that the increase in the $K_{m(app)}$ value at a low flow rate is due to film diffusion or a liquid channeling factor. In addition, several experimental studies have shown similar flow dependency of $K_{m(app)}$ (Lilly et al., 1966; Shiraishi et al., 1996; Ozdural et al., 2001). They explained the importance of mass transfer outside a solid catalyst with the fact that the apparent Michaelis constant determined in a packed column reactor varied with the flow rate of the liquid. On the contrary, Matosevic et al. (2011b) found an increase in $K_{m(app)}$ with increasing flow rate of substrate through a surface derivatised capillary containing immobilised TK enzyme. With lower operating flow rates of 0.33-3 µL/min and

reduced enzyme concentration compared to the packed tube reactor, the mass transfer effect observed was not as pronounced as in our system.

(a)
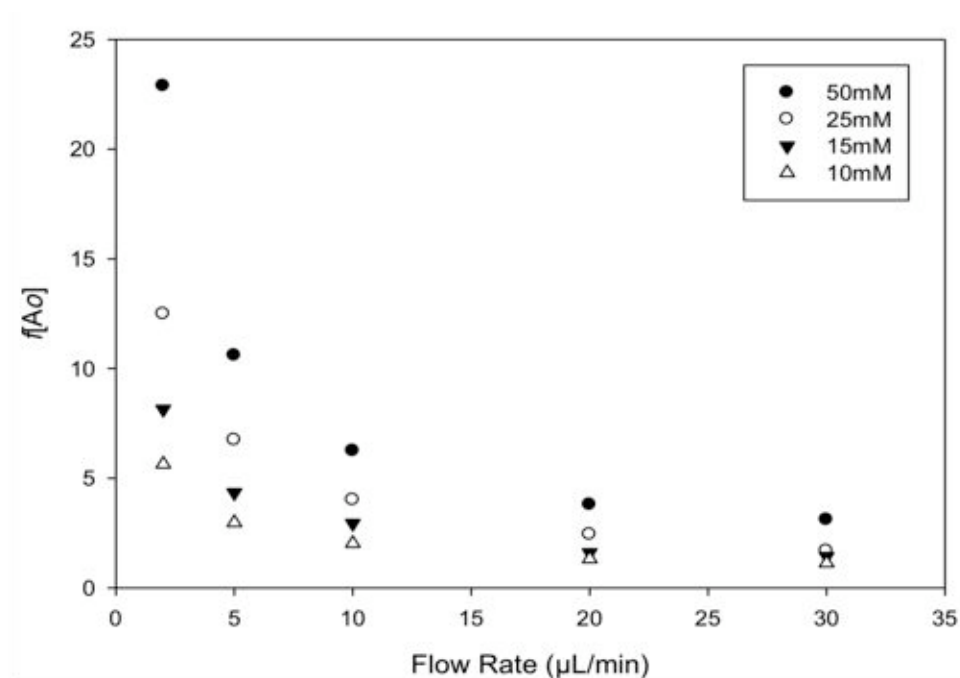
(b)
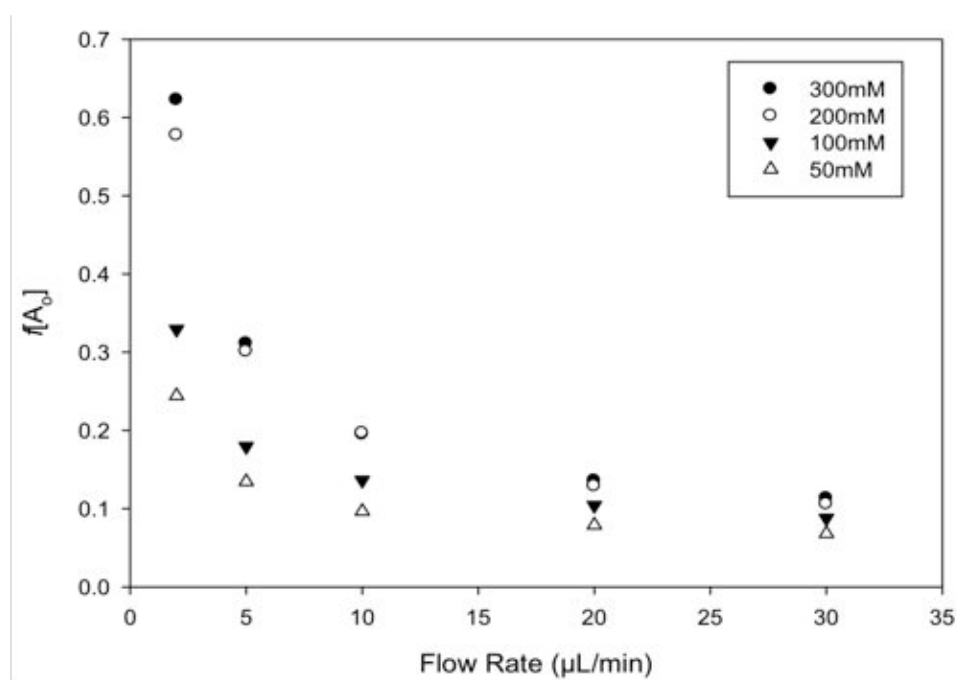
Figure 5.1: Bioconversions using different substrate concentration at flow rates ranging from 2 μL/min-30 μL/min. (a) Continuous-flow TK-catalysed reaction at different GA concentration (10-50 mM) with HPA concentration was kept at 100 mM (b) Continuous-flow TAm-catalysed reaction at different ERY concentration (50-300 mM) with MBA concentration was kept at 10 mM.

178

(a)
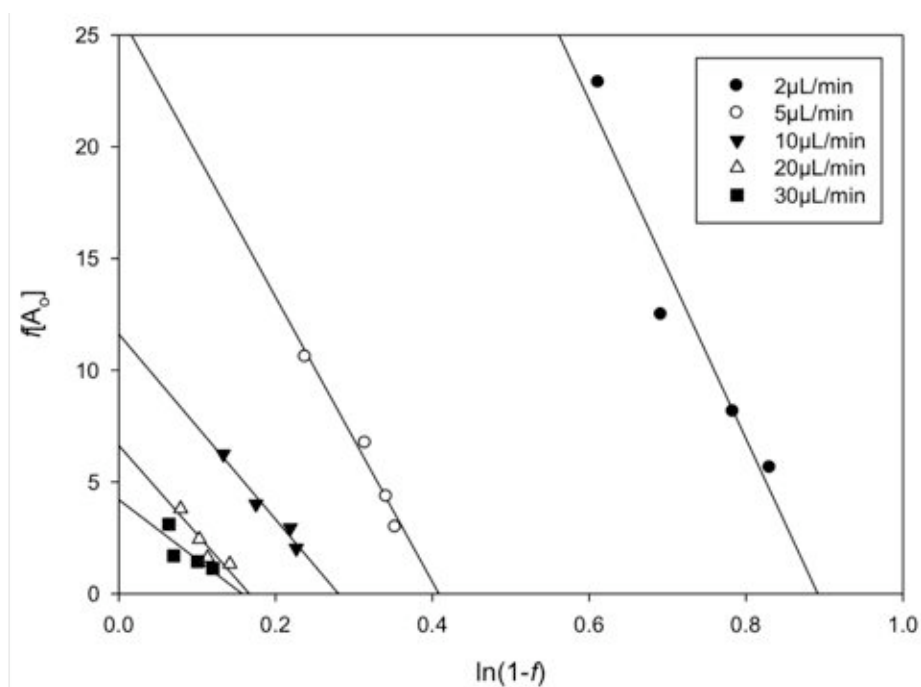
(b)
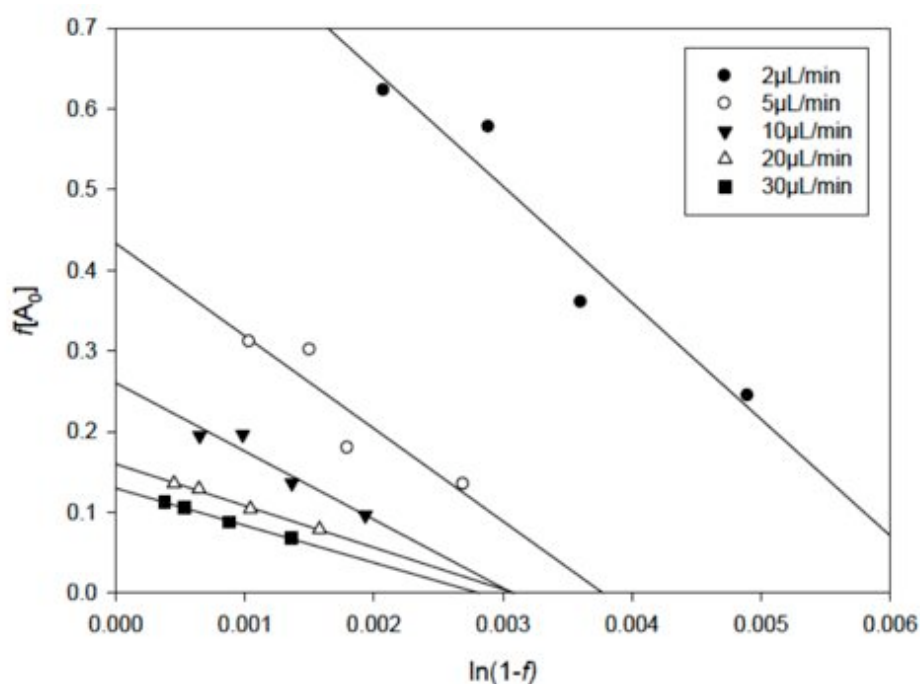
Figure 5.2: Kinetics determination using Lilly-Hornby model for continuous-flow mode reaction. Data to obtain these plots was taken from Figure 5.1. (a) TK-catalysed reaction and (b) TAm-catalysed reaction. Solid lines fitted by linear regression. Values of $K_{m\ (app)}$ and C for the continuous flow reactions could be obtained from these plots.
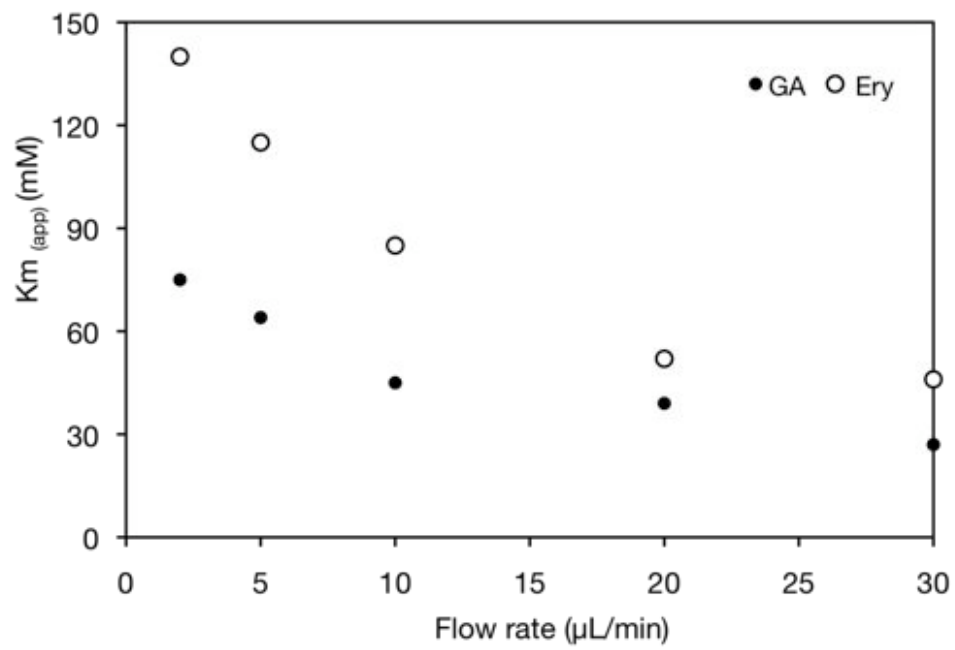
Figure 5.3: $K_{m\ (app)}$ values for GA and ERY ranging from 2 μL/min-30 μL/min. Data to obtain this plot was taken from Figure 5.2.

The reactor capacity (C) values obtained were nearly constant for all experiments, with an average of 12.88±0.27 mM/min and 0.28±0.027 mM/min for GA and ERY, respectively. These values were then used to determine the turnover number, k_{cat} which was 32 s^{-1} for TK and 0.058 s^{-1} for TAm. These values were approximately 3 times less than k_{cat} values in solution-phase (Section 3.2.5 and Section 3.3.6). This apparent loss in activity may be due to the inaccessibility of some enzyme molecules that were immobilised in the packed tube to the substrate molecules. The intrinsic compressibility of porous agarose beads resulted in highly compact packing, which created a barrier to the accessibility of the substrate to those enzyme molecules located within the beads packing. In addition, non-uniform enzyme distributions within the support would also affect the apparent kinetic parameters where the catalyst immobilised on the surface can render far greater enzyme utilization efficiency compared to the catalyst in the interior core configuration (Dalvie and Baltus, 1992; Juang and Weng, 1984). Finally, altered conformation of enzyme and steric hindrance could also contribute to the loss of activity of the immobilised enzyme (Krenková & Foret, 2004; Delouise & Miller, 2005; Kerby et al., 2006).

5.4 Effect of substrate residence time

Characteristic operating parameters for continuous reactor is the dilution rate, D (h^{-1}) and the average residence time, τ (h). These parameters are related as follows:

$$\tau = \frac{1}{D} = \frac{V}{Q}$$

In continuous reactor operation, the amount of material that can be processed over a given period of time is represented by the volumetric flow rate, Q (mL.h^{-1}). Therefore, for a given throughput, the reactor size V (mL) and associated capital and operating costs are minimised when τ is made as small as possible (Doran, 2013).

The average residence time is also known as a space time or holding time is inversely proportional to the dilution rate. At high dilution rate, conversion of substrate to product decreases. In the continuous flow of TK-catalysed and TAm-catalysed reactions in the packed tube IEMR, the product formation was proportional to the space time (τ) at the range of higher flow rates (10-30 µL/min) (Figure 5.4). This pattern started to level-off at higher space time (1-5 µL/min) which displayed similar trend as $K_{m(app)}$ on the flow rates (Figure 5.3). This situation can be explained by the presence of a diffusion layer surrounding the immobilised enzymes (Lilly et al., 1966). At higher flow rates, the mass transfer of the substrate and the product through the layer are improved which resulted in higher conversion of the substrate. This finding shows that the rate of enzyme reaction is highly affected by the diffusion rate presence in the immobilised enzyme system.

(a)
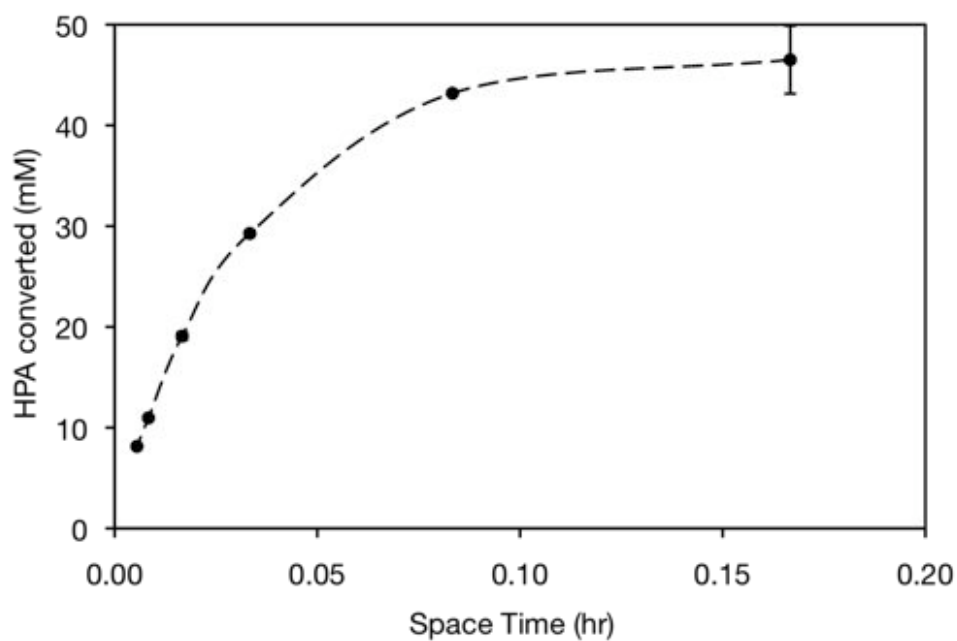
(b)
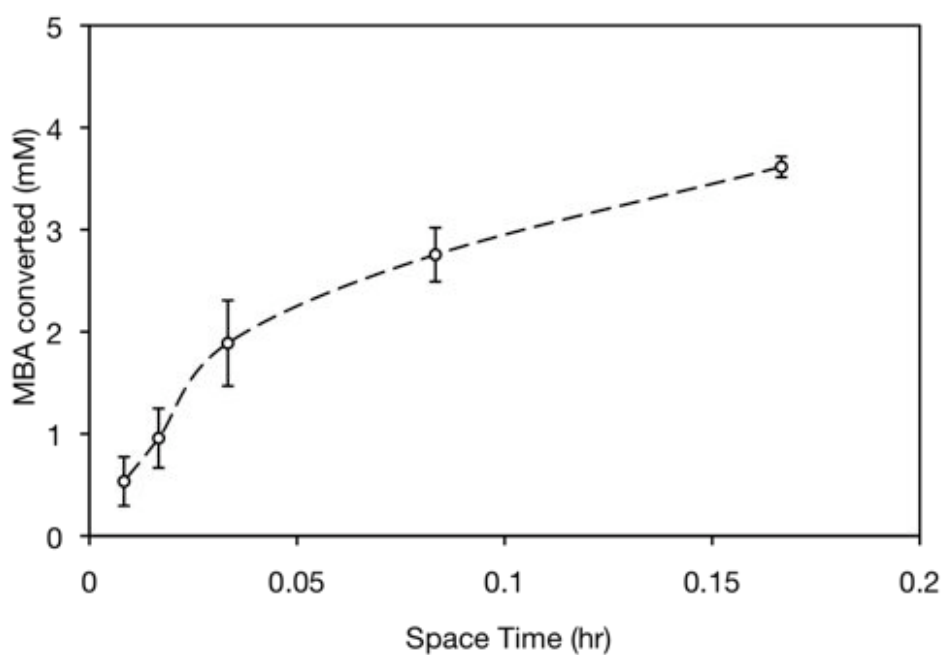
Figure 5.4: Analysis of space time with respect to the converted substrate in the continuous flow microreactor. (a) The relation of space time with HPA converted to erythrulose in TK-catalysed reaction, (b) The relation of space time with MBA converted to AP in TAm-catalysed reaction. Error bars represent one standard deviation about the mean (n = 3)

5.5 Summary

In this chapter, the kinetic evaluation of transketolase and transaminase in continuous flow mode was successfully demonstrated using Lilly-Hornby (1966) kinetics model in the packed tube IEMR. Conversion yield shown to increase with the substrate concentration as seen in the standard TK and TAm reaction profile in solution-phase. Moreover, no significant inhibition by the products was observed within the substrates concentration range studied.

The $K_{m(app)}$ for both enzymes showed to be a function of flow rate whereby the $K_{m(app)}$ decreases with increasing flow rate. The dependency of the $K_{m(app)}$ on the flow rate can be explained by the presence of the diffusion layer surrounding the immobilised enzyme and the effect was reduced at higher flow rates as displayed in Figure 5.3. In addition, the $K_{m(app)}$ values for both enzymes at the highest flow rate (30 μL/min) were found to be smaller than that for the soluble enzyme. This behaviour might be attributed to the increased affinity of the immobilised enzyme to the substrate, due to the reduced mass transfer effect at high flow rate. Furthermore, values of k_{cat} calculated were three times smaller than those measured in free solution. There are several possible explanations for the reduced k_{cat} obtained in the immobilised form, these include the imperfect immobilisation, non-uniform distribution of the enzyme and steric hindrance.

The enzyme kinetics of transketolase and transaminase enzyme was successfully demonstrated in this chapter. The kinetic model system adopted in this analysis allows for the evaluation for any mass transfer effects that may be present and can alter the overall enzyme kinetics. Nevertheless, the findings showed that the apparent Michaelis Menten constant of both enzymes to be affected by the mass transfer effect which was also observed in many other studies (Lilly et al., 1966; Shiraishi et al., 1996; Ozdural et al., 2001). In conclusion, this packed tube IEMR system has a potential to be used to characterise kinetics of various biochemical reactions based on the simplicity of the system. The continuous flow operation eliminates dead time, improve mixing problem and the immobilised enzymes can be reused and easily recovered.

6 Multi-step enzymatic reaction in packed tube IEMR

6.1 Introduction

The production of complex organic compounds through integration of multi-step synthesis provides an attractive alternative for the creation of molecules with increased complexity and defined functions or properties. However, the traditional pathway for multi-step synthesis usually adopted the batch and iterative step-by-step transformation of starting materials into desired product. Each synthesis step usually is completed with the product removal from the reaction mixture and purified to remove any undesired components that have adverse effect with the subsequent synthetic transformations (Webb & Jamison, 2010). This approach is considered time consuming and commonly wasteful and pose clear contradiction with the single-cell multi-step biosynthetic pathways found in nature (Dewick, 2009). Alternatively, the multi-step syntheses can be performed by integrating multiple synthetic steps into a single and continuous flow operation without having to isolate the intermediate products.
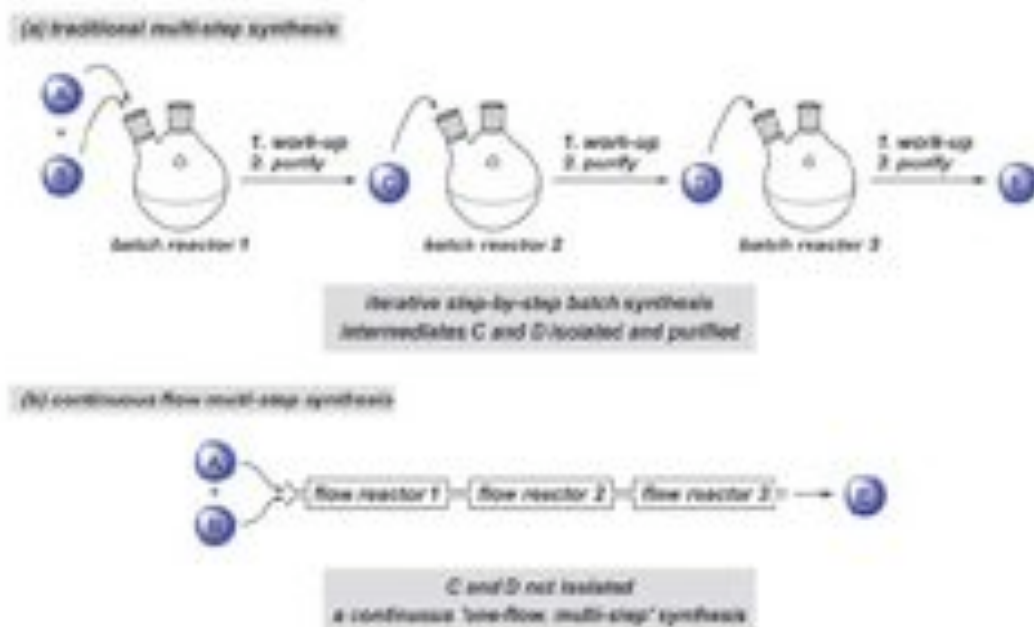
Figure 6.1: Multi-step synthesis strategies. Image reproduced from (Webb & Jamison, 2010).

The use of biocatalysts in product synthesis is well documented and has proven to be an extremely advantageous technology (Section 1.4). This approach is particularly appealing since biocatalysts are intrinsically "green" (biodegradable), highly selective and most importantly they are compatible with each other within certain ranges of operating conditions (Ricca et al., 2011). The cooperation of immobilised catalysts in the continuous flow system further extends the potential for revolutionizing the synthesis process (Section 1.5).

The combination of transketolase and transaminase enzyme reactions in series has the potential to create chiral amino-alcohols from achiral starting compounds. This *de novo* designed pathway for the synthesis of optically pure amino alcohols comprises of the formation of asymmetric carbon-carbon bond catalyses by transketolase and subsequently the addition of the chiral amino group by transaminase. This model reaction was previously demonstrated by Ingram et al. (2007) using transketolase from *E.coli* and β-alanine: pyruvate aminotransferase (β-A:P TAm) from *Pseudomonas aeruginosa* overexpressed in a single host for the biocatalytic synthesis of 2-amino-1,3,4-butanetriol (ABT) in a one-pot process in microwell format. The reaction however showed to be limited due to the low activity of the β-A:P TAm causing a low overall yield of the reaction. The two step synthesis of the ABT was further investigated by Rios-Solis et al. (2011) where they paired the wild-type *E. coli* TK with ω-transaminase from *C. violaceum* that showed higher yields and stereoselectivities. The 87% mol/mol yield for ABT synthesis represented an improvement of 4-fold in yield in a quarter of the reaction time compared to the previous work (Ingram et al., 2007).

Apart from the microwell format, the production of ABT through multi-step enzymatic reaction was also performed in a microreactor system. Matosevic et al. (2011b) exploited the advantages of microreactor system that is otherwise unachievable in a conventional microwell-based system. To demonstrate the feasibility of performing the continuous flow TK-TAm enzymatic reaction using immobilised enzymes, Matosevic et al. (2011b) derivatised the inner surface of a fused silica capillary ("open-tubular" reactor). The dual TK-TAm reaction reached

5% conversion over 1 hour at an initial MBA concentration of 10 mM.

In this chapter, the synthesis of the ABT compound in a packed tube IEMR was performed using two model reaction systems. The first model system was a two-enzyme route with sequential use of transketolase (pQR 791) and ω-transaminase (pQR 801) as previously demonstrated (Matosevic et al., 2011b; Rios-Solis et al., 2011). The first step of the dual reaction involved the reaction catalysed by transketolase (pQR 791) between hydroxypyruvate (HPA) and glycolaldehdye (GA) producing L-erythrulose (ERY), and subsequently transaminase (pQR 801) catalysed the second part by aminating ERY using S-methylbenzylamine (MBA) to produce the chiral amino alcohol product of ABT. Demonstration of the synthesis of ABT was executed by connecting single TK and TAm IEMR in series (Figure 6.2). The second model reaction was the three-step enzymatic reaction through sequential use of ω-transaminase (pQR 1021), transketolase (pQR 791) and ω-transaminase (pQR 1021). Instead of using HPA as the starting material that is a rather expensive substrate, serine (SER) and GA were used which were converted into HPA by TAm in the first part of the three-steps reaction. Subsequently, TK catalyzed the reaction between HPA and the remaining GA into ERY. The three-step enzymatic reaction was completed by the reaction catalysed by the second TAm between ERY and SER to produce the chiral amino alcohol, ABT. Three single IEMRs were cascaded in series to allow the multi-step enzymatic reaction (Figure 6.3).

Demonstration of the synthesis of the ABT product via the dual and three-step reaction and the monitoring of each component can provide a full profile of the bioconversion. In order to achieve this, the stability and reactivity of reaction components (substrates and products) in the presence of different enzymes were investigated to access any effect on the enzyme kinetics and aid in identifying the optimal parameters for the multi-step enzymatic reactions.

The key objectives of this chapter are:

- Demonstration of the dual enzyme reaction involving TK and TAm immobilised in series to produce the chiral amino alcohol product, ABT.

- Demonstration of the three-step enzyme reaction comprised of the sequential TAm, TK and TAm reaction conducted in three single IEMRs cascaded in series to synthesise ABT.

-
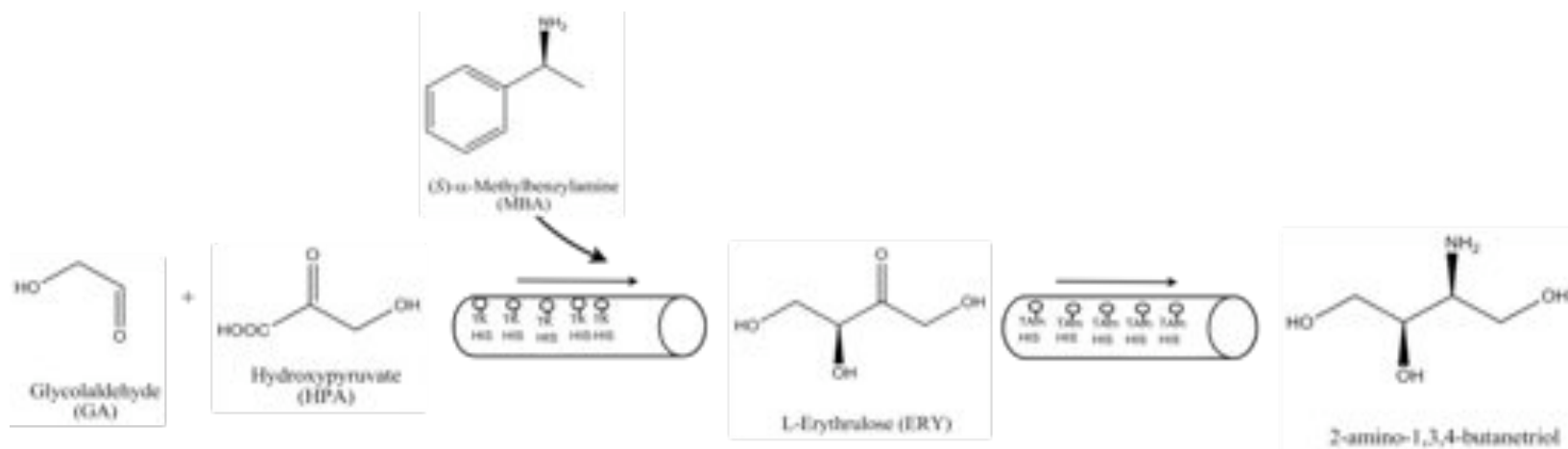
Figure 6.2: Schematic diagram of continuous flow dual reaction kinetics. The dual reaction system consists of two packed tube IEMR connected in series. His$_6$-transketolase (pQR 791) and His$_6$-transaminase (pQR 801) are immobilised inside each of the IEMR.
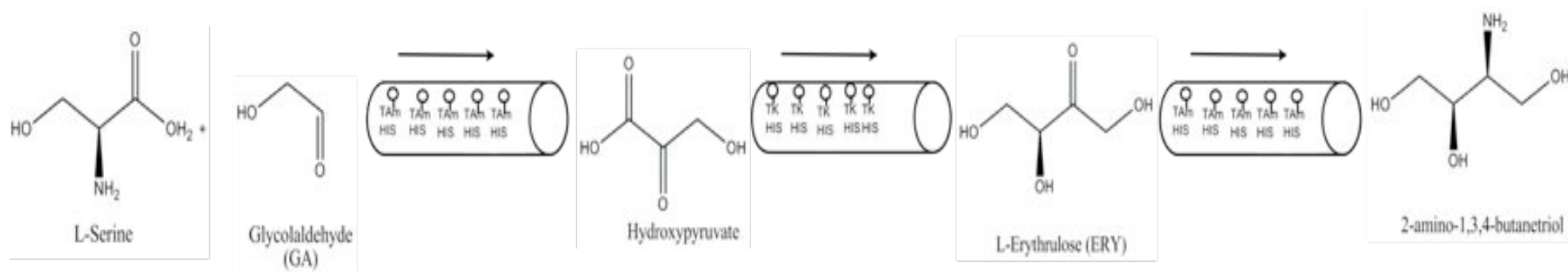
Figure 6.3: Schematic diagram of continuous flow three steps enzyme reaction kinetics. The three steps enzyme reaction system consists of three packed tube IEMR connected in series. His$_6$- transaminase (pQR 1021) and His$_6$-transketolase (pQR 791) are immobilised inside each of the IEMR.

6.2 Dual TK-TAm reaction

6.2.1 Setup of the dual microreactor system and immobilisation of enzymes

The dual enzyme reaction was executed by connecting single TK and TAm IEMR (2x5 cm) in series that gives a total reaction volume of ~10 μL each (Figure 2.4). The immobilisation of both His_6-TK and His_6-TAm were performed separately on each IEMR before assembly following the procedure previously described (Section 2.10.2.2). Immobilisation was performed with purified solutions of both enzymes preparations at a concentration of 0.2-2.0 mg/mL. Quantification of the immobilised enzyme was carried out based on the elution sample (Section 2.10.2.2) obtained once the reaction was completed. The measurement of the enzyme concentration was determined by absorbance measurement at 280 nm and validated via Bradford assay at 595 nm on a bench scale spectrophotometer (Section 2.2.3.2).

6.2.2 Stability of TK and TAm reaction components in the dual enzymatic reaction

The stability of each enzyme reaction component is paramount in the multi-step enzymatic syntheses. Thus, some compromises have to be made regarding the optimum conditions for each enzyme. One of the important factors to look at is the buffer condition. It was previously reported that the optimal buffer condition for TK and TAm were Tris-HCl (Hibbert et al., 2005; Cázares et al., 2010) and HEPES (Kaulmann et al., 2007; Smithies et al., 2009) buffer respectively. Stability of HPA towards HEPES buffer was found to be detrimental to the substrate (Matosevic et al., 2011b). Similar finding was also reported previously whereby HEPES buffer was found to greatly affect the stability of both substrates, HPA and GA (Chauhan et al., 1996). On the other hand, the stability of the transaminase substrate MBA in the presence of TK substrates was proved to be high in Tris-HCl (Matosevic et al., 2011b). Based on these considerations and the preliminary data of enzymatic activity in a batch solution (Chapter 3), Tris-HCl buffer was selected for the dual TK-TAm reaction.

Moreover, the presence of TK cofactors (Mg^{2+} and TPP) did not pose any negative effect on the TAm bioconversion and likewise the effect of PLP on the TK bioconversion was minimal (Rios-Solis et al., 2011). In addition, the coupled reaction was performed at pH 7.5, which was previously shown to be suitable for both enzymes (Mitra et al., 1998; Kaulmann et al., 2007).

6.2.3   Stability of MBA substrate in His$_6$-TK immobilised microreactor

The stability of the TAm reaction component MBA in Tris-HCl (pH: 7.5) buffer was investigated in TK packed tube IEMR. Reaction mixture of TK reaction (60 mM GA and HPA, cofactors) with the addition of 6 mM MBA was continuously fed into the packed tube IEMR at various flow rates (1-30 µL/min). Another set of TK reaction with similar condition (without MBA) was also run as a control. The utilisation of MBA and ERY production were measured by HPLC at different flow rates. No observable depletion of MBA was observed which showed that there was no activity of TK towards MBA. In addition, the reaction profiles of ERY formation for both conditions displayed very similar results; the slight difference might be due to the experimental errors (Figure 6.4). This suggested that the presence of MBA in the TK reaction mixture does not pose any significant effect on the reaction.
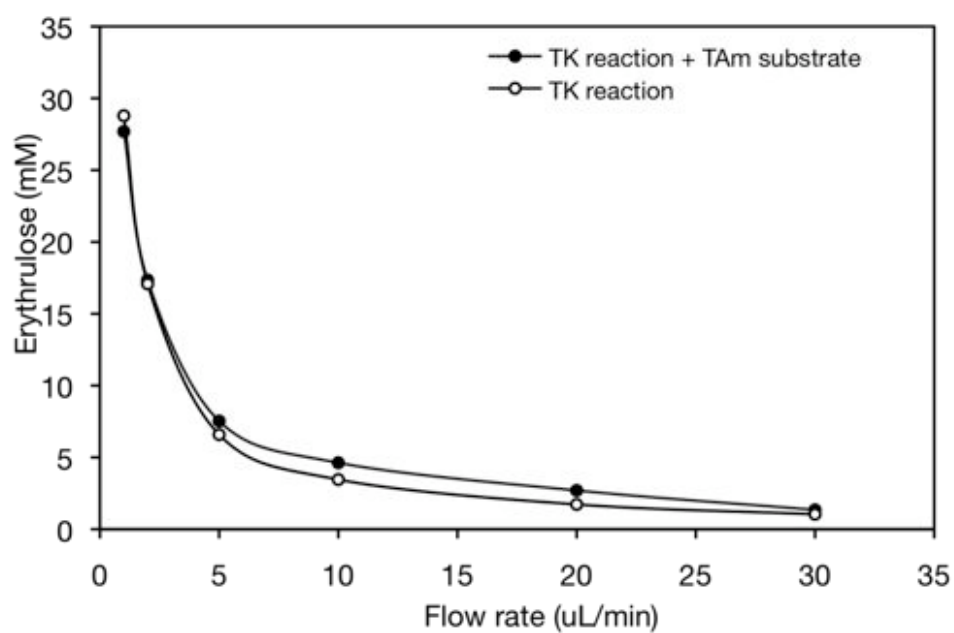
Figure 6.4: Reaction profile of the transketolase reaction in the presence of the TAm substrate. Two sets of TK reactions were conducted; one in the presence of TAm substrate, MBA and a TK control reaction. This result showed that the presence of MBA in the TK reaction mixture does not have any effect on the TK reaction.

6.2.4 Demonstration of the dual model reaction

In order to achieve the synthesis of the chiral amino alcohol ABT, the dual TK-TAm reaction system via two packed tube IEMRs was performed directly from achiral substrates GA and HPA with MBA as the amino donor. The reaction was performed in the presence of both enzymes cofactors in Tris-HCl buffer at pH 7.5 and room temperature. The reaction was monitored for ERY, AP and ABT production via HPLC analysis.

Substrates mixture of both enzymes, with initial concentrations of 60 mM (GA and HPA, each) and 6 mM (MBA), were fed together in the presence of cofactors (Section 2.12.1). Higher initial substrate concentration of GA and HPA (10x more) compared to MBA were used which resulted in higher ERY formation to shift the equilibrium towards ABT production in the second step of the reaction. Substrate mixtures were loaded into the feed reservoir in a 1 mL syringe and dispensed via a syringe pump connected to the first IEMR. In the first part of the dual reaction, His_6-TK catalysed the conversion of the achiral substrates HPA and GA to form ERY. The product of the first reaction was then continuously fed to the second IEMR containing the immobilised His_6-TAm. The dual reaction was completed with the amination of ERY with MBA as the amino donor to produce the final target reaction product, ABT. This dual TK-TAm reaction was conducted in continuous flow mode at various flow rates ranging from 1-30 μL/min, which corresponds to residence times from 0.33 to 10 minutes per individual reaction step.

6.2.4.1 Dual TK-TAm reaction in packed tube IEMR

The profile of the dual TK-TAm reaction can be monitored by measuring the substrate and product composition at certain time period, which can give the complete mass balance of the reaction. However the target product of the dual reaction, ABT, cannot be quantified based on the formation of the by-product, AP, due to the presence of the side reactions between the residual TK substrates, HPA and GA in the transaminase-catalysed reaction (Chen et al., 2006; Kaulmann et al.,

2007; Rios-Solis et al., 2011). Therefore the quantification of the ABT has to be performed via the derivatisation process (Section 2.8) prior to the HPLC assay.

With an initial substrate concentration of 6 mM MBA, the coupled reaction reached approximately 83% conversion in 20 minutes at the lowest flow rate (Figure 6.5). This corresponds to a specific activity of 0.03 $\mu mol/min/mg_{TAm}$. On the other hand, the formation of ABT was not increase proportionally with AP and the trend became more apparent at higher flow rates. This result was anticipated as higher residual concentrations of HPA and GA from the TK-catalysed reaction were fed into the second step, which resulted in more side reactions. Consequently, the formation of ABT was greatly reduced and the detection of the product became more error prone especially at flow rates between 10-30 $\mu L/min$.

The production of the ABT in the final step of the TK-TAm reaction is dependent on the formation of ERY in the first part of TK-catalysed reaction. In order to estimate the conversion yield of GA and HPA to ERY in the first reaction, a separate experiment was conducted. A single IEMR was prepared with immobilised TK. Similar enzyme and substrate concentrations were used to match the condition in the coupled reaction. Based on Figure 6.6, the reaction reached a conversion of 90% in 10 minutes at the lowest flow rate with a specific activity of 8.20 $\mu mol/min/mg_{TK}$. This suggested that a total of 54 mM ERY was fed to the second IEMR in the coupled reaction. Therefore, about 9% of the relative amount of ERY supplied by the TK step was aminated by TAm in the second reaction. Based on these results, it is apparent that the transketolase is more active than transaminase for the model reaction under the conditions investigated. A similar trend was also observed in the rates of catalysis of the two enzymes in batch solution as well as other studies reported elsewhere (Ingram et al., 2007; Matosevic et al., 2011; Rios-Solis et al., 2011). Nevertheless, low specific activity of TAm was not only due to the slow amination rate of the enzyme but also due to the presence of side reactions with residual HPA and GA. Kaulmann et al. (2007) reported that TAm has the affinity to catalyse the amination of both HPA and GA leading to the reduced

formation of ABT at higher flow rates when higher residual concentrations of HPA and GA from the TK-catalysed reaction were present.

(a)
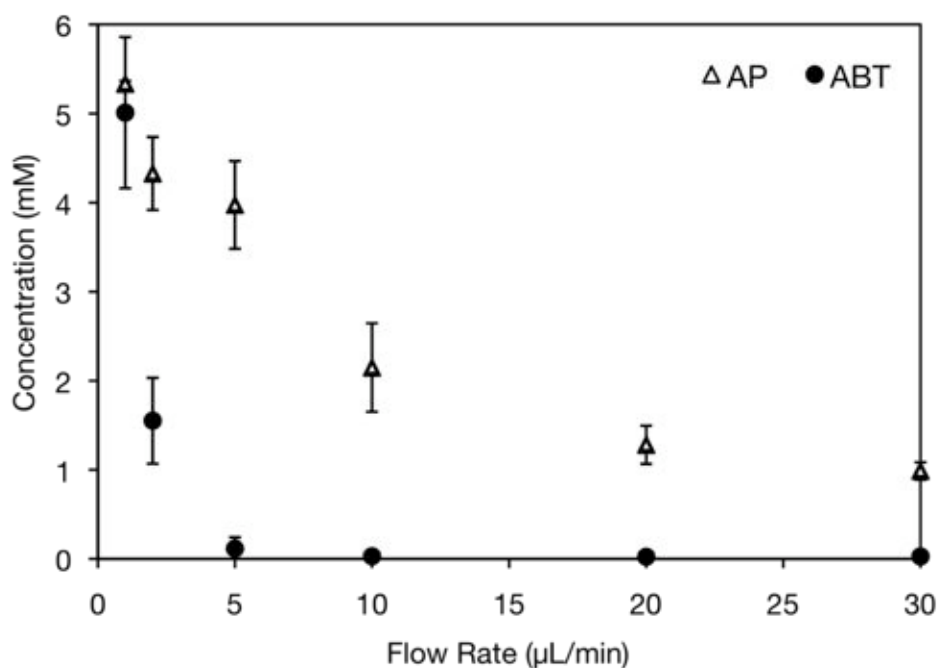
(b)
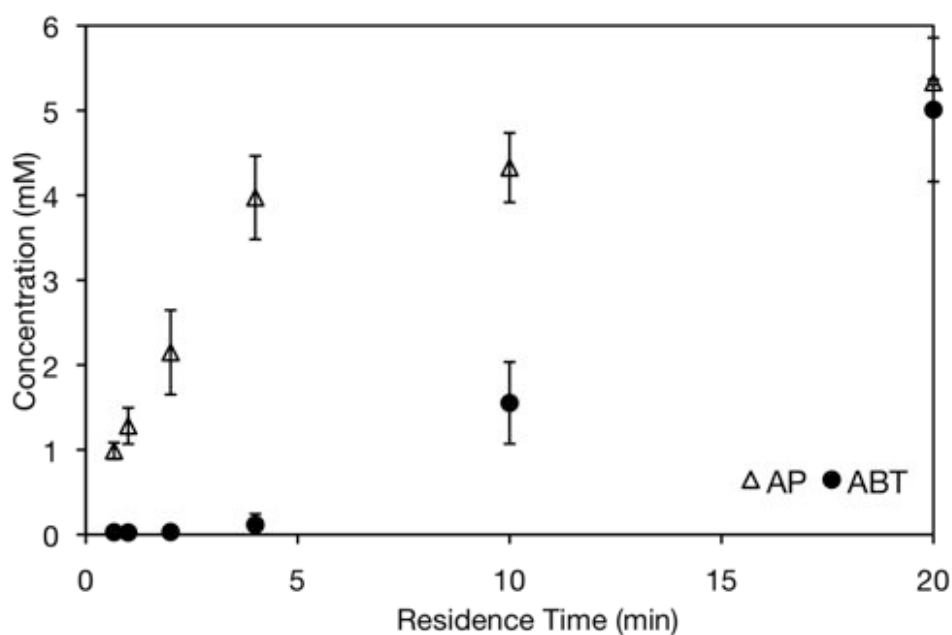
Figure 6.5: Dual TK-TAm reaction in IEMR. Graph showing the formation of the ABT and by-product AP in the TK-TAm dual reaction as a function of (a) flow rate and (b) residence time. Initial substrates concentration of 60 mM (GA and HPA each) and 6 mM MBA in 50 mM Tris−HCl buffer, pH 7.5 with cofactors thiamine pyrophosphate (TPP), 2.4 mM and $MgCl_2$, 9 mM and 0.2 mM PLP at room temperature The concentration of immobilised enzyme was 1.1 ± 0.15 mg/mL for TAm and 0.15 ± 0.006 mg/mL for TK. Error bars represent one standard deviation about the mean (n = 3).

(a)
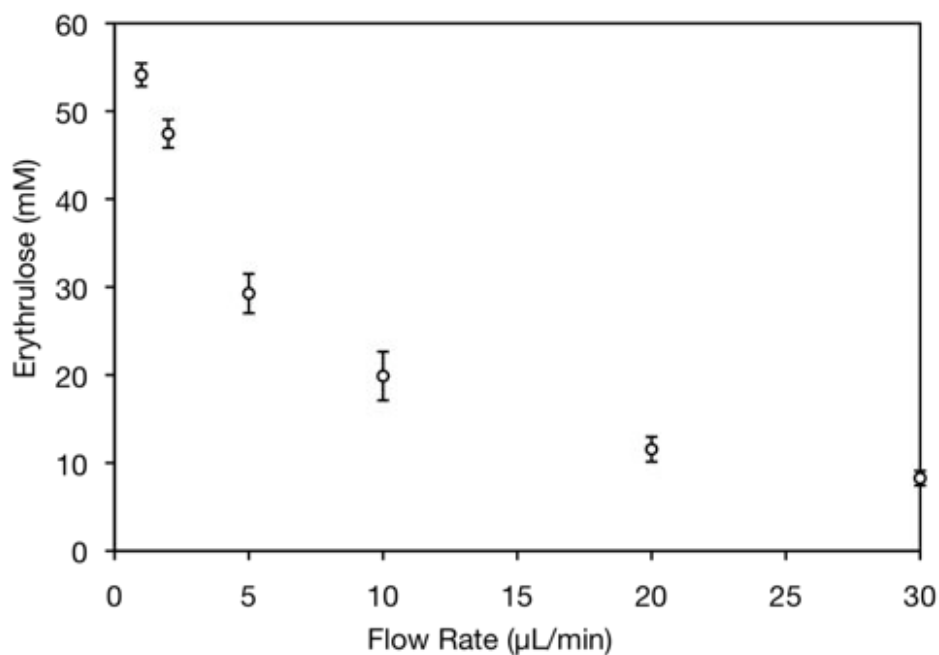
(b)
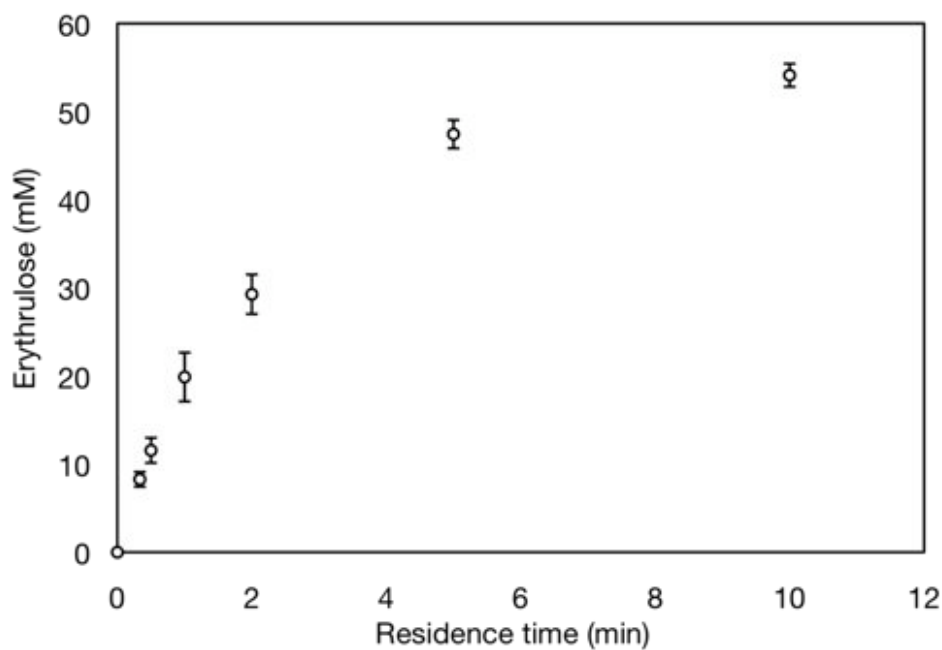
Figure 6.6: Production of erythrulose in the first TK-catalysed step in the dual TK-TAm reaction. Graph showing the formation of the ERY in the first step of the TK-TAm dual reaction as a function of (a) flow rate and (b) residence time. Initial substrates concentration of 60 mM (GA and HPA each) and 6 mM MBA in 50 mM Tris−HCl buffer, pH 7.5 with cofactors thiamine pyrophosphate (TPP), 2.4 mM and $MgCl_2$, 9 mM and 0.2 mM PLP at room temperature The concentration of immobilized TK enzyme was 0.15 ± 0.006 mg/mL. Error bars represent one standard deviation about the mean (n = 3).

6.2.4.2 Side reaction of HPA and GA towards TAm reaction

The effect of the presence of GA and HPA in the second step of TAm-catalysed reaction was investigated. Several sets of reactions catalysed by TAm (constant enzyme concentration) were performed with variation in the substrate added in the reaction. The reactions were conducted in batch solution whereby the final concentration of each substrate was kept constant to allow direct comparison of their respective initial rate. The reactions were monitored for the formation of acetophenone by HPLC analysis. Results from Figure 6.7 confirmed that GA and HPA were reactive towards TAm as previously reported (Chen et al., 2006; Kaulmann et al., 2007; Rios-Solis et al., 2011). The GA appeared to be more reactive with an initial rate of 0.0239 mM/min compared to 0.0108 mM/min for HPA. Moreover, TAm showed higher affinity towards GA compared to ERY, which would explain the low formation of ABT at higher flow rates. Therefore, the key point for this TK-TAm reaction was to match the TK and TAm activity to reduce the HPA and GA side reaction by TAm, and ultimately to achieve the highest possible ABT yield.
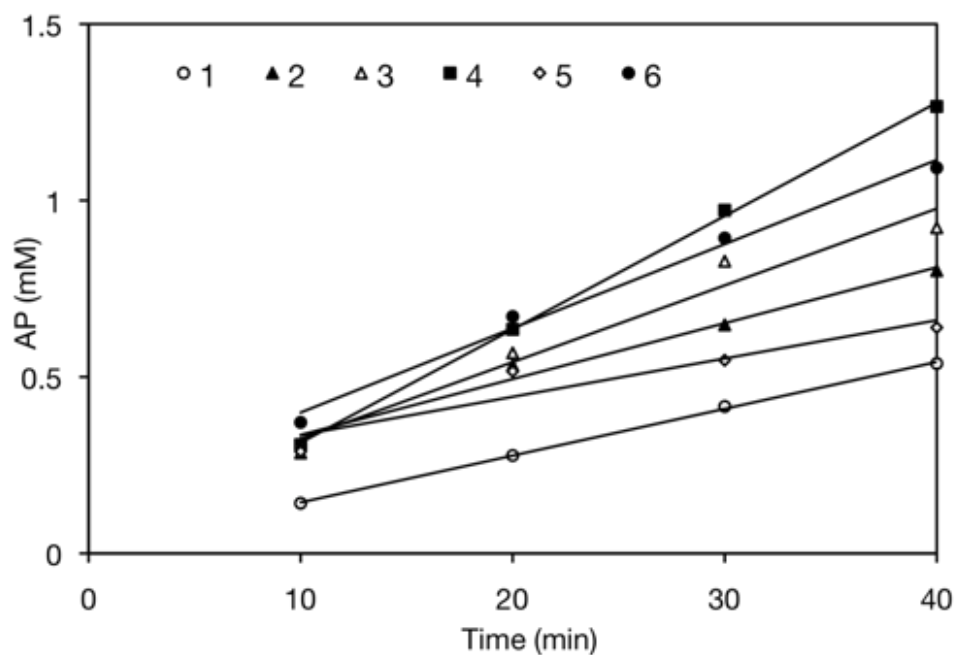
Figure 6.7: Profiles of the TAm-catalysed reaction with various substrate conditions. Graph showing the production of acetophenone catalysed by TAm in batch solution. Different substrate conditions were tested and the initial rate of each condition was determined. Reaction conditions: 5 mM MBA, 50 mM acceptor, 0.2 mM PLP, pH 7.5 in Tris-HCl buffer, 0.16 mg/mL TAm. Substrate mixture: [1] MBA+ERY, [2] MBA+ERY+HPA, [3] MBA+ERY+GA, [4] MBA+ERY+HPA+GA, [5] MBA+HPA, [6] MBA+GA.

6.3　Three step enzymatic reaction

The synthesis of the chiral amino alcohol, ABT in this model system would require a three-step enzyme sequential reaction, consisting of ω-TAm (pQR 1021)-TK (pQR 791)-ω-TAm (pQR 1021) catalysed reaction conducted in series. Preliminary studies were performed in our research group and identified ω-TAm (pQR 1021) from *Rhodobacter sphaeroides* to be one of the possible catalytic candidates for the synthesis of HPA. This enzyme was also reported to have high affinity towards serine as amino donor and high reactivity towards aldehydes as amino acceptor (Villegas, 2013). Moreover, ω-TAm (pQR 1021) showed to have better reaction rate on the amination of erythrulose compared to the ω-TAm (pQR 801) (Villegas, 2013). Therefore, this enzyme was chosen and incorporated into the three-step enzymatic reaction for the production of ABT (Figure 6.8).

Standard activity of the ω-TAm (pQR 1021) enzyme in solution was carried out to get preliminary data on the enzyme activity. ω-TAm (pQR 1021) activity was demonstrated using serine (SER) and glycolaldehyde (GA) model substrates with the cofactor pyridoxal phosphate (PLP) to produce hydroxypyruvate (HPA) and ethanol amine. This model system represents the first step reaction for the production of the chiral amino alcohol, ABT (Figure 6.8). The reaction was conducted in glass vials with a total reaction volume of 300 μL at room temperature following the procedure in Section 2.7.3. The reaction was evaluated by quantifying the product of HPA by HPLC (Section 2.8).

Based on Figure 6.9, the specific activity of TAm (pQR 1021) calculated was 0.02±0.009 μmol/min/mg This value was approximately 7 times lower than the specific activity of TAm (pQR 801) calculated based on the investigated conditions (Section 3.3.2). The low value obtained showed that the amination rate of the amino acceptor was slow in spite of the high amino donor concentration employed to shift the equilibrium of the reaction thus obtaining a higher conversion yield. Therefore, further considerations have to be taken to compensate for the low reaction rate.
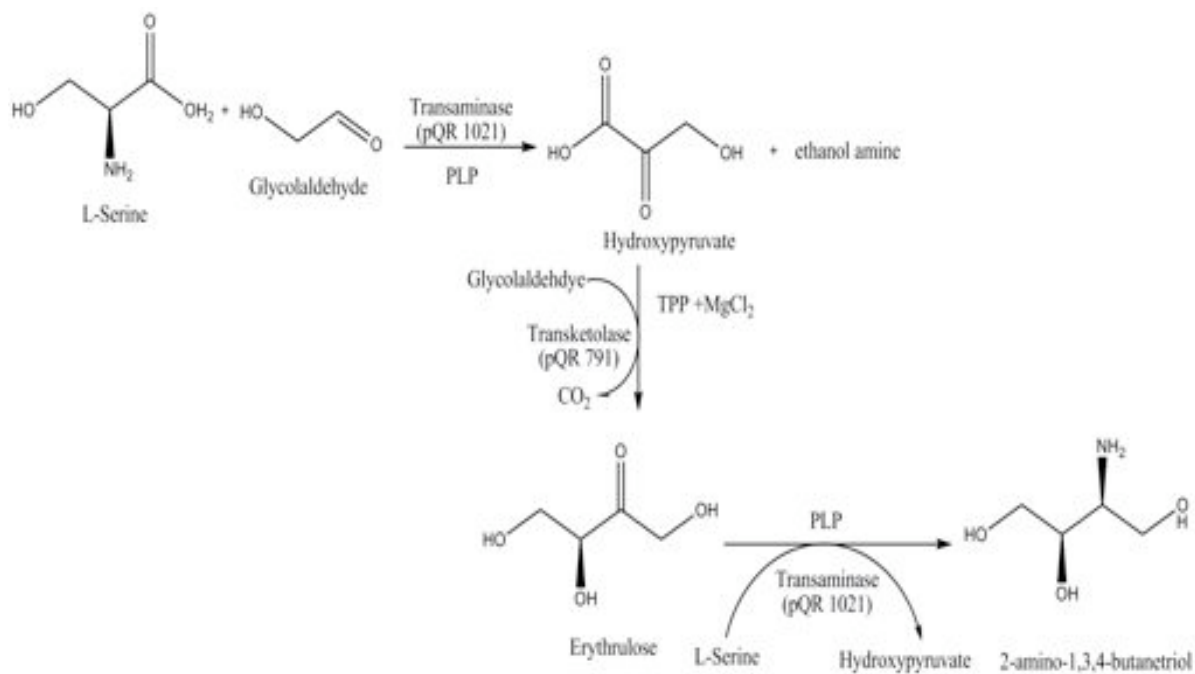
Figure 6.8: Reaction scheme for the synthesis of 2-amino-1,3,4-butanetriol (ABT) via the TAm-TK-TAm enzymes pathway. The three-step enzyme reaction pathway showing the first TAm-catalysed production of hydroxypyruvate (HPA) followed by the TK-catalysed production of eryhtrulose (ERY) and the multi-step reaction is completed with the amination ERY into ABT by the second TAm enzyme. Substrates required for the second (glycolaldehyde) and third step (serine) were recycled from the initial substrates mixture supplied in the beginning of the reaction.
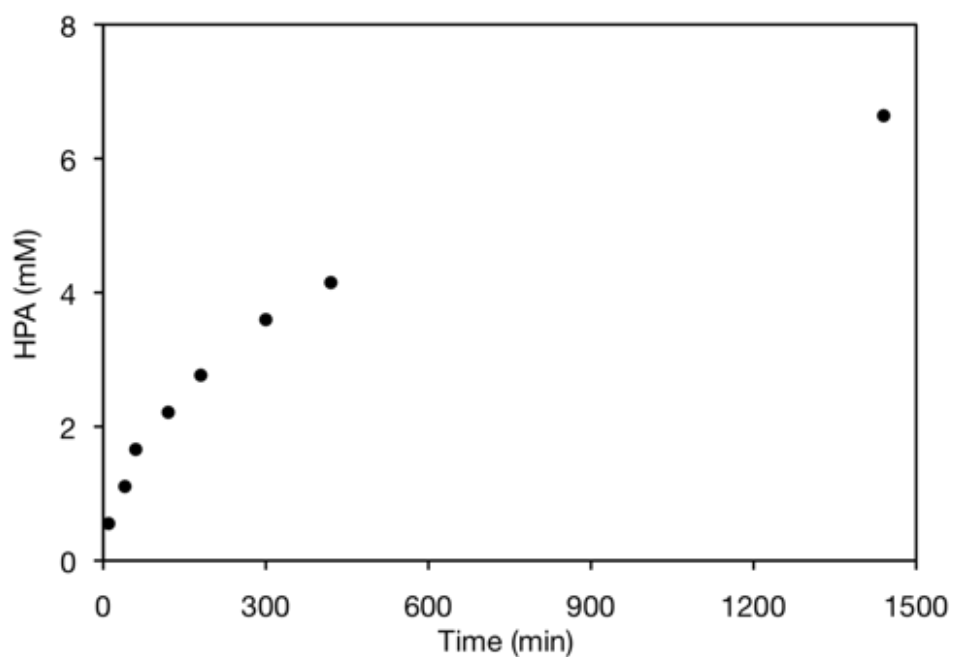
Figure 6.9: Reaction profile of His$_6$-TAm (pQR 1021) in solution phase. The TAm reaction profile with model substrate of 100 mM serine (SER) and 10 mM glycolaldehyde (GA) in 50 mM Tris−HCl buffer, pH 7.5 with cofactor 0.2 mM pyridoxal phosphate (PLP) at room temperature. The purified enzyme was used with a concentration of 1.1 mg/mL.

6.4   Setup of the three step microreactor system

The three step enzyme reaction was executed by connecting three separate packed tube IEMRs (2x10 cm and 1x5 cm) in series that gives a total reaction volume of ~2x20 µL and 10 µL respectively (Figure 2.5). The immobilisation of both His$_6$-TK (pQR 791) and His$_6$-TAm (pQR 1021) were performed separately on each IEMR before assembly following the procedure previously described (Section 2.10.2.2). Immobilisation was performed with purified solutions of both enzymes preparations at a concentration of 0.2-3.5 mg/mL. Quantification of the immobilised enzyme was carried out based on the elution sample (Section 2.10.2.2) obtained once the enzyme assay was completed. The measurement of the enzyme concentration was determined by absorbance measurement at 280 nm and validated via the Bradford assay at 595 nm on a bench scale spectrophotometer (Section 2.2.3.2).

6.4.1   Integration of Actipix online detection

6.4.1.1 Absorptivity of TAm reaction components

The monitoring of the first step reaction in the three-step enzymatic reaction was performed via the online UV detection system, Actipix. The production of HPA in this step was monitored at UV absorbance of 210 nm. It was previously reported that the product HPA absorbs UV light at 210 nm (Miller et al., 2007) while both of the substrates (SER and GA) and by-product ethanol amine have negligible absorbance at the same wavelength. In order to determine the absorbance of the species, measurements at 210 nm were initially carried out on a bench scale spectrophotometer at room temperature. Solution of substrates was prepared in 50 mM Tris-HCl (pH: 7.5) and the reading confirmed low absorptivity at this wavelength. To eliminate background interference by PLP, absorbance readings were blanked with the initial absorbance of the PLP-substrates mixture.

In order to validate the previous results, the substrate solutions were run through the Actipix detector and the reading was observed. Results obtained were in agreement as in the spectrophotometer. The detection of product through the Actipix detector was calibrated with solutions of standard HPA measured at different concentrations

(Figure 6.10). This calibration curve was used to quantify the HPA production in the first step of the TAm-catalysed reaction.

(a)
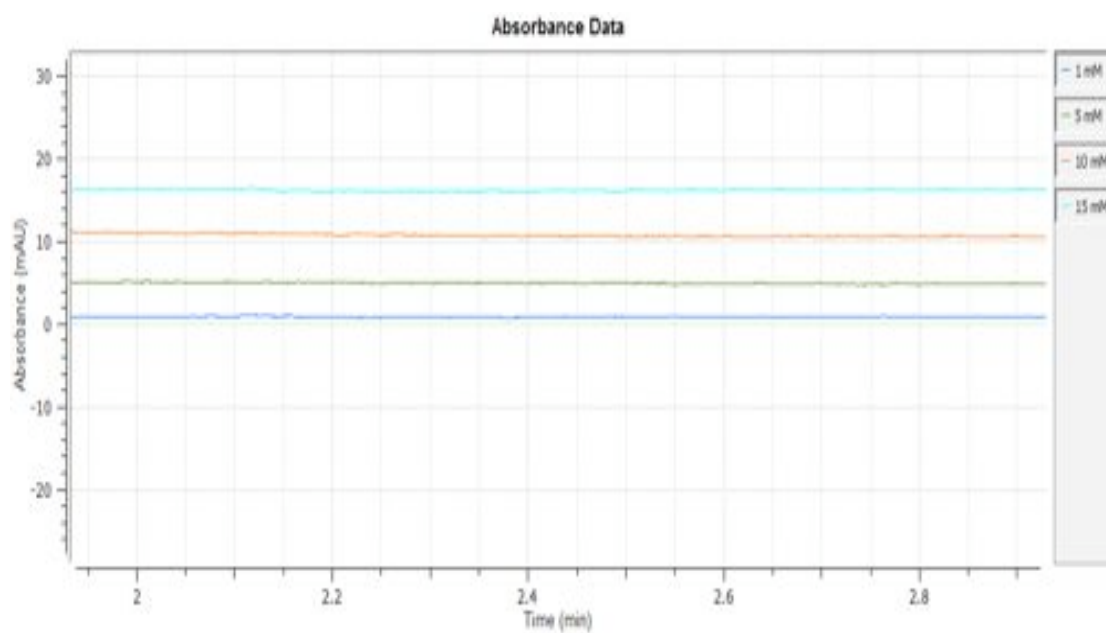
(b)
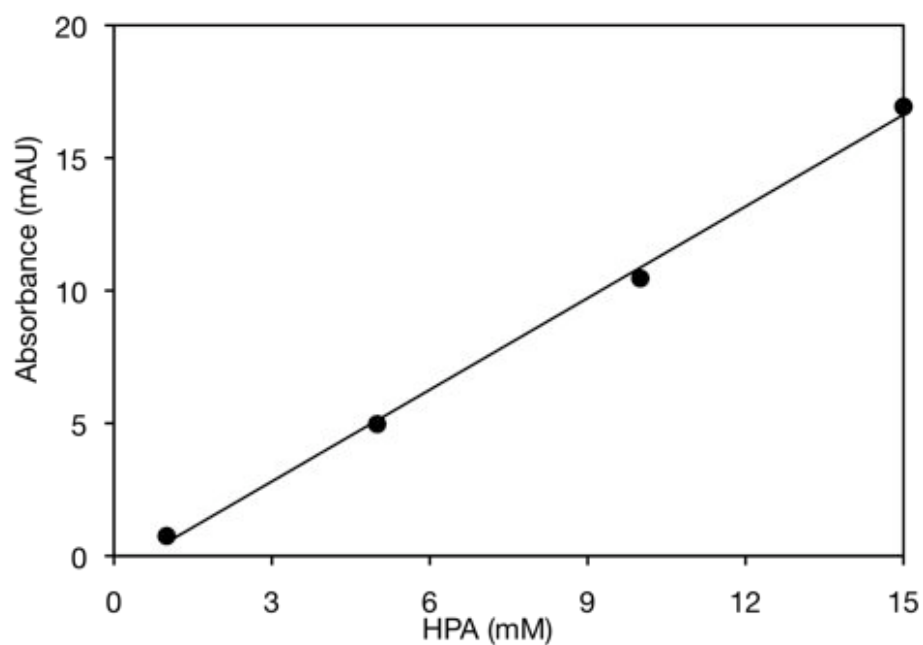
Figure 6.10: Actipix online detection of hydroxypyruvate at 210 nm. (a) HPA absorbance at various concentrations (1-5 mM). The absorbance values were used to construct the (b) calibration curve for the quantification of HPA product in the first reaction of the three-step enzymatic reaction in packed tube IEMR.

6.4.2 Operational stability of TAm pQR 1021 in packed tube IEMR

The operational stability of TAm in the packed tube IEMR was investigated over 8 hours in continuous mode reaction. This data is crucial to ensure no degradation of enzyme activity during the reaction that may compromise the obtained data. The operational stability of the immobilised His_6-TAm was evaluated continuously at a flow rate of 5 µL/min. Samples were taken every hour to measure the conversion of SER and GA to HPA product. Immobilised His_6-TAm was found to remain stable during the first 7 hours of reaction with 100% productivity (Figure 6.11). However, the activity of immobilised TAm started to decline slightly after 8 hours, which accounted for about 15% of the initial enzyme activity. Nonetheless, immobilised TAm (pQR 1021) in the packed tube IIEMR displayed an improved enzyme stability compared to immobilised TAm (pQR 801) as previously discussed (Section 4.3.2).
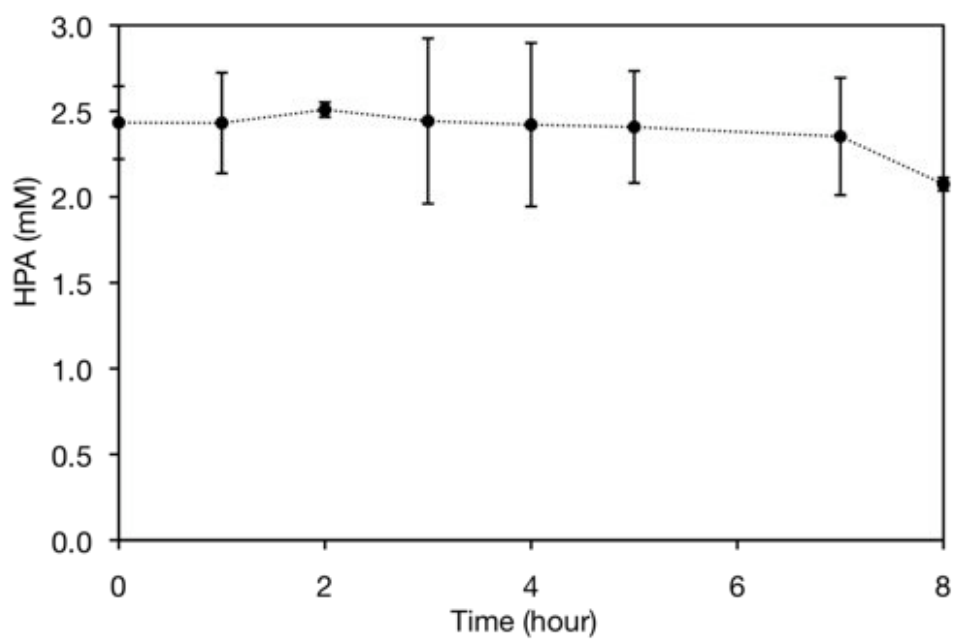
Figure 6.11: Operational stability of ω-TAm (pQR 1021) in a packed tube IEMR. The reaction was performed with 100 mM serine (SER) and 50 mM glycolaldehyde (GA) in 50 mM Tris−HCl buffer, pH 7.5 with cofactor 0.2 mM pyridoxal phosphate (PLP) at room temperature with enzyme concentration of 1.3 mg/mL. Error bars represent one standard deviation about the mean (n = 2).

6.4.3　Demonstration of the three step enzymatic reaction

The production of chiral amino alcohol, ABT in the three-step enzymatic reaction was performed via three packed tube IEMRs using serine (SER) as the amino donor and glycolaldehyde (GA) as the amino acceptor. The reaction was performed in the presence of both cofactors in 50 mM Tris-HCl, pH 7.5 at room temperature. The reaction profile of this multi-step enzyme reaction was assessed separately by monitoring the production of HPA in the first step, ERY in the second step and the final product of ABT and HPA. The product analyses were performed via HPLC and online detection system Actipix (first step).

Substrate mixtures with initial concentrations of 100 mM SER and 40 mM GA were fed together in the presence of cofactors (Section 2.12.2). In the first part of the three-step reaction, His_6-TAm catalysed the conversion of the substrates SER and GA to form HPA. The product of the first reaction was then continuously fed to the second IEMR containing the immobilised His_6-TK, which catalysed the reaction between HPA and GA into ERY. The multi-step reaction was completed with the amination of ERY by the second His_6-TAm to produce the final target product, ABT (Figure 6.8). This three-step TAm-TK-TAm reaction was conducted in continuous flow mode at various flow rates ranging from 0.5-10 μL/min, which correspond to residence times from 1 to 100 minutes.

6.4.3.1 Three-step enzymatic reaction in packed tube IEMR

Based on the preliminary enzyme activity data in solution phase of TAm (pQR 1021), this enzyme showed a lower activity in the enzyme model system investigated compared to the TAm (pQR 801). In this particular enzyme reaction, the residence time needs to be adjusted so that it is sufficiently long to provide detectable level of substrate-to-product conversion. Therefore, the dimension of the individual IEMR was modified whereby the reaction volume for TAm (pQR 1021) was increased to 20 μL. This reflects the length of the IEMR from 5 cm to 10 cm (Figure 2.5). Moreover, the residence time was also extended by supplying the substrate at a much lower flow rate of 0.5 μL/min.

With an initial substrate concentration of 100 mM SER and 40 mM GA, the three-step reaction reached approximately 6% conversion of ABT production at the lowest flow rate (Figure 6.12). This corresponds to a specific activity of 0.9 nmol/min/mg$_{TAm}$ in the final step reaction. The low conversion of the final step was anticipated by the presence of side reactions from the residual HPA and GA which was also shown in the dual enzyme reaction (Section 6.2.4.2). The effect of the side reactions was more pronounced at higher flow rates as a higher proportion of residual GA and HPA were fed continuously from the previous steps. As a result, the formation of ABT was greatly reduced and the detection of the product was only assessable at lower flow rates of 0.5-1 µL/min. The effect of the side reaction in the final step was further discussed in Section 6.4.3.2.

Apart from the side reaction effect, the low production of the ABT in the final step of the TAm-TK-TAm reaction is highly dependent on the formation of ERY in the second step and subsequently the formation of HPA in the first step reaction. The conversion of SER and GA in the first step of reaction (TAm step) was monitored online via the Actipix detection system. The production of the HPA recorded was shown to be increasing with lower flow rates, which was expected as the residence time increases (Figure 6.13). The conversion of the first TAm-catalysed reaction reached ~27% which equates to ~11 mM of HPA at 0.5 µL/min. The HPA produced was then fed into the TK-catalysed reaction, which later reacted with GA to produce ERY. Based on Figure 6.13, about ~10 mM of ERY was produced, which suggested that almost 100% conversion was reached at 0.5 µL/min. These correspond to a specific activity of 0.013 µmol/min/mg$_{TAm}$ and 0.29 µmol/min/mg$_{TK}$. Therefore, a total of ~10 mM ERY was fed to the final IEMR, whereby about 6% of the relative amount of ERY supplied by the TK step was aminated by TAm to produce ABT.

The TAm-catalysed reaction showed a consistently lower level of activity compared to TK as previously reported in the dual TK-TAm reaction as well as other studies reported elsewhere (Ingram et al., 2007; Matosevic et al., 2011b; Rios-Solis et al., 2011). While these systems were not directly comparable, these data showed the

importance of matching the rates of the two enzymes to achieve optimal conversion rates.

(a)

(b)
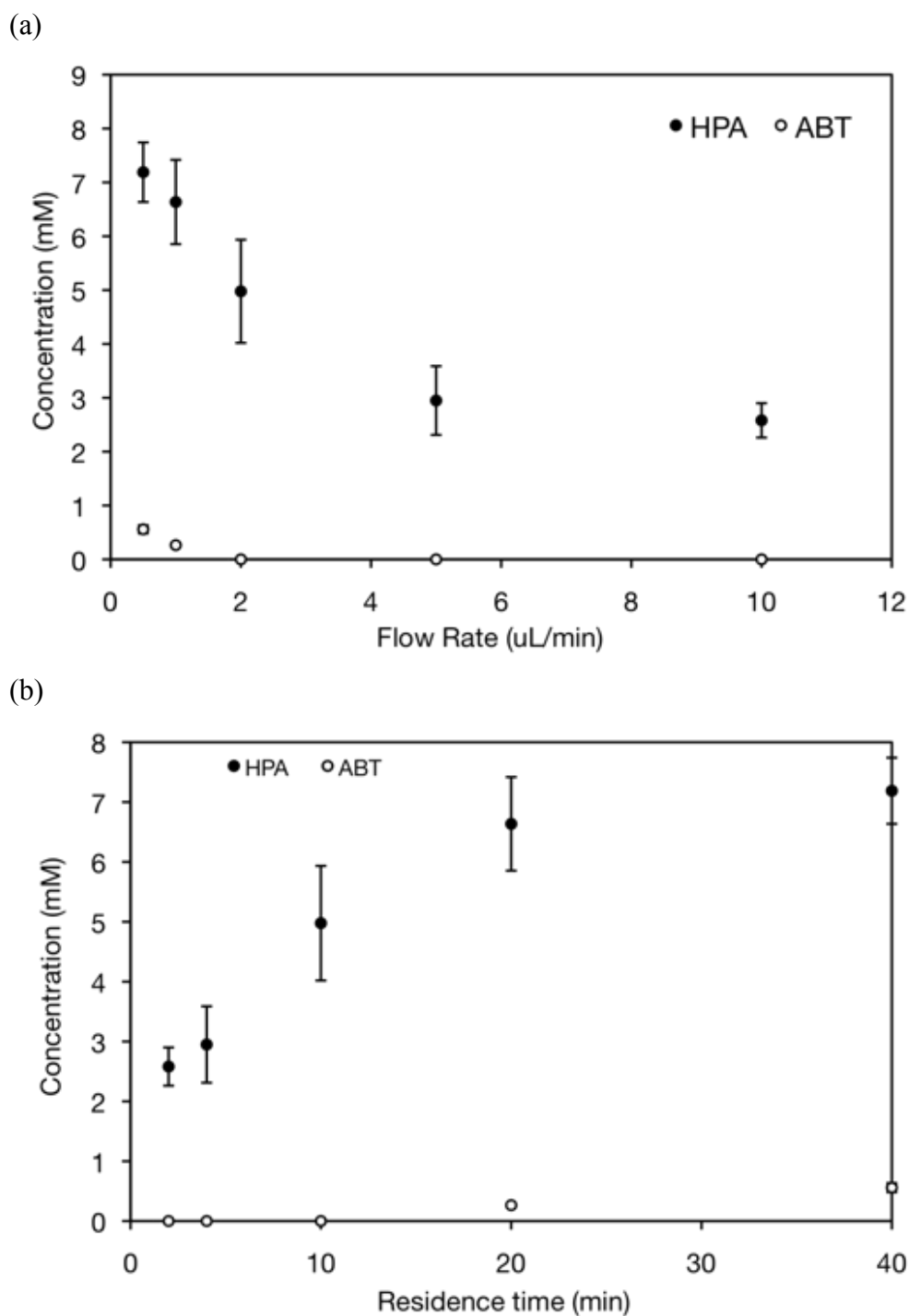
Figure 6.12: Three-step TAm-TK-TAm reaction in packed tube IEMR. Graph showing the formation of the ABT and by-product HPA in the final step of the TAm-TK-TAm reaction as a function of (a) flow rate and (b) residence time. Initial substrate concentrations of 100 mM serine and 40 mM glycolaldehyde in 50 mM Tris−HCl buffer, pH 7.5 with cofactors thiamine pyrophosphate (TPP), 2.4 mM and $MgCl_2$, 9 mM and 0.2 mM PLP at room temperature The concentration of immobilised enzyme was 3.0-3.3 mg/mL for TAm and 0.15 mg/mL for TK. Error bars represent one standard deviation about the mean (n = 3).
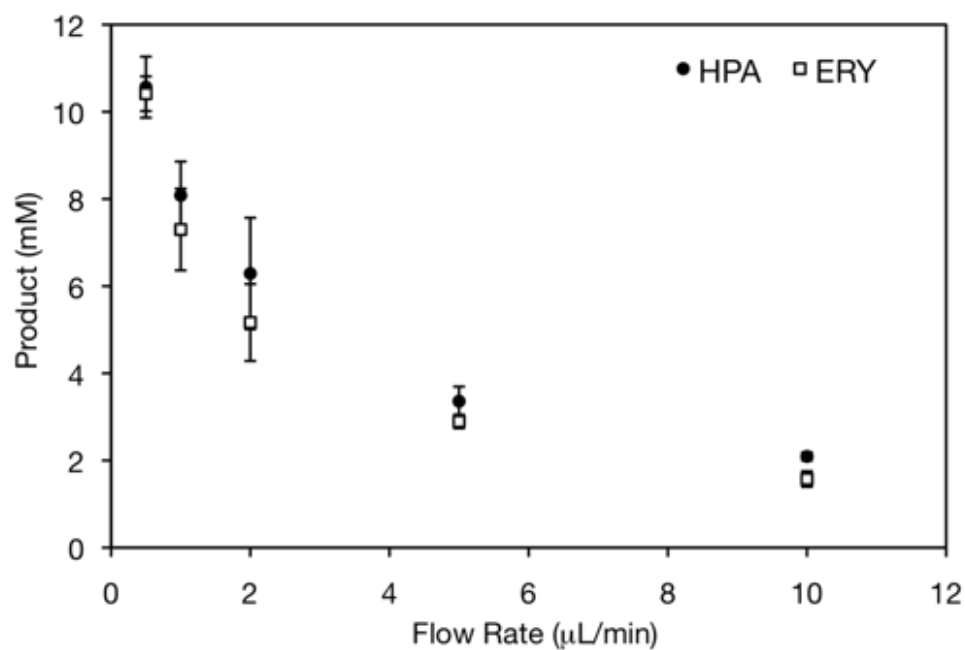
Figure 6.13: Product profile of the first and second reaction in the three-step enzymatic reaction in packed tube IEMR. Graph showing the formation of the HPA and ERY, which were the product of the first and second step respectively. Initial substrate concentration of 100 mM serine and 40 mM glycolaldehyde in 50 mM Tris−HCl buffer, pH 7.5 with cofactors thiamine pyrophosphate (TPP), 2.4 mM and $MgCl_2$, 9 mM and 0.2 mM PLP at room temperature The concentration of immobilised enzyme was 3.0-3.3 mg/mL for TAm and 0.15 mg/mL for TK. Error bars represent one standard deviation about the mean (n = 3).

6.4.3.2 Side reaction study in three step enzymatic reaction

The risk of having multiple side reactions becomes more critical as the number of cascade reactions increases. This happens when the initial substrates serve more than one enzyme in the multi-step reaction or the product of the earlier step has affinity towards the subsequent enzyme step reaction. Particularly for the continuous three-step enzymatic reaction, the effect of the side reaction is more apparent at higher flow rates, which reflects on the higher proportion of the residual substrates from the previous steps. In the TAm-TK-TAm catalysed reaction, the side reactions effect is only present in the final TAm-catalysed reaction, where the enzyme shows reactivity towards GA and HPA. As discussed previously in Section 6.2.4.2, GA and HPA were reported to serve as substrates, not just for TK but also for TAm (Chen et al., 2006; Kaulmann et al., 2007; Rios-Solis et al., 2011). The reactivity of GA and ERY towards TAm (pQR 1021) was investigated (Figure 6.14). The amination rates of GA by TAm was shown to be approximately three times higher compared to ERY. This result was in line with the low formation of ABT, which suggested that the affinity of TAm towards GA was higher compared to ERY. Moreover, the reactivity of GA was expected to be higher as the concentration of the residual substrate was about 20 mM, which was two times more than the ERY available.

Apart from HPA and GA, the presence of the by-product ethanolamine from the first step TAm-catalysed reaction was also investigated. Two sets of TAm reactions were run, one as a control and the other one with the addition of pure ethanolamine. No significant different in the TAm enzyme activity was observed, which showed that this compound was not reactive towards TAm (data not shown).
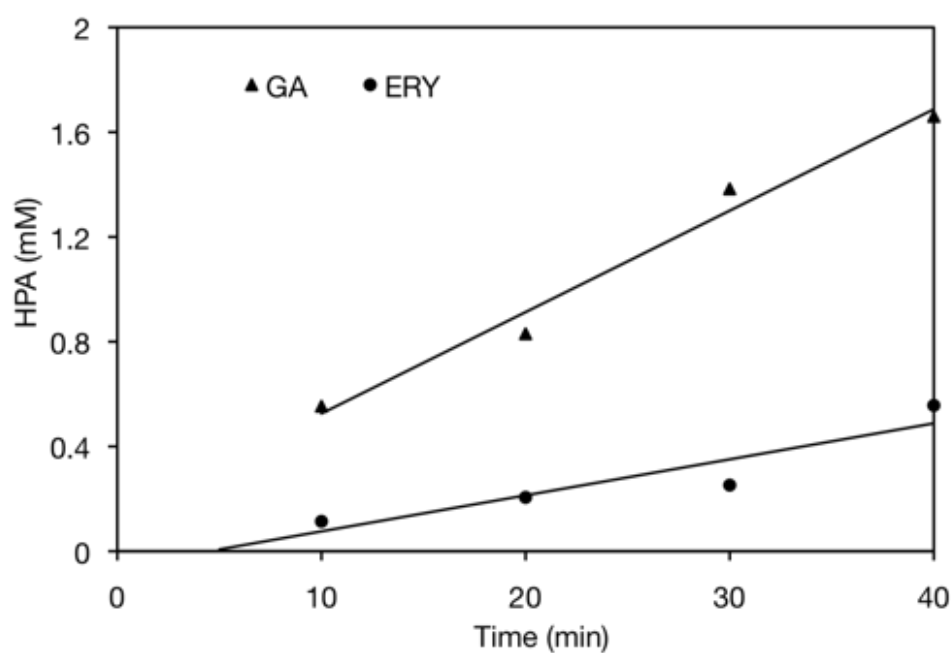
Figure 6.14: Reactivity of GA and ERY towards TAm (pQR 1021). Standard activity assay of TAm (pQR 1021) with GA and ERY as the amino acceptor in batch solution. Initial substrate concentration of 100 mM serine and 10 mM glycolaldehyde and erythrulose in 50 mM Tris−HCl buffer, pH 7.5 with cofactor 0.2 mM PLP at room temperature.

6.5 Summary

In this chapter, the demonstration of the multiple enzyme reactions involving the immobilised transketolase and transaminase were successfully performed in the packed tube IEMR. Individual units of IEMRs were connected in series to allow for the dual and three step enzymatic reaction to synthesise 2-amino-1,3,4 butanetriol (ABT).

In the dual enzyme reaction the production of ABT achieved approximately 83% conversion in 20 minutes at the lowest flow rate (Figure 6.5). Conversely, lower conversion yield was obtained in the three step reaction where the reaction only managed to achieved ~6% conversion at the lowest flow rate (Figure 6.12). The low production of the final product ABT in this reaction was due to the severe side reactions caused by the residual substrates. The low conversion rate of the ω-TAm (pQR1021) further hampered the overall reaction rates in the three- step reaction.

Investigations on the stability of the reaction components in free solution were performed. HPA and GA were found to be reactive towards both ω-TAm enzymes, which explains the presence of the side reactions in both model systems. Due to the significant effect imposed by the side reaction on the yield of the final product, future consideration to overcome this constraint is very important. Apart from that, the final product yield was highly dependent on the previous bioconversion steps. As the reaction rate of TAm was much slower than that of TK, finding the best matching enzyme combinations would improve the final yield in the multi-step enzyme reaction.

7 Conclusions and Future Work

7.1 Summary of project achievements

In this thesis, the development and characterisation of prototype immobilised enzyme microreactors (IEMR) were successfully achieved. The development of the IEMR was accomplished using His_6-tagged transketolase (TK) and transaminase (TAm) enzyme immobilised onto Ni-NTA agarose beads that were packed into tubes and work as a packed bed system. This microreactor system, based on the reversible immobilisation of His_6-tagged enzymes was implemented for the quantitative evaluation of TK and TAm bioconversion kinetics. Ultimately, several IEMR units were connected in series to enable the synthesis of a chiral pharmaceutical intermediate, ABT. The ability to synthesise this compound in relatively short time proves this IEMR system as a powerful tool for the construction and evaluation of *de novo* pathways as well as for rapid determination of various enzymes kinetics.

Initially in Chapter 3, the kinetics performance of both enzymes were evaluated in batch solution phase. The characterisation of the enzymes based on several parameters was also investigated. Data gathered from the specific activity for both enzymes showed that the conversion rate of TAm (Section 3.3.2) was relatively slower (~150x) compared to TK (Section 3.2.2) based on the investigated conditions. This preliminary data highlights the importance of matching the rates of the two enzymes to achieve optimal conversion rates in the multi-step enzymatic reactions (Chapter 6).

Furthermore, the principle of continuous flow kinetics was successfully demonstrated on the TK (Section 4.2.2.3) and TAm (Section 4.4.2) individually. The catalytic performance of both enzymes displayed consistent dependency on substrate concentration and residence time. Moreover, the product formation showed to be proportional to the space time at higher flow rates and started to level off as the flow rate was reduced. This condition can be explained by the presence of a diffusion layer surrounding the immobilised enzymes (Section 5.4). In addition,

the application of online UV detection system (Section 4.4), Actipix was integrated with the TAm packed tube IEMR and was successfully demonstrated to detect the by-product, HPA, in the single enzyme system.

In Chapter 5, the kinetic performance of TK and TAm in a continuous flow reaction was investigated using the Lilly-Hornby (1966) kinetics model in the packed tube IEMR. The findings showed the $K_{m(app)}$ for both enzymes to be dependent on the flow rates whereby higher $K_{m\,(app)}$ values were observed at lower flow rates and vice versa. A similar trend was also reported by other researchers, while factors of mass transfer and liquid channeling were believed to be the potential cause of this condition. Furthermore, the turnover number k_{cat} calculated were approximately 3 times less than k_{cat} values in solution-phase (Section 3.2.5 and Section 3.3.6). This apparent loss in activity may be due to the inaccessibility of some enzyme molecules to the substrates, altered conformation of the enzyme and a steric hindrance factor.

The versatility of the IEMR was further demonstrated in the multistep enzymatic reaction to synthesis the complex chiral aminodiol (Chapter 6). Two model systems were studied with the final target product of 2-amino-1,3,4 butanetriol (ABT). In the first model system the production of ABT achieved approximately 83% conversion in 20 minutes at the lowest flow rate (Figure 6.5). On the other hand, the bioconversion of TAm in the three-step reaction only managed to achieve ~6% of ABT production at the lowest flow rate (Figure 6.12). Reduced activity observed in the latter system was due to the severe side reactions coming from the residual substrates. While both of the model systems were not directly comparable, the production of the final product was highly dependent on the previous bioconversion steps. Therefore, finding the best matching enzyme combinations would improve the final yield in the multi-step enzyme reaction.

This *in vitro* study of the multi-step enzymatic reaction however provides insight into the behaviour of *de novo* engineered pathway prior to cloning them into engineered whole cell biocatalysts. Besides that, there is a huge potential of this

system to be further developed to ensure improved yields are achieved. While this system has been proved to work and has produced reproducible results, there is still room for improvements to be made. Generally, the main issue faced here is the low final product yield in the three-step enzyme reaction, which directly related with the side reactions. This problem stemmed from the low conversion rate of the TAm (pQR 1021)-catalysed reaction and subsequently affects the overall conversion rates of the system. This suggests that future efforts to improve the performance would require a comprehensive approach using both enzyme engineering and microfabrication methods.

7.2   Future work

Whilst the overall aim of this project was achieved, future work is required to improve the multi-step reaction to further increase reaction yields, and to enable better integration of analytical techniques. The main setback in the multi-step enzymatic reaction was the low yield of ABT production. As discussed before, the rate of conversion for the TAm reaction was relatively low compared to TK, which in turn affected the overall conversion. A possible strategy to improve this condition is by having higher enzyme loading for the slower enzyme reaction, which in this case is the TAm-catalysed reaction. Modification on the IEMR by increasing the reactor volume can be obtained by either increasing the length or the diameter of the reactor. However, any changes made on the dimensions of the reactor have to be within the maximum limit of the pressure drop in the IEMR (Section 4.3.1) and factors such as channeling effect and blockage should be considered.

Another approach aimed to improving the performance of the multi-step reaction is by reducing the effect of the side reaction (especially at high flow rate) that promotes unfavourable equilibria. In each case of the model system, the residual substrates (HPA and GA) need to be removed in order to overcome this constraint and hence increase the formation of the target product. One of the strategies to tackle this problem is by applying the *in situ* substrate removal technique (ISPR). This method not only helps improving the conversion rate but also provides further benefit for the subsequent downstream processing (Lye & Woodley 1999). Several

techniques of ISPR can be adopted which include ion exchange, complex formation and physical adsorption (Lye & Woodley 1999). Nevertheless, further study has to be performed to determine the suitable ISPR method, potentially using absorbent resins with binding selectivity that are easily incorporated in the IEMR system. This can be achieved by adding an additional packed tube containing the adsorbent resin next to the respected IEMR to remove the unwanted compound.

Apart from the ISPR method, the excessive amount of the residual substrates could be recycled back into the system. This option offers a good prospect on the overall multi-step reaction where it utilises the most of the total substrate concentration feed in the beginning of the reaction. An additional connector (eg: shut-off valve from Presearch Ltd) can be added into the system to allow for the recycling mode. Alternatively, a chip based microreactor could be used while maintaining the Ni-NTA beads as the immobilisation method. With various types of microfabrication available (Section 1.3.2), multiple channels can be easily constructed on a single chip with flexibility in the design that would fit with the intended biocatalytic model system. Moreover, the versatility of microfabrication would allow the channel dimension to be adjusted to suit the need of matching the activities of transketolase and transaminase to get optimum conversion rate in the multi-step enzyme reaction (Boehm et al., 2013).

With the main target to achieve higher yields for the production of chiral aminodiols, a different set of substrates can be tested using the transketolase-transaminase model pathway. Rios-Solis et al. (2011) reported that higher yields were achieved when using isopropylamine (IPA) as the amino donor compared to MBA. This compound showed to have negligible side reactions with transaminase and obtained 87% yield for ABT synthesis and 90% yield for 2-aminopentane-1,3-diol (APD) and available at a relatively low price. Moreover, ongoing research to increase the size of TK and TAm libraries is significant to improve the performance of *de novo* design of synthetic pathway to create chiral amino alcohols that are useful in many industrial synthon. Protein engineering strategies could be applied to generate more stable biocatalysts with new substrate specificity or enzyme with improved affinity for existing substrates (Hibbert et al., 2007, 2008; Cázares et al.,

2010; Payongsri et al., 2012). Apart from this, a genome-mining approach can also be adopted to find more stable homologues in the sequenced genome libraries that is available online (Liolios et al., 2006). Besides that, a mix-and-match of different combination of TK and TAm enzymes can be implemented to create wide range of amino alcohols (Ingram et al., 2007; Smith et al., 2009).

Another important aspect to be addressed for future work is to improve the characterisation of the transaminase stability. Based on the results obtained in Section 4.3.2, the stability of TAm was found to be less stable in immobilised form compared to the enzyme in solution. Apart from the suggested reasons discussed, a study on enzyme degradation can be conducted to further investigate the effect of immobilisation on the enzyme stability. Several methods can be performed for the analysis, which include circular dichroism, mass spectrometry, SDS-PAGE and size exclusion chromatography. The enzyme required for the analysis can be easily recovered by treating the IEMR with elution buffer.

Finally, it would be desireable to demonstrate the whole multi-step reaction (each individual step) integrated with direct analytical techniques. Apart from minimizing the dead time for analyzing the sample, this would allow for more efficient monitoring of the enzyme activities without having to analyze the individual step separately. This was partly demonstrated in the three-step enzymatic reaction (Section 6.4.1) where the UV online detection system was installed to monitor the production of HPA in the first reaction. However, this system was unable to be integrated in other bioconversion steps (dual system) due to the overlapping absorptivites of HPA and ERY. Alternatively, introducing different substrates as discussed previously can minimise this problem. In addition, the analytical assay could be performed directly by coupling the microreactor with the HPLC system, which would provide real time reaction data (Mark et al., 2010).

8 References

Abad, J.M., Mertens, S.F.L., Pita, M., Fernández, V.M., Schiffrin, D.J., 2005. Functionalization of thioctic acid-capped gold nanoparticles for specific immobilization of histidine-tagged proteins. J. Am. Chem. Soc. 127, 5689–5694.

Adeosun, J.T., Lawal, A., 2009. Numerical and experimental studies of mixing characteristics in a T-junction microchannel using residence-time distribution. Chem. Eng. Sci. 64, 2422–2432.

Alam, M.N.H.Z., Pinelo, M., Samanta, K., Jonsson, G., Meyer, A., Gernaey, K. V, 2011. A continuous membrane microbioreactor system for development of integrated pectin modification and separation processes. Chem. Eng. J. 167, 418–426.

Amankwa, L.N., Kuhr, W.G., 1992. Trypsin-Modified Fused-Silica Capillary Microreactor for Peptide Mapping by Capillary Zone Electrophoresis. Anal. Chem. 1610–1613.

An, R., Hoffman, M.D., Donoghue, M.A., Hunt, A.J., Jacobson, S.C., 2008. Water-assisted femtosecond laser machining of electrospray nozzles on glass microfluidic devices. Opt. Express 16, 15206–15211.

Anderson, J.R., Chiu, D.T., Jackman, R.J., Cherniavskaya, O., McDonald, J.C., Wu, H., Whitesides, S.H., Whitesides, G.M., 2000. Fabrication of topologically complex three-dimensional microfluidic systems in PDMS by rapid prototyping. Anal. Chem. 72, 3158–3164.

Anderson, N.G., 2001. Practical use of continuous processing in developing and scaling up laboratory processes. Org. Process Res. Dev. 5, 613–621.

Anderson, R.C., Su, X., Bogdan, G.J., Fenton, J., 2000. A miniature integrated device for automated multistep genetic assays. Nucleic Acids Res. 28, E60.

Andrić, P., Meyer, A.S., Jensen, P.A., Dam-Johansen, K., 2010. Reactor design for minimizing product inhibition during enzymatic lignocellulose hydrolysis: II. Quantification of inhibition and suitability of membrane reactors. Biotechnol. Adv. 28, 407–425.

Arnau, J., Lauritzen, C., Petersen, G.E., Pedersen, J., 2006. Current strategies for the use of affinity tags and tag removal for the purification of recombinant proteins. Protein Expr. Purif. 48, 1–13.

Aucamp, J.P., Martinez-Torres, R.J., Hibbert, E.G., Dalby, P. a, 2008. A microplate-based evaluation of complex denaturation pathways: structural stability of *Escherichia coli* transketolase. Biotechnol. Bioeng. 99, 1303–10.

Babich, L., Hartog, A.F., van Hemert, L.J.C., Rutjes, F.P.J.T., Wever, R., 2012. Synthesis of Carbohydrates in a Continuous Flow Reactor by Immobilized Phosphatase and Aldolase. Chem. Sus. Chem. 5, 2348–2353.

Baker, C.A., Duong, C.T., Grimley, A., Roper, M.G., 2009. Recent advances in microfluidic detection systems. Bioanalysis 1, 967–975.

Becker, H., Gärtner, C., 2008. Polymer microfabrication technologies for microfluidic systems. Anal. Bioanal. Chem. 390, 89–111.

Beebe, D.J., Mensing, G.A., Walker, G.M., 2002. Physics and applications of microfluidics in biology. Annu. Rev. Biomed. Eng. 4, 261–286.

Benninger, R.K.P., Hofmann, O., Önfelt, B., Munro, I., Dunsby, C., Davis, D.M., Neil, M.A.A., French, P.M.W., de Mello, A.J., 2007. Fluorescence-Lifetime Imaging of DNA–Dye Interactions within Continuous-Flow Microfluidic Systems. Angew. Chem. Int. Ed. Engl. 46, 2228–2231.

Berne, C., Betancor, L., Luckarift, H.R., Spain, J.C., 2006. Application of a microfluidic reactor for screening cancer prodrug activation using silica-immobilized nitrobenzene nitroreductase. Biomacromolecules 7, 2631–2636.

Blacklock, T.J. et al, 1993. An enantioselective synthesis of the topically active carbonic anhydrase inhibitor MK-0507: 5, 6-dihydro- (S)-4-(ethylamino)-(S)-6-methyl-4H-thieno[2, 3-b]thiopyran-2- sulfonamide 7, 7-dioxide hydrochloride. J. Org. Chem. 58, 1672–1679.

Block, H., Maertens, B., Spriestersbach, A., Brinker, N., Kubicek, J., Fabis, R., Labahn, J., Schäfer, F., 2009. Immobilized-metal affinity chromatography (IMAC): a review. Methods Enzymol. 463, 439–73.

Boehm, C.R., Freemont, P.S., Ces, O., 2013. Design of a prototype flow microreactor for synthetic biology in vitro. Lab. Chip 13, 3426–3432.

Bolte, J., Demuynck, C., Samaki, H., 1987. Utilization of enzymes in organic chemistry: Transketolase catalyzed synthesis of ketoses. Tetrahedron Lett. 28, 5525–5528.

Bradford, M.M., 1976. A rapid and sensitive method for the quantitation of microgram quantities of protein using the principle of protein dye binding. Anal. Biochem. 72, 248–254.

Brands, K.M.J., Payack, J.F., Rosen, J.D., Nelson, T.D., Candelario, A., Huffman, M.A., Zhao, M.M., Li, J., Craig, B., Song, Z.J., Tschaen, D.M., Hansen, K., Devine, P.N., Pye, P.J., Rossen, K., Dormer, P.G., Reamer, R.A., Welch, C.J., Mathre, D.J., Tsou, N.N., McNamara, J.M., Reider, P.J., 2003. Efficient synthesis of NK(1) receptor antagonist aprepitant using a crystallization-induced diastereoselective transformation. J. Am. Chem. Soc. 125, 2129–2135.

Breslauer, D.N., Lee, P.J., Lee, L.P., 2006. Microfluidics-based systems biology. Mol. Biosyst. 2, 97–112.

Brivio, M., Verboom, W., Reinhoudt, D.N., 2006. Miniaturized continuous flow reaction vessels: influence on chemical reactions. Lab. Chip 6, 329–344.

Brocklebank, S.P., Mitra, R.K., Woodley, J.M., Lilly, M.D., 1996. Carbon-Carbon Bond Synthesis: Preparation and use of immobilized transketolase. Ann. N. Y. Acad. Sci. 799, 729–736.

Brunhuber, N.M., Blanchard, J.S., 1994. The biochemistry and enzymology of amino acid dehydrogenases. Crit. Rev. Biochem. Mol. Biol. 29, 415–467.

Buckland, B.C., Drew, S.W., Connors, N.C., Chartrain, M.M., Lee, C., Salmon, P.M., Gbewonyo, K., Zhou, W., Gailliot, P., Singhvi, R., Olewinski, R.C., Sun, W.J., Reddy, J., Zhang, J., Jackey, B.A., Taylor, C., Goklen, K.E., Junker, B., Greasham, R.L., 1999. Microbial conversion of indene to indandiol: a key intermediate in the synthesis of CRIXIVAN. Metab. Eng. 1, 63–74.

Cha, T., Guo, A., Zhu, X.-Y., 2005. Enzymatic activity on a chip: the critical role of protein orientation. Proteomics 5, 416–419.

Chaga, G., Bochkariov, D.E., Jokhadze, G.G., Hopp, J., Nelson, P., 1999. Natural poly-histidine affinity tag for purification of recombinant proteins on cobalt(II)-carboxymethylaspartate crosslinked agarose. J. Chromatogr. A 864, 247–256.

Chakrabarty, K., Zeng, J., 2005. Design automation for microfluidics-based biochips. ACM J. Emerg. Technol. Comput. Syst. 1, 186–223.

Chao, Y.P., Lai, Z.J., Chen, P., Chern, J.T., 1999. Enhanced conversion rate of L-phenylalanine by coupling reactions of aminotransferases and phosphoenolpyruvate carboxykinase in *Escherichia coli* K-12. Biotechnol. Prog. 15, 453–458.

Chatterjee, S., Schoepe, J., Lohmer, S., Schomburg, D., 2005. High level expression and single-step purification of hexahistidine-tagged L-2-hydroxyisocaproate dehydrogenase making use of a versatile expression vector set. Protein Expr. Purif. 39, 137–143.

Chauhan, R.P., Powell, L.W., Woodley, J.M., 1997. Boron based separations for in situ recovery of L-erythrulose from transketolase-catalyzed condensation. Biotechnol. Bioeng. 56, 345–51.

Chauhan, R.P., Woodley, J.M., Powell, L.W., 1996. In Situ Product Removal from *E. coli* Transketolase-catalyzed Biotransformationsa. Ann. N. Y. Acad. Sci. 799, 545–554.

Chen, B., Baganz, F., Woodley, J., 2007. Modelling and optimisation of a transketolase-mediated carbon-carbon bond formation reaction. Chem. Eng. Sci. 62, 3178–3184.

Chen, B., Sayar, A., Kaulmann, U., Dalby, P., Ward, J., Woodley, J., 2006. Reaction modelling and simulation to assess the integrated use of transketolase and omega-transaminase for the synthesis of an aminotriol. Biocataly. Biotransformation 24, 449–457.

Chen, B.H., Micheletti, M., Baganz, F., Woodley, J.M., Lye, G.J., 2009. An efficient approach to bioconversion kinetic model generation based on automated microscale experimentation integrated with model driven experimental design. Chem. Eng. Sci. 64, 403–409.

Chen, J., Chen, J., 1998. Preparation and characterization of immobilized phospholipase A 2 on chitosan beads for lowering serum cholesterol concentration. J. Mol. Catal., B. Enzym. 5, 483-489.

Cheung, R., Wong, J., Ng, T., 2012. Immobilized metal ion affinity chromatography: a review on its applications. Appl. Microbiol. Biotechnol. 96, 1411–1420.

Cho, B.-K., Seo, J.-H., Kang, T.-W., Kim, B.-G., 2003. Asymmetric synthesis of L-homophenylalanine by equilibrium-shift using recombinant aromatic L-amino acid transaminase. Biotechnol. Bioeng. 83, 226–234.

Cho S, Kang DK, Choo J, de Mello AJ, C.S., 2011. Recent advances in microfluidic technologies for biochemistry and molecular biology. BMB Rep. 44, 705–712.

Chow, A.W., 2002. Lab-on-a-chip: Opportunities for chemical engineering. AIChE Journal 48, 1590–1595.

Christen, Metzler, 1985. Transaminase. Wiley Interscience.

Cobb, K.A., Novotny, M., 1989. High-sensitivity peptide mapping by capillary zone electrophoresis and microcolumn liquid chromatography, using immobilized trypsin for protein digestion. Anal. Chem. 61, 2226–2231.

Cohen, S.A., Michaud, D.P., 1993. Synthesis of a fluorescent derivatizing reagent, 6-aminoquinolyl-N-hydroxysuccinimidyl carbamate, and its application for the analysis of hydrolysate amino acids via high-performance liquid chromatography. Anal. Biochem. 211, 279–287.

Cooney, M.J., 2011. Kinetic measurements for enzyme immobilization. Methods Mol. Biol. 679, 207–225.

Crump, S.P., Rozzell, J.D., 1992. Biocatalytic production of amino acids by transamination. Wiley, New York.

Cryer, A., Bartley, W., 1974. The effect of storage on enzyme activities in tissues. Biochem. J. 144, 433–434.

Cázares, A., Galman, J.L., Crago, L.G., Smith, M.E.B., Strafford, J., Ríos-Solís, L., Lye, G.J., Dalby, P.A., Hailes, H.C., Cazares, A., Rios-Solis, L., 2010. Non-[α]-hydroxylated aldehydes with evolved transketolase enzymes. Org. Biomol Chem. 8, 1301–1309.

D. Chambers, R., C. H. Spink, R., 1999. Microreactors for elemental fluorine. Chem. Commun. 883–884.

Dalmas, V., Demuynck, C., 1993. Study of the specificity of a spinach transketolase on achiral substrates. Tetrahedron Asymmetry 4, 2383–2388.

Dalvie, S.K., Baltus, R.E., 1992. Distribution of immobilized enzymes on porous membranes. Biotechnol. Bioeng. 40, 1173–1180.

Delle Monache, G., Misiti, D., Zappia, G., 1999. A stereocontrolled synthesis of (−)-detoxinine from l-ascorbic acid. Tetrahedron: Asymmetry 10, 2961–2973.

Delouise, L. A., Miller, B.L., 2005. Enzyme immobilization in porous silicon: quantitative analysis of the kinetic parameters for glutathione-S-transferases. Anal. Chem. 77, 1950–6.

Demuynck, C., Bolte, J., Hecquet, L., Dalmas, V., 1991. Enzyme-catalyzed synthesis of carbohydrates: synthetic potential of transketolase. Tetrahedron Lett. 32, 5085–5088.

Denbigh, K.G., 1944. Velocity and yield in continuous reaction systems. Trans. Faraday Soc. 40, 352–373.

Derewenda, Z.S., 2004. The use of recombinant methods and molecular engineering in protein crystallization. Methods 34, 354–363.

DeSantis, G., Wong, K., Farwell, B., Chatman, K., Zhu, Z., Tomlinson, G., Huang, H., Tan, X., Bibbs, L., Chen, P., Kretz, K., Burk, M.J., 2003. Creation of a productive, highly enantioselective nitrilase through gene site saturation mutagenesis (GSSM). J. Am. Chem. Soc. 125, 11476–11477.

Dewick, P.M., 2009. Medicinal Natural Products: A Biosynthetic Approach, 3rd ed. Wiley.

Dittrich, P.S., Manz, A., 2006. Lab-on-a-chip: microfluidics in drug discovery. Nat. Rev. Drug Discov. 5, 210–218.

Doran, P.M., 2013. Bioprocess engineering principles, 2nd ed. Academic Press.

Eadie, G.S., 1942. The inhibition of cholinesterase by physostigmine and prostigmine. J. Biol. Chem. 146, 85–93.

Effenberger, F., Null, V., Ziegler, T., 1992. Preparation of optically pure L-2-hydroxyaldehydes with yeast transketolase. Tetrahedron Lett. 33, 5157–5160.

Ehrfeld, W., Hessel, V., Lowe, H., 2000. Microreactors. Wiley.

Ehrfeld, W., 1999. Microreaction technology: industrial prospects : IMRET 3 : proceedings of the Third International Conference on Microreaction Technology, Springer.

Eijsink, V.G.H., Gåseidnes, S., Borchert, T. V, Van Den Burg, B., 2005. Directed evolution of enzyme stability. Biomol. Eng. 22, 21–30.

Eisfeld, B., Schnitzlein, K., 2001. The influence of confining walls on the pressure drop in packed beds. Chem. Eng. Sci. 56, 4321–4329.

Ekström, S., Onnerfjord, P., Nilsson, J., Bengtsson, M., Laurell, T., Marko-Varga, G., 2000. Integrated microanalytical technology enabling rapid and automated protein identification. Anal. Chem. 72, 286–293.

Emory, J.M., Soper, S.A., 2008. Charge-coupled device operated in a time-delayed integration mode as an approach to high-throughput flow-based single molecule analysis. Anal. Chem. 80, 3897–3903.

Euler, H., Pope, T.H., 1912. General chemistry of the enzymes. New York, J. Wiley & Sons, 1912.

Fan, Z.H., Mangru, S., Granzow, R., Heaney, P., Ho, W., Dong, Q., Kumar, R., 1999. Dynamic DNA hybridization on a chip using paramagnetic beads. Anal. Chem. 71, 4851–4859.

Federspiel, M., Fischer, R., Hennig, M., Mair, H.-J., Oberhauser, T., Rimmler, G., Albiez, T., Bruhin, J., Estermann, H., Gandert, C., Göckel, V., Götzö, S., Hoffmann, U., Huber, G., Janatsch, G., Lauper, S., Röckel-Stäbler, O., Trussardi, R., Zwahlen, A.G., 1999. Industrial Synthesis of the Key Precursor in the Synthesis of the Anti-Influenza Drug Oseltamivir Phosphate. Org. Process Res. Dev. 3, 266–274.

Fernandes, P., 2010. Enzymes in Food Processing: A Condensed Overview on Strategies for Better Biocatalysts. Enzyme research, doi: 10.4061/2010/862537

Fessner, W.D., Helaine, V., 2001. Biocatalytic synthesis of hydroxylated natural products using aldolases and related enzymes. Curr. Opin. Biotechnol. 12, 574–586.

Fischer, H., Polikarpov, I., Craievich, A.F., 2004. Average protein density is a molecular-weight-dependent function. Protein Sci. 13, 2825–2828.

Fisher, J.P., Dean, D., Engel, P.S., Mikos, A.G., 2001. Photoinitiated polymerization of biomaterials. Annu.Rev. Mater.Res. 31, 171–181.

Fodor, S.P., Read, J.L., Pirrung, M.C., Stryer, L., Lu, A.T., Solas, D., 1991. Light-directed, spatially addressable parallel chemical synthesis. Science 251, 767–773.

Folch, A., 2013. Introduction to BioMEMS. CRC Press, Taylor & Francis Group, 97-98.

Forsberg, E.M., Green, J.R.A., Brennan, J.D., 2004. Continuous flow immobilized enzyme reactor-tandem mass spectrometry for screening of AChE inhibitors in complex mixtures. Anal. Chem. 83, 5230–5236.

French, C., Ward, J.M., 1996. Production and Modification of *E. coli* Transketolase for Large-Scale Biocatalysisa. Ann. N. Y. Acad. Sci. 799, 11–18.

Friedrich, M., Perne, R., 1995. Design and control of batch reactors: -An industrial viewpoint-. Comput. Chem. Eng. 19, 357–368.

Frédéric, B., (2012, February16). Microfluidics sector poised for 23% growth. Retrieved from http://memsblog.wordpress.com/2012/02/16/microfluidics-sector-poised-for-23-growth/

Gao, J., Xu, J., Locascio, L.E., Lee, C.S., 2001. Integrated microfluidic system enabling protein digestion, peptide separation, and protein identification. Anal. Chem. 73, 2648–2655.

Gleason, N.J., Carbeck, J.D., 2004. Measurement of enzyme kinetics using microscale steady-state kinetic analysis. Langmuir 20, 6374–81.

Goldberg, K., Edegger, K., Kroutil, W., Liese, A., 2006. Overcoming the thermodynamic limitation in asymmetric hydrogen transfer reactions catalyzed by whole cells. Biotechnol. Bioeng. 95, 192–198.

Greenberg, W.A., Varvak, A., Hanson, S.R., Wong, K., Huang, H., Chen, P., Burk, M.J., 2004. Development of an efficient, scalable, aldolase-catalyzed process for enantioselective synthesis of statin intermediates. Proc. Natl. Acad. Sci. U. S. A. 101, 5788–5793.

Greenway, G.M., Haswell, S.J., Morgan, D.O., Skelton, V., Styring, P., 2000. The use of a novel microreactor for high throughput continuous flow organic synthesis. Sens. Actuators B. Chem. 63, 153–158.

Guilbault, G.G., Kauffmann, J.M., Patriarche, G.J., 1991. Immobilized enzyme electrodes as biosensors. Biosystems 14, 209–262.

Guo, J., Frost, J.W., 2004. Synthesis of aminoshikimic acid. Org. Lett. 6, 1585–1588.

Guo, Z., Xu, S., Lei, Z., Zou, H., Guo, B., 2003. Immobilized metal-ion chelating capillary microreactor for peptide mapping analysis of proteins by matrix assisted laser desorption/ ionization-time of flight-mass spectrometry. Electrophoresis 24, 3633–3639.

Gyamerah, M., Willetts, A.J. 1997. Kinetics of overexpressed transketolase from *Escherichia coli* JM 107/pQR 700. Enzyme Microb. Technol. 20, 127–134.

Gärtner, C., Klemm, R., Becker, H., Gmbh, C., Promenade, C., Jena, D.2007. Methods and instruments for continuous-flow PCR on a chip. Proceedings of SPIE. doi: 10.1117/12.713797

Hadd, A.G., Raymond, D.E., Halliwell, J.W., Jacobson, S.C., Ramsey, J.M., 1997. Microchip device for performing enzyme assays. Anal. Chem. 69, 3407–3412.

Hammond, J.B., Kruger, N.J., 1988. The bradford method for protein quantitation. Methods Mol. Biol. 3, 9–15.

Hanes, C.S., 1932. Studies on plant amylases: The effect of starch concentration upon the velocity of hydrolysis by the amylase of germinated barley. Biochem. J. 26, 1406–1421.

Hansen, C.M., Shultz, T.D., 2001. Stability of Vitamin B-6–Dependent Aminotransferase Activity in Frozen Packed Erythrocytes Is Dependent on Storage Temperature. J. Nutr. 131 , 1581–1583.

Haswell, S.J., Skelton, V., 2000. Chemical and biochemical microreactors. Trends Analyt. Chem. 19, 389–395.

Hayashi, K., Takahashi, J., Horiuchi, T., Iwasaki, Y., Haga, T., 2008. Development of Nanoscale Interdigitated Array Electrode as Electrochemical Sensor Platform for Highly Sensitive Detection of Biomolecules. J. Electrochem. Soc. 155, J240.

Henkes, S., Sonnewald, U., Badur, R., Flachmann, R., Stitt, M., 2001. A Small Decrease of Plastid Transketolase Activity in Antisense Tobacco Transformants Has Dramatic Effects on Photosynthesis and Phenylpropanoid Metabolism. Plant Cell 13 , 535–551.

Heule, M., Rezwan, K., Cavalli, L., Gauckler, L.J., 2003. A Miniaturized Enzyme Reactor Based on Hierarchically Shaped Porous Ceramic Microstruts. Adv. Mater. 15, 1191–1194.

Hibbert, E.G., Baganz, F., Hailes, H.C., Ward, J.M., Lye, G.J., Woodley, J.M., Dalby, P. a, 2005. Directed evolution of biocatalytic processes. Biomol. Engin. 22, 11–9.

Hibbert, E.G., Senussi, T., Costelloe, S.J., Lei, W., Smith, M.E.B., Ward, J.M., Hailes, H.C., Dalby, P.A., 2007. Directed evolution of transketolase activity on non-phosphorylated substrates. J. Biotechnol. 131, 425–432.

Hibbert, E.G., Senussi, T., Smith, M.E.B., Costelloe, S.J., Ward, J.M., Hailes, H.C., Dalby, P.A., 2008. Directed evolution of transketolase substrate specificity towards an aliphatic aldehyde. J. Biotechnol. 134, 240–245.

Hickey, A.M., Marle, L., McCreedy, T., Watts, P., Greenway, G.M., Littlechild, J.A., 2007. Immobilization of thermophilic enzymes in miniaturized flow reactors. Biochem. Soc. Trans. 35, 1621–1623.

Hickey, A.M., Ngamsom, B., Wiles, C., Greenway, G.M., Watts, P., Littlechild, J.A., 2009. A microreactor for the study of biotransformations by a cross-linked γ-lactamase enzyme. Biotechnol. J. 4, 510–516.

Hisamoto, H., Shimizu, Y., Uchiyama, K., Tokeshi, M., Kikutani, Y., Hibara, A., Kitamori, T., 2003. Chemicofunctional membrane for integrated chemical processes on a microchip. Anal. Chem. 75, 350–354.

Hobbs, G.R., Lilly, M.D., Turner, N.J., Ward, J.M., Willets, A.J., Woodley, J.M., 1993. Enzyme-catalysed carbon-carbon bond formation: use of transketolase from *Escherichia coli*. J. Chem. Soc. 10, 165–166.

Hofstee, B.H.J., 1952. On the Evaluation of the Constants V_m and K_M in Enzyme Reactions. Science 116 , 329–331.

Holden, M.A., Jung, S.-Y., Cremer, P.S., 2004. Patterning Enzymes Inside Microfluidic Channels via Photoattachment Chemistry. Anal. Chem. 76, 1838–1843.

Holt, R.A., 1996. Microbial asymmetric reduction in the synthesis of a drug intermediate. Chim. Oggi. 14, 17–20.

Honda, T., Miyazaki, M., Nakamura, H., Maeda, H., 2005. Immobilization of enzymes on a microchannel surface through cross-linking polymerization. Chem. Commun. 5062–5064.

Hong, J., Edel, J.B., DeMello, A.J., Andrew, J., 2009. Micro- and nanofluidic systems for high-throughput biological screening. Drug Discov. Today 14, 134–146.

Hsieh, F., Keshishian, H., Muir, C., 1998. Automated high throughput multiple target screening of molecular libraries by microfluidic MALDI-TOF MS. J. Biomol. Screen. 189-198.

Huh, D., Gu, W., Kamotani, Y., Grotberg, J.B., Takayama, S., 2005. Microfluidics for flow cytometric analysis of cells and particles. Physiol. Meas. 26, R73–R98.

Ingram, C.U., Bommer, M., Smith, M.E.B., Dalby, P.A., Ward, J.M., Hailes, H.C., Lye, G.J., 2007. One-Pot Synthesis of Amino-Alcohols Using a *De-Novo* Transketolase and b-Alanine : Pyruvate Transaminase Pathway in *Escherichia coli.* Biotechnol. Bioeng. 96, 559–569.

Jahromi, R.R.F., Morris, P., Martinez-Torres, R.J., Dalby, P.A., 2011. Structural stability of *E. coli* transketolase to temperature and pH denaturation. J. Biotechnol. 155, 209–216.

Jiang, H., Yuan, H., Liang, Y., Xia, S., Zhao, Q., Wu, Q., Zhang, L., Liang, Z., Zhang, Y., 2012. A hydrophilic immobilized trypsin reactor with N-vinyl-2-pyrrolidinone modified polymer microparticles as matrix for highly efficient protein digestion with low peptide residue. J. Chromatogr. A 1246, 111–116.

Johnson, T.J., Ross, D., Gaitan, M., Locascio, L.E., 2001. Laser modification of preformed polymer microchannels: application to reduce band broadening around turns subject to electrokinetic flow. Anal. Chem. 73, 3656–3661.

Jones, D.G., 1985. Stability and storage characteristics of enzymes in sheep blood. Res. Vet. Sci. 38, 307–311.

Joye, D.D., 2003. Pressure drop correlation for laminar, mixed convection, aiding flow heat transfer in a vertical tube. IJHFF 24, 260–266.

Juang, H.D., Weng, H.S., 1984. Performance of biocatalysts with nonuniformly distributed immobilized enzyme. Biotechnol. Bioeng. 26, 623–626.

Jähnisch, K., Hessel, V., Löwe, H., Baerns, M., 2004. Chemistry in microstructured reactors. Angew. Chem. Int. Edt. Engl. 43, 406–446.

Kang, Q., Shen, D., Li, Q., Hu, Q., Dong, J., Du, J., Tang, B., 2008. Reduction of the Impedance of a Contactless Conductivity Detector for Microchip Capillary Electrophoresis: Compensation of the Electrode Impedance by Addition of a Series Inductance from a Piezoelectric Quartz Crystal. Anal. Chem. 80, 7826–7832.

Kato, M., Sakai-Kato, K., Jin, Kubota, K., Miyano, H., Toyo'oka, T., Dulay, M.T., Zare, R.N., 2004. Integration of On-Line Protein Digestion, Peptide Separation, and Protein Identification Using Pepsin-Coated Photopolymerized Sol−Gel Columns and Capillary Electrophoresis/Mass Spectrometry. Anal. Chem. 76, 1896–1902.

Kaulmann, U., Smithies, K., Smith, M., Hailes, H., Ward, J., 2007. Substrate spectrum of ω-transaminase from *Chromobacterium violaceum* DSM30191 and its potential for biocatalysis. Enzyme Microb. Technol. 41, 628–637.

Kawakami, K., Sera, Y., Sakai, S., Ono, T., Ijima, H., 2004. Development and Characterization of a Silica Monolith Immobilized Enzyme Micro-bioreactor. Ind. Eng. Chem. Res. 44, 236–240.

Ke, C., Berney, H., Mathewson, A., Sheehan, M.M., 2004. Rapid amplification for the detection of *Mycobacterium tuberculosis* using a non-contact heating method in a silicon microreactor based thermal cycler. Sens. Actuators B Chem. 102, 308–314.

Kerby, M.B., Legge, R.S., Tripathi, A., 2006. Measurements of kinetic parameters in a microfluidic reactor. Anal. Chem. 78, 8273–80.

Kim, D., Goldberg, I.B., Judy, J.W., 2009. Microfabricated electrochemical nitrate sensor using double-potential-step chronocoulometry. Sens. Actuators B Chem. 135, 618–624.

Kim, W., Guo, M., Yang, P., Wang, D., 2007. Microfabricated monolithic multinozzle emitters for nanoelectrospray mass spectrometry. Anal. Chem. 79, 3703–3707.

King, J., Laemmli, U.K., 1971. Polypeptides of the tail fibres of bacteriophage T4. J. Mol. Biol. 62, 465–477.

Kirst, H.A., Yeh, W.-K., Zmijewski, M.J., 2001. Enzyme Technologies For Pharmaceutical And Biotechnological Applications. CRC Press.

Kobayashi, J., Mori, Y., Okamoto, K., Akiyama, R., Ueno, M., Kitamori, T., Kobayashi, S., 2004. A Microfluidic Device for Conducting Gas-Liquid-Solid Hydrogenation Reactions. Science 304 , 1305–1308.

Kobayashi, T., Moo-Young, M., 1973. The kinetic and mass transfer behavior of immobilized invertase on ion-exchange resin beads. Biotechnol. Bioeng. 15, 47–67.

Kobori, Y., Myles, D.C., Whitesides, G.M., 1992. Substrate specificity and carbohydrate synthesis using transketolase. J. Org. Chem. 57, 5899–5907.

Kochetov, G.A., 1982. Structure of the Active Center of Transketolase. Ann. N. Y. Acad. Sci. 378, 306–311.

Kochetov, G.A., Solocbeva, O.N., 1977. Synthesis and some properties of immobilized transketolase. Biokhimiia 42, 1872–1877.

Koh, W., Pishko, M., 2005. Immobilization of multi-enzyme microreactors inside microfluidic devices. Sens. Actuators B Chem. 106, 335–342.

Krenková, J., Foret, F., 2004. Immobilized microfluidic enzymatic reactors. Electrophoresis 25, 3550–3563.

Kuan, I., Liao, R., Hsieh, H., Chen, K., Yu, C., 2008. Properties of *Rhodotorula gracilis* D-amino acid oxidase immobilized on magnetic beads through his-tag. J. Biosci. Bioeng. 105, 110–5.

Kundu, S., Bhangale, A.S., Wallace, W.E., Flynn, K.M., Guttman, C.M., Gross, R.A., Beers, K.L., 2011. Continuous flow enzyme-catalyzed polymerization in a microreactor. J. Am. Chem. Soc. 133, 6006–6011.

Ladero, M., Ruiz, G., Pessela, B., Vian, A., Santos, A., Garciaochoa, F., 2006. Thermal and pH inactivation of an immobilized thermostable β-galactosidase from *Thermus sp.* strain T2: Comparison to the free enzyme. Biochem. Eng. J. 31, 14–24.

Laser, D.J., Santiago, J.G., 2004. A review of micropumps. J. Micromec. Microeng. 14, R35–R64.

Lee, S.B., Kim, S.M., Ryu, D.D.Y., 1979. Effects of external diffusion and design geometry on the performance of immobilized glucose isomerase reactor system. Biotechnol. Bioeng. 21, 2023–2043.

Lee, S.J., Lee, S.Y., 2004. Micro total analysis system (micro-TAS) in biotechnology. Appl. Microbiol. Biotechnol. 64, 289–299.

Lee, T.M., Hsing, I.M., Lao, A.I., Carles, M.C., 2000. A miniaturized DNA amplifier: its application in traditional Chinese medicine. Anal. Chem. 72, 4242–4247.

Lemke, E.A., Gambin, Y., Vandelinder, V., Brustad, E.M., Liu, H.-W., Schultz, P.G., Groisman, A., Deniz, A.A., 2009. Microfluidic device for single-molecule experiments with enhanced photostability. J. Am. Chem. Soc. 131, 13610–13612.

Li, H.-F., Lin, J.-M., Su, R.-G., Cai, Z.W., Uchiyama, K., 2005. A polymeric master replication technology for mass fabrication of poly(dimethylsiloxane) microfluidic devices. Electropohoresis 26, 1825–1833.

Lilly, M.D., Chauhan, R., French, C., Gyamerah, M., Hobbs, G.R., Humprey, A., Isupov, M., Littlechild, J.A., Mitra, R.K., Morris, K.G., Rupprecth, M., Turner, N.J., Ward, J.M., Willets, A.J., Woodley, J.M., 1996. Carbon–Carbon Bond Synthesis: The Impact of rDNA Technology on the Production and Use of *E. coli* Transketolase. Ann. N. Y. Acad. Sci. 782, 513–525.

Lilly, M.D., Hornby, W.E., Crook, E.M., 1966. The Kinetics of Carboxymethylcellulose-Ficin in Packed Beds Na-benzoylarginine. Methods 718–723.

Lin, J., Ostovic, D., Vacca, J., 2002. The Integration of Medicinal Chemistry, Drug Metabolism, and Pharmaceutical Research and Development in Drug

Discovery and Development, Integration of Pharmaceutical Discovery and Development SE - 11. Springer US, pp. 233–255.

Lineweaver, H., Burk, D., 1934. The Determination of Enzyme Dissociation Constants. J. Am. Chem. Soc. 56, 658–666.

Liolios, K., Tavernarakis, N., Hugenholtz, P., Kyrpides, N.C., 2006. The Genomes On Line Database (GOLD) v.2: a monitor of genome projects worldwide. Nucleic Acids Res. 34 , 332–334.

Liu, Z., Zhang, J., Chen, X., Wang, P.G., 2002. Combined biosynthetic pathway for de novo production of UDP-galactose: Catalysis with multiple enzymes immobilized on agarose beads. Chem. Bio. Chem. 3, 348–355.

Lombardi, D., Dittrich, P.S., 2010. Advances in microfluidics for drug discovery. Expert Opin. Drug Discov. 5, 1081–1094.

Luckarift, H.R., Ku, B.S., Dordick, J.S., 2007. Silica-Immobilized Enzymes for Multi-Step Synthesis in Microfluidic Devices. Biotechnol. Bioeng. 98, 701–705.

Lye, G.J., Woodley, J.M., 1999. Application of in situ product-removal techniques to biocatalytic processes. Trends Biotechnol. 17, 395–402.

MacInnes, J.M., Chen, Z., Allen, R.W.K., 2005. Investigation of alternating-flow mixing in microchannels. Chem. Engin. Sci. 60, 3453–3467.

Maehara, S., Taneda, M., Kusakabe, K., 2008. Catalytic synthesis of hydrogen peroxide in microreactors. Chem. Eng. Res. Des. 86, 410–415.

Malek, C.G.K., 2006. Laser processing for bio-microfluidics applications (part I). Anal. Bioanal. Chem. 1351–1361.

Manz, A., Graber, N., Widmer, H.M., 1990. Miniaturized total chemical analysis systems: A novel concept for chemical sensing. Sens. Actuators B Chem. 1, 244–248.

Manz, A., Miyahara, Y., Miura, J., Watanabe, Y., Miyagi, H., Sato, K., 1990. Design of an open-tubular column liquid chromatograph using silicon chip technology. Sens. Actuators B Chem 1, 249–255.

Mao, H., Yang, T., Cremer, P.S., 2002. Design and characterization of immobilized enzymes in microfluidic systems. Anal. chem. 74, 379–85.

Mark, D., Haeberle, S., Roth, G., Von Stetten, F., Zengerle, R., 2010. Microfluidic lab-on-a-chip platforms: requirements, characteristics and applications. Chem. Soc. Rev. 39, 1153–82.

Markoglou, N., Hsuesh, R., Wainer, I.W., 2004. Immobilized enzyme reactors based upon the flavoenzymes monoamine oxidase A and B. J. Chromatogr. B, 804, 295–302.

Martinez-Torres, R., Aucamp, J., George, R., Dalby, P., 2007. Structural stability of *E.coli* transketolase to urea denaturation. Enzyme Microb. Technol. 41, 653–662.

Matosevic, S., Lye, G.J., Baganz, F., 2009. Design and characterization of a prototype enzyme microreactor: quantification of immobilized transketolase kinetics. Biotechnology progress 26, 118–26.

Matosevic, S., Lye, G.J., Baganz, F., 2011b. Immobilised enzyme microreactor for screening of multi-step bioconversions: Characterisation of a de novo transketolase-ω-transaminase pathway to synthesise chiral amino alcohols. J. Biotechnol.155, 320–9.

Matosevic, S., Micheletti, M., Woodley, J.M., Lye, G.J., Baganz, F., 2008. Quantification of kinetics for enzyme-catalysed reactions: implications for diffusional limitations at the 10 ml scale. Biotechnol. Lett. 30, 995–1000.

Matosevic, S., Szita, N., Baganz, F., 2011a. Fundamentals and applications of immobilized microfluidic enzymatic reactors. J. Chem. Tech. Biotechnol. 86, 325–334.

Matsuura, S., Ishii, R., Itoh, T., Hamakawa, S., Tsunoda, T., Hanaoka, T., Mizukami, F., 2011. Immobilization of enzyme-encapsulated nanoporous material in a microreactor and reaction analysis. Chem. Engin. J. 167, 744–749.

Mehta, P.K., Hale, T.I., Christen, P., 1993. Aminotransferases: demonstration of homology and division into evolutionary subgroups. FEBS J. 214, 549–61.

Meining, W., Mörtl, S., Fischer, M., Cushman, M., Bacher, A., Ladenstein, R., 2000. Refined structure of transketolase from *Saccharomyces cerevisiae* at 2.0 A resolution. J. Mol. Biol. 289, 885–891.

Mellors, J.S., Gorbounov, V., Ramsey, R.S., Ramsey, J.M., 2008. Fully integrated glass microfluidic device for performing high-efficiency capillary electrophoresis and electrospray ionization mass spectrometry. Anal. Chem. 80, 6881–6887.

Michaelis, L., Menten, M., 1913. Die Kinetik der Invertinwerkung. Biochem Z 49, 333–369.

Miller, E.M., Wheeler, A.R., 2008. A Digital Microfluidic Approach to Homogeneous Enzyme Assays. Anal. Chem. 80, 1614–1619.

Miller, O.J., Hibbert, E.G., Ingram, C.U., Lye, G.J., Dalby, P.A., 2007. Optimisation and evaluation of a generic microplate-based HPLC screen for transketolase activity. Biotechnol. Lett. 29, 1759–1770.

Mishra, R.K., Coates, C.M., Revell, K.D., Turos, E., 2007. Synthesis of 2-Oxazolidinones from β-Lactams: Stereospecific Total Synthesis of (−)-Cytoxazone and All of Its Stereoisomers. Org. Lett. 9, 575–578.

Mitra, R., Woodley, J., Lilly, M., 1998. *Escherichia coli* transketolase-catalysed carbon-carbon bond formation: biotransformation characterisation for reactor evaluation and selection. Enzyme Microb. Technol 22, 64–70.

Mitra, R.K., Woodley, J.M., 1996. A useful assay for transketolase in asymmetric syntheses. Biotechnol. Tech. 10, 167–172.

Miyazaki, M., Kaneno, J., Kohama, R., Uehara, M., Kanno, K., 2004. Preparation of functionalized nanostructures on microchannel surface and their use for enzyme microreactors. Chem. Eng. J. 101, 277–284.

Miyazaki, M., Kaneno, J., Uehara, M., Fujii, M., 2003. Simple method for preparation of nanostructure on microchannel surface and its usage for enzyme-immobilization. Chem Commun. 648 – 649.

Miyazaki, M., Kaneno, J., Yamaori, S., Honda, T., Briones, M.P.P., Uehara, M., Arima, K., Kanno, K., Yamashita, K., Yamaguchi, Y., Nakamura, H., Yonezawa, H., Fujii, M., Maeda, H., 2005. Efficient immobilization of enzymes on microchannel surface through His-tag and application for microreactor. Protein Pept. Lett. 12, 207–210.

Miyazaki, M., Maeda, H., 2006. Microchannel enzyme reactors and their applications for processing. Trends Biotechnol. 24, 463–470.

Muller, Y.A., Lindqvist, Y., Furey, W., Schulz, G.E., Jordan, F., Schneider, G.,

1993. A thiamin diphosphate binding fold revealed by comparison of the crystal structuresof transketolase, pyruvate oxidase and pyruvate decarboxylase. Structure 1, 95–103.

Nakamura, H., 2004. A simple method of self assembled nano-particles deposition on the micro-capillary inner walls and the reactor application for photo-catalytic and enzyme reactions. Chem. Engin. J. 101, 261–268.

Neuhoff, V., Stamm, R., Eibl, H., 1985. Clear background and highly sensitive protein staining with Coomassie Blue dyes in polyacrylamide gels: A systematic analysis. Electrophoresis 6, 427–448.

Ngamsom, B., Hickey, A.M., Greenway, G.M., Littlechild, J.A., Watts, P., Wiles, C., 2010. Development of a high throughput screening tool for biotransformations utilising a thermophilic l-aminoacylase enzyme. J. Mol. Catal. B Enzym. 63, 81–86.

Nidetzky, B., 2013. Smart enzyme immobilization in microstructured reactors. Chemistry Today 31(3), 50–55.

Nomura, A., Shin, S., Mehdi, O.O., Kauffmann, J.-M., 2004. Preparation, characterization, and application of an enzyme-immobilized magnetic microreactor for flow injection analysis. Anal. Chem. 76, 5498–5502.

Nouaimi, M., Möschel, K., Bisswanger, H., 2001. Immobilization of trypsin on polyester fleece via different spacers. Enzyme Microb. Technol. 29, 567–574.

Oh, K.W., Ahn, C.H., 2006. A review of microvalves. J. Micromech. Microeng 16, 13–39.

Ozdural, A.R., Tanyolaç, D., Demircan, Z., Boyaci, İ.H., Mutlu, M., Webb, C., 2001. A new method for determination of apparent kinetics parameters in

recirculating packed-bed immobilized enzyme reactors. Chem. Eng. Sci. 56, 3483–3490.

Pace, C.N., Vajdos, F., Fee, L., Grimsley, G., Gray, T., 1995. How to measure and predict the molar absorption coefficient of a protein. Protein Sci. 4, 2411–2423.

Park, J., Li, J., Han, A., 2010. Micro-macro hybrid soft-lithography master (MMHSM) fabrication for lab-on-a-chip applications. Biomed. Microdevices 12, 345–351.

Payongsri, P., Steadman, D., Strafford, J., MacMurray, A., Hailes, H.C., Dalby, P.A., 2012. Rational substrate and enzyme engineering of transketolase for aromatics. Org. Biomol. Chem. 10, 9021–9029.

Pihl, J., Karlsson, M., Chiu, D.T., 2005. Microfluidic technologies in drug discovery. Drug Discov. Today 10, 1377–1383.

Pollack, M.G., Shenderov, A.D., Fair, R.B., 2002. Electrowetting-based actuation of droplets for integrated microfluidics. Lab. Chip 2, 96–101.

Pollard, D., Truppo, M., Pollard, J., Chen, C., Moore, J., 2006. Effective synthesis of (S)-3,5-bistrifluoromethylphenyl ethanol by asymmetric enzymatic reduction. Tetrahedron: Asymmetry 17, 554–559.

Pollard, D.J., Woodley, J.M., 2007. Biocatalysis for pharmaceutical intermediates: the future is now. Trends Biotechnol. 25, 66–73.

Ponomareva, E.A., Volokitina, M. V, Vinokhodov, D.O., Vlakh, E.G., Tennikova, T.B., 2012. Biocatalytic reactors based on ribonuclease A immobilized on macroporous monolithic supports. Anal. Bioanal. Chem. 405, 2195-2206.

Punta, M., Coggill, P.C., Eberhardt, R.Y., Mistry, J., Tate, J., Boursnell, C., Pang, N., Forslund, K., Ceric, G., Clements, J., Heger, A., Holm, L., , Sonnhammer, E.L.L., Eddy, S.R., Bateman, A., Finn, R.D. 2012. The Pfam protein families database. Nucleic Acids Res. 40, D290-301.

Qu, H., Wang, H., Huang, Y., Zhong, W., Lu, H., Kong, J., Yang, P., Liu, B., 2004. Stable microstructured network for protein patterning on a plastic microfluidic channel: strategy and characterization of on-chip enzyme microreactors. Anal. Chem. 76, 6426–6433.

Quiram, D.J., Jensen, K.F., Schmidt, M.A., Mills, P.L., Ryley, J.F., Wetzel, M.D., Kraus, D.J., 2007. Integrated Microreactor System for Gas-Phase Catalytic Reactions. 3. Microreactor System Design and System Automation. Ind. Eng. Chem. Res. 46, 8319–8335.

Ricca, E., Brucher, B., Schrittwieser, J.H., 2011. Multi-Enzymatic Cascade Reactions: Overview and Perspectives. Adv. Synth. Catal. 353, 2239–2262.

Richter, T., Shultz-Lockyear, L.L., Oleschuk, R.D., Bilitewski, U., Harrison, D.J., 2002. Bi-enzymatic and capillary electrophoretic analysis of non-fluorescent compounds in microfluidic devices: Determination of xanthine. Sens. Actuators B Chem. 81, 369–376.

Rios-Solis, L., Halim, M., Cázares, A., Morris, P., Ward, J.M., Hailes, H.C., Dalby, P.A., Baganz, F., Lye, G.J., 2011. A toolbox approach for the rapid evaluation of multi-step enzymatic syntheses comprising a "mix and match" E. coli expression system with microscale experimentation. Biocatal. Biotransformation 29, 192–203.

Roberts, M.A., Rossier, J.S., Bercier, P., Girault, H., 1997. UV Laser Machined Polymer Substrates for the Development of Microdiagnostic Systems. Anal. Chem. 69, 2035–42.

Roth, B.D., 2002. The discovery and development of atorvastatin, a potent novel hypolipidemic agent. Prog. Med. Chem. 40, 1–22.

Sakai-Kato, K., Kato, M., Ishihara, K., Toyo'oka, T., 2004. An enzyme-immobilization method for integration of biofunctions on a microchip using a water-soluble amphiphilic phospholipid polymer having a reacting group. Lab. Chip 4, 4–6.

Sakai-Kato, K., Kato, M., Toyo'oka, T., 2002. On-line trypsin-encapsulated enzyme reactor by the sol-gel method integrated into capillary electrophoresis. Anal. Chem. 74, 2943–2949.

Sakai-Kato, K., Kato, M., Toyo'oka, T., 2003. Creation of an On-Chip Enzyme Reactor by Encapsulating Trypsin in Sol−Gel on a Plastic Microchip. Anal. Chem. 75, 388–393.

Sayer, C., Isupov, M.N., Westlake, A., Littlechild, J.A. 2013. Structural studies of *Pseudomonas* and *Chromobacterium* ω-aminotransferases provide insights into their differing substrate specificity. Acta Cryst. D69, 564-576.

Schilling, E.A., Kamholz, A.E., Yager, P., 2002. Cell lysis and protein extraction in a microfluidic device with detection by a fluorogenic enzyme assay. Anal. Chem. 74, 1798–1804.

Schmid, A., Dordick, J.S., Hauer, B., Kiener, A., Wubbolts, M., Witholt, B., 2001. Industrial biocatalysis today and tomorrow. Nature 409, 258–268.

Schoevaart, R., Van Rantwijk, F., Sheldon, R.A., 2000. A Four-Step Enzymatic Cascade for the One-Pot Synthesis of Non-natural Carbohydrates from Glycerol. J. Org. Chem. 65, 6940–6943.

Schwarz, H., Hinz, H.J., Mehlich, A., Tschesche, H., Wenzel, H.R., 1987. Derivative sspectroscopy applied to tyrosyl chromophores. Studies on

ribonuclease, lima bean inhibitors, insulin, and pancreatic trypsin inhibitor. Biochemistry (Mosc.) 26, 2011–2024.

Schwarz, M.A., Hauser, P.C., 2001. Recent developments in detection methods for microfabricated analytical devices. Lab. Chip 1, 1–6.

Seong, G.H., Crooks, R.M., 2002. Efficient Mixing and Reactions within Microfluidic Channels Using Microbead-Supported Catalysts. J. Am. Chem. Soc. 124, 13360–13361.

Seong, G.H., Heo, J., Crooks, R.M., 2003. Measurement of enzyme kinetics using a continuous-flow microfluidic system. Analytical chemistry 75, 3161–7.

Sevostyanova, I. a, Solovjeva, O.N., Kochetov, G. a, 2004. A hitherto unknown transketolase—catalyzed reaction. Biochem. Biophys. Res. Commun. 313, 771–774.

Shin, J., Kim, B., 2002. Exploring the Active Site of Amine : Pyruvate Aminotransferase on the Basis of the Substrate Structure-Reactivity Relationship : How the Enzyme Controls Substrate Specificity and Stereoselectivity. Society 2848–2853.

Shin, J.-S., Kim, B.-G., 1998. Kinetic modeling of ω-transamination for enzymatic kinetic resolution of α-methylbenzylamine. Biotechnol. Bioeng. 60, 534–540.

Shin, J.-S., Kim, B.-G., 1999. Asymmetric synthesis of chiral amines with ω-transaminase. Biotechnol. Bioeng. 65, 206–211.

Shin, J.-S., Yun, H., Jang, J.-W., Park, I., Kim, B.-G., 2003. Purification, characterization, and molecular cloning of a novel amine:pyruvate transaminase from *Vibrio fluvialis* JS17. Appl. Microbiol. Biotechnol. 61, 463–71.

Shin, J.S., Kim, B.G., 1997. Kinetic resolution of alpha-methylbenzylamine with omicron-transaminase screened from soil microorganisms: application of a biphasic system to overcome product inhibition. Biotechnol. Bioeng. 55, 348–358.

Shin, J.S., Kim, B.G., Liese, A., Wandrey, C., 2001. Kinetic resolution of chiral amines with omega-transaminase using an enzyme-membrane reactor. Biotechnol. Bioeng. 73, 179–187.

Shiraishi, F., Hasegawa, T., Kasai, S., Makishita, N., Miyakawa, H., 1996. Bed Immobilized Enzyme Reactor. Chem. Eng. Sci. 51, 2847–2852.

Smith, M.E.B., Chen, B.H., Hibbert, E.G., Kaulmann, U., Smithies, K., Galman, J.L., Baganz, F., Dalby, P.A., Hailes, H.C., Lye, G.J., Ward, J.M., Woodley, J.M., Micheletti, M., 2009. A Multidisciplinary Approach Toward the Rapid and Preparative-Scale Biocatalytic Synthesis of Chiral Amino Alcohols: A Concise Transketolase-/ω-Transaminase-Mediated Synthesis of (2S,3S)-2-Aminopentane-1,3-diol. Org. Process Res. Dev. 14, 99–107.

Smith, M.E.B., Kaulmann, U., Ward, J.M., Hailes, H.C., 2006. A colorimetric assay for screening transketolase activity. Bioorg. Med. Chem. 14, 7062–5.

Smithies, K., Smith, M.E.B., Kaulmann, U., Galman, J.L., Ward, J.M., Hailes, H.C., 2009. Stereoselectivity of an ω-transaminase-mediated amination of 1,3-dihydroxy-1-phenylpropane-2-one. Tetrahedron Asymmetry 20, 570–574.

Sprenger, G.A.G., Schörken, U., Sahm, H., Schorken, U., 1995. Transketolase A of *Escherichia coli* K12 Purification and properties of the enzyme from recombinant strains. Eur. J. Biochem. 230, 525–532.

Srinivasan, A., Bach, H., Sherman, D.H., Dordick, J.S., 2004. Bacterial P450-catalyzed polyketide hydroxylation on a microfluidic platform. Biotechnol. Bioeng. 88, 528–535.

Srinivasan, R., Hsing, I.-M., Berger, P.E., Jensen, K.F., Firebaugh, S.L., Schmidt, M.A., Harold, M.P., Lerou, J.J., Ryley, J.F., 1997. Micromachined reactors for catalytic partial oxidation reactions. AIChE Journal 43, 3059–3069.

Stewart, J.D., 2001. Dehydrogenases and transaminases in asymmetric synthesis. Curr. Opin. Chem. Biol. 5, 120–9.

Svedendahl Humble, M., Engelmark Cassimjee, K., Håkansson, M., Kimbung, Y.R., Walse, B., Abedi, V., Federsel, H.-J., Berglund, P., Logan, D.T., 2012. Crystal structures of the *Chromobacterium violaceum* ω-transaminase reveal major structural rearrangements upon binding of coenzyme PLP. FEBS J..279, 779-792

Szakonyi, Z., 2008. Synthesis and application of monoterpene-based chiral aminodiols. Tetrahedron 64, 1034–1039.

Takayama, S., McGarvey, G.J., Wong, C.H., 1997. Microbial aldolases and transketolases: new biocatalytic approaches to simple and complex sugars. Annu. Rev. Microbiol. 51, 285–310.

Tao, F., Zhang, Y., Ma, C., Xu, P., 2011. One-pot bio-synthesis: N-acetyl-d-neuraminic acid production by a powerful engineered whole-cell catalyst. Sci. Rep. 1, 1–7.

Taylor, P.P., Pantaleone, D.P., Senkpeil, R.F., Fotheringham, I.G., 1998. Novel biosynthetic approaches to the production of unnatural amino acids using transaminases. Trends Biotechnol. 16, 412–418.

Thorsen, T., Maerkl, S.J., Quake, S.R., 2002. Microfluidic large-scale integration. Science 298, 580–584.

Tischer, W., Kasche, V., 1999. Immobilized enzymes: crystals or carriers? Trends Biotechnol. 17, 326–335.

Toda, I., 1975. Interparticle Mass Transfer Study with a Packed Column of Immobilized Microbes. Biotechnol. Bioeng. XVII, 1729–1747.

Tong, L., Righini, M., Gonzalez, M.U., Quidant, R., Käll, M., 2009. Optical aggregation of metal nanoparticles in a microfluidic channel for surface-enhanced Raman scattering analysis. Lab. Chip 9, 193–195.

Tran, R., Joseph, J.R., Sinclair, A., Bracewell, D., Zhou, Y., Titchener-Hooker, N.J., 2007. A framework for the prediction of scale-up when using compressible chromatographic packings. Biotechnol. Prog. 23, 413–22.

Turner, N.J., 2000. Applications of transketolases in organic synthesis. Curr. Opin. Biotechnol. 11, 527–531.

Urban, P.L., Goodall, D.M., Bruce, N.C., 2006. Enzymatic microreactors in chemical analysis and kinetic studies. Biotechnol. Adv. 24, 42–57.

Verpoorte, E., Rooij, N.F.D.E., 2003. Microfluidics Meets MEMS. Proceedings of IEEE. 91, 930-953.

Villegas, M.F., 2013. Novel coupled reactions for the synthesis of chiral amino compound. PhD Thesis. Department of Biochemical Engineering. University College London.

Wang, C., Li, S.-J., Wu, Z.-Q., Xu, J.-J., Chen, H.-Y., Xia, X.-H., 2010. Study on the kinetics of homogeneous enzyme reactions in a micro/nanofluidics device. Lab. Chip 10, 639–646.

Wang, C., Oleschuk, R., Ouchen, F., Li, J., Thibault, P., Harrison, D.J., 2000. Integration of immobilized trypsin bead beds for protein digestion within a

microfluidic chip incorporating capillary electrophoresis separations and an electrospray mass spectrometry interface. RCM 14, 1377–1383.

Wang, J., Chatrathi, M.P., Tian, B., Polsky, R., 2000. Microfabricated electrophoresis chips for simultaneous bioassays of glucose, uric acid, ascorbic acid, and acetaminophen. Anal. Chem. 72, 2514–2518.

Watts, P., 2004. Continuous flow microreactors for drug discovery. Curr. Op. Drug Discov. Dev. 7, 807–812.

Webb, D., Jamison, T.F., 2010. Continuous flow multi-step organic synthesis. Chem. Sci. 1, 675-680

Wen, E., Asiaie, R., Horváth, C., 1990. Dynamics of capillary electrochromatography. II. Comparison of column efficiency parameters in microscale high-performance liquid chromatography and capillary electrochromatography. J. Chromatogr 507, 349–366.

Wheeler, A.R., Throndset, W.R., Whelan, R.J., Leach, A.M., Zare, R.N., Liao, Y.H., Farrell, K., Manger, I.D., Daridon, A., 2003. Microfluidic device for single-cell analysis. Anal. Chem. 75, 3581–3586.

Whitesides, G.M., 2006. The origins and the future of microfluidics. Nature 442, 368–373.

Wilson, N.G., McCreedy, T., 2000. On-chip catalysis using a lithographically fabricated glass microreactor-the dehydration of alcohols using sulfated zirconia. Chem. Commun. 0, 733–734.

Woodley, J.M., Mitra, R.K., Lilly, M.D., 1996. Carbon-Carbon Bond Synthesis. Reactor Design and Operation for Transketolase-catalyzed Biotransformations. Ann. N. Y. Acad. Sci. 799, 729–736.

Woolley, A.T., Mathies, R.A., 1994. Ultra-high-speed DNA fragment separations using microfabricated capillary array electrophoresis chips. Proc. Natl. Acad. Sci. U. S. A. 91, 11348–11352.

Wu, G., Irvine, J., Luft, C., Pressley, D., Hodge, C.N., Janzen, B., 2003. Assay development and high-throughput screening of caspases in microfluidic format. Comb. Chem. High Throughput Screen. 6, 303–312.

Wu, H., Tian, Y., Liu, B., Lu, H., Wang, X., Zhai, J., Jin, H., Yang, P., Xu, Y., Wang, H., 2004. Titania and alumina sol-gel-derived microfluidics enzymatic-reactors for peptide mapping: design, characterization, and performance. J. Proteome Res. 3, 1201–1209.

Xue, Q., Wainright, A., Gangakhedkar, S., Gibbons, I., 2001. Multiplexed enzyme assays in capillary electrophoretic single-use microfluidic devices. Electrophoresis 22, 4000–4007.

Yasohara, Y., Kizaki, N., Hasegawa, J., Takahashi, S., Wada, M., Kataoka, M., Shimizu, S., 1999. Synthesis of optically active ethyl 4-chloro-3-hydroxybutanoate by microbial reduction. Appl. Microbiol. Biotechnol. 51, 847–851.

Yeo, L.Y., Chang, H.-C., Chan, P.P.Y., Friend, J.R., 2011. Microfluidic devices for bioapplications. Small 7, 12–48.

Yi, S.-S., Lee, C., Kim, J., Kyung, D., Kim, B.-G., Lee, Y.-S., 2007. Covalent immobilization of ω-transaminase from *Vibrio fluvialis* JS17 on chitosan beads. Process Biochem. 42, 895–898.

Yin, H., Killeen, K., Brennen, R., Sobek, D., Werlich, M., Van De Goor, T., 2005. Microfluidic chip for peptide analysis with an integrated HPLC column, sample enrichment column, and nanoelectrospray tip. Anal. Chem. 77, 527–533.

Yun, H., Hwang, B.-Y., Lee, J.-H., Kim, B., 2005. Use of enrichment culture for directed evolution of the *Vibrio fluvialis* JS17 omega-transaminase, which is resistant to product inhibition by aliphatic ketones. Appl. Environ. Microbiol. 71, 4220–4224.

Yun, H., Lim, S., Cho, B.-K., Kim, B.-G., 2004. omega-Amino acid:pyruvate transaminase from *Alcaligenes denitrificans* Y2k-2: a new catalyst for kinetic resolution of beta-amino acids and amines. Appl. Environ. Microbiol. 70, 2529–2534.

Zhang, C., Xing, D., Li, Y., 2007. Micropumps, microvalves, and micromixers within PCR microfluidic chips: Advances and trends. Biotechnology Advances 25, 483–514.

Zhang, N., Yeung, E.S., 1998. On-line coupling of polymerase chain reaction and capillary electrophoresis for automatic DNA typing and HIV-1 diagnosis. J. Chromatogr. B Biomed. Sci. Appl. 714, 3–11.

Zimmermann, F.T., Schneider, A., Schörken, U., Sprenger, G.A., Fessner, W.-D., 1999. Efficient multi-enzymatic synthesis of d-xylulose 5-phosphate. Tetrahedron: Asymmetry 10, 1643–1646.
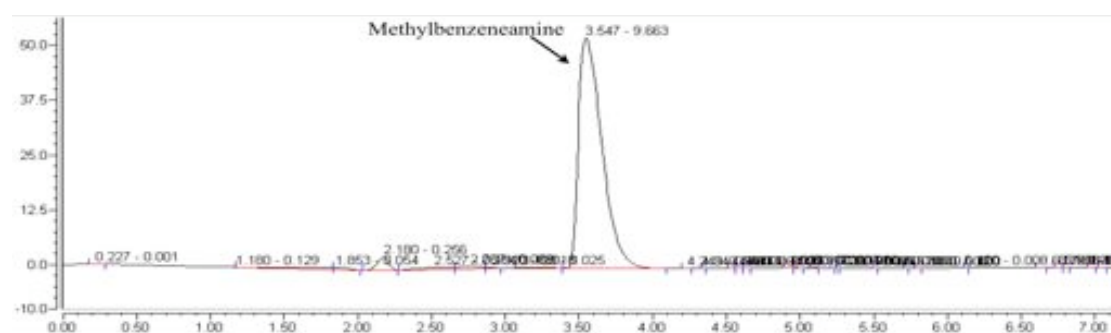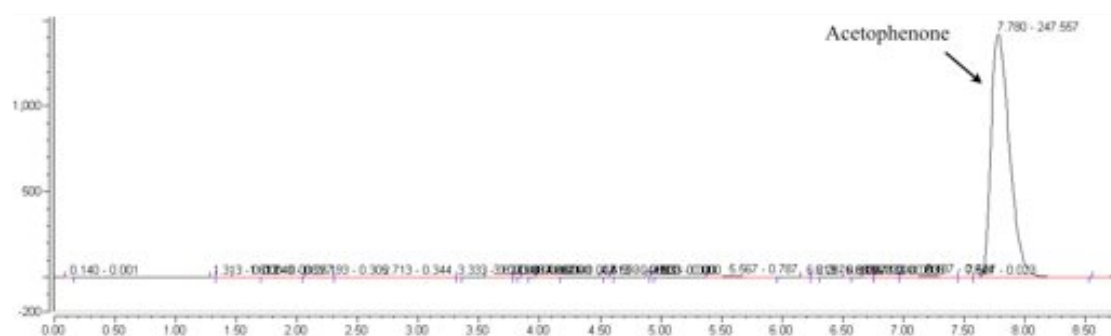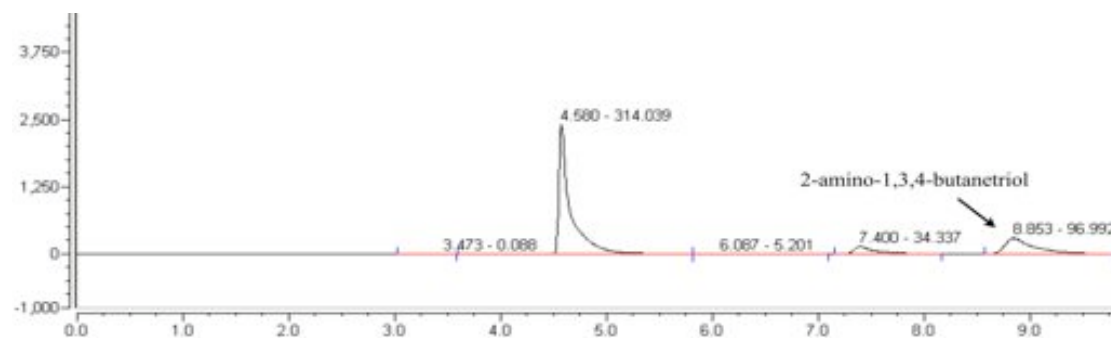
Appendix 1: HPLC Traces

(1)
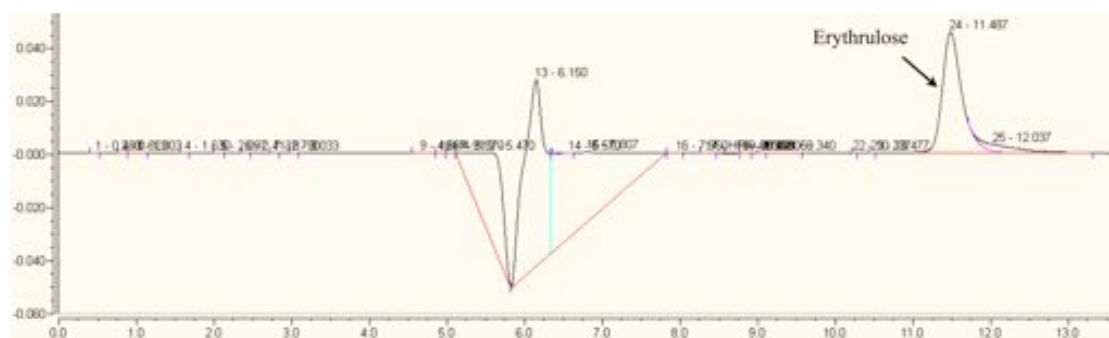
(2)
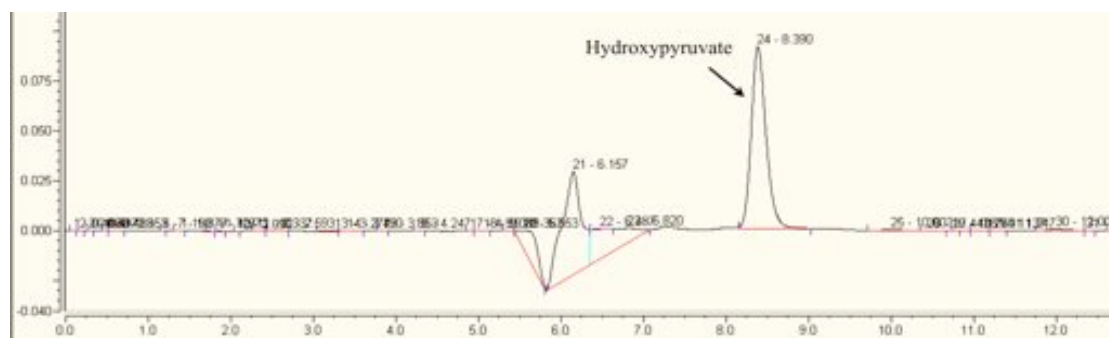
(3)

(4)

(5)

Appendix 2: Enzyme Binding on Surface

Fischer et al. (2004) showed that the average density for proteins of MW>20 kDa is approximately 1.4g/cm^3. The MW of each TK unit is ~72.5 kDa. Avogadro's constant, N_A is 6.02 x 10^{23} mol^{-1}. Therefore the radius each TK molecule can be estimated as follows:

$$\text{Protein volume} \approx \frac{4}{3}\pi r^3$$

Or,

$$\frac{MW}{\rho N_A} = \frac{4}{3}\pi r^3$$

Rearranging and substituting,

$$r = \sqrt[3]{\frac{3}{4\pi}\frac{MW}{\rho N_A}}$$

$$r = \sqrt[3]{\frac{3}{4\pi}\frac{72500}{1.4x(6x10^{23})}}$$

This gives r≈0.0027 μm and the area occupied can be approximated to the circular area:

$$\text{Protein Area, A} = \pi r^2$$

$$A = \pi x 0.0027^2 = 2.3x10^{-5}\mu m^2$$

And,

The surface area available on the capillary can be calculated by assuming area of cylinder with internal diameter (ID) of 200 μm and length of 40 cm that is 250 mm^2 = 250 x 10^6 μm^2.

Finally,

$$\text{Protein molecules} = \frac{\text{Capillary Area}}{\text{Protein Area}} = \frac{250x10^6}{2.29x10^{-5}} = 1.09x10^{13}\text{molecules}$$

$$\text{Moles of TK} = \frac{\text{Molecules}}{N_A} = \frac{1.09x10^{13}}{6.02x10^{23}} = 1.8x10^{-11}\text{moles}$$

Therefore, the mass of TK immobilized on the microcapillary surface can be estimated:

$$\text{Mass of TK} = \text{Moles x MW} = 1.8\text{x}10^{-11}\text{moles x } 72500 = 1.3 \ \mu\text{g}$$